Mathematical Modelling of a Pulse Combustor of the Helmholtz-type

P.A. van Heerbeek

August 2008

TUDelft

Delft University of Technology
Faculty of Electrical Engineering, Mathematics and Computer Science
Delft Institute of Applied Mathematics

Mathematical Modelling of a Pulse Combustor of the Helmholtz-type

A thesis submitted to the
Delft Institute of Applied Mathematics
in partial fulfillment of the requirements

for the degree

MASTER OF SCIENCE
in
APPLIED MATHEMATICS

by

PIETER ANTHON VAN HEERBEEK

Delft, the Netherlands
August 2008

TUDelft

MSc THESIS APPLIED MATHEMATICS

"Mathematical Modelling of a Pulse Combustor of the Helmholtz-type"

PIETER ANTHON VAN HEERBEEK

Delft University of Technology

Daily supervisor

Dr.ir. M.B. van Gijzen

Responsible professor

Prof. dr.ir. C. Vuik

Other thesis committee members

Ir. M.R. de la Fonteijne

Ir. H.F.M. Corstens

August 2008

Delft, the Netherlands

Contact information

Delft University of Technology

P.A. van Heerbeek

Delft University of Technology
Delft Institute of Applied Mathematics
Mekelweg 4 (Room HB07.030)
2628 CD Delft
The Netherlands

E-mail: `P.A.vanHeerbeek@student.tudelft.nl`

DLF Sustainable
Sustainable Technology & Environmental Solutions

Ir. M.R. de la Fonteijne

DLF Sustainable
P.O. Box 1077
2600 BB Delft
The Netherlands

Mobile: +31 621885101
E-mail: `marcel@dlfsustainable.nl`
Web-site: `www.dlfsustainable.nl`

# Mathematical modelling of a pulse combustor of the Helmholtz-type

Preface

This report is my Master's thesis for the study "Applied Mathematics" at the Delft University of Technology (TU Delft). The project is conducted in collaboration with DLF Sustainable and aims at developing mathematical tools to aid in the design of pulse combustors and to gain insight into the physical processes that make them work (or not).

At the start of the research project, DLF Sustainable was already involved in a joint research project on pulse combustion with the Eindhoven University of Technology (TU Eindhoven). A small pulse combustor has been made available for experimenting (see Figure 1a). The pulse combustor is much simpler in design than the industrial pulse combustors of interest to DLF Sustainable (see Figure 1b), but the working principles are basically the same. Experimental research with the pulse combustor at the TU Eindhoven can be useful for validation of a mathematical model. Research at the TU Eindhoven is mainly progressed via Bachelor's thesis projects, which are concentrated on zero-dimensional models of pulse combustors from literature. I have taken note of two Bachelor's theses on pulse combustion [31, 33], produced at the TU Eindhoven. They will be mentioned at the appropriate places in this report.

Pieter van Heerbeek,
August 2008, Delft.

(a) Small pulse combustor at TUE
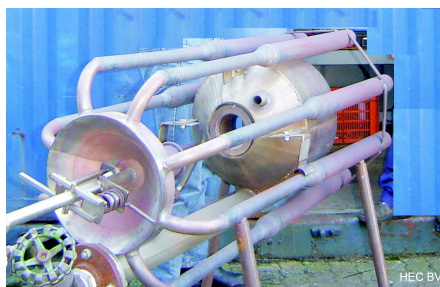
(b) An advanced pulse combustor

Figure 1: Two pulse combustors: (a) a small pulse combustor made available for experimenting at the TU Eindhoven (TUE), photo (a) is from Tiemessen and Bastiaans [31]; (b) an advanced pulse combustor.

x

DLF Sustainable is a specialist in the field of thermodynamics, with a focus on sustainable energy generation and energy saving in an industrial environment. Keywords are: biomass gasification, pyrolysis, CHP, solar power, PV, cogen.

Because pulse combustion can have a positive impact on reducing environmental emission, DLF Sustainable asked Pieter van Heerbeek to investigate pulse combustion from a theoretical point of view. In this study Pieter van Heerbeek examined thoroughly several models from literature, in order to be capable of defining goals for the second part of his Master's thesis. This resulted in several corrections of models shown in literature, the results of which are presented in a poster session on the Combura 2007 symposium at NBC in Nieuwegein (Holland) on the 10th of October 2007.

In this second part, the steady-state points were examined in more detail in relation to stable pulse combustion. He showed under which circumstances pulse combustion will occur. This resulted in a poster presentation at the ECMI conference in July 2008 and an article to be published.

Pieter showed himself to be a nice and intelligent person with a high level of integrity. I am very pleased to see the enthusiasm of Pieter doing this study and I appreciate his sound working attitude.

Thanks Pieter, I wish you all the best with your future plans.

Marcel de la Fonteijne,
DLF Sustainable.

Contents

Chapter 1

Introduction

1.1 Background and motivation

The company DLF Sustainable in Delft is a specialist in the field of thermo-dynamic applications. Examples of industrial applications are: gas fired installations (for direct or indirect heat generation, central heating boilers), dryers (for feed stock, industrial sewage/sludge), incinerators (for hazardous waste, thermal oxidation of gases/fluids/solids) and gasifiers (for biomass gasification). This list is by no means exhaustive.

During years of experience in the field and doing research, DLF Sustainable has developed an advanced pulse combustor for industrial applications such as mentioned above (see Figure 1.1). Compared to conventional (steady flow) combustion systems, this type of combustor can achieve production increases as high as 40%, and fuel savings of 10–50%, depending on the application. Also, it produces very low emissions of harmful substances. These advantages are typical of pulse combustors and can be related to the generation of intense oscillatory fluid motions (sound waves) in the combustion system, which is a fundamental part of the operating conditions. The high-intensity sound waves cause enhanced heat and mass transfer, higher combustion intensities, lower emissions of nitrogen oxides (NO_x) and higher thermal efficiencies, all by a considerable factor of magnitude compared to conventional combustion systems [9,10,14,16,22]. Also, usually pulse combustors provide their own means for pumping fuel and air, obviating the need for extra devices such as fans or a chimney. This may lead to more compact designs. The mentioned advantages make pulse combustion a practically, economically and environmentally attractive technique for burning and heating applications.

There are disadvantages to pulse combustion. First, the process is inherently noisy. At higher frequencies this is not a major obstacle, since the sound and associated vibrations can then be damped by conventional methods of isolation. And sometimes the sound generated is a plus. For example in drying applications, where sound induced oscillations in a drying chamber not only increase the drying rates, but also prevent depositing of substances on the walls. A more serious problem results from the highly coupled physical and chemical processes in a working pulse combustor, such as the interaction between (turbulent) combustion and the system's acoustics. These interactions cause problems when

(a) Advanced pulse combustor in action   (b) Close-up of pulse combustor
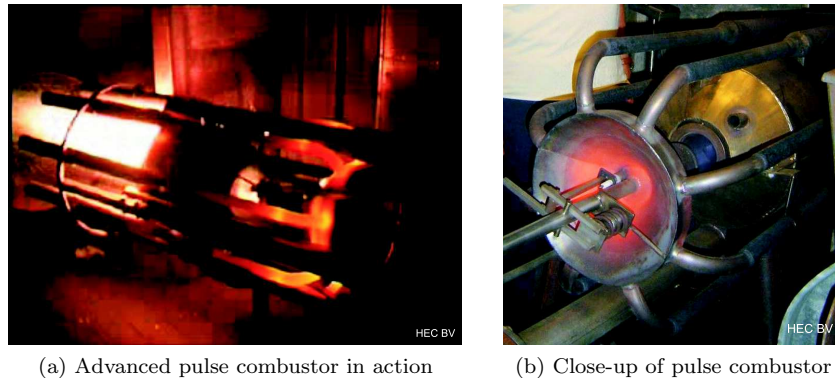
Figure 1.1: A gas-fired pulse combustor with a secondary burner. (a) The
pulse combustor in operation, the eight tailpipes are glowing. In the secondary
burner, pulverized brown coal is ignited by a flame from the pulse combustor's
aerovalve. (b) A close-up of the pulse combustor, showing the gas supply at the
front, and a flame from the aerovalve entering the secondary burner.

trying to scale up or improve upon a working design. Adjusting the geometry
of the pulse combustor may produce the desired effect, but sometimes it may
be detrimental to the system's performance instead. Therefore, improvement of
a design is mainly a process by trial-and-error.

To aid in the design of pulse combustors and to get a better understanding
of the fundamental physical processes that govern the pulse combustion phe-
nomenon, a mathematical model capturing the most important aspects of pulse
combustion is desired. The work reported here is a preparing step for research
aimed at developing such a mathematical model.

1.2   Objective and outline

The goal of this work is (a) to describe the physics behind three simple models
for pulse combustion and to present their mathematical formulation, and (b) to
determine conditions under which these models can describe stable operation of
a pulse combustor.

The three models are lumped parameter models: physical processes are mod-
elled by spatial averaging. In this way, modelling of the details of the pulse
combustion process is avoided, while one tries to retain the most important
characteristics.

This report is organized in the following way. The basic principles of pulse
combustion operation are described in Chapter 2. Of special interest is the
Rayleigh criterion. It is a condition under which periodic heat release may
drive acoustic oscillations, which is a fundamental part of the pulse combustion
process. In each of the Chapters 3–5, one simple mathematical model from
literature is described and analyzed in detail. Conclusions of the study of these
models are presented at the end of the relevant chapters. In Chapter 3 a model
presented by Kilicarslan [17] is discussed. Shortcomings of this model to describe
a pulse combustion process were reason to study the model of Ahrens et al. [2],

that provided the basis for Kilicarslan's model. The model of Ahrens et al. is discussed in Chapter 4. The mathematical model of Richards et al. [25] is the third model that was studied. It includes physical processes that were neglected in the other two models; it is described in Chapter 5. Finally, in Chapter 6 overall conclusions are presented, and suggestions for future research are given. suggested. Computational analysis of the three models was performed using MATLAB [29] software. The codes that were used, can be found in the appendices.

Chapter 2

Working principles of pulse combustion

The principles of operation of a pulse combustor are based on a coupling between intermittent (pulse) combustion and (resonant) acoustics in the burner system. The interaction of the system's acoustics with the combustion process (e.g. fuel supply, mixing processes, reaction rates, etc.) is such that the resulting intermittent combustion process feeds energy into the acoustical oscillations.

Although the acoustical oscillations in a pulse combustor are obviously driven by the combustion process, the term 'combustion-driven oscillations' is generally associated with disturbances (instabilities) of a steady combustion process. Putnam et al. [22] distinguished between combustion-driven oscillations, which may be harmful in devices designed for steady combustion, and pulse combustion, where oscillations are deliberately stimulated in order to obtain increased mixing rates, higher heat transfer rates, etc. A condition under which unsteady combustion may drive pressure waves, that is often mentioned in the study of combustion instabilities, is Rayleigh's criterion. It will be discussed below, after describing the operation of a typical pulse combustor.

2.1   A typical pulse combustion cycle

Figure 2.1 depicts an idealized cycle of operation of a pulse combustor with an aerodynamic valve (or, aerovalve). In the first stage of the cycle (1), a combustible mixture in the combustion chamber ignites, and a burning region expands, driving gases into the tailpipe (to the right) and through the aerovalve (to the left). In the second stage of the cycle (2), when most of the fuel has been consumed, the gases continue their motion due to inertia, thereby lowering the pressure in the combustion chamber. Eventually, the pressure in the combustion chamber falls below atmospheric pressure. Then the third phase of the cycle starts (3). Fresh air (and fuel) enter the combustion chamber, following the remnant of combustion products from the aerovalve. Due to inertia, the flow in the tailpipe takes longer to slow down and it may reverse its direction at a later moment. In the last stage of the cycle (4), inertia of the gases flowing toward the combustion chamber cause the pressure to rise above the ambient pressure. Then, the cycle is started anew with the ignition of the combustible mixture.
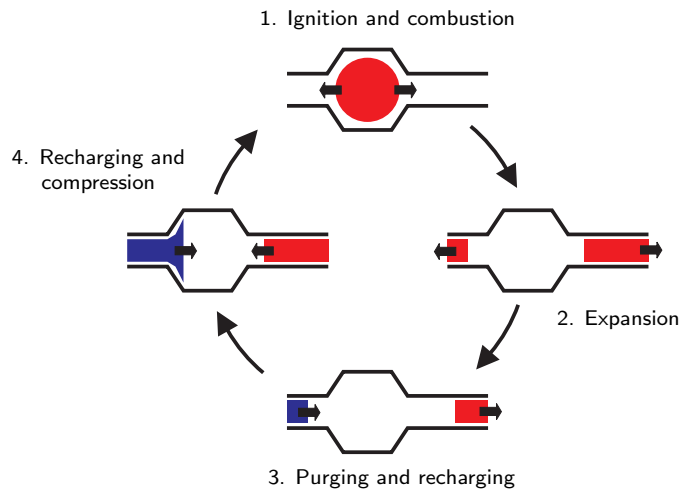
Figure 2.1: An idealized (aerovalved) pulse combustion cycle (adapted from Putnam et al. [22]). With a flapper valve, the flow in the direction of the valve is completely blocked during the expansion phase.

The exact ignition mechanism is not clear; it may be caused by flame remnants, contact with hot combustion products, or a hot-spot in the combustion chamber.

There are many different types of pulse combustors. A pulse combustor can be mechanically valved (e.g., it may be equipped with flapper valves or with reed valves), or aerodynamically valved. In case of mechanical valves, back flow through the valve is prevented: flow through the valves only occurs in stages 3 and 4 of Figure 2.1. Also, an aerovalve may be designed to greatly resist back flow, acting somewhat like a badly leaking flapper valve. There is a great variety in the geometry of pulse combustors, too. Typical examples are pulse combustors of the Helmholtz-type, the Schmidt (or, quarter-wave) type, and the Rijke-type. The pulse combustor sketched in Figure 2.1 is of the Helmholtz-type: a volume (the combustion chamber) acts like a Helmholtz resonator on the tailpipe gases. A Schmidt-type pulse combustor typically consists of a tube closed at one end (where combustion takes place) and open at the other end; it acts like a quarter-wave tube. In a Rijke-type pulse combustor, combustion takes place in the lower half of a vertical tube, acting like a Rijke-tube. In this configuration, the combustion process is typically enhanced by (acoustical) velocity fluctuations. Other configurations are possible. In a review article on pulse combustion, Putnam et al. [22] provide a historic overview of pulse combustor designs, and describe the operating characteristics of mechanically valved and aerovalved pulse combustors.

2.2 Rayleigh's criterion

A pulse combustor can be viewed as a harmonic resonator used to store acoustical energy. Moments of low pressure are used for refueling, while periodic combustion sustains the acoustical oscillations by feeding energy to the resonator. A widely used condition under which periodic heat release (e.g. by combustion)

can sustain acoustical oscillations, is Rayleigh's criterion. In short, it states that acoustical oscillations are stimulated when heat is released in phase with the pressure variations, while the oscillations are damped when heat is released out of phase.

In 1878, Rayleigh [23] formulated it as follows:

> "If heat be periodically communicated to, and abstracted from, a mass of air vibrating (for example) in a cylinder bounded by a piston, the effect produced will depend upon the phase of the vibration at which the heat transfer takes place. If heat be given to the air at the moment of greatest condensation, or taken from it at the moment of greatest rarefaction, the vibration is encouraged. On the other hand, if heat be given at the moment of greatest rarefaction, or abstracted at the moment of greatest condensation, the vibration is discouraged."

He also noted that the frequency can be changed, depending on the phase of heat release:

> "If the air be at its normal density at the moment when the transfer of heat takes place, the vibration is neither encouraged nor discouraged, but the pitch is altered. Thus the pitch is raised, if heat be communicated a quarter period before the phase of greatest condensation, and the pitch is lowered if the heat be communicated a quarter period after the phase of greatest condensation."

Rayleigh remarked that in general heat release produces both kinds of effects. He went on to illustrate the principle by successfully applying it to explain certain acoustical phenomena.

2.2.1   A heuristic explanation

Intuitively, Rayleigh's criterion is easily understood. For example, consider a volume of air vibrating in a surrounding fluid. Energy of condensation of the volume (i.e. its potential energy) and kinetic energy of the surroundings are exchanged through work performed on the boundaries of the volume. Heat addition will cause the volume of air to expand, obtaining a new equilibrium volume. When heat is added to the volume at a moment of condensation, the action of the volume of air is supported in converting potential energy into kinetic energy (or vice versa), and the vibration is encouraged. On the other hand, when heat is added at a moment of rarefaction, the action of the volume of air on the surroundings is counteracted, and the vibration is discouraged. The greater the pressure difference of the volume and the surroundings, the more work is done per unit of expansion. Thus, the effect of heat addition is greater if the condensation is greater. When the volume of air is at its equilibrium pressure, it is not doing any work on the surroundings, and heat addition will neither encourage nor discourage the vibration.

The effect of (periodic) heat release on the frequency of the vibration can be understood intuitively, too. If heat is added before the moment of greatest condensation, the induced expansion works against the compression by the surroundings, and the state of greatest condensation is reached sooner. Therefore,

the frequency is increased. If heat is added after the moment of greatest condensation, the induced expansion works with the expansion by the surroundings, and the state of greatest rarefaction is reached later. Therefore, the frequency is decreased.

2.2.2   A mathematical formulation

An often used mathematical formulation of the Rayleigh criterion for maintenance of oscillations is

$$\int_0^{T_P} \int_V p'Q' \, dV \, dt > 0, \tag{2.1}$$

where the product of the pressure fluctuations p' and the fluctuations in heat release Q' is integrated over the volume V and the time interval $[0, T_P]$, with T_P a period of oscillation. It can be viewed as an expression of the heuristic argument put forward in the previous subsection. More generally, in order for the heat release to provide the oscillations with sufficient energy to overcome energy losses, the integral on the left-hand side should be great enough to overcome the sum of the energy losses $(\sum_i L_i)$ occurring in the volume over a period of oscillation:

$$\frac{\gamma - 1}{\gamma p_0} \int_0^{T_P} \int_V p'Q' \, dV \, dt > \sum_i L_i. \tag{2.2}$$

The factor $\frac{\gamma-1}{\gamma p_0}$ is introduced in anticipation of analysis later in this chapter; it cannot be missed for dimensional reasons. Energy losses may be associated with viscous dissipation, heat conduction, energy fluxes through the boundary of the volume, etc. This is a generalized version of the Rayleigh criterion.

In an article on the energy transfer to small disturbances in fluid flow, Chu [6] has provided a foundation for expressions like (2.1) and (2.2), quantifying the conditions under which heat release encourages fluctuations in fluid flow. In this report, no quantification of the Rayleigh criterion is used, therefore the article of Chu will not be discussed at length here. However, to illustrate how the Rayleigh criterion may appear from the general equations of fluid motion, a simplified derivation may be insightful. Such a derivation will be considered next. For details on the derivation, see the paper by Chu [6].

Consider a uniform homogeneous perfect gas at rest: its state may be expressed by velocity $\mathbf{u}_0 = \mathbf{0}$, pressure $p = p_0$, density $\rho = \rho_0$ and temperature $T = T_0$, all constant. Assume that the specific heats for constant pressure c_p and constant volume c_v are constant, and that effects of viscosity and heat conduction may be neglected. Now introduce some small heat release Q', and associated *small* disturbances in velocity ($\mathbf{u}'$), pressure (p'), density (ρ'), and temperature (T'). The disturbances are considered small if: $|\mathbf{u}'|/c_0 \ll 1$ (with c_0 the speed of sound of the undisturbed fluidum), $|p'/p_0| \ll 1$, $|\rho'/\rho_0| \ll 1$, and $|T'/T_0| \ll 1$. Now, substitution of $p = p_0 + p'$, $\mathbf{u} = \mathbf{u}_0 + \mathbf{u}'$, etc., in the continuity equation, the momentum equation, the energy equation, and the state equation, and neglecting cross-products of fluctuations, leads to the following

equations for the disturbances in the fluid flow:

$$\frac{\partial \rho'}{\partial t} + \rho_0 \nabla \cdot \mathbf{u}' = 0, \qquad \text{(continuity)} \qquad (2.3)$$

$$\rho_0 \frac{\partial \mathbf{u}'}{\partial t} = -\nabla p', \qquad \text{(momentum)} \qquad (2.4)$$

$$\rho_0 c_v \frac{\partial T'}{\partial t} + p_0 \nabla \cdot \mathbf{u}' = Q', \qquad \text{(energy)} \qquad (2.5)$$

$$\frac{T'}{T_0} + \frac{\rho'}{\rho_0} = \frac{p'}{p_0}. \qquad \text{(state)} \qquad (2.6)$$

To see how the heat release Q' drives the pressure disturbances, substitute T' from the state equation (2.6) into the energy equation (2.5), and then write the time-derivative of ρ' in terms of the rate of expansion $(\nabla \cdot \mathbf{u}')$ using the continuity equation (2.3). Using $\gamma = c_p/c_v$ and the perfect gas properties $p_0 = R\rho_0 T_0$ and $R = c_p - c_v$, with R the gas constant, this gives

$$\frac{1}{\gamma p_0} \frac{\partial p'}{\partial t} + \nabla \cdot \mathbf{u}' = \frac{Q'}{c_p \rho_0 T_0}. \qquad (2.7)$$

Differentiating this equation with respect to time, and eliminating the time derivative of the rate of expansion $(\frac{\partial}{\partial t}\nabla \cdot \mathbf{u}')$ by substitution of the momentum equation (2.4) after taking the divergence, leads to

$$\frac{\partial^2 p'}{\partial t^2} - c_0^2 \nabla^2 p' = (\gamma - 1)\frac{\partial Q'}{\partial t}, \qquad (2.8)$$

where the relation $c_0^2 = \gamma p_0/\rho_0$ for speed of sound has been used. This is an inhomogeneous wave equation, with the time-derivative of the heat release rate as source term.

An expression for the acoustic energy can be derived from the momentum equation equation (2.4) and equation (2.7), leading to a quantification of the Rayleigh criterion. Adding the product of p' and equation (2.7) to the inner product of $\mathbf{u}'$ and equation (2.4), and using $\rho_0 c_0^2 = \gamma p_0$ and $\frac{1}{c_p \rho_0 T_0} = \frac{\gamma - 1}{\gamma p_0}$, yields

$$\frac{\partial}{\partial t}\left[\frac{1}{2}\frac{p'^2}{\rho_0 c_0^2} + \frac{1}{2}\rho_0 \mathbf{u}' \cdot \mathbf{u}'\right] + \nabla \cdot (p'\mathbf{u}') = \frac{\gamma - 1}{\gamma p_0} p'Q'. \qquad (2.9)$$

This is an equation for the acoustic energy: the two terms in the square brackets are the energy associated with compression (first term, a potential energy) and the kinetic energy (second term), and the divergence on left-hand side expresses the flux of acoustic energy. The right-hand side shows a source term for the production of acoustic energy. Integrated over a volume V with boundary S and a period of oscillation $[0, T_P]$, this equation provides a quantification of Rayleigh's criterion: in order for the acoustic disturbances to be maintained, the relation between the pressure fluctuations p' and heat release Q' should satisfy the inequality

$$\frac{\gamma - 1}{\gamma p_0} \int_0^{T_P} \int_V p'Q' \, dV \, dt > \int_0^{T_P} \int_S p'\mathbf{u}' \cdot \mathbf{n} \, dS \, dt, \qquad (2.10)$$

where $\mathbf{n}$ denotes the outwardly directed normal on the surface S. To convert the volume integral of the divergence to the surface integral, Gauss' theorem has been used.

In his article, Chu [6] included viscous and heat conduction terms, source terms for mass and heat, and body forces. Taking the fluxes across the boundary of the volume of interest equal to zero, he derived an expression that generalizes the acoustic energy of the fluctuations to an expression including the fluctuations in entropy. If heat conduction can be neglected, and without mass sources and body forces, his expression for the rate of change of the energy of fluctuations splits into two distinct expressions:

$$\frac{\partial}{\partial t} \int_V \left[\frac{1}{2} \frac{p'^2}{\rho_0 c_0^2} + \frac{1}{2} \rho_0 \mathbf{u}' \cdot \mathbf{u}' \right] dV = \frac{(\gamma - 1)}{\gamma p_0} \int_V p' Q' \, dV - \int_V \Phi' \, dV, \qquad (2.11)$$

where Φ' is a viscous dissipation term, and

$$\frac{\partial}{\partial t} \int_V \left[\frac{1}{2} \frac{(\gamma - 1)}{\gamma} p_0 \left(\frac{S'}{R} \right)^2 \right] dV = \frac{1}{c_p} \int_V S' Q' \, dV, \qquad (2.12)$$

where S' is the fluctuation in entropy. The last equation can be obtained directly from the energy equation if it is expressed in terms of entropy instead of temperature: $\rho_0 T_0 \frac{\partial S'}{\partial t} = Q'$. Based on equation (2.11), the Rayleigh criterion may be expressed as

$$\int_0^{T_P} \int_V p' Q' \, dV \, dt > \frac{\gamma p_0}{(\gamma - 1)} \int_0^{T_P} \int_V \Phi' \, dV \, dt, \qquad (2.13)$$

but equation (2.12) shows that the Rayleigh criterion does not tell the whole story. If heat is released in phase with the entropy fluctuations, the flow may become unstable, even without any pressure fluctuations. If heat conduction cannot be neglected, the contributions of source terms to the energy of fluctuations cannot be split into an acoustical part and an entropic part, as was done with (2.11) and (2.12).

Further, Chu [6] applied the theory of the energy of fluctuations to study transfer of energy from a steady main stream, with extra source terms derived from the main stream. He then discussed the special case of a two-dimensional parallel shear flow as main stream, showing the work done by the Reynolds stress and the transport of entropy spottiness across the temperature shear layers as production terms of the energy of fluctuations.

In a closely related article, Nicoud and Poinsot [20] first derived an exact nonlinear equation, similar to the equation for the energy of fluctuations. From this, they derived an equation for the energy of fluctuations by linearization. They mentioned an extra production term for the energy of fluctuations, that appears to be missing in the derivation by Chu: $-\frac{p_0}{R C_p} S' \mathbf{u}' \cdot \nabla S_0$, where S_0 is the entropy of the mean flow. After an estimation of the order of magnitude of the extra term, they noted that it may be larger that the classic Rayleigh term. They concluded that for the investigation of combustion instabilities, the energy of fluctuations should be used instead of Rayleigh's criterion.

Chapter 3

A model suggested by Kilicarslan

Note: In a Bachelor's thesis project at the Eindhoven University of Technology, Tiemessen and Bastiaans [31] adjusted the model of Kilicarslan [17], which is discussed in this chapter, with the purpose of predicting the frequency of an experimental aerovalved pulse combustor. This report was studied, but the discussion in this chapter focuses only on the work presented by Kilicarslan.

In this chapter a zero-dimensional model for a gas-fired flapper-valved pulse combustor of the Helmholtz-type, presented in an article by Kilicarslan [17], will be examined. Figure 3.1 shows a schematic of the modelled pulse combustor. In the model, the combustion chamber is taken as control volume and an energy balance for this control volume is formulated. The amount of energy in the control volume is changed by reactants mixture entering the control volume, by combustion inside the control volume and by products leaving the control volume via the tailpipe. The inflow of reactants mixture is modelled by quasi-steady flow orifice equations and depends upon the pressure difference between the combustion chamber pressure and the supply pressure (assumed to be atmospheric). The tailpipe flow is modelled as a plug flow, i.e., of constant density and solely driven by the pressure difference over the tailpipe. The heat release by combustion is assumed to be equal to the heat of combustion of the reactants mixture entering the combustion chamber. No energy losses, e.g., by viscous effects or heat transfer, are modelled. The gases are assumed to be perfect. The specific heats of the reactants entering the combustion chamber, of the gases inside it, and of the products leaving it to the tailpipe, are assumed to be constant and all equal. Apparently, some kind of average value is used. This is also assumed for the gas constants of the reactants, the products, and the mixture inside the combustion chamber.

From the mathematical model, Kilicarslan derived a frequency of operation for the pulse combustor. In the article, the theoretical frequency of operation is compared to experimental results with a tunable pulse combustor. In the experiments, the tailpipe length, tailpipe diameter, combustion chamber volume and supply pressure were varied.

Below, the derivation of the mathematical model of Kilicarslan is given,
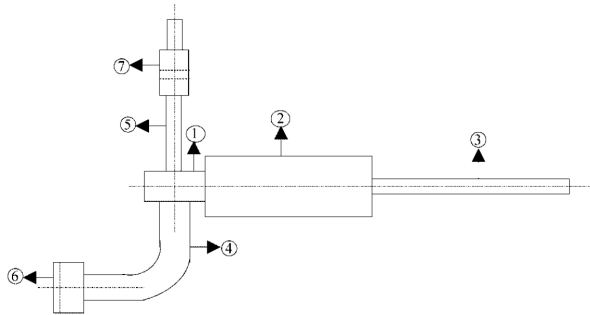
Figure 3.1: A schematic of the modelled gas-fired pulse combustor. (1) Mixer head, (2) combustion chamber, (3) tailpipe, (4) air supply, (5) gas supply, (6,7) flapper valves. The figure is taken from the article by Kilicarslan [17].

largely following Kilicarslan's presentation in [17]. The nomenclature is changed to ease the comparison with the other models examined in this report. As will be seen, the model for the heat release implies a timing of heat release such that the oscillatory motions necessary for pulse combustion operation are damped. Therefore, this model is not a proper description of a working pulse combustor. In the derivation of the theoretical frequency, Kilicarslan assumed that the damping that results from the (incorrect) modelling of the heat release is negligible. The fact that the Rayleigh criterion is not satisfied, which is an indication that the model does not correctly describe a pulse combustion process, manifests itself in the (neglected) damping term. This may be the reason why the incorrect modelling of the heat release has gone unnoticed.

3.1   Nomenclature

Roman symbols

A–C	Auxiliary constants, see (3.18)–(3.20)	
A_{tp}	Area of tailpipe cross-section	$[\,\mathrm{m}^2\,]$
A_v	Effective flow area air/gas valve	$[\,\mathrm{m}^2\,]$
C_D	Discharge coefficient of valve	$[\,-\,]$
c_p	Specific heat for constant pressure	$[\,\mathrm{J/kg\,K}\,]$
c_v	Specific heat for constant volume	$[\,\mathrm{J/kg\,K}\,]$
e	Specific internal energy	$[\,\mathrm{J/kg}\,]$
E	Total energy	$[\,\mathrm{J}\,]$
f	Frequency	$[\,\mathrm{Hz}\,]$
F	Auxiliary function, see (3.21)	
h	Specific enthalpy	$[\,\mathrm{J/kg}\,]$
k_g	Gas valve parameter	$[\,\mathrm{kg}^{1/2}\,\mathrm{m}^{1/2}\,]$
L_{tp}	Tailpipe length	$[\,\mathrm{m}\,]$
$\dot{m}$	Mass flux	$[\,\mathrm{kg/s}\,]$

Continued on next page

Roman symbols, continued

p	Gauge pressure (in combustion chamber)	$[\,\text{Pa}\,]$
P	Pressure (in combustion chamber)	$[\,\text{Pa}\,]$
$\dot{Q}$	Rate of heat release	$[\,\text{J/s}\,]$
r	Air-fuel mass ratio	$[\,-\,]$
R	Specific gas constant	$[\,\text{J/kg\,K}\,]$
t	Time	$[\,\text{s}\,]$
T	Temperature	$[\,\text{K}\,]$
V	Volume	$[\,\text{m}^3\,]$

Greek symbols

ΔH_f	Heat of combustion per unit fuel mass	$[\,\text{J/kg}\,]$
γ	Ratio of specific heats, $= c_p/c_v$	$[\,-\,]$
ω_0	Angular frequency	$[\,\text{rad/s}\,]$
ρ	Density	$[\,\text{kg/m}^3\,]$

Subscripts

0	initial/standard/ambient value
a	air (oxidizer)
cc	combustion chamber
e	exit combustion chamber/entrance tailpipe
g	gas (fuel)
p	products (burnt reactants)
r	reactants (fuel and oxidizer)
tp	tailpipe

3.2 Derivation of model equations

The combustion chamber is chosen as a control volume. See Figure 3.2 for a schematic of the control volume and sign conventions. Reactants entering the combustion chamber consist of premixed air and gas with a constant air-fuel ratio r (on mass basis). All reactants are assumed to be converted to products by combustion. The products leave the combustion chamber through the tailpipe.

The gases are assumed to be perfect, i.e., (i) they obey the ideal gas law:

$$P = \rho RT, \tag{3.1}$$

where P is the pressure, ρ the density, R the specific gas constant and T the temperature of the gas, and (ii) the ratio of specific heats, γ, is constant:

$$\gamma = \frac{c_p}{c_v} = \text{constant}, \tag{3.2}$$

where c_p and c_v are the specific heat for constant pressure and volume, respectively. Since the molecular weight is constant the specific gas constant does not vary in absence of chemical reaction. In that case the specific heats are both constant and the specific internal energy and specific enthalpy can be written as

$$e = c_v T, \tag{3.3}$$
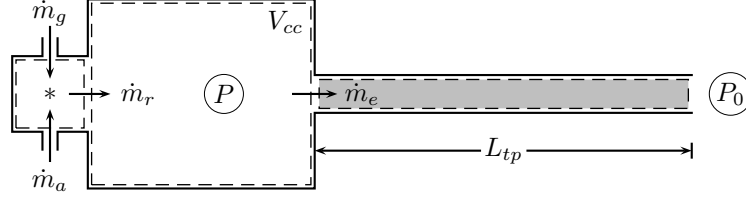
Figure 3.2: Control volume (i.e., the combustion chamber, with volume V_{cc}) of the modelled pulse combustor, with sign conventions and (some) model parameters. The values of the mass fluxes $\dot{m}_g$, $\dot{m}_a$, $\dot{m}_r$ and $\dot{m}_e$ are taken positive in the directions indicated. Mixing of gas and air takes place in the mixer head ($*$) and the reactants entering the combustion chamber are assumed to be perfectly mixed.

and

$$h = c_p T, \tag{3.4}$$

respectively. Kilicarslan assumes that the ratios of the specific heats for constant volume to the specific gas constants are equal for reactants and products, thus

$$\left(\frac{c_v}{R}\right)_r = \left(\frac{c_v}{R}\right)_p = \frac{c_v}{R} = \frac{1}{\gamma - 1} = \text{constant}. \tag{3.5}$$

The reactants occupy a volume V_r of the combustion chamber and the products occupy a volume V_p. The combustion chamber is assumed to be fully occupied at all times, thus, with V_{cc} denoting the volume of the combustion chamber:

$$V_r + V_p = V_{cc}. \tag{3.6}$$

The state variables of the reactants and products are assumed to be uniform throughout their volumes and the pressures of the reactants, P_r, and products, P_p, associated with the volumes V_r and V_p, respectively, are assumed to be equal at all times:

$$\rho_r R_r T_r = P_r = P = P_p = \rho_p R_p T_p. \tag{3.7}$$

3.2.1   Conservation of energy

An energy balance over the control volume (i.e., the combustion chamber) yields

$$\frac{dE_{cc}}{dt} = \dot{Q} + h_r \dot{m}_r - h_e \dot{m}_e, \tag{3.8}$$

where E_{cc} is the total energy in the combustion chamber, $\dot{Q}$ is the rate of heat release by combustion, $\dot{m}_r$ and $\dot{m}_e$ are the mass fluxes into and out of the combustion chamber, respectively, and h_r and h_e are the specific (sensible) enthalpies[1] of the reactants and products, respectively. Under the assumptions

---

[1] A standardized (or, absolute) enthalpy (per unit mass) $h(T)$ at a temperature T can be written as $h(T) = h_f^\circ(T_{\text{ref}}) + \Delta h_s(T)$, where $h_f^\circ(T_{\text{ref}})$ is the enthalpy of formation of the substance (associated with the chemical bonds) at a certain reference temperature T_{ref} and $\Delta h_s(T)$ is the sensible enthalpy change, i.e., the difference in enthalpy when going from the

mentioned above the total energy in the combustion chamber can be written as

$$E_{cc} = \rho_r e_r V_r + \rho_p e_p V_p = \frac{c_v}{R}(P_r V_r + P_p V_p) = \frac{PV_{cc}}{\gamma - 1}. \tag{3.9}$$

The rate of heat release $\dot{Q}$ in the combustion chamber is given by

$$\dot{Q} = \dot{m}_r \frac{\Delta H_f}{1 + r} = \dot{m}_r(h_e - h_r), \tag{3.10}$$

where ΔH_f is the heat of combustion per unit mass of fuel.

3.2.2   Mass flow rate into combustion chamber

The mass flow rate for the reactants (gas and air separately) are modelled by quasi-steady orifice flow equations, assuming the flapper valves to be either fully open or fully closed. In order to keep the air-fuel ratio, r, constant the pressure at the gas-supply is assumed to be equal to the atmospheric pressure, P_0, at which the air is supplied. This yields for the time-dependent mass flow rate of gas, $\dot{m}_g$,

$$\dot{m}_g(t) = k_g \sqrt{|p|}\, \mathbf{1}_{(-\infty,0)}(p), \tag{3.11}$$

where k_g is a constant parameter corresponding to the flow through the gas valve, p is the gauge pressure of the combustion chamber, i.e., $p = P - P_0$, and $\mathbf{1}_X(x)$ is an indicator function equal to one if x is an element of the set $X \subset \mathbf{R}$ and zero otherwise. Thus, there is only inflow if the pressure in the combustion chamber is below the atmospheric pressure. Since $\sqrt{|p|} = \sqrt{-p}$ for $p < 0$, expression (3.11) could equivalently be written with $-p$ instead of the absolute value $|p|$. The form given in (3.11) is preferred in order to avoid confusion about the meaning of $\sqrt{-p}$ for $p > 0$. The constant k_g is given by

$$k_g = \sqrt{2\rho_g}C_{D,g}A_{v,g}, \tag{3.12}$$

where ρ_g is the density of the gas, $C_{D,g}$ is a discharge coefficient of the gas valve and $A_{v,g}$ is the effective flow area of the gas valve (see Ahrens et al. [2]).

For the mass flow rate of air, $\dot{m}_a$, a similar expression can be written with corresponding parameters ρ_a, $C_{D,g}$ and $A_{v,a}$. Using the air-fuel ratio, r, the mass flow rate of the reactants can be expressed as $\dot{m}_r = \dot{m}_g(1 + r)$, thus

$$\dot{m}_r(t) = k_g(1 + r)\sqrt{|p|}\, \mathbf{1}_{(-\infty,0)}(p). \tag{3.13}$$

Note that for $p < 0$ the air-fuel ratio is given by $r = \dot{m}_a/\dot{m}_g$, yielding

$$r = \sqrt{\frac{\rho_a}{\rho_g}}\frac{C_{D,a}A_{v,a}}{C_{D,g}A_{v,g}}. \tag{3.14}$$

---

reference temperature T_{ref} to the temperature T: $\Delta h_s = \int_{T_{\mathrm{ref}}}^{T} dh$. The heat of combustion (Δh_f) at a certain reference state is defined as the difference of the standardized enthalpies of the reactants (h_{reac}) and the products (h_{prod}) at that reference state and, thus, is equal to the difference in enthalpies of formations at that reference state: $\Delta h_f(T_{\mathrm{ref}}) = h_{\mathrm{reac}}(T_{\mathrm{ref}}) - h_{\mathrm{prod}}(T_{\mathrm{ref}}) = h_{f,\mathrm{reac}}^{\mathrm{o}}(T_{\mathrm{ref}}) - h_{f,\mathrm{prod}}^{\mathrm{o}}(T_{\mathrm{ref}})$. In the derivation of the model equations, the enthalpies of formation are contained in the heat release term, so the enthalpies h_r and h_e in the derivation are sensible enthalpies, or sensible enthalpy changes. See, for example, [32, p.24–31] for details.

3.2.3 Coupling to tailpipe dynamics by conservation of momentum

The flow in the tailpipe is assumed to behave like a plug flow: it is considered to be of constant density and moving frictionlessly under the influence of the pressure difference between tailpipe inlet and exit. Conservation of momentum in the tailpipe gives the following differential equation for the mass flow rate $\dot{m}_e$ into the tailpipe:

$$L_{tp}\frac{d\dot{m}_e}{dt} = pA_{tp}, \tag{3.15}$$

where L_{tp} is the tailpipe length and A_{tp} the area of its cross-section.

3.2.4 Complete set of model equations

Substitution of the total energy (3.9), the rate of heat release (3.10) and the mass flow rate of reactants (3.13) into the energy balance equation (3.8) together with equation (3.15) for conservation of momentum lead to the following system of first-order nonlinear differential equations

$$\frac{dp}{dt} = AF(p) - B\,\dot{m}_e, \tag{3.16}$$

$$\frac{d\dot{m}_e}{dt} = C\,p, \tag{3.17}$$

where

$$A = k_g(1+r)\frac{(\gamma-1)h_e}{V_{cc}}, \tag{3.18}$$

$$B = \frac{(\gamma-1)h_e}{V_{cc}}, \tag{3.19}$$

$$C = \frac{A_{tp}}{L_{tp}}, \tag{3.20}$$

$$F(p) = \sqrt{|p|}\,\mathbf{1}_{(-\infty,0)}(p), \tag{3.21}$$

with (see expression (3.10))

$$h_e = \left(h_r + \frac{\Delta H_f}{1+r}\right). \tag{3.22}$$

By differentiating equation (3.16) and substitution of equation (3.17) a single second-order nonlinear differential equation is derived. Note that the function $F(p)$ is not differentiable in $p = 0$. Thus, its derivative $F'(p)$ is not properly defined in that point; it will be defined as $F'(0) \equiv 0$, i.e., equal to the right-hand derivative of F in $p = 0$. This yields the model equation of Kilicarslan for the gauge pressure p in the combustion chamber:

$$\frac{d^2p}{dt^2} - AF'(p)\frac{dp}{dt} + BCp = 0, \tag{3.23}$$

where

$$F'(p) = \frac{dF}{dp} = -\frac{1}{2\sqrt{|p|}}\,\mathbf{1}_{(-\infty,0)}(p). \tag{3.24}$$

The mathematical model is completed by supplying appropriate initial conditions, e.g., prescribing the initial gauge pressure, $p(0) = p_0$, and initial mass flux out of the combustion chamber, $\dot{m}_e(0) = \dot{m}_{e,0}$.

3.3   Prediction of frequency of pulse combustion

Kilicarslan uses equation (3.23) to estimate the frequency of a stable pulse combustion process. Without giving much justification it is implicitly assumed that the damping term $-AF'(p)\frac{dp}{dt}$ of equation (3.23) is of negligible effect on the frequency of the pulse combustion process. In that case the approximated frequency of the simulated combustion process, f_0, is given by

$$f_0 = \frac{\omega_0}{2\pi} = \frac{1}{2\pi}\sqrt{BC} = \frac{\sqrt{(\gamma-1)h_e}}{2\pi}\sqrt{\frac{A_{tp}}{V_{cc}L_{tp}}}, \qquad (3.25)$$

where ω_0 is the angular frequency associated with the harmonic oscillator described by ignoring the damping term $-AF'(p)\frac{dp}{dt}$ in equation (3.23). Note that this is simply the frequency of a Helmholtz resonator without resistance in the case that the speed of sound is given by that in the tailpipe: $\sqrt{\gamma R T_e} = \sqrt{(\gamma-1)c_p T_e} = \sqrt{(\gamma-1)h_e}$, where T_e is the temperature in the tailpipe, i.e., at the exit of the combustion chamber. (See Thompson [30, pp. 549–550] for a derivation of the resonant frequency of a Helmholtz resonator.)

3.4   Comments on the mathematical model

3.4.1   Damping effects

The model equation (3.23) can be written as

$$\ddot{x} + h(x, \dot{x}) + \omega_0^2 x = 0, \qquad (3.26)$$

where $x = p(t)$, ω_0 is given by expression (3.25), a dot denotes a time derivative and $h(x, \dot{x})$ is defined by

$$h(x, \dot{x}) = -AF'(x)\dot{x}, \qquad (3.27)$$

with $F'(x)$ given by (3.24). The equation can be interpreted as describing a linear oscillator with nonlinear damping. Following the analysis of Jordan and Smith [13, pp. 16–17], we can write the total mechanical energy $\mathcal{E}$ of the oscillator as

$$\mathcal{E} = \mathcal{T} + \mathcal{V} = \frac{1}{2}\dot{x}^2 + \frac{1}{2}\omega_0^2 x^2, \qquad (3.28)$$

where $\mathcal{T} = \frac{1}{2}\dot{x}^2$ and $\mathcal{V} = \frac{1}{2}\omega_0^2 x^2$ are the kinetic energy and a potential energy, respectively. Along a phase path $(x(t), \dot{x}(t))$ the energy variation with time is given by

$$\frac{d\mathcal{E}}{dt} = \frac{d\mathcal{T}}{dt} + \frac{d\mathcal{V}}{dt} = \dot{x}\ddot{x} + \omega_0^2 x\dot{x} = -h(x, \dot{x})\dot{x}. \qquad (3.29)$$

Integration of this expression with respect to time from t_0 to t_1 gives

$$\mathcal{E}(t_1) - \mathcal{E}(t_0) = -\int_{t_0}^{t_1} h(x, \dot{x})\dot{x}\,dt. \qquad (3.30)$$

Because $h(x, \dot{x})\dot{x} = -AF'(x)\dot{x}^2 \geq 0$ for all times (and strictly so if $x < 0$) the energy will be decreasing as time passes. The amplitudes of oscillation in x, i.e., in the gauge pressure p in the combustion chamber, will be diminishing in time and never increasing. Thus, the mathematical model presented by Kilicarslan cannot describe a stable operating pulse combustor.

3.4.2   Using Rayleigh's criterion to explain damping effect

Above it was found that the amount of damping (in the sense of energy loss per unit of time) is related to $-AF'(p)(\frac{dp}{dt})^2 \geq 0$, which is proportional to the parameter A. This parameter is given by expressions (3.18) and (3.22) and it comes from mass flow of reactants into the combustion chamber (part of the sum in A proportional to h_r, see (3.22)) and from heat release in the combustion chamber (part of A proportional to ΔH_f, see (3.22)). On noting that the mass flow rate into the combustion chamber occurs when the gauge pressure is negative and the rate of heat release is modelled to be proportional to the mass flow rate an explanation for the damping is given by application of the Rayleigh's criterion. At the moment of greatest *rarefaction* both mass and heat are added to the combustion chamber, both with the effect of diminishing the pressure amplitude. In pulse combustors the heat release should be greatest at moments of greatest *condensation* thereby amplifying the oscillatory motion.

Clearly the heat release is modelled incorrectly in the work of Kilicarslan. His mathematical model for pulse combustion is largely based on that of Ahrens et al. [2]. The main difference is in the modelling of the heat release. That is why in the next chapter the model of Ahrens et al. will be examined.

3.5   Numerical implementation and experiments

The system of model equations (3.16)–(3.22) is numerically implemented using MATLAB [29] software. The standard MATLAB ODE-solver ode45[2] is used to solve the equations. The implementation in MATLAB is straightforward; the codes can be found in Appendix A.

In order to solve the model equations numerically, the model parameters need to be specified, as well as the initial conditions. For the purpose of showing the damping of the pressure fluctuations in the mathematical model, one or two sets of parameters will suffice. In the experiments of Kilicarslan, the gas supply pressure and geometrical properties of the combustor (the volume of the combustion chamber, and the tailpipe length and diameter) were varied. For the numerical evaluation of the model equations, the gas supply pressure will be chosen equal to the air supply pressure of 1 atm. The other parameters that were varied in the experiments are listed in Table 3.1, along with ranges over which they were varied and the values that were selected for the numerical evaluation of the model equations. These parameters are chosen such that they lie somewhere in the middle of the intervals over which they were varied.

Except for the gas and air supply pressure (the latter equal to 1 atm), none of the other model parameters were specified by Kilicarslan. Nor is the kind of gas mentioned that was used in the experiments. Therefore, for the numerical evaluation of the model equations, the model parameters are assigned rather arbitrary, although reasonable, values. In order to obtain reasonable values, the article of Ahrens, et al. [2] (upon which a large part of Kilicarslan's analysis is based) was consulted. The heat of combustion of the fuel used for the numerical

---

[2]The MATLAB function ode45 is part of a suite of ODE-solvers. It is an implementation of a one-step method with adaptive step-size control that uses two explicit Runge-Kutta methods, based on the Dormand-Prince (4,5) pair. That is, it uses fifth and fourth order Runge-Kutta formulae to obtain an estimate for the local error in order to determine the step-size. See [28] for a comprehensive description of the MATLAB ODE suite.

Parameter	Range in experiments	Value used	Unit
D_{tp}	$0.038 - 0.051$	0.042	m
L_{tp}	$1 - 3$	2	m
V_{cc}	1.739800×10^{-3} 2.609705×10^{-3} 3.479607×10^{-3}	2.609705×10^{-3}	m^3

Table 3.1: Model parameters connected to the shape of the pulse combustor, the ranges over which the values of these parameters are varied in the experiments of Kilicarslan, and the values used in the numerical evaluation of Kilicarslan's model equations.

evaluation is that of methane (CH_4). The reference temperature and pressure for the heat of combustion are 298.15 K and 1 atm, respectively. The lower heating value (LHV) is used, since part of the heat released is used to evaporate formed water from the reference temperature to the temperature of the products. The discharge coefficients of the valves are chosen the same as in the article of Ahrens et al., who, lacking information for a correct value, chose rather arbitrarily the value 0.6. Air property values (at 300 K and 1 atm) are used for the gas constant and the heat capacity at constant pressure. The value used for the effective flow area of the gas valve is based on that of a pulse combustor of comparable dimensions mentioned in the article of Ahrens et al., and is about 1/100 of the value used for the area of the tailpipe cross-section. Thus, the gas valve diameter is in the order of a tenth of the diameter of the tailpipe. It is assumed that the dimensions of the air valve are such that the air-fuel ratio, r, is constant at the stoichiometric value. This ratio is easily calculated by using the common approximation of air as consisting of 21% oxygen (O_2) and 79% nitrogen (N_2) (by volume), i.e., for each mole of O_2 there is $\frac{79}{21} \approx 3.76$ moles of N_2 in air. Then, using the chemical balance

$$CH_4 + 2\,(O_2 + 3.76\,N_2) \quad \longrightarrow \quad CO_2 + 2\,H_2O\ (g) + 7.52\,N_2, \qquad (3.31)$$
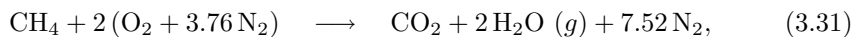
the air-fuel ratio (on mass basis) is given by

$$r = \frac{2\,(MW_{O_2} + 3.76 \times MW_{N_2})}{MW_{CH_4}} = \frac{2\,(31.999 + 3.76 \times 28.013)}{16.043} \approx 17.12, \quad (3.32)$$

where MW_X denotes the molecular weight of a substance X. The values of the molecular weights are obtained from [27, Table 2, p.343].

Some auxiliary constants are needed to compute the model parameters. All values used in the numerical evaluation of the model equations are listed in Table 3.2 (in addition to Table 3.1).

The initial conditions are chosen as indicated in Table 3.3. That is, the initial gauge pressure is equal to the atmospheric pressure (thus, the initial pressure in the combustion chamber is twice the atmospheric pressure) and the initial mass flux into the tailpipe is zero, making the initial pressure a (local) maximum.

The pressure development in the combustion chamber over time predicted by the model equations is shown in Figure 3.3. The figure shows such strong damping that not even one cycle is completed. In order to get some kind of oscillations into the system, the model parameters are adjusted. Oscillation can

Parameter	Value used	Unit	Comment
A_{tp}	$= \pi D_{tp}^2/4$	m^2	
$A_{v,g}$	6.26×10^{-5}	m^2	Ahrens, et al.
$C_{D,g}$	0.6	$-$	Ahrens, et al.
c_p	1009.7	$\mathrm{J/kg\,K}$	air prop., [27, p.346]
h_e	$= h_r + \frac{\Delta H_f}{1+r}$	$\mathrm{J/kg}$	
h_r	$= c_p T_0$	$\mathrm{J/kg}$	
k_g	$= \sqrt{2\rho_g C_{D,g} A_{v,g}}$	$\mathrm{kg}^{1/2}\,\mathrm{m}^{1/2}$	
MW_g	16.043	$\mathrm{kg/kmol}$	mol. weight, [27, p.343]
P_0	1.01325×10^5	Pa	$= 1\,\mathrm{atm}$
r	17.12	$-$	stoich. ratio, computed
R_a	287	$\mathrm{J/kg\,K}$	air prop., [27, p.343]
R_g	$= R_u/\mathrm{MW}_g$	$\mathrm{J/kg\,K}$	
R_u	8.31441×10^3	$\mathrm{J/kmol\,K}$	univ. gas const., [27, in back]
T_0	300	K	
ΔH_f	50.016×10^6	$\mathrm{J/kg}$	LHV, [32, p.543]

Table 3.2: Model parameters (and auxiliary values to compute model parameters) used for the numerical evaluation of Kilicarslan's model equations. Parameters are taken from work of Ahrens et al. [2], computed, or looked up in tables in [27] or [32].

Initial condition	Value used	Unit
$p(0)$	1.01325×10^5	Pa
$\dot{m}_e(0)$	0	kg/s

Table 3.3: Initial conditions used for the numerical evaluation of Kilicarslan's model equations.
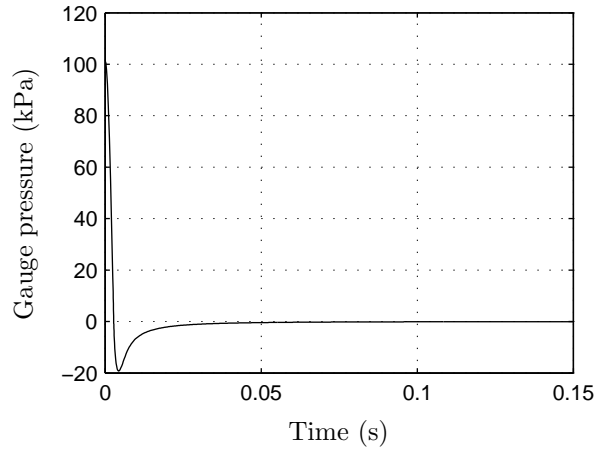
Figure 3.3: Development of the pressure in the combustion chamber over time, as predicted by the model equations of Kilicarslan. The model parameters were given 'reasonable' values; very strong damping results.
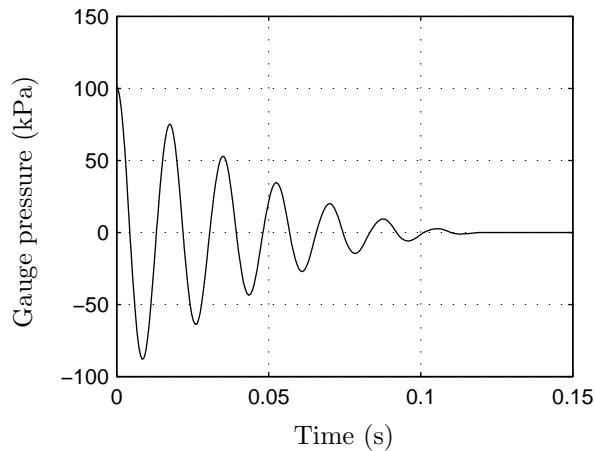
Figure 3.4: Development of the pressure in the combustion chamber over time, as predicted by the model equations of Kilicarslan. Model parameters were changed significantly in order to achieve oscillations. Still, very strong damping remains.

be achieved by decreasing the damping, for example by decreasing the effective flow area of the gas valve, $A_{v,g}$: that decreases k_g, see (3.12), which decreases the constant A, see (3.18), decreasing the damping term in (3.22). If the effective flow area of the air valve is decreased by the same factor, the air-fuel ratio will be unchanged (see (3.14)). An increase of the frequency can be achieved by, for example, increasing the volume of the combustion chamber, or decreasing the tailpipe length, as is suggested by the formula for the frequency of operation (see (3.25)). Only with the use of very different values can some oscillations in the system be achieved. Figure 3.4 shows the results after halving the effective flow area of the gas valve, and taking ten times the combustion chamber volume and a quarter of the tailpipe length used above. Still, the damping is very strong.

It is clear that the model equations cannot correctly describe a stable operating pulse combustor.

3.6 Conclusions

Kilicarslan [17] has suggested a lumped parameter model for a gas-fired Helmholtz pulse combustor with flapper valves. In his paper, an energy balance analysis of the combustion chamber, with simple steady-flow orifice equations describing the reactants inflow and a certain heat release model for the combustion, is linked to a plug flow description of the products in the tailpipe. It leads to a second order differential equation for the pressure in the combustion chamber. Neglecting the damping term, an approximation for the operating frequency of the pulse combustor is arrived at.

In this chapter, the model mentioned above has been examined analytically and numerically. The derivation of the model equations has been given, largely following Kilicarslan's presentation. The heat release model of Kilicarslan comes

down to releasing an amount of heat equal to the heat of combustion of the reactants entering the combustion chamber, at the moment of entrance. This can be viewed as burning the entering reactants upon entrance into the combustion chamber. By Rayleigh's criterion, this timing of heat release would dampen oscillations in the system, rather than amplify them. A simple analysis of the model equations shows that pressure fluctuations in the combustion chamber are indeed damped, according to the mathematical model. A numerical investigation of the model equations shows that the damping predicted by the mathematical model is very strong for 'reasonable' choices of the model parameters. It can be concluded that the mathematical model suggested by Kilicarslan cannot describe a stable operating pulse combustor.

The predicted value of the frequency is obtained by neglecting the damping term in the mathematical model, assuming that the damping effect is of negligible effect upon the operating frequency. In the article by Kilicarslan no investigation into the mathematical model is made, except for the predicted frequency, which may explain why the failure of the model to describe a stable pulse combustor has gone unnoticed.

The model may be corrected by modelling the heat release in a different way, allowing for reactants to build up in the combustion chamber and igniting them at a more convenient moment, satisfying Rayleigh's criterion. Since Kilicarslan's model is very similar to the lumped model presented by Ahrens et al. [2], in fact only differing in the way the heat release is modelled, the latter model is worth investigating.

Chapter 4

A model suggested by Ahrens, et al

The mathematical model of Kilicarslan presented in the previous chapter is largely based on that of Ahrens et al. [2], which will be investigated in this chapter. The only real difference is in the modelling of the heat release by combustion. Ahrens et al. assume the reaction zone to be separated in a cool zone occupied by the reactants and a hot zone occupied by the combustion products. Combustion is assumed to take place in a thin flame sheet separating the two zones. The heat release is modelled by the movement of an equivalent plane flame sheet spanning the combustion chamber cross-section, moving at a pressure-independent 'flame speed'. In this way, if the density of the reactants in the combustion chamber increases, more reactants mass is burnt and more heat is released. At constant temperature of the reactants, an increase in density means an increase in pressure. Thus, with this heat release model, more heat is released at moments of increased pressure, thereby satisfying Rayleigh's criterion.

The assumptions lead to a second-order differential equation, similar to the one given by Kilicarslan, but with a different damping term. According to the mathematical model of Ahrens et al., the heat release indeed amplifies the pressure oscillations. Also, in accordance with Rayleigh's criterion, the entrance of reactants at moments of low pressure attenuates the pressure oscillations. Ahrens et al. assume that stable operation of a pulse combustor can be described by choosing the model parameters (e.g., the constant flame speed), such that these two counteracting effects are in balance. As in the approach of Kilicarslan, the frequency of operation is estimated by neglecting the damping term.

In this chapter, the mathematical model suggested by Ahrens et al. will be investigated, largely following the presentation given in their article. The nomenclature is adjusted in order to ease the comparison of the three models described in this report. In the end, it will be shown that the assumption that stable operation of a pulse combustor can be described by balancing the two counteracting damping effects, is questionable.

4.1   Nomenclature

Roman symbols

A_b	Area of combustion chamber cross-section	$[\,\mathrm{m}^2\,]$
A_{tp}	Area of tailpipe cross-section	$[\,\mathrm{m}^2\,]$
A_v	Effective flow area air/gas valve	$[\,\mathrm{m}^2\,]$
C_D	Discharge coefficient	$[-]$
c_p	Specific heat for constant pressure	$[\,\mathrm{J/kg\,K}\,]$
c_v	Specific heat for constant volume	$[\,\mathrm{J/kg\,K}\,]$
e	Specific internal energy	$[\,\mathrm{J/kg}\,]$
E	Total energy	$[\,\mathrm{J}\,]$
f	Frequency	$[\,\mathrm{Hz}\,]$
h	Specific enthalpy	$[\,\mathrm{J/kg}\,]$
k_g	Gas valve parameter	$[\,\mathrm{kg}^{1/2}\,\mathrm{m}^{1/2}\,]$
L_{tp}	Tailpipe length	$[\,\mathrm{m}\,]$
$\dot{m}$	Mass flux	$[\,\mathrm{kg/s}\,]$
p	Gauge pressure (in combustion chamber)	$[\,\mathrm{Pa}\,]$
P	Pressure (in combustion chamber)	$[\,\mathrm{Pa}\,]$
$\dot{Q}$	Rate of heat release	$[\,\mathrm{J/s}\,]$
r	Air-fuel mass ratio	$[-]$
R	Specific gas constant	$[\,\mathrm{J/kg\,K}\,]$
t	Time	$[\,\mathrm{s}\,]$
T	Temperature	$[\,\mathrm{K}\,]$
U_f	Model parameter related to flame speed	$[\,\mathrm{m/s}\,]$
V	Volume	$[\,\mathrm{m}^3\,]$

Greek symbols

ΔH_f	Heat of combustion per unit mass fuel	$[\,\mathrm{J/kg}\,]$
γ	Ratio of specific heats, $= c_p/c_v$	$[-]$
ω_0	Angular frequency	$[\,\mathrm{rad/s}\,]$
ρ	Density	$[\,\mathrm{kg/m}^3\,]$

Subscripts

0	initial/standard/ambient value
a	air (oxidizer)
b	concerning burning of reactants
cc	combustion chamber
e	exit combustion chamber/entrance tailpipe
g	gas (fuel)
p	products (burnt reactants)
r	reactants (fuel and oxidizer)
tp	tailpipe

4.2   Derivation of model equations

Since Kilicarslan based his mathematical model of a pulse combustor largely on the work by Ahrens et al., the derivations of the model equations are nearly equivalent. The derivation of the model equations of Ahrens et al. will not be
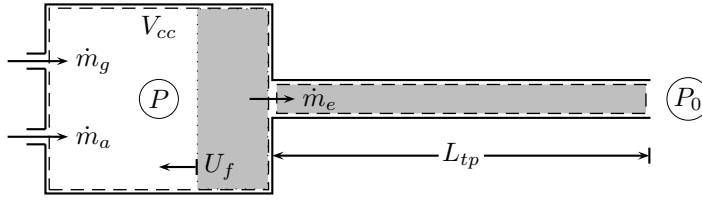
Figure 4.1: Control volume (i.e., the combustion chamber, with volume V_{cc}) of the modelled pulse combustor, with sign conventions and (some) model parameters. The values of the mass fluxes $\dot{m}_g$, $\dot{m}_a$ and $\dot{m}_e$ and the 'flame speed' U_f are taken positive in the directions indicated.

described here in great detail. Rather, only deviations from the derivation of Kilicarslan's model given in the previous chapter, will be highlighted.

Ahrens et al. assume that the burning process inside the combustion chamber takes place in a thin zone (a moving flame front) separating a cold zone containing the reactants, perfectly mixed, from a hot zone containing the combustion products. The state variables are assumed to be uniform in both the zones. The volumes of the two zones add up to the volume of the combustion chamber. Apart from the modelling of the heat release this more clearly defined picture of the combustion process seems to be the only difference with Kilicarslan's presentation. Figure 4.1 shows a schematic of the pulse combustor, with model parameters and sign conventions.

4.2.1 Conservation of energy

The assumptions described in Chapter 3 for the derivation of Kilicarslan's model equations of the gases behaving as perfect gases, of the ratio of specific heats being constant and of the ratio of specific heats for the reactants and products being equal, are also applied here. Taking the combustion chamber as a control volume together with the assumptions on the uniform properties in the two zones lead to the same energy balance equation as (3.8):

$$\frac{dE_{cc}}{dt} = \dot{Q} + h_r \dot{m}_r - h_e \dot{m}_e, \tag{4.1}$$

where E_{cc} is the total energy in the combustion chamber, $\dot{Q}$ is the rate of heat release by combustion, $\dot{m}_r$ and $\dot{m}_e$ are the mass fluxes into and out of the combustion chamber, respectively, and h_r and h_e are the specific (sensible) enthalpies[1] of the reactants and products, respectively. As before (see expression (3.9)), the total energy in the combustion chamber can be written as:

$$E_{cc} = \frac{PV_{cc}}{\gamma - 1}, \tag{4.2}$$

where $\gamma = c_p/c_v$ is the ratio of specific heat for constant pressure, c_p, and for constant volume, c_v, P is the pressure and V_{cc} is the volume of the combustion

---

[1]See footnote on page 14

chamber. The rate of heat release $\dot{Q}$ in the combustion chamber is given by

$$\dot{Q} = \dot{m}_b \frac{\Delta H_f}{1+r} = \dot{m}_b (h_e - h_r), \tag{4.3}$$

where $\dot{m}_b$ is the mass burning rate of the reactant mixture (to be specified later), ΔH_f is the heat of combustion per unit mass of fuel, r is the air-fuel ratio on mass basis and h_e and h_r are the enthalpies leaving the combustion chamber to the tailpipe and entering the combustion chamber, respectively. Note that Kilicarslan assumed the mass burning rate to be equal to the mass rate of reactants entering the combustion chamber, i.e., $\dot{m}_b = \dot{m}_r$, and thus assumed burning the exact amount of mass entering the chamber at the exact moment of entrance. In Chapter 3 it was shown that then the burning occurs at an inconvenient moment of rarefaction of the gases in the combustion chamber.

4.2.2   Rate of heat release

The heat release is modelled by specifying the burning rate of the reactant mixture. The mass burning rate caused by the flame separating the zones of unburnt (reactants) and burnt gases (products) is assumed to be equivalent to that of a plane flame sheet across a cross-section of the combustion chamber, moving at a certain pressure-independent 'flame speed' U_f relative to the unburnt gases. Denoting the area of the cross-section of the combustion chamber by A_b the mass burning rate is given by

$$\dot{m}_b = \rho_r A_b U_f, \tag{4.4}$$

where ρ_r is the density of the reactants. With T_0 denoting the constant temperature of the reactants and using the perfect gas law there follows

$$\dot{m}_b = \frac{P}{RT_0} A_b U_f = \frac{P_0 + p}{RT_0} A_b U_f, \tag{4.5}$$

where $p = P - P_0$ is the combustion chamber gauge pressure with P_0 the atmospheric pressure and R is the specific gas constant of the reactants. Note that the mass burning rate, and thus the rate of heat release, is directly proportional to the pressure in the combustion chamber. So for this model of the heat release Rayleigh's criterion for amplification of the pressure amplitude is fulfilled at all times.

In their article, Ahrens et al. stress that U_f is not to be regarded as a flame velocity (i.e., the velocity at which the flame front spreads in the combustion chamber), but rather as a system parameter related to the combustion process that attains has a certain value if the pulse combustor is operating stably. Although not explicitly stated, it is clear from the article that U_f is assumed to be constant throughout the derivation of the model equations.

4.2.3   Mass of reactants in combustion chamber

To be able to use the above given model of reactants burning process at all times, it is assumed that there is a certain amount of reactants in the combustion

chamber present at all times. The rate of change of the total mass of reactants present in the combustion chamber, M_r, is given by

$$\frac{dM_r}{dt} = \dot{m}_r - \dot{m}_b, \tag{4.6}$$

i.e., by the mass flow rate of reactants entering the combustion chamber minus the mass burning rate of the reactants. In the article of Ahrens et al., this requirement is used only for a stably operating pulse combustor, where there should not be any accumulation or depletion of reactants in the combustion chamber over a cycle. Then the requirement on the mass flow and mass burning rates amounts to

$$\int_{\text{cycle}} (\dot{m}_r - \dot{m}_b) dt = 0, \tag{4.7}$$

where the integration is taken over a period of one cycle.

4.2.4 Mass flow rate into combustion chamber

The modelling of the mass flow rate through the valves as done by Ahrens et al. is already treated above in the derivation of the mass flow rates in Kilicarslan's mathematical model. The result for the mass flow rate of reactants into the reaction chamber is, see (3.13):

$$\dot{m}_r(t) = k_g (1 + r) \sqrt{|p|} \, \mathbf{1}_{(-\infty, 0)}(p), \tag{4.8}$$

where k_g is a constant parameter corresponding to the flow through the gas valve and $\mathbf{1}_X(x)$ is an indicator function equal to one if x is an element of the set $X \subset \mathbf{R}$ and zero otherwise. The constant k_g is given by, see (3.12):

$$k_g = \sqrt{2\rho_g} C_{D,g} A_{v,g}, \tag{4.9}$$

where ρ_g is the density of the gas, $C_{D,g}$ is a discharge coefficient of the gas valve and $A_{v,g}$ is the effective flow area of the gas valve. The constant air-fuel ratio is given by, see (3.14):

$$r = \sqrt{\frac{\rho_a}{\rho_g}} \frac{C_{D,a} A_{v,a}}{C_{D,g} A_{v,g}}, \tag{4.10}$$

where ρ_a is the density of the air, $C_{D,a}$ is a discharge coefficient of the air valve and $A_{v,a}$ is the effective flow area of the air valve.

4.2.5 Coupling to tailpipe dynamics by conservation of momentum

Modelling of the tailpipe flow is done as shown above in the derivation of Kilicarslan's model. Thus, see (3.15):

$$L_{tp} \frac{d\dot{m}_e}{dt} = p A_{tp}, \tag{4.11}$$

where L_{tp} is the tailpipe length and A_{tp} the area of its cross-section.

4.2.6   Complete set of model equations

The equations above lead to the following system of first-order nonlinear differential equations

$$\frac{dp}{dt} = AF(p) + B(p + P_0) - C\,\dot{m}_e \tag{4.12}$$

$$\frac{d\dot{m}_e}{dt} = Dp \tag{4.13}$$

where

$$A = k_g(1+r)\frac{\gamma-1}{V_{cc}}h_r \tag{4.14}$$

$$B = \frac{A_b U_f}{RT_0}\frac{\gamma-1}{V_{cc}}\frac{\Delta H_f}{1+r} \tag{4.15}$$

$$C = \frac{(\gamma-1)h_e}{V_{cc}} \tag{4.16}$$

$$D = \frac{A_{tp}}{L_{tp}} \tag{4.17}$$

$$F(p) = \sqrt{|p|}\,\mathbf{1}_{(-\infty,0)}(p) \tag{4.18}$$

with (see expression (4.3))

$$h_e = \left(h_r + \frac{\Delta H_f}{1+r}\right). \tag{4.19}$$

By differentiating equation (4.12) and substitution of equation (4.13) a single second-order nonlinear differential equation is derived. As before, the function $F(p)$ is not differentiable in $p = 0$ and its derivative $F'(p)$ will defined as $F'(0) \equiv 0$, i.e., equal to the right-hand derivative of F in $p = 0$. This yields a model equation for the gauge pressure p is the combustion chamber equivalent to that of Ahrens et al.:

$$\frac{d^2p}{dt^2} - (AF'(p) + B)\frac{dp}{dt} + CDp = 0, \tag{4.20}$$

where

$$F'(p) = \frac{dF}{dp} = -\frac{1}{2\sqrt{|p|}}\,\mathbf{1}_{(-\infty,0)}(p). \tag{4.21}$$

To the system of first-order differential equations (4.12)–(4.13), or the second-order differential equation (4.20), appropriate initial conditions must be added, for example by prescribing the initial gauge pressure, $p(0) = p_0$, and the initial mass flux out of the combustion chamber, $\dot{m}_e(0) = \dot{m}_{e,0}$.

The requirement that reactants must be present in the combustion chamber at all times, is presented by the inequality $M_r(t) > 0$ for all t. The total mass of the reactants in the combustion chamber, M_r, satisfies the differential equation (see (4.6))

$$\frac{dM_r}{dt} = \dot{m}_r - \dot{m}_b, \tag{4.22}$$

with $\dot{m}_r$ and $\dot{m}_b$ given by (4.8) and (4.5), respectively. This differential equation should be supplemented with an initial condition, for example by specifying the total mass of reactants $M_{r,0}$ present in the combustion chamber at a certain starting point $t = 0$:

$$M_r(0) = M_{r,0}. \tag{4.23}$$

4.3 Prediction of frequency of pulse combustion

In the article by Ahrens et al., it is noted that the differential equation (4.20) is similar to one describing a linear oscillator with nonlinear damping. The equation can be written as

$$\ddot{x} + h(x, \dot{x}) + \omega_0^2 x = 0, \tag{4.24}$$

where $x = p(t)$, a dot denotes a time derivative, the nonlinear damping term $h(x, \dot{x})$ is defined by

$$h(x, \dot{x}) = -(AF'(x) + B)\dot{x}, \tag{4.25}$$

with $F'(x)$ given by (4.21) and ω_0 is defined as

$$\omega_0 = \sqrt{CD} = \sqrt{(\gamma - 1)h_e} \sqrt{\frac{A_{tp}}{V_{cc}L_{tp}}}. \tag{4.26}$$

It is also noted that the contributions to the damping term by heat release $(-B\dot{x})$ and by reactants mass inflow $(-AF'(x)\dot{x})$ are of opposite sign, since $F'(x) \leq 0$ for all x. Thus, they have counteracting effects on the oscillations, the heat release amplifying the oscillations and the mass inflow of reactants attenuating them.

Ahrens et al. note that for an undamped oscillation the frequency, f_0, would be given by

$$f_0 = \frac{\omega_0}{2\pi} = \frac{\sqrt{(\gamma - 1)h_e}}{2\pi} \sqrt{\frac{A_{tp}}{V_{cc}L_{tp}}}. \tag{4.27}$$

They also mention that "in principle the damping term will cause a frequency shift from the undamped value," but that in their results this shift was very small. The frequency f_0 can be used as an estimate for the frequency of oscillations of a stable pulse combustion process. They also mention that f_0 is the frequency of a Helmholtz resonator. (Note that $\sqrt{(\gamma - 1)h_e} = \sqrt{(\gamma - 1)c_p T_e} = \sqrt{\gamma R T_e}$, which is the speed of sound in the tailpipe.)

4.4 Searching for a stable oscillation

Ahrens et al. mention that they have solved the model equations numerically and that they found that for a stable oscillating solution the model parameter U_f and the amplitude of the oscillation $p_{\max}$ must both have a specific value for each set of the other model parameters. They proceed by formulating two stability criteria, which are analyzed under simplifying assumptions. The analysis yields two expressions relating U_f and $p_{\max}$, with which the unique values for these parameters can be estimated.

One of the stability criteria is the requirement that there is no accumulation or depletion of reactants in the combustion chamber over a cycle. The other stability criterion is that the pressure amplitude of the oscillations, and the mean pressure, should be independent of time. Ahrens et al. note that in the present case the mean pressure should be zero, as a consequence of the assumption that there is no friction in the tailpipe.

4.4.1   No accumulation/depletion of reactants

The requirement of no accumulation or depletion of reactants is formulated by equation (4.7), repeated here for convenience:

$$\int_{\text{cycle}} (\dot{m}_r - \dot{m}_b)dt = 0, \tag{4.28}$$

with $\dot{m}_b$ and $\dot{m}_r$ given by expressions (4.5) and (4.8), respectively, also repeated here for convenience:

$$\dot{m}_r(t) = k_g(1+r)\sqrt{|p|}\,\mathbf{1}_{(-\infty,0)}(p), \tag{4.29}$$

$$\dot{m}_b = \frac{P_0 + p}{RT_0}A_b U_f. \tag{4.30}$$

Imposing the simplifying assumption that the pressure variation in time is of the form

$$p(t) = -p_{\max}\cos(\omega_0 t), \tag{4.31}$$

and using the substitution $\tau = \omega_0 t$, Ahrens et al. show that evaluation of the integral in (4.28) leads to

$$2k_g(1+r)\sqrt{p_{\max}}\int_0^{\frac{\pi}{2}}\sqrt{\cos\tau}\,d\tau - 2\pi\frac{P_0}{RT_0}A_b U_f = 0. \tag{4.32}$$

The integral in this equation can be evaluated using complete elliptic integrals K and E, and is given by Ahrens et al. to be

$$I = \int_0^{\frac{\pi}{2}}\sqrt{\cos\tau}\,d\tau = 2\sqrt{2}E\left(\tfrac{1}{2}\sqrt{2}\right) - \sqrt{2}K\left(\tfrac{1}{2}\sqrt{2}\right). \tag{4.33}$$

This gives the relation between $p_{\max}$ and U_f:

$$U_f = \frac{I}{\pi}RT_0\frac{k_g(1+r)}{P_0 A_b}\sqrt{p_{\max}}. \tag{4.34}$$

Ahrens et al. evaluate the integral to give $I/\pi = 0.375$ (thus, $I = 1.1781$), which is different from a MATLAB evaluation based on a quadrature algorithm (using the function `quad`) giving $I = 1.1981$ (thus, $I/\pi = 0.381$). Formula (4.33) is correct and can be derived as follows. Using the relation $\cos\tau = 1 - 2\sin^2(\tau/2)$, the integral I can be written as

$$I = \int_0^{\frac{\pi}{2}}\sqrt{\cos\tau}\,d\tau = 2\int_0^{\frac{\pi}{4}}\sqrt{1 - 2\sin^2\hat{\tau}}\,d\hat{\tau} = 2\,E\left(\frac{\pi}{4}, \sqrt{2}\right), \tag{4.35}$$

where $E(\varphi, k) \equiv \int_0^\varphi \sqrt{1 - k^2\sin^2\phi}\,d\phi$ has been used as definition for the incomplete integral of the second kind, with amplitude φ and modulus k. The modulus in the right-hand side of (4.35) is greater than unity. Most tables on elliptic integrals only deal with moduli less than or equal to unity, as does the MATLAB function `ellipke`[2] for evaluating complete elliptic integrals. A transformation can be applied to express the right-hand side of (4.35) in terms of

---

[2]Note that the MATLAB function `ellipke` evaluates the complete integrals of the first and second kind for the *parameter* m as argument. The parameter m is related to the *modulus* k by $m = k^2$.

incomplete integrals of the first and second kind with a modulus less than unity (see [5, 114.01, p. 12]): if $k_1 = 1/k$ and $\sin \varphi_1 = k \sin \varphi$, then

$$E(\varphi, k) = k_1[k^2 E(\varphi_1, k_1) + (1 - k^2)F(\varphi_1, k_1)], \tag{4.36}$$

where $F(\varphi, k)$ denotes the incomplete integral of the first kind with amplitude φ and modulus k. It follows that

$$
\begin{aligned}
I &= 2E\left(\frac{\pi}{4}, \sqrt{2}\right) = \sqrt{2}\left[2E\left(\frac{\pi}{2}, \frac{1}{\sqrt{2}}\right) - F\left(\frac{\pi}{2}, \frac{1}{\sqrt{2}}\right)\right] \\
&= 2\sqrt{2}E\left(\tfrac{1}{2}\sqrt{2}\right) - \sqrt{2}K\left(\tfrac{1}{2}\sqrt{2}\right).
\end{aligned}
\tag{4.37}
$$

As a check for the evaluation of the integral I using the MATLAB function `ellipke`, the integral was also evaluated using Table 17.2 in [1, pp. 610–611] for the complete elliptic integrals. Both methods of evaluation yield $I = 1.1981$, consistent with the value previously found by using the MATLAB quadrature function and different from the value given by Ahrens et al. In order to avoid further confusion, the value for the integral I in (4.34) will not be substituted; if needed, the value $I = 1.1981$ can be used as the correct value, or the value $I = 1.1781$ can be used for easy comparison with derived quantities in the article by Ahrens et al.

Note that the value of I in (4.34) comes from the integral of the reactants mass flux $\dot{m}_r$ over a cycle and depends on the pressure variation $p(t)$ as function of time. In general, for $p(t)$ not prescribed, I could be defined as

$$I = \frac{1}{2T_P} \int_{\text{cycle}} \sqrt{|\widehat{p}(t)|} \mathbf{1}_{(-\infty,0)}(\widehat{p}(t)) \, dt, \tag{4.38}$$

with $\widehat{p} = p/p_{\max}$ giving the 'shape' of the pressure variation over time, and T_P the period of oscillation. If the second criterion of stability is invoked, i.e., the mean pressure variation over a cycle is zero, the integral over the mass burning rate $\dot{m}_b$ is the same as before and expression (4.34) is valid for I as just given. Thus, the exact relationship between U_f and $p_{\max}$ is given by expression (4.34) for some value of I, which was approximated above by assuming the pressure variation to be sinusoidal with frequency $\frac{\omega_0}{2\pi}$, giving $I = 1.1981$.

4.4.2 Zero mean pressure

In order to arrive at another expression relating U_f and $p_{\max}$, Ahrens et al. use the stability criterion that the mean pressure variation over a cycle must be zero. They use some simplifying assumptions, based on a general shape of the pressure variation as function of time. In Figure 4.2 a sketch of the pressure variation as function of the time is shown for a cycle, with some typical points in time marked on the time axis. The simplifying assumptions, which are not motivated, come down to the following (referring to Figure 4.2):

- the maximum variation in pressure is as great above zero as below zero, i.e., $p_{\max} = -p_{\min}$;

- the ratios of the shaded areas above and below the time axis to the total areas above and below the time axis, respectively, are equal. Thus,

$$\frac{\int_{t_1}^{t_2} p(t) \, dt}{\int_{t_0}^{t_2} p(t) \, dt} = \frac{\int_{t_2}^{t_3} p(t) \, dt}{\int_{t_2}^{t_4} p(t) \, dt}. \tag{4.39}$$
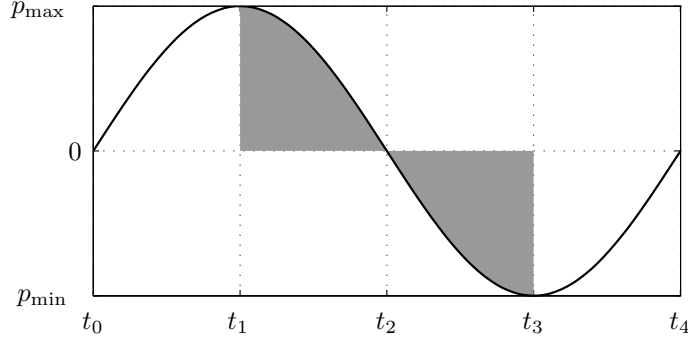
Figure 4.2: Sketch of the gauge pressure as function of the time during a cycle. The marked times on the time axis are: t_0, start of the cycle ($p = 0$); t_1, moment of maximum pressure ($p = p_{max}$); t_2, moment of zero pressure ($p = 0$); t_3, moment of minimum pressure ($p_{min} < 0$); and t_4, end of the cycle ($p = 0$).

With the mean pressure variation being zero, the last assumption is equivalent to assuming that the shaded areas are of equal size, with the integrals of opposite sign:

$$\int_{t_1}^{t_2} p(t)\, dt = -\int_{t_2}^{t_3} p(t)\, dt. \tag{4.40}$$

Integration of the second-order nonlinear differential equation (4.20) from time τ_0 to time τ_1 gives

$$
\begin{aligned}
0 &= \int_{\tau_0}^{\tau_1} \left(\frac{d^2 p}{dt^2} - (AF'(p) + B)\frac{dp}{dt} + CDp \right) dt \\
&= \left[\frac{dp(t)}{dt} - (AF(p(t)) + Bp(t)) \right]_{t=\tau_0}^{\tau_1} + CD \int_{\tau_0}^{\tau_1} p(t)\, dt, \tag{4.41}
\end{aligned}
$$

where the term with square brackets denotes the difference of the term evaluated for the superscript and the term evaluated for the subscript, $[f(t)]_{t=a}^{b} = f(b) - f(a)$. It follows that

$$\int_{\tau_0}^{\tau_1} p(t)\, dt = -\frac{1}{CD}\left[\frac{dp(t)}{dt} - (AF(p(t)) + Bp(t)) \right]_{t=\tau_0}^{\tau_1}. \tag{4.42}$$

Using the expressions $-p(t_3) = -p_{min} = p_{max} = p(t_1)$ and $p(t_2) = 0$, and the function $F(p) = \sqrt{|p|}\mathbf{1}_{(-\infty,0)}(p)$ (see (4.18)), gives

$$AF(p) + Bp = \begin{cases} B\, p_{max}, & t = t_1 \\ 0, & t = t_2 \\ A\sqrt{p_{max}} - B\, p_{max}, & t = t_3 \end{cases} \tag{4.43}$$

With $\frac{dp(t)}{dt} = 0$ for $t = t_1, t_3$, and using expression (4.42), it is easy to show that the assumption (4.40) leads to $B\, p_{max} = A\sqrt{p_{max}} - B\, p_{max}$, or

$$\sqrt{p_{max}} = \frac{A}{2B} = \frac{k_g(1+r)^2 h_r RT_0}{2A_b U_f \Delta H_f}, \tag{4.44}$$

where the expressions (4.14) and (4.15) for A and B, respectively, have been substituted. (Note that the value of $\frac{dp}{dt}(t = t_2)$ is not needed, since it appears on both sides of the equal sign, and thus drops from the equation.) This is the second relation between $p_{\max}$ and U_f given by Ahrens et al.

Actually, the derivation of expression (4.44) given by Ahrens et al. is somewhat more elaborate than presented above. In the process of deriving this expression, they determine the exact solution of the pressure variation in the interval of the cycle where the pressure is positive. In such an interval, the nonlinear contribution to the damping term caused by the reactants inflow is zero, so that the exact solution in the interval is easily found. From this exact solution, Ahrens et al. infer an additional requirement on the model parameters that need to be fulfilled in order to get a stable operation of the pulse combustor. Some comments on this will be given below in Section 4.5, entitled "Comments on the mathematical model."

4.4.3 Combining the two stability criteria

Substitution of expression (4.34) for U_f into (4.44) leads in a straightforward way to the unique pressure amplitude expressed in the model parameters:

$$p_{\max} = \left(\frac{2I}{\pi}\right)^{-1} \frac{P_0(1+r)h_r}{\Delta H_f}. \tag{4.45}$$

Back-substitution of this expression into (4.34) gives an expression of U_f in other model parameters than $p_{\max}$:

$$U_f = \sqrt{\frac{I}{2\pi}} \frac{RT_0(1+r)^{3/2}}{A_b\sqrt{P_0}} \sqrt{\frac{h_r}{\Delta H_f}}. \tag{4.46}$$

These expressions for the model parameters U_f and $p_{\max}$ are used as estimates for the values that are necessary for a stable oscillation of the pressure in the combustion chamber. More accurate values can be obtained by solving the model equations numerically and requiring the fulfillment of the two stability criteria. Some comments on the imposed requirements to obtain a stable oscillating pressure amplitude are given in the next section.

4.5   Comments on the mathematical model

The process of pulse combustion as modelled by Ahrens et al. is one of combustion inducing pressure increase, resulting in products outflow and a drop in pressure (eventually dropping below ambient pressure), whereupon the cycle starts anew with the inflow of reactants. The heat release as modelled by Ahrens et al. satisfies Rayleigh's criterion at all times and therefore the combustion process continuously amplifies pressure oscillations. The amplitude of the pressure oscillations would grow without limit, if it were not for some limiting factors.

For stable operation of a pulse combustor the model presented by Ahrens et al. requires a balance between damping of pressure oscillations by reactants inflow and amplification thereof by combustion. The model parameters U_f (which is associated with the combustion process and firing rate of the pulse

combustor) and $p_{\max}$ (the amplitude of the pressure oscillations) are determined by requiring such a balance.

As mentioned by Ahrens et al., many pulse combustion phenomena are not represented in the model. This raises the question whether the damping by reactants inflow is indeed the most important limiting factor. This question is addressed in this section.

4.5.1   Damping effects

Without the nonlinear damping term $-AF'(p)\frac{dp}{dt}$ in model equation (4.20) caused by the reactants inflow, an analytical solution of the model equation can be to obtained by elementary methods. Then, given initial conditions $p(0) = 0$ and $\frac{dp}{dt}(t = 0) = \dot{p}_0$ for some $\dot{p}_0 > 0$ at a starting point $t = 0$, and provided the solution $p(t)$ of the model equation will return to zero in a finite time span, the solution would be given by

$$p(t) = \frac{\dot{p}_0}{\beta} e^{\alpha t} \sin(\beta t), \qquad (4.47)$$

where

$$\alpha = \frac{B}{2} \qquad (4.48)$$

and

$$\beta = \frac{1}{2}\sqrt{|B^2 - 4CD|}. \qquad (4.49)$$

Thus, without damping by reactants inflow the pressure amplitude would be amplified each (half-)cycle by the same factor. During the half-cycles that the gauge pressure is positive, there is no reactants inflow and the exact solution of the model equations is given by (4.47). (At least, if the pressure does return to zero after the start of the half-cycle. Conditions for this will be discussed below.) From (4.47) it is clear that the greater (i.e., the more positive) the rate of change of the gauge pressure $\frac{dp}{dt}$ at the beginning of the half-cycle is, the greater is the pressure amplitude during the half-cycle and the more negative is the rate of change of the gauge pressure at the end of the half-cycle.

During the half-cycle that the gauge pressure is negative, the inflow of reactants counteracts the amplification of the pressure amplitude. However, since $F'(p) = -1/(2\sqrt{|p|})$ for $p < 0$ (see (4.21)), the damping effect is less for more negative gauge pressure. At the beginning of reactants inflow (then $p = 0$) the gauge pressure grows negative more rapidly if the rate of change of the gauge pressure $\frac{dp}{dt}$ is more negative, resulting in less damping during the cycle. Thus, if the damping by reactants inflow during a cycle is not sufficient to counteract the amplification of the pressure amplitude by combustion, the rate of change of the gauge pressure at the beginning of the reactants inflow will be more negative in the next cycle, resulting in even less damping. On the other hand, if the damping by reactants inflow is greater than the amplification by combustion, the rate of change of the gauge pressure at the moment of reactants inflow for the next cycle will be less negative than that in the previous cycle, resulting in even more damping. From this it may be expected that either the pressure amplitude will grow without limit (if the damping is not strong enough) or the pressure oscillations will die out (if the damping is too strong). The numerical

results in the next section confirm these expectations of the behaviour of the solution of the model equations.

From this it may be concluded that, according to the mathematical model of Ahrens et al., the damping by reactants inflow does not drive a pulse combustion system toward stable operation. 'Stable' operation requires an exact relationship between the initial rate of change of the gauge pressure, $\dot{p}_0$ (or, equivalently, the pressure amplitude p_{max} sought after in Section 4.4), and the model parameter U_f. Any deviation from that relationship and the pressure oscillations will die out or grow without limit. This suggests that other damping factors than reactants inflow are responsible for stabilizing a pulse combustion system. Therefore, the premise that the model parameter U_f (related to the combustion) can be obtained by requiring a balance between the effects of combustion and reactants inflow on the pressure oscillations seems questionable. If other factors are indeed important in limiting pressure oscillations, one might even strive for system parameters that, according to the model of Ahrens et al., would let the pressure oscillations grow without limit. A real pulse combustor designed with such parameters could operate stably due to damping by other factors than reactants inflow.

4.5.2 Requirement of presence of reactants in combustion chamber and burning rate modelling

One requirement for stable operation of a pulse combustor that Ahrens et al. used to determine the model parameter U_f, is that there should be no reactants mass build up or depletion in the combustion chamber. This in fact excludes one physical process that could be a limiting factor on growth of the pressure amplitude in a real pulse combustor: if all the reactants in the combustion chamber are consumed by combustion, there will be no extra heat release, and thus no extra rise in pressure. Ahrens et al. mention that the presence of reactants in the combustion chamber throughout the combustion cycle "appears to be consistent with the observed operation of pulse combustion burners." But this does not mean that the burning model prescribing the burning rate of reactants $\dot{m}_b$ expressed by (4.5) is an appropriate one throughout the cycle. One may expect that when the reactants run low, the reaction rate is no longer representable by the thin flame sheet across the entire combustion chamber cross-section moving at a certain flame speed U_f, but instead might be described by such a flame sheet (using the same flame speed U_f) across a smaller area. Then, as opposed to the burning model of Ahrens et al., reactants could be present throughout the cycle while the heat release diminishes significantly if most of the reactants are consumed by combustion, thereby limiting the amplification of the pressure oscillations. Thus, the requirement in the model of Ahrens et al. that there is always some reactants mixture present in the combustion chamber, combined with the burning model that prescribes the consumption of the mixture at a certain rate only dependent on the pressure in the combustion chamber, seems to impose a limit on the capability of the model to describe stable operating pulse combustors.

4.5.3   Conditions for oscillatory solutions

In the analysis on the damping effects, it was assumed that the solution $p(t)$ of
the model equations starting at some point $t = 0$ in time, with initial conditions
$p(0) = 0$ and $\frac{dp}{dt}(t = 0) = \dot{p}_0 > 0$, would return to zero in a finite time span.
With the nonlinear damping term in model equation (4.20) being zero if $p > 0$,
it is easy to show that for the gauge pressure to return to zero the relation $B^2 -
4CD < 0$, or equivalently $B/\sqrt{CD} < 2$, must be satisfied: if this condition is
satisfied, the solution of the model equations will be oscillatory on time intervals
of positive gauge pressure; otherwise, it will be continuously increasing in time.
Formulated in model parameters, the condition is

$$\frac{A_b U_f \Delta H_f}{RT_0(1 + r)} \sqrt{\frac{(\gamma - 1)L_{tp}}{h_e A_{tp} V_{cc}}} < 2 \tag{4.50}$$

(see (4.15), (4.16) and (4.17) for expressions of B, C and D in model parame-
ters). Similar arguments[3] lead Ahrens et al. to suspect that stable pulse combus-
tor operation may be impossible for model parameters not satisfying inequality
(4.50). They mention that in practice this condition is usually met, so that it
is not a serious restriction in the design of pulse combustors. They also men-
tion that the condition could not be put to the test in their article, since for
all the pulse combustors they used data of, the system parameters satisfied the
condition.

   According to the model of Ahrens et al., sets of system parameters not
satisfying inequality (4.50) result in a continuously increasing pressure in the
combustion chamber. This would ultimately result in the consumption of all
the reactants present in the combustion chamber, which violates a criterion of
Ahrens et al. for stable pulse combustion burner operation. Considering the
discussion above on the requirement of presence of reactant mixture throughout
a cycle in combination with the burning rate model used by Ahrens et al., it
seems questionable to consider inequality (4.50) as a restriction on design choices
of the system parameters for pulse combustors. For a better understanding
of the conditions under which a pulse combustion burner may operate stably,
additional physical processes should be included in the model and/or physical
processes should be modelled in greater detail (for example the burning rate).

4.6   Numerical implementation and experiments

The system of model equations (4.12)–(4.19) is numerically implemented using
MATLAB [29] software. The standard MATLAB ODE-solver `ode45`[4] is used to
solve the equations. The implementation in MATLAB is straightforward; the
codes used can be found in Appendix B.

   In order to solve the model equations numerically, the model parameters
and the initial conditions need to be specified. The model parameters chosen
by Ahrens et al. that are related to the dimensions of a pulse combustor are

---

[3]They use the exact solution of the model equations for positive gauge pressure, but state
incorrectly that the condition $B/\sqrt{CD} < 2$ must hold, for otherwise the gauge pressure "would
approach zero asymptotically and, therefore, cannot switch over to the negative pressure
regime."

[4]See footnote 2 on page 18

Parameter	Value used	Unit
A_b	8.11×10^{-3}	m^2
A_{tp}	7.92×10^{-4}	m^2
$A_{v,g}$	6.26×10^{-5}	m^2
L_{tp}	1.52	m
r	19.8	–
V_{cc}	1.97×10^{-3}	m^3

Table 4.1: Model parameters associated with pulse combustor dimensions as used for numerical evaluation of the model equations. Values are taken from Table 1 (AGA experimental burner No. 2) in the article [2] of Ahrens et al.

based on existing pulse combustion burners. In their article, the dimensional properties of the burners are presented clearly in Table 1 on AGA Experimental Burners. Of these, the dimensions associated with burner No. 2 are used for the numerical evaluation of the model equations in this report. This choice is made, because of the available data presented in the table this particular burner operates with the gas pressure supplied at the ambient (atmospheric) value, which is an assumption used in developing the model equations. Other listed pulse combustion burners operate with a slightly pressurized gas supply. There is one other burner listed operating with the gas pressure supplied at the ambient value: it has the same dimensions except for a tailpipe that is more than twice as long. The burner with the shorter tailpipe is listed operating with a mean chamber pressure that is less than that with the burner with the longer tailpipe ($7,421\,\mathrm{Pa}$ versus $11,204\,\mathrm{Pa}$). Since no friction was assumed in the derivation of the model equations, the mean chamber pressure should be zero in the mathematical model. The influence of friction in the tailpipe is less with the burner with the shorter tailpipe, thus that tailpipe length is chosen to numerically evaluate the model equations. The values chosen for the model parameters related to the dimensions of the pulse combustor are listed in Table 4.1.

The other model parameters that are needed for the numerical evaluation of the model equations, and some auxiliary parameters used to compute the model parameters, are listed in Table 4.2. As in the article of Ahrens et al., the values chosen for the model parameters are based on methane as fuel and air property values. The parameter values needed are computed or looked up in literature (see the caption of the table). For the ambient temperature and associated air property values $T_0 = 300$ K is used, almost equal to the value of $T_0 = 530°$ R used by Ahrens et al. Since the appropriate values for the discharge coefficients $C_{D,g}$ of the gas valves of the pulse combustion burners were unknown to Ahrens et al., they chose (rather arbitrarily) the value $C_{D,g} = 0.6$ for it.

The initial conditions needed for numerical evaluation of the model equations (4.12)–(4.19) are chosen in the following way. The numerical evaluation is chosen to start at a point in time ($t = 0$) of maximum gauge pressure p_0, thus $\frac{dp}{dt}(t = 0) = 0$. Substitution of $\frac{dp}{dt}(t = 0)$ and $p(0) = p_0$ in differential equation (4.12) for

Parameter	Value used	Unit	Comment
$C_{D,g}$	0.6	–	
c_p	1009.7	J/kg K	air prop., [27, p.346]
h_e	$= h_r + \frac{\Delta H_f}{1+r}$	J/kg	
h_r	$= c_p T_0$	J/kg	
k_g	$= \sqrt{2\rho_g} C_{D,g} A_{v,g}$	$\mathrm{kg}^{1/2}\,\mathrm{m}^{1/2}$	
MW_g	16.043	kg/kmol	mol. weight, [27, p.343]
P_0	1.01325×10^5	Pa	$= 1\,\mathrm{atm}$
R_a	287	J/kg K	air prop., [27, p.343]
R_g	$= R_u/\mathrm{MW}_g$	J/kg K	
R_u	8.31441×10^3	J/kmol K	univ. gas const., [27, in back]
T_0	300	K	
ΔH_f	50.016×10^6	J/kg	LHV [32, p.543]
ρ_g	$= P_0/(R_g T_0)$	$\mathrm{kg/m}^3$	

Table 4.2: Model parameters (and auxiliary values to compute model parameters) used for the numerical evaluation of the model equations of Ahrens et al. The value of the parameter $C_{D,g}$ is that chosen by Ahrens et al. [2]; the other parameter values are based on air property values (as used by Ahrens et al.) at a reactants temperature of 300 K (close to the choice of 530° R of Ahrens et al.) and the fuel choice of methane. The reference temperature and pressure for the LHV of methane is 298.15 K and 1 atm, respectively. The air and fuel properties were looked up in tables in [27] and [32].

the rate of change of the gauge pressure yields the following initial conditions:

$$p(0) = p_0, \qquad (4.51)$$

$$\dot{m}_e(0) = \dot{m}_{e,0} = \frac{B}{C}(p_0 + P_0), \qquad (4.52)$$

where $\dot{m}_{e,0}$ denotes the prescribed initial mass flux into the pulse combustor tailpipe.

The initial (maximum) gauge pressure should be related to the model parameter U_f in some way in order to obtain a 'stable' oscillating solution. As a first guess, the values of p_0 and U_f are chosen as those given by $p_{\max}$ and U_f in expressions (4.45) and (4.46), respectively, that resulted from the analysis of Ahrens et al. The value of I in these expressions is chosen to be consistent with the (incorrect) value used by Ahrens et al., i.e. $I/\pi = 0.375$, so that $p_{\max}$ and U_f are given by

$$p_{\max} = \frac{1}{0.75} \frac{P_0(1+r)h_r}{\Delta H_f}, \qquad (4.53)$$

$$U_f = \sqrt{0.1875} \frac{RT_0(1+r)^{3/2}}{A_b\sqrt{P_0}} \sqrt{\frac{h_r}{\Delta H_f}}. \qquad (4.54)$$

This first choice of parameters p_0 ($= p_{\max}$) and U_f does not result in a stable oscillating solution: the initial oscillation quickly dies out. Keeping U_f and $p_{\max}$ constant at the values chosen above, the initial gauge pressure p_0 is adjusted

(a) $p_0 = 1.242p_{max}$

(b) $p_0 = 1.243p_{max}$
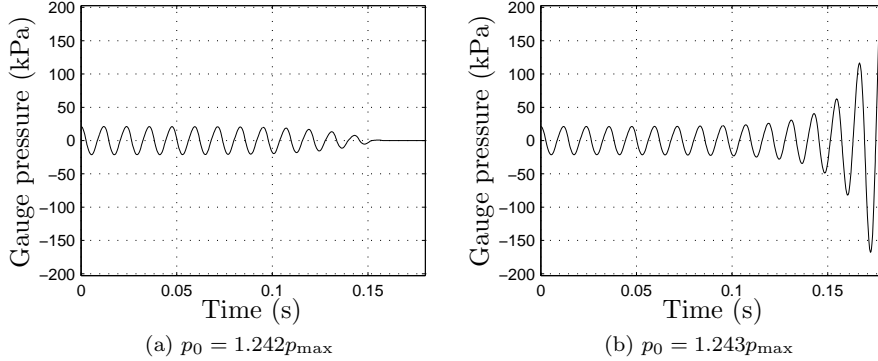
Figure 4.3: Gauge pressure as function of time for different, but very close, initial conditions $p_0 = (1 + \delta)p_{max}$: (a) $\delta = 0.242$, (b) $\delta = 0.243$.

(increased if the oscillations die out, decreased if the amplitude of oscillations grows continuously) by choosing it to be a multiple of p_{max}:

$$p_0 = (1 + \delta)p_{max}, \qquad (4.55)$$

for a certain $\delta > -1$. This procedure for searching a 'stable' oscillating solution will yield a set of parameters p_0 and U_f satisfying only the requirement of zero mean gauge pressure in the combustion chamber, not the requirement of the presence of reactants in the combustion chamber throughout the cycle. However, for illustrating that the sought-after stable oscillating solution does not exist (i.e., the pressure oscillations will either grow without limit, or they will die out), it will suffice. The solution of the model equations will show a similar behaviour for the pair of model parameters p_0 and U_f for which the requirement on the reactants appears to be satisfied. Of course, the fulfillment of this requirement cannot be maintained if the pressure oscillations grow too large, or die away.

Figure 4.3 shows plots of the computed gauge pressure versus time for the values $\delta = 0.242$ and $\delta = 0.243$. The difference of the initial gauge pressures is very small and the computed gauge pressures appear to be oscillating stably in the beginning. However, after some time has passed, the graphs show significantly different behaviour of the gauge pressure: for $\delta = 0.242$ the oscillations die out, while for $\delta = 0.243$ the amplitude increases without bounds.

The difference in evolution of the computed gauge pressure for the two choices of δ is illustrated by the phase diagram shown in Figure 4.4. The phase path associated with $\delta = 0.242$ starts at $(0, 1.242p_{max})$ and spirals inwardly to the origin. The phase path associated with $\delta = 0.243$ starts at $(0, 1.243p_{max})$ and spirals outwardly.

The graphs clearly shows the influence of the damping: around $p = 0$, where for $p < 0$ the damping is the greatest, the rate of change of the gauge pressure in absolute sense is decreased and change in gauge pressure is severely inhibited. The graphs suggest the existence of a limit cycle for a value of δ somewhere between 0.242 and 0.243. However, for a value of δ slightly different the damping will continuously increase or decrease and while for some time the phase paths may stay close to the limit cycle, they will eventually diverge.
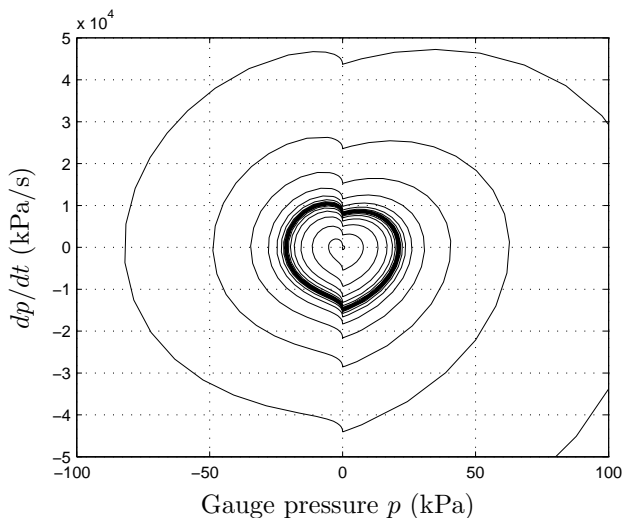
Figure 4.4: Trajectories in phase plane corresponding to the nonlinear model equation (4.20) for two different, but very close, initial conditions. One trajectory, corresponding to an initial condition $p_0 = 1.242 p_{max}$, spirals inwardly toward the origin. The other trajectory, corresponding to the initial condition $p_0 = 1.243 p_{max}$, spirals outwardly.

4.7   Conclusions

In their article [2] Ahrens et al. present a lumped parameter model for a pulse combustion burner. An energy balance analysis of the combustion chamber, with simple steady-flow orifice equations describing the reactants inflow and a heat release given by combustion of the reactants at a constant volumetric rate, is linked to a plug flow description of the products in the tailpipe. No energy losses, for example by friction in the tailpipe or heat transfer to the combustion chamber wall, are modelled. The analysis of Ahrens et al. leads to a second-order differential equation for the gauge pressure in the combustion chamber with a negative (linear) damping term associated with the combustion process and a positive (nonlinear) damping term associated with the inflow of reactants. The constant volumetric burning rate is equivalent to that of a thin flame sheet across the combustion chamber moving at a certain constant 'flame speed'. Ahrens et al. found this constant 'flame speed' and the amplitude of the pressure variation in the combustion chamber to be uniquely determined if the solution of their model equation is to satisfy two criteria for stable pulse combustion burner operation. One criterion they mention is that the mean gauge pressure in the combustion chamber should be zero (since no energy losses are modelled). The other criterion is that there should be no accumulation or depletion of reactants in the combustion chamber. Also, the model equations of Ahrens et al. impose a certain condition on the model parameters which must be satisfied for the solution to be oscillatory. Ahrens et al. conclude from this that a pulse combustion burner with design parameters not satisfying that condition might not work properly.

In this chapter, the mathematical model presented by Ahrens et al. has been examined analytically and numerically. The derivation of the model equations has been given, largely following the presentation of Ahrens et al. The analysis shows that the impact of damping of the pressure oscillation by inflow of reactants diminishes if the amplitude of the oscillation increases. According to the model equations, the inflow of reactants causes pressure oscillations either to die out or to continuously increase in amplitude. Other physical processes than the inflow of reactants, for example a burning rate that is different from the one used in the model, seem to be responsible for reaching a stable oscillation. The premise that model parameters of a stably operating pulse combustor should satisfy the conditions that yield a 'stable' oscillatory solution of the model equations, is therefore questionable. Besides the inflow of reactants, other physical processes that may influence the stability of oscillations should be included in the model in order to gain more insight in the conditions under which a pulse combustor may operate properly.

Chapter 5

A model suggested by Richards, et al

Note: In a Bachelor's thesis project at the Eindhoven University of Technology, Van Mullem and Bastiaans [33] examined the model of Richards et al. [25], which is discussed in this chapter. They gave a quick investigation into the effect of changing the air/fuel ratio. This report was studied, but the discussion in this chapter focuses only on the work presented by Richards et al.

Richards et al. [25] introduced a mathematical model to describe a combustion system with a continuous fuel supply. This is different from a typical pulse combustor, where fuel periodically enters the combustion chamber because of time-dependent pressure differences over valves. They show that pulsation can occur even for a continuous fuel supply. To indicate the impact of heat transfer on the pulsating process, they termed it *thermal pulse combustion*.

The model is a lumped parameter model, taking the combustion chamber as a control volume. The amount of energy in the combustion chamber is changed by inflow of reactants, combustion, outflow of combustion products, and heat transfer to the chamber wall. The combustion process is modelled by a one-step Ahrrenius law for a bimolecular reaction between fuel and oxidizer. The gases in the combustion chamber are assumed to be well-stirred. The tailpipe flow is modelled as a slug flow, i.e. of constant density and driven by the pressure difference over the tailpipe. Flow from the combustion chamber into the tailpipe is assumed to be isentropic. Wall friction of the tailpipe gases is taken into account. It is assumed that the gases are perfect, and that all mixtures of reactants and products have the same (constant) specific heats. By applying conservation of mass, energy and species to the control volume, and coupling this to the tailpipe dynamics by conservation of momentum, Richards et al. derived a system of four ordinary differential equations.

The numerical results obtained by Richards et al. showed three possible modes of operation, depending on the model parameters: steady combustion, flame extinction, or oscillatory combustion. The influence of microscale mixing was also investigated numerically. The numerical results showed a qualitative agreement to experimental data.

In this chapter, the mathematical model suggested by Richards et al. will be

investigated. The nomenclature used by Richards et al. is adjusted in order to ease the comparison with the other models that are investigated in this report. The numerical results of Richards et al. will be reproduced (for as far as this was possible). As will be seen in the discussion of the results in this report, the phase difference between heat release and the acoustic oscillations provides an intuitive explanation of the system's behaviour. Although the importance of the phase difference may be obvious from Rayleigh's criterion, Richards et al. did not give it much attention in the discussion of their results.

5.1   Nomenclature

Roman symbols

A–G	Auxiliary constants	
$\widehat{A}$	Kinetic constant for fuel reaction	$[\,\mathrm{m^3/kg\,s\,K^{\frac{1}{2}}}\,]$
A'	Modified kinetic constant, $= A\rho_0\sqrt{T_0}S_r$	$[\,\mathrm{1/s}\,]$
A_{tp}	Area of tailpipe cross-section	$[\,\mathrm{m^2}\,]$
A_s	Surface area of combustion zone	$[\,\mathrm{m^2}\,]$
c_p	Specific heat for constant pressure	$[\,\mathrm{J/kg\,K}\,]$
c_v	Specific heat for constant volume	$[\,\mathrm{J/kg\,K}\,]$
D_{tp}	Tailpipe diameter	$[\,\mathrm{m^2}\,]$
e	Specific internal energy	$[\,\mathrm{J/kg}\,]$
E_A	Activation energy	$[\,\mathrm{J/mol}\,]$
f	Friction coefficient (in tailpipe)	$[\,-\,]$
F_f	Friction force (in tailpipe)	$[\,\mathrm{N}\,]$
h	Specific enthalpy	$[\,\mathrm{J/kg}\,]$
$\widehat{h}$	Heat transfer coefficient	$[\,\mathrm{W/m^2\,K}\,]$
L_1	First characteristic length, $= V_{cc}/A_s$	$[\,\mathrm{m}\,]$
L_2	Second characteristic length, $= V_{cc}/A_{tp}$	$[\,\mathrm{m}\,]$
L_{tp}	Tailpipe length	$[\,\mathrm{m}\,]$
M	Mach number	$[\,-\,]$
$\dot{m}$	Mass flow rate	$[\,\mathrm{kg/s}\,]$
$\mathrm{MW_X}$	Molecular weight of chemical compound X	$[\,\mathrm{g/mol}\,]$
$\mathbf{n}$	Outward normal on control volume boundary	$[\,-\,]$
P	Pressure (in combustion chamber)	$[\,\mathrm{Pa}\,]$
$\mathbf{q}$	Heat flow per unit of area	$[\,\mathrm{J/m^2\,s}\,]$
$\dot{Q}$	Rate of heat release per unit volume	$[\,\mathrm{J/m^3\,s}\,]$
R	Specific gas constant	$[\,\mathrm{J/kg\,K}\,]$
$\dot{R}_f$	Fuel reaction rate	$[\,\mathrm{kg/m^3\,s}\,]$
$\dot{R}_o$	Oxygen reaction rate	$[\,\mathrm{kg/m^3\,s}\,]$
R_u	Universal gas constant	$[\,\mathrm{J/mol\,K}\,]$
RR	Auxiliary reaction rate	$[\,\mathrm{1/s}\,]$
$\widehat{RR}$	Auxiliary reaction rate, modified for mixing time	$[\,\mathrm{1/s}\,]$
S_r	Stoichiometric oxygen-fuel mass ratio	$[\,-\,]$
t	Time	$[\,\mathrm{s}\,]$

Roman symbols, continued

T	Temperature	$[\mathrm{K}]$
$\widetilde{T}_{\mathrm{act}}$	Dimensionless activation temperature, $= E_A/R_u T_0$	$[-]$
T_w	Wall temperature of combustion chamber	$[\mathrm{K}]$
u	Velocity of tailpipe plug flow	$[\mathrm{m/s}]$
u_c	Characteristic tailpipe velocity, $= \dot{m}_i/\rho_0 A_{tp}$	$[\mathrm{m/s}]$
$\mathbf{v}$	Velocity vector (in tailpipe)	$[\mathrm{m/s}]$
v^2	$= \mathbf{v} \cdot \mathbf{v}$	$[\mathrm{m^2/s^2}]$
V	Volume	$[\mathrm{m^3}]$
Y	Mass fraction (in combustion chamber)	$[-]$
Z	Auxiliary parameter, $= \dot{m}/V$	$[\mathrm{kg/m^3\,s}]$

Greek symbols

γ	Ratio of specific heats, $= c_p/c_v$	$[-]$
ΔH_f	Heat of combustion per unit mass fuel	$[\mathrm{J/kg}]$
Ω	Control volume	$[-]$
ρ	Density	$[\mathrm{kg/m^3}]$
τ_c	Combustion time, $= c_p\rho_0 T_0/\dot{Q}$	$[\mathrm{s}]$
τ_{cm}	Combined combustion and mixing time, $= \tau_c + \tau_m$	$[\mathrm{s}]$
τ_f	Flow time, $= \rho_0/Z_i$	$[\mathrm{s}]$
τ_{HT}	Heat transfer time, $= L_1 c_p \rho_0 T_0/\widehat{h} T_w$	$[\mathrm{s}]$
τ_m	Mixing time	$[\mathrm{s}]$
τ_{wall}	Friction shear stress at tailpipe wall	$[\mathrm{N/m^2}]$
χ_{X}	molal fraction of chemical compound X	$[-]$

Other symbols

$\sim$	(Over variable) Indicates normalized variable
$\partial\Omega$	Boundary of control volume

Subscripts

0	initial/standard/ambient value
cc	combustion chamber
e	exit combustion chamber/entrance tailpipe
f	fuel (except for F_f and τ_f, see above)
i	inlet of combustion chamber
mix	mixture
o	oxygen
w	combustion chamber wall

Superscripts

$*$	average value
tot	total (or, stagnation) variables

5.2 Derivation of model equations

In this section the derivation of the model equations will be given, largely following the presentation of Richards et al. For clarity, some in-between steps in
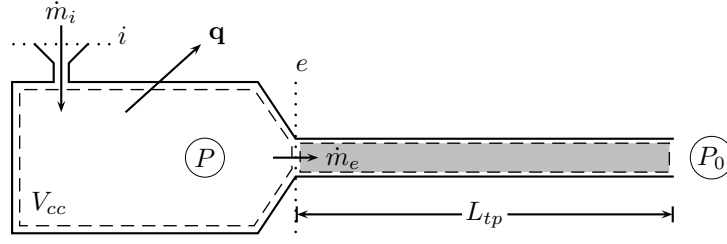
Figure 5.1: Control volume (i.e., the combustion chamber, with volume V_{cc}) of the modelled thermal pulse combustor, with sign conventions and (some) model parameters. The values of the mass fluxes $\dot{m}_i$ at the inlet i, and $\dot{m}_e$ at the tailpipe entrance e are taken positive in the directions indicated. The heat flux $\mathbf{q}$ is directed outward of the combustion chamber.

the derivation are added where Richards et al. only show the resulting equations or mention the way to get them.

5.2.1   Conservation of energy

The combustion chamber is chosen as a control volume. Let Ω denote the control volume and $\partial\Omega$ its boundary. See Figure 5.1 for a schematic of the control volume and sign conventions. Conservation of energy over this control volume is expressed by

$$\frac{d}{dt}\int_{\Omega}\rho(e+\tfrac{1}{2}v^2)\,dV = -\int_{\partial\Omega}\rho\mathbf{v}\cdot\mathbf{n}(e+\tfrac{1}{2}v^2)\,dA - \int_{\partial\Omega}P\mathbf{v}\cdot\mathbf{n}\,dA$$
$$+ \int_{\Omega}\dot{Q}\,dV - \int_{\partial\Omega}\mathbf{q}\cdot\mathbf{n}\,dA \quad (5.1)$$

where ρ is the density, e is the specific internal energy, P is the pressure, $\dot{Q}$ is the rate of heat release per unit volume, $\mathbf{v}$ is the fluid velocity, v^2 denotes $\mathbf{v}\cdot\mathbf{v}$, $\mathbf{q}$ is the heat flow per unit area out of the control volume, and $\mathbf{n}$ is the outwardly directed normal on the boundary. The integral on the left-hand side represents the rate of change of the total amount of energy in the control volume. The first integral on the right-hand side is the energy flux through the boundary out of the control volume. The second integral on the right-hand side is the rate of flow work done by the control volume. The third integral on the right-hand side is the rate of heat release inside the control volume and the last integral is the heat flux through the boundary out of the control volume.

It is assumed that the specific kinetic energy inside the control volume is negligibly small compared to the specific internal energy. The gases (reactants and the products) are assumed to be perfect, i.e., they obey the perfect gas law

$$P = \rho R T, \quad (5.2)$$

with R the gas constant and T the temperature, and the ratio of specifics heats is constant:

$$\gamma = \frac{c_p}{c_v} = \text{constant}, \quad (5.3)$$

where c_p is the specific heat for constant pressure and c_v is the specific heat for constant volume. Also, the specific heats and gas constants of the reactants are assumed to be equal to those of the products. The control volume is considered to be well-mixed and therefore the state variables are considered to have a uniform value over the volume. With the specific internal energy given by

$$e = c_v T, \tag{5.4}$$

and with the relation

$$R = c_p - c_v, \tag{5.5}$$

and under the assumptions mentioned above, the left-hand side of equation (5.1) can be written as

$$\frac{d}{dt} \int_\Omega \rho(e + \frac{1}{2}v^2) \, dV = V_{cc} \frac{1}{\gamma - 1} \frac{dP}{dt}, \tag{5.6}$$

where V_{cc} is the volume of the combustion chamber.

The conditions at the inlet and exit of the combustion chamber are assumed to arise from isentropic acceleration of the gases to their inlet and outlet velocities. Thus,

$$\left(\frac{T^{\text{tot}}}{T}\right)_{i/e} = \left(1 + \frac{\gamma - 1}{2} M^2\right)_{i/e} = \left(\frac{P^{\text{tot}}}{P}\right)_{i/e}^{\frac{\gamma - 1}{\gamma}} = \left(\frac{\rho^{\text{tot}}}{\rho}\right)_{i/e}^{\gamma - 1}, \tag{5.7}$$

with the subscript i/e denoting the variables at either the inlet (i) or exit (e) of the combustion chamber. Here T^{tot}, P^{tot} and ρ^{tot} are the total, or stagnation, temperature, pressure and density, respectively. (See Thompson [30, pp. 267–268] for a derivation of these equations.) Because inside the combustion chamber $v^2/2$ is set to zero (it is assumed to be negligibly small compared to the specific internal energy), the state variables inside the combustion chamber are equal to their total state variables:

$$T_{cc}^{\text{tot}} = T, \quad P_{cc}^{\text{tot}} = P, \quad \rho_{cc}^{\text{tot}} = \rho, \tag{5.8}$$

where the subscript cc expresses the correspondence to the state variables inside the control volume (i.e., inside the combustion chamber). The Mach number at the inlet is assumed to be negligibly small, $M_i \approx 0$. For the total temperatures at the inlet and exit there follows

$$c_p T_{i/e} + \frac{v_{i/e}^2}{2} = c_p \left(1 + \frac{1}{2c_p} M_{i/e}^2 \gamma R\right) T_{i/e}$$
$$= c_p \left(1 + \frac{\gamma - 1}{2} M_{i/e}^2\right) T_{i/e} = c_p T_{i/e}^{\text{tot}}. \tag{5.9}$$

Thus, using the relation $R = c_p - c_v$ (5.5) and with $T_i^{\text{tot}} = T_i$ and $T_e^{\text{tot}} = T$,

$$\int_{\partial\Omega} \mathbf{v} \cdot \mathbf{n} \left(\rho(e + \frac{v^2}{2}) + P\right) dA = \int_{\partial\Omega} \rho\mathbf{v} \cdot \mathbf{n} \left(\frac{v^2}{2} + e + RT\right) dA$$
$$= \int_{\partial\Omega} \rho\mathbf{v} \cdot \mathbf{n} \left(c_p T + \frac{v^2}{2}\right) dA = c_p(\dot{m}_e T - \dot{m}_i T_i), \tag{5.10}$$

where use is made of the identities $(\rho\mathbf{v}\cdot\mathbf{n})_i = -\dot{m}_i$ and $(\rho\mathbf{v}\cdot\mathbf{n})_e = \dot{m}_e$, the subscripts indicating values at inlet and exit and $\dot{m}_e$ being the mass flow rate at the entrance of the tailpipe. Note that this result could have been obtained easier by using the specific enthalpy $h = e + P/\rho = c_p T$ and using the fact that an isentropic flow is adiabatic (i.e., no change in heat content) so that for a perfect gas the enthalpy does not change.

It should be stressed that in the derivation of equation (5.10), use of the relation $T_e^{\text{tot}} = T$, prescribing the total temperature at the tailpipe entrance by isentropic acceleration of gases from the combustion chamber, is valid only for flow exiting the combustion chamber. For flow in the reverse direction, from tailpipe into the combustion chamber, the total temperature at the tailpipe entrance only *contributes* to the temperature in the combustion chamber, and should be independent from it. This means that for flow into the combustion chamber (i.e. when $\dot{m}_e < 0$), the term $c_p\dot{m}_e T$ in equation (5.10) should be replaced by $c_p\dot{m}_e T_e^{\text{tot}}$ for some appropriate T_e^{tot} based on the temperature and velocity of the tailpipe gases. Although Richards et al. do not explicitly describe how they implemented the isentropic acceleration/deceleration of the tailpipe gases, the term $c_p\dot{m}_e T$ appears in their formulas, without making any distinction between the cases $\dot{m}_e < 0$ and $\dot{m}_e \geq 0$. It introduces a modelling error. Most of the numerical results show a negative mass flux at the tailpipe entrance (i.e., flow into the combustion chamber) only for a small portion of a cycle, and at a relatively low value in absolute sense. Therefore the effect of the modelling error may be small, although this should be confirmed more rigorously. It would be preferable to correct the model equations to account for flow from the tailpipe back into the combustion chamber, but since this chapter is focused on evaluation of the model and numerical results presented by Richards et al., this will not be pursued here. For the remainder of the derivation of the model equations, it will be assumed that the effect of flow from the tailpipe back into the combustion chamber is negligible.

The heat flux per unit of area at the boundary of the control volume given by Newton's cooling law is $\mathbf{q}\cdot\mathbf{n} = \widehat{h}(T - T_w)$, where T_w is the combustion chamber wall temperature and $\widehat{h}$ is a heat transfer coefficient. With $\widehat{h}$ assumed to be constant and the assumption of uniformity inside the control volume, the last two integrals of equation (5.1) are given by

$$\int_\Omega \dot{Q}\,dV = \dot{Q}V_{cc}, \qquad (5.11)$$

$$\int_{\partial\Omega} \mathbf{q}\cdot\mathbf{n}\,dA = -\widehat{h}(T_w - T)A_s, \qquad (5.12)$$

where A_s is the surface area of the combustion zone.

For convenience Richards et al. introduce the following definitions:

$$Z_i = \frac{\dot{m}_i}{V_{cc}}, \qquad (5.13)$$

$$Z_e = \frac{\dot{m}_e}{V_{cc}}, \qquad (5.14)$$

$$L_1 = \frac{V_{cc}}{A_s}, \qquad (5.15)$$

They call the parameter L_1 the first characteristic length and announce a second characteristic length to be introduced later. It will be associated with a

characteristic velocity in the tailpipe.

Substituting the expressions for the integrals (5.6), (5.10)–(5.12) in the energy balance equation (5.1) and using the definitions (5.13)–(5.15), the energy balance equation (5.1) can be written as

$$\frac{1}{\gamma - 1} \frac{dP}{dt} = c_p(T_i Z_i - T Z_e) + \dot{Q} + \frac{\widehat{h}}{L_1}(T_w - T). \qquad (5.16)$$

5.2.2 Conservation of mass

Under the assumption of uniformity, conservation of mass over the control volume gives $d(\rho V_{cc})/dt = \dot{m}_i - \dot{m}_e$. With the definitions (5.13)–(5.14) this yields

$$\frac{d\rho}{dt} = Z_i - Z_e. \qquad (5.17)$$

5.2.3 Introducing dimensionless state variables and characteristic times

The dimensionless state variables $\widetilde{P}$, $\widetilde{T}$ and $\widetilde{\rho}$ are introduced by

$$\widetilde{P} = \frac{P}{P_0}, \qquad (5.18)$$

$$\widetilde{T} = \frac{T}{T_0}, \qquad (5.19)$$

$$\widetilde{\rho} = \frac{\rho}{\rho_0}, \qquad (5.20)$$

where P_0 is the ambient pressure, T_0 is the ambient temperature and $\rho_0 = P_0/RT_0$ (these constants are characteristic state parameters). Using these relations in the energy conservation equation (5.16) with $T_i = T_0$ and $P_0 = \rho_0 T_0 R$, and noting that $\frac{P_0}{\gamma - 1} = \frac{c_p}{\gamma} \rho_0 T_0$ yields

$$\frac{d\widetilde{P}}{dt} = \gamma \left(\frac{Z_i}{\rho_0} + \frac{\dot{Q}}{c_p \rho_0 T_0} + \frac{\widehat{h} T_w}{L_1 c_p \rho_0 T_0} \right) - \gamma \left(\frac{Z_e}{\rho_0} + \frac{\widehat{h}}{L_1 c_p \rho_0} \right) \widetilde{T}. \qquad (5.21)$$

For the mass conservation equation (5.17) it is easy to see that

$$\frac{d\widetilde{\rho}}{dt} = \frac{Z_i}{\rho_0} - \frac{Z_e}{\rho_0}. \qquad (5.22)$$

At this point Richards et al. introduce the following 'characteristic times' that are recognizable in the equations (5.21)–(5.22):

$$\tau_f = \frac{\rho_0}{Z_i}, \qquad (5.23)$$

$$\tau_{HT} = \frac{L_1 c_p \rho_0 T_0}{\widehat{h} T_w} \qquad (5.24)$$

$$\tau_c = \frac{c_p \rho_0 T_0}{\dot{Q}}. \qquad (5.25)$$

They call τ_f a flow time, indicating the time that it takes non-reacting isothermal gases to pass through the combustion chamber. It can be compared to the

cold residence time of a steady-state reactor, but since in the pulsating case it is not a residence time, the term 'flow time' was introduced for τ_f. The characteristic time τ_{HT} is associated with the heat transfer and τ_c is associated with the combustion process. Note that τ_c is not a constant because of $\dot{Q}$ in the denominator (to be modelled later). Since a characteristic parameter is usually a constant, it may be confusing to call τ_c a characteristic time. Also, it will be shown later (see p. 67) that the 'characteristic time' τ_{HT} is not characteristic for the heat transfer process, contrary to what the terminology may suggest. Nonetheless, in this report the terminology of Richards et al. is followed, and the constant τ_{HT} and variable τ_c will be called characteristic times.

Using the characteristic times in the energy and mass conservation equations (5.21)–(5.22) gives

$$\frac{d\widetilde{P}}{dt} = \gamma \left(\frac{1}{\tau_f} + \frac{1}{\tau_c} + \frac{1}{\tau_{HT}} \right) - \gamma \left(\frac{Z_e}{\rho_0} + \frac{1}{\tau_{HT}} \frac{T_0}{T_w} \right) \widetilde{T} \qquad (5.26)$$

and

$$\frac{d\widetilde{\rho}}{dt} = \frac{1}{\tau_f} - \frac{Z_e}{\rho_0}. \qquad (5.27)$$

Richards et al. use a differential equation for the temperature rather than the mass conservation equation (5.27). It is derived as follows. Using the characteristic state parameters (5.18)–(5.20) and the perfect gas law gives $\widetilde{P} = \widetilde{\rho}\widetilde{T}$ and using the mass conservation equation (5.27) it follows that

$$\frac{d\widetilde{P}}{dt} = \frac{d}{dt}(\widetilde{\rho}\widetilde{T}) = \widetilde{T}\frac{d\widetilde{\rho}}{dt} + \widetilde{\rho}\frac{d\widetilde{T}}{dt} = \widetilde{T}\left(\frac{1}{\tau_f} - \frac{Z_e}{\rho_0} \right) + \frac{\widetilde{P}}{\widetilde{T}}\frac{d\widetilde{T}}{dt}. \qquad (5.28)$$

Solving for $\frac{d\widetilde{T}}{dt}$ gives

$$\frac{d\widetilde{T}}{dt} = \frac{\widetilde{T}}{\widetilde{P}}\frac{d\widetilde{P}}{dt} - \left(\frac{1}{\tau_f} - \frac{Z_e}{\rho_0} \right)\frac{\widetilde{T}^2}{\widetilde{P}}. \qquad (5.29)$$

With substitution of $\frac{d\widetilde{P}}{dt}$ from equation (5.26) the time derivative of the dimensionless temperature is expressed in terms of the dimensionless pressure and temperature:

$$\frac{d\widetilde{T}}{dt} = \gamma \left(\frac{1}{\tau_f} + \frac{1}{\tau_c} + \frac{1}{\tau_{HT}} \right)\frac{\widetilde{T}}{\widetilde{P}} - \left((\gamma - 1)\frac{Z_e}{\rho_0} + \frac{1}{\tau_f} + \frac{\gamma}{\tau_{HT}}\frac{T_0}{T_w} \right)\frac{\widetilde{T}^2}{\widetilde{P}}. \qquad (5.30)$$

5.2.4 Rate of heat release and mass fractions in combustion chamber

The rate of heat release (per unit of volume), $\dot{Q}$, is simply the heat of reaction per unit of fuel mass, ΔH_f, times the fuel mass reaction rate (per unit of volume), $\dot{R}_f$, i.e.

$$\dot{Q} = \Delta H_f \dot{R}_f. \qquad (5.31)$$

The mass fuel rate of reaction is modelled by a bimolecular reaction rate law between fuel and oxygen:

$$\dot{R}_f = \widehat{A}T^{1/2}\rho^2 Y_o Y_f \exp(-E_A/R_u T). \qquad (5.32)$$

where $\widehat{A}$ is some kinetic constant, Y_f and Y_o are the mass fractions of fuel and oxygen, respectively, E_A is the activation energy and R_u is the universal gas constant. The mass oxygen rate of reaction is simply the stoichiometric oxygen-fuel mass ratio, S_r, times the mass fuel rate of reaction:

$$\dot{R}_o = S_r \dot{R}_f. \tag{5.33}$$

Relations for the mass fractions Y_f and Y_o can be derived by considering mass conservation of species in the control volume under the assumption of uniformity inside the control volume. Mass conservation of species for the fuel, for example, is expressed by

$$\frac{d}{dt} \int_\Omega \rho Y_f dV = -\int_{\partial\Omega} \rho Y_f \mathbf{v} \cdot \mathbf{n} dA - \int_\Omega \dot{R}_f dV, \tag{5.34}$$

where the left-hand side is the amount of fuel mass added to the control volume per unit of time, the first integral on the right-hand side is the fuel mass flux out of the control volume and the second integral on the right-hand side is the amount of fuel mass consumed by combustion in the control volume per unit of time. Under the assumption of uniformity inside the control volume this leads to

$$\frac{d}{dt}(\rho Y_f) = -(Y_{f,e} Z_e - Y_{f,i} Z_i) - \dot{R}_f, \tag{5.35}$$

where $Y_{f,i}$ and $Y_{f,e}$ are the fuel mass fractions at the inlet and exit of the combustion chamber, respectively. Applying the chain rule of differentiation yields

$$\rho \frac{dY_f}{dt} + Y_f \frac{d\rho}{dt} = -(Y_{f,e} Z_e - Y_{f,i} Z_i) - \dot{R}_f. \tag{5.36}$$

This equation can be expressed in the dimensionless pressure and temperature by using the identities $\rho = \rho_0 \widetilde{\rho}$ and $\widetilde{\rho} = \widetilde{P}/\widetilde{T}$ and substitution of the mass conservation equation (5.27) for $\frac{d\widetilde{\rho}}{dt}$:

$$\frac{\widetilde{P}}{\widetilde{T}} \frac{dY_f}{dt} = -\left(\frac{1}{\tau_f} - \frac{Z_e}{\rho_0}\right) Y_f - (Y_{f,e} \frac{Z_e}{\rho_0} - Y_{f,i} \frac{Z_i}{\rho_0}) - \frac{\dot{R}_f}{\rho_0}. \tag{5.37}$$

From (5.31) and (5.25) it follows that

$$\frac{\dot{R}_f}{\rho_0} = \frac{\dot{Q}}{\rho_0 \Delta H_f} = \frac{1}{\tau_c} \frac{c_p T_0}{\Delta H_f} \tag{5.38}$$

and with $\frac{Z_i}{\rho_0} = \frac{1}{\tau_f}$ by definition of τ_f (see (5.23)) equation (5.37) can be written as

$$\frac{\widetilde{P}}{\widetilde{T}} \frac{dY_f}{dt} = -\left(Y_{f,e} \frac{Z_e}{\rho_0} - Y_{f,i} \frac{1}{\tau_f}\right) - \left(\frac{1}{\tau_f} - \frac{Z_e}{\rho_0}\right) Y_f - \frac{1}{\tau_c} \frac{c_p T_0}{\Delta H_f}. \tag{5.39}$$

With the assumption of uniformity inside the control volume it follows that $Y_{f,e} = Y_f$, thus

$$\frac{dY_f}{dt} = \frac{\widetilde{T}}{\widetilde{P}} \left(\frac{1}{\tau_f}(Y_{f,i} - Y_f) - \frac{1}{\tau_c} \frac{c_p T_0}{\Delta H_f}\right). \tag{5.40}$$

Note that the relation $Y_{f,e} = Y_f$ used in the derivation of equation (5.40) is valid only for flow from the combustion chamber into the tailpipe. For flow in the

reverse direction, from the tailpipe into the combustion chamber, the fuel present in the tailpipe only contributes to the mass fuel fraction in the combustion chamber, and should be independent from it. Equation (5.40) is used as model equation by Richards et al. without making any distinction between $Z_e \geq 0$ (i.e., flow is from the combustion chamber into the tailpipe) and $Z_e < 0$ (i.e., flow is from the tailpipe into the combustion chamber). Recall that the model equations of this chapter are derived under the assumption that the flow from the tailpipe back into the combustion chamber is negligible (see the discussion in the first new paragraph after equation (5.10) on page 48).

The equation for conservation of the oxygen mass fraction can be derived in a completely analogous manner, leading to a similar expression only differing in the last term because the reaction rate is a factor S_r higher (see (5.33) and (5.38)):

$$\frac{dY_o}{dt} = \frac{\widetilde{T}}{\widetilde{P}} \left(\frac{1}{\tau_f} (Y_{o,i} - Y_o) - \frac{1}{\tau_c} \frac{S_r c_p T_0}{\Delta H_f} \right). \tag{5.41}$$

An expression for the characteristic combustion time τ_c in terms of the mass fractions and the dimensionless pressure $\widetilde{P} = P/P_0$ and temperature $\widetilde{T} = T/T_0$ is given by

$$\begin{aligned} \frac{1}{\tau_c} &\overset{(5.25)}{=} \frac{\dot{Q}}{c_p \rho_0 T_0} \overset{(5.31)}{=} \frac{\dot{R}_f \Delta H_f}{c_p \rho_0 T_0} \\ &\overset{(5.32)}{=} \frac{\Delta H_f}{c_p T_0} \rho_0 T_0^{1/2} \widehat{A} \frac{\widetilde{P}^2}{\widetilde{T}^{3/2}} Y_o Y_f \exp \left(-\frac{E_A}{R_u T_0 \widetilde{T}} \right). \end{aligned} \tag{5.42}$$

Richards et al. simplified the equations by assuming stoichiometric inlet conditions and complete combustion, i.e., burnt fuel is completely converted to carbon dioxide and water molecules. Then, at all times the oxygen mass fraction is given by $Y_o = S_r Y_f$. Substituting this expression for Y_o in (5.42) and writing $A' = \widehat{A} \rho_0 T_0^{1/2} S_r$ and $\widetilde{T}_{\text{act}} = E_A / R_u T_0$ gives

$$\frac{1}{\tau_c} = A' \frac{\Delta H_f}{c_p T_0} \frac{\widetilde{P}^2}{\widetilde{T}^{3/2}} Y_f^2 \exp(-\widetilde{T}_{\text{act}} / \widetilde{T}). \tag{5.43}$$

Values used by Richards et al. for propane reaction were obtained from a paper by Kretschmer and Odgers [18] and are given by $A' = 3.85 \times 10^8 \, \text{s}^{-1}$ and $\widetilde{T}_{\text{act}} = 50$, where the value $\widetilde{T}_{\text{act}}$ corresponds to an activation energy of 30 kcal/kmol.

Richards et al. remark that this reaction rate can be used for fuel lean combustion, although the computed oxygen levels will be artificially low in that case. But this seems to be inconsistent with the general reaction rate that is described in the paper of Kretschmer and Odgers [18], on which Richards et al. based their reaction rate parameters. The general reaction rate that is given in the article of Kretschmer and Odgers depends on the equivalence ratio, which is absent in the reaction rate that Richards et al. prescribed. How the reaction rate of Richards et al. is distilled from the one given by Kretschmer and Odgers should be examined more closely.

5.2.5 Coupling to tailpipe dynamics by conservation of momentum

For the coupling of gases exiting the combustion chamber with the dynamics in the tailpipe it is assumed that the gases in the tailpipe move as a slug flow, i.e., moving as a whole under the pressure difference between the entrance of the tailpipe and the exit of the tailpipe (at atmospheric pressure). A certain wall friction force F_f is assumed to be acting in the tailpipe. Applying Newton's law then gives

$$(P_e - P_0)A_{tp} + F_f = \int_{\Omega_{tp}} \rho \, dV \, \frac{du}{dt}, \tag{5.44}$$

where A_{tp} is the tailpipe cross-section area, u is the velocity of the tailpipe gases (taken positive if directed toward the tailpipe exit), and the integral is taken over the tailpipe volume. Richards et al. approximate the volume integral of the density in the tailpipe by

$$\int_{\Omega_{tp}} \rho \, dV = \rho_e A_{tp} L_{tp}, \tag{5.45}$$

where L_{tp} is the tailpipe length (i.e., $A_{tp}L_{tp}$ is the tailpipe volume), yields

$$(P_e - P_0)A_{tp} + F_f = \rho_e A_{tp} L_{tp} \frac{du}{dt}. \tag{5.46}$$

Note that Richards et al. assume that the (average) density in the tailpipe at any moment is equal to the density of the gases entering the tailpipe at that moment. This means that at moments of low density at the tailpipe entrance, the mass of the gases in the tailpipe is underestimated, while it is overestimated when the density is high. Therefore an error in the velocity of the gases in the tailpipe is produced. The impact of the error introduced in the velocity is not clear. The fact that the velocity appears not only in the momentum equation, but, via the mass outflow ($\dot{m}_e$), also in the model equations for the pressure and temperature, obscures it even further.

The issue can easily be resolved by introducing an extra differential equation, which describes the rate of change of the average density in the tailpipe. Using $\rho_{tp} = \frac{m_{tp}}{V_{tp}}$ for the average density in the tailpipe, where m_{tp} denotes the mass of the tailpipe gases and $V_{tp} = L_{tp}A_{tp}$ is the tailpipe volume, and assuming that the tailpipe gases are of uniform density and flow toward the tailpipe exit, it follows that

$$\frac{d\rho_{tp}}{dt} = \frac{1}{V_{tp}} \lim_{\Delta t \to 0} \frac{\Delta m_{tp}}{\Delta t} = \frac{(\rho_e - \rho_{tp})A_{tp}u}{V_{tp}} = \frac{(\rho_e - \rho_{tp})u}{L_{tp}}. \tag{5.47}$$

Instead of the density ρ_e at the tailpipe entrance, the average density of the tailpipe gases ρ_{tp} should be used in the derivation of the momentum equation.

Preliminary results incorporating the adjustments to the tailpipe density as described above, suggest that the modifications may have a significant effect. For example, under the default parameter values introduced later in this chapter, adjusting the momentum equation as described above decreases the peak-to-peak pressure amplitude of oscillations in the combustion system from $71\,\text{kPa}$ to $47\,\text{kPa}$, and increases the frequency from $150\,\text{Hz}$ to $164\,\text{Hz}$. However, since

this chapter is focused on evaluation of the model and numerical results of Richards et al., the differential equation for the average density in the tailpipe and associated changes to the model equations are not implemented here.

A characteristic velocity u_c and an associated second characteristic length L_2 are defined by

$$u_c \equiv \frac{\dot{m}_i}{\rho_0 A_{tp}} = \frac{Z_i}{\rho_0} \frac{V_{cc}}{A_{tp}} = \frac{1}{\tau_f} \frac{V_{cc}}{A_{tp}} \qquad (5.48)$$

and

$$L_2 \equiv \frac{V_{cc}}{A_{tp}}. \qquad (5.49)$$

Thus $L_2 = u_c \tau_f$, expressing the characteristic length L_2 in terms of the characteristic velocity u_c and the flow time τ_f. Introducing the dimensionless velocity $\widetilde{u} = u/u_c$ and the dimensionless state variables $\widetilde{P}_e = P_e/P_0$, $\widetilde{T}_e = T_e/T_0$, $\widetilde{\rho}_e = \rho_e/\rho_0$, equation (5.46) can be written as

$$P_0(\widetilde{P}_e - 1)A_{tp} + F_f = A_{tp}L_{tp}\rho_0\widetilde{\rho}_e \frac{L_2}{\tau_f} \frac{d\widetilde{u}}{dt} \qquad (5.50)$$

and thus

$$\frac{d\widetilde{u}}{dt} = (\widetilde{P}_e - 1) \frac{P_0\tau_f}{L_{tp}L_2\rho_0\widetilde{\rho}_e} + \frac{\tau_f}{L_2} \frac{F_f}{A_{tp}L_{tp}\rho_0\widetilde{\rho}_e}. \qquad (5.51)$$

The friction force in the tailpipe is given by the product of the surface area of the tailpipe wall and the friction shear stress at the wall. Taking the tailpipe to be cylindrical, its surface area is given by $\pi D_{tp}L_{tp}$, where D_{tp} is the tailpipe diameter. Using Schlichting's [26, pp. 596–597] friction shear stress on the tailpipe wall $\tau_{\text{wall}} = \frac{1}{8}f\rho_e u^2$, where f is the dimensionless coefficient of resistance (here called the friction coefficient), the wall friction force can be expressed as

$$F_f = -\frac{1}{8}(\pi D_{tp} L_{tp})f\rho_e u^2 \frac{u}{|u|} = -\frac{\pi}{8}D_{tp} L_{tp} f\rho_0\widetilde{\rho}_e \left(\frac{L_2}{\tau_f}\right)^2 \widetilde{u}^2 \frac{\widetilde{u}}{|\widetilde{u}|}, \qquad (5.52)$$

where the factor $-u/|u|$ gives the right direction of the friction force, i.e., against the flow direction. Substitution of this expression for the friction force into equation (5.51) and using the relations $P_e = \rho_e RT_e$, $P_0 = \rho_0 RT_0$ (thus $\widetilde{\rho}_e = \widetilde{P}_e/\widetilde{T}_e$) and $A_{tp} = \frac{\pi}{4}D_{tp}^2$ gives

$$\frac{d\widetilde{u}}{dt} = (\widetilde{P}_e - 1) \frac{RT_0\tau_f}{L_{tp}L_2} \frac{\widetilde{T}_e}{\widetilde{P}_e} - \frac{L_2 f}{2D_{tp}\tau_f} \frac{\widetilde{u}^3}{|\widetilde{u}|}. \qquad (5.53)$$

5.2.6   Complete set of model equations

As mentioned before, the state variables in the tailpipe entrance are obtained by isentropic acceleration of the gases leaving the combustion chamber to the tailpipe entrance Mach number. For completeness, the equations relating the pressures and temperatures in the tailpipe and the combustion chamber are worked out below. Richards et al. do not explicitly describe how the state variables at the tailpipe entrance are obtained, except that isentropic acceleration/deceleration is used.

By using the total state relations (5.7), the state variables in the tailpipe can be expressed in their total (or, stagnation) variables, which, for flow from

the combustion chamber into the tailpipe, are equal to the state variables in the combustion chamber. Using the Mach number $M_e = u/\sqrt{\gamma R T_e}$ for the tailpipe flow, this yields

$$\frac{T}{T_e} = 1 + \frac{\gamma - 1}{2} M_e^2 = 1 + \frac{\gamma - 1}{2} \frac{u^2}{\gamma R T_e}, \tag{5.54}$$

$$\frac{P}{P_e} = \left(\frac{T}{T_e} \right)^{\frac{\gamma}{\gamma - 1}}. \tag{5.55}$$

Solving equation (5.54) for T_e gives

$$T_e = T - \frac{\gamma - 1}{2} \frac{u^2}{\gamma R} = T \left(1 - \frac{\gamma - 1}{2} \frac{u^2}{\gamma R T} \right). \tag{5.56}$$

Thus, the temperature and pressure at the tailpipe entrance, in normalized form, are given by

$$\widetilde{T}_e = \widetilde{T} \left(1 - \frac{\gamma - 1}{2} \left(\frac{L_2}{\tau_f} \right)^2 \frac{\widetilde{u}^2}{\gamma R T_0 \widetilde{T}} \right), \tag{5.57}$$

$$\widetilde{P}_e = \widetilde{P} \left(\frac{\widetilde{T}_e}{\widetilde{T}} \right)^{\frac{\gamma}{\gamma - 1}}. \tag{5.58}$$

Note that, because the state variables at the tailpipe entrance are derived from those in the combustion chamber (via isentropic acceleration), these equations are valid only for flow from the combustion chamber into the tailpipe.

The last term that needs to be specified to complete the mathematical model is Z_e/ρ_0. This term is specified by considering mass conservation: with $\dot{m}_e = A_{tp} \rho_e u$ it follows that

$$\frac{\dot{m}_e}{\rho_0} = A_{tp} u_c \widetilde{\rho}_e \widetilde{u} = A_{tp} \frac{L_2}{\tau_f} \widetilde{\rho}_e \widetilde{u} \tag{5.59}$$

and thus, by definitions of Z_e and L_2 and since $\widetilde{\rho}_e = \widetilde{P}_e/\widetilde{T}_e$,

$$\frac{Z_e}{\rho_0} = \frac{\dot{m}_e}{\rho_0 V_{cc}} = \frac{A_{tp}}{V_{cc}} \frac{L_2}{\tau_f} \widetilde{\rho}_e \widetilde{u} = \frac{1}{\tau_f} \frac{\widetilde{P}_e}{\widetilde{T}_e} \widetilde{u}, \tag{5.60}$$

completing the model equations.

The model equations are summarized by

$$\frac{d\widetilde{P}}{dt} = \gamma \left(\frac{1}{\tau_f} + \frac{1}{\tau_c} + \frac{1}{\tau_{HT}} \right) - \gamma \left(\frac{Z_e}{\rho_0} + \frac{1}{\tau_{HT}} \frac{T_0}{T_w} \right) \widetilde{T}, \tag{5.61}$$

$$\frac{d\widetilde{T}}{dt} = \gamma \left(\frac{1}{\tau_f} + \frac{1}{\tau_c} + \frac{1}{\tau_{HT}} \right) \frac{\widetilde{T}}{\widetilde{P}}$$
$$\quad - \left((\gamma - 1) \frac{Z_e}{\rho_0} + \frac{1}{\tau_f} + \frac{\gamma}{\tau_{HT}} \frac{T_0}{T_w} \right) \frac{\widetilde{T}^2}{\widetilde{P}}, \tag{5.62}$$

$$\frac{d\widetilde{u}}{dt} = (\widetilde{P}_e - 1) \frac{R T_0 \tau_f}{L_{tp} L_2} \frac{\widetilde{T}_e}{\widetilde{P}_e} - \frac{L_2 f}{2 D_{tp} \tau_f} \frac{\widetilde{u}^3}{|\widetilde{u}|}, \tag{5.63}$$

$$\frac{dY_f}{dt} = \frac{\widetilde{T}}{\widetilde{P}} \left(\frac{1}{\tau_f} (Y_{f,i} - Y_f) - \frac{1}{\tau_c} \frac{c_p T_0}{\Delta H_f} \right). \tag{5.64}$$

The time-dependent variables at the tailpipe entrance (found from isentropic acceleration of the gases in the combustion chamber) and the time-dependent combustion time τ_c are given by

$$\widetilde{T}_e = \widetilde{T}\left(1 - \frac{\gamma-1}{2}\left(\frac{L_2}{\tau_f}\right)^2 \frac{\widetilde{u}^2}{\gamma R T_0 \widetilde{T}}\right), \tag{5.65}$$

$$\widetilde{P}_e = \widetilde{P}\left(\frac{\widetilde{T}_e}{\widetilde{T}}\right)^{\frac{\gamma}{\gamma-1}}, \tag{5.66}$$

$$\frac{Z_e}{\rho_0} = \frac{1}{\tau_f}\frac{\widetilde{P}_e}{\widetilde{T}_e}\widetilde{u}, \tag{5.67}$$

$$\frac{1}{\tau_c} = A'\frac{\Delta H_f}{c_p T_0}\frac{\widetilde{P}^2}{\widetilde{T}^{3/2}}Y_f^2 \exp(-\widetilde{T}_{\text{act}}/\widetilde{T}). \tag{5.68}$$

The constant parameters are given by

$$L_1 = \frac{V_{cc}}{A_s}, \tag{5.69}$$

$$L_2 = \frac{V_{cc}}{A_{tp}}, \tag{5.70}$$

$$\tau_f = \frac{\rho_0}{Z_i} = \frac{\rho_0 V_{cc}}{\dot{m}_i}, \tag{5.71}$$

$$\tau_{HT} = \frac{c_p L_1 \rho_0 T_0}{\widehat{h}T_w}. \tag{5.72}$$

5.3 Numerical implementation

In this and the following section, the system of model equations (5.61)–(5.72) is numerically investigated. This section focuses on the numerical implementation of the model equations. Numerical results will be discussed in the next section. First the system of model equations (5.61)–(5.72) is rewritten to a form more suitable for numerical implementation, as will be explained below.

5.3.1 Rewriting the model equations

Close inspection of the system of equations (5.61)–(5.72) reveals that numerical implementation of several parameters needs to be done carefully. It concerns the 'characteristic times': τ_f, τ_c and τ_{HT}. Of these parameters, only the inverse of τ_c and τ_{HT} are used, while τ_f shows up in the equations both inverted and not inverted. For the sake of numerical experimenting, it is useful if in the numerical implementation of the model equations the heat transfer to the combustion chamber wall can be 'turned off' (for example by specifying $\widehat{h} = 0$) or that the combustion process can be 'turned off' (for example by specifying $\Delta H_f = 0$). A glance at expression (5.72) for τ_{HT} (with $\widehat{h}$ in its denominator) makes it clear that this parameter should be implemented numerically by specifying and using only its inverse. The same goes for τ_c (see expression (5.68)), although the factor $\frac{1}{\tau_c}$ in the term $\frac{1}{\tau_c}\frac{c_p T_0}{\Delta H_f}$ in equation (5.64) should be substituted by the expression (5.68), yielding $A'\frac{\widetilde{P}^2}{\widetilde{T}^{3/2}}Y_f^2 \exp(-\widetilde{T}_{\text{act}}/\widetilde{T})$ for the term in equation

(5.64). Implementing τ_f so that its inverse $\frac{1}{\tau_f} = \frac{\dot{m}_i}{\rho_0 V_{cc}}$ may take the value 0 is rather complicated (if not impossible) because both τ_f (in (5.63)) and $\frac{1}{\tau_f}$ (in (5.61)–(5.65) and in (5.67)) are used. It is useful to be able to freely specify the mass influx $\dot{m}_i$, and thus $1/\tau_f$, including the value 0 because then the model equations can be used to describe a pulse combustor with varying mass inflow (e.g., in the case of a combustor equipped with flapper valves). The problems with the parameter τ_f arise from the non-dimensionalizing of the velocity of the fluid in the tailpipe with the factor $u_c = L_2/\tau_f$ (see expressions (5.48) and (5.49)). It is clear that in case of a pulse combustor with flapper valves, for example, the mass inflow and the fluid velocity in the tailpipe are hardly directly related. A more natural factor for non-dimensionalizing the fluid velocity in the tailpipe would be the speed of sound of the ambient environment $\sqrt{\gamma R T_0}$, with which the speed in the tailpipe (and thus the particle velocity in the tailpipe) can be compared. Retracing the steps leading to the system of model equations (5.61)–(5.72) shows that all the parameters τ_f in equations (5.61), (5.62) and (5.64) are related to the mass influx $\dot{m}_i$, while all those in equation (5.63) and expressions (5.65) and (5.67) are related to the tailpipe fluid velocity u_c. Thus, the problem with τ_f can be solved by introducing a different characteristic velocity in cases where τ_f is related to (the inverse of) the tailpipe velocity and numerically implementing and using only the inverse of τ_f where τ_f is related to (the inverse of) the mass influx. Then the value $\dot{m}_i = 0$ can be used (yielding $\frac{1}{\tau_f} = 0$).

The system of model equations (5.61)–(5.72) will now be rewritten, taking into account the comments mentioned above. A characteristic speed for the fluid velocity in the tailpipe is denoted by u_0 in order to avoid confusion with the u_c used earlier. The following substitutions are made in the model equations (5.61)–(5.72). The parameter $1/\tau_f$ is replaced by the constant A in equations where it is associated with the mass influx, thus in model equations (5.61), (5.62) and (5.64); it is replaced by u_0/L_2 where it is associated with the tailpipe fluid velocity, thus in (5.63), (5.65) and (5.67). The parameter $1/\tau_c$ (see (5.68)) is written as $1/\tau_c = B \cdot RR$, with $B = \frac{\Delta H_f}{c_p T_0}$ and RR the reaction rate per unit of mass $RR = \frac{\dot{R}_f}{\rho_0} = A' \frac{\tilde{P}^2}{\tilde{T}^{3/2}} Y_f^2 \exp(-\tilde{T}_{\text{act}}/\tilde{T})$ (see (5.38)). To be able to vary the wall temperature T_w independently of the heat transfer coefficient $\widehat{h}$ the parameter $\frac{1}{\tau_{HT}}$ is replaced by $\frac{1}{\tau_{HT}} = CD$ with $C = \frac{\widehat{h}}{c_p L_1 \rho_0}$ and $D = \frac{T_w}{T_0}$. For ease of notation three extra constants are introduced. Two are given by the constants in the two terms of the equation (5.63) for the tailpipe fluid velocity: $E = \frac{RT_0}{L_{tp} u_0}$ and $F = \frac{f u_0}{2 D_{tp}}$. (Note that the substitution $u_0 = \frac{L_2}{\tau_f}$ is applied.) The term $\frac{\tilde{u}^3}{|\tilde{u}|}$ in the same equation is replaced with the equivalent $\tilde{u}|\tilde{u}|$, thereby avoiding divisions by zero. The third extra constant, G, is given by defining $\widetilde{Z}_e \equiv \frac{\tilde{P}_e}{\tilde{T}_e} \tilde{u}$ (cf. expression (5.67), coming from (5.60)) and requiring that $G\widetilde{Z}_e = \frac{Z_e}{\rho_0}$. Using expression (5.60) this gives $G = \frac{u_0}{L_2}$. The differential equation for the temperature (5.62) is replaced by the equivalent equation (5.29) from which the final form was found. Since $\frac{d\tilde{P}}{dt}$ must be computed anyway, this saves some computations and is more compact. Note that the equation for the temperature (5.62) could also be replaced by the much simpler equation for the density (5.27), and then use the perfect gas law to obtain the temperature. In

order to be able to make a direct comparison of the results obtained here with those obtained by Richards et al., this will not be implemented.

The adjusted equations are:

$$\frac{d\widetilde{P}}{dt} = \gamma \left(A + B \cdot RR + CD - (C + G\widetilde{Z}_e)\,\widetilde{T} \right), \tag{5.73}$$

$$\frac{d\widetilde{T}}{dt} = \left(\frac{d\widetilde{P}}{dt} - (A - G\widetilde{Z}_e)\widetilde{T} \right) \frac{\widetilde{T}}{\widetilde{P}}, \tag{5.74}$$

$$\frac{d\widetilde{u}}{dt} = E(\widetilde{P}_e - 1) \frac{\widetilde{T}_e}{\widetilde{P}_e} - F\,\widetilde{u}\,|\widetilde{u}|, \tag{5.75}$$

$$\frac{dY_f}{dt} = (A(Y_{f,i} - Y_f) - RR) \frac{\widetilde{T}}{\widetilde{P}}, \tag{5.76}$$

where RR, $\widetilde{P}_e$, $\widetilde{T}_e$ and $\widetilde{Z}_e$ are functions of $\widetilde{P}$, $\widetilde{T}$, $\widetilde{u}$ and Y_f given by

$$RR = A' \frac{\widetilde{P}^2}{\widetilde{T}^{3/2}} Y_f^2 \exp(-\widetilde{T}_{\mathrm{act}}/\widetilde{T}), \tag{5.77}$$

$$\widetilde{T}_e = \widetilde{T} \left(1 - \frac{\gamma - 1}{2} \frac{u_0^2}{\gamma R T_0} \frac{\widetilde{u}^2}{\widetilde{T}} \right), \tag{5.78}$$

$$\widetilde{P}_e = \widetilde{P} \left(\frac{\widetilde{T}_e}{\widetilde{T}} \right)^{\frac{\gamma}{\gamma-1}}, \tag{5.79}$$

$$\widetilde{Z}_e = \frac{\widetilde{P}_e}{\widetilde{T}_e} \widetilde{u} \tag{5.80}$$

and A, B, C, D, E, F and G are constants given by

$$A = \frac{1}{\tau_f} = \frac{\dot{m}_i}{\rho_0 V_{cc}}, \tag{5.81}$$

$$B = \frac{\Delta H_f}{c_p T_0}, \tag{5.82}$$

$$C = \frac{\widehat{h}}{L_1 c_p \rho_0}, \tag{5.83}$$

$$D = \frac{T_w}{T_0}, \tag{5.84}$$

$$E = \frac{R T_0}{L_{tp} u_0}, \tag{5.85}$$

$$F = \frac{u_0 f}{2 D_{tp}}, \tag{5.86}$$

$$G = \frac{u_0}{L_2}. \tag{5.87}$$

The constants L_1 and L_2 are the two characteristics lengths introduced before. Their definitions are repeated below for convenience:

$$L_1 = \frac{V_{cc}}{A_s}, \tag{5.88}$$

$$L_2 = \frac{V_{cc}}{A_{tp}}. \tag{5.89}$$

Variable	Initial value	Unit
$\widetilde{P}$	1.0	–
$\widetilde{T}$	5.0	–
$\widetilde{u}$	0.0	–
Y_f	0.06	–

Table 5.1: Initial conditions for the numerical evaluation of model equations (5.73)–(5.89). These are the same initial conditions as used by Richards et al. [25].

The adjusted model equations can be implemented numerically without difficulty.

5.3.2 Specifying model parameters and initial conditions

The system of model equations (5.73)–(5.89) is numerically implemented using MATLAB [29] software. The standard MATLAB ODE-solver `ode45`[1] is used to solve the equations. The implementation in MATLAB is straightforward; the codes used can be found in Appendix C.

In order to evaluate the system of model equations (5.73)–(5.89) numerically, the model parameters and suitable initial conditions need to be specified. Where possible, these are chosen equal to those used by Richards et al. The initial conditions and most parameter values are stated clearly in the article of Richards et al., but some critical parameter values are not specified explicitly. This causes some difficulties in trying to reproduce their numerical results. The choices for the model parameters not specified by Richards et al. are discussed below.

The initial conditions used by Richards et al. are given in Table 5.1; they are also used for the numerical evaluation in this report. The values correspond to a combustion chamber that is filled with a stoichiometric fuel-air mixture at ambient pressure, with no outflow and a temperature that is high enough to get the combustion process going immediately. This choice of initial conditions (for the temperature in particular) may be unrealistic, but Richards et al. mention that the choice of initial conditions did not affect the final results.

The model parameters that are specified explicitly by Richards et al., and that are used for the numerical evaluation of the model equations in this report, are given in Table 5.2. Richards et al. based these values on properties of the thermal pulse combustor they used in experiments, running on propane as fuel.

Values for the model parameters that are not specified explicitly by Richards et al., are presented in Table 5.3. The choices for the ambient pressure P_0 and temperature T_0 are natural. The choice for R (equal to that of air) is less natural than it seems; this will be discussed below. Choosing the specific heat, c_p, and the ratio of specific heats, γ, is more difficult, since they depend on the temperature of the mixture in the combustion chamber, as well as on its composition. Note that because of the relation $R = c_p - c_v = c_p \frac{\gamma - 1}{\gamma}$ used in the derivation of the model equations, the parameters c_p, γ and R cannot be specified independently of each other. The values chosen for c_p and γ are based

---

[1]See footnote 2 on page 18

Parameter	Value used	Unit
A'	3.85×10^8	s^{-1}
D_{tp}	0.0178	m
f	0.030	–
$\widehat{h}$	120	$\text{W/m}^2/\text{K}$
L_1	0.0119	m
L_2	0.8486	m
L_{tp}	0.6100	m
$\widetilde{T}_{\text{act}}$	50	–
T_w	1000	K
$Y_{f,i}$	0.06	–
τ_f	0.030	s

Table 5.2: Model parameters for the evaluation of model equations (5.73)–(5.89), as specified by Richards et al. in their article [25].

Parameter	Value used	Unit
c_p	1350	$\text{J/kg} \cdot \text{K}$
P_0	1.01325×10^5	Pa
R	287	$\text{J/kg} \cdot \text{K}$
T_0	300	K
u_0	$= \sqrt{\gamma R T_0}$	m/s
ΔH_f	5×10^7	J/kg
γ	$= c_p/(c_p - R)$	–
ρ_0	$= P_0/R T_0$	kg/m^3

Table 5.3: Model parameters for the numerical evaluation of model equations (5.73)–(5.89) that are not (explicitly) specified by Richards et al. in their article [25].

on those specified in some articles in which the model equations of Richards et al. are used. These choices will be discussed below.

Specifying the gas constant

The gas constant R is chosen to be that of air (i.e., $R = 287\,\mathrm{J/kg \cdot K}$, see Table 2, p.343 of Reference [27]). This seems a natural choice, since it is used in the derivation of the model equations to define the ambient density $\rho_0 = P_0/RT_0$. But it should be noted that it is also used as the gas constant of the mixture in the combustion chamber, as can be seen from the relation $P = \rho RT$. Since the value of the gas constant depends on the composition of the mixture, some kind of average value should be specified. Given that the fuel is propane (C_3H_8), as used by Richards et al., the gas constants for the reactants (R_r) and the products (R_p) are easily calculated from the molecular weights of the compounds forming the mixtures. From the reaction equation

$$C_3H_8 + 5\,(O_2 + 3.76\,N_2) \quad \longrightarrow \quad 3CO_2 + 4\,H_2O\ (g) + 18.8\,N_2, \qquad (5.90)$$

it follows that the molecular weights of the reactants (MW_r) and products (MW_p) are given by

$$
\begin{aligned}
MW_r &= \chi_{C_3H_8}MW_{C_3H_8} + \chi_{O_2}MW_{O_2} + \chi_{N_2}MW_{N_2} \qquad (5.91) \\
&= \frac{44.094 + 5 \cdot 31.999 + 18.8 \cdot 28.013}{24.8} = 29.465\,\mathrm{g/mol}
\end{aligned}
$$

and

$$
\begin{aligned}
MW_p &= \chi_{CO_2}MW_{CO_2} + \chi_{H_2O}MW_{H_2O} + \chi_{N_2}MW_{N_2} \qquad (5.92) \\
&= \frac{3 \cdot 44.010 + 4 \cdot 18.015 + 18.8 \cdot 28.013}{25.8} = 28.323\,\mathrm{g/mol}.
\end{aligned}
$$

Here χ_X denotes the molal fraction of a compound X. The values for the molecular weights of the compounds are obtained from Reference [27, Table 2, p.344]. The gas constants are given by $R_r = R_u/MW_r = 282.2\,\mathrm{J/kg \cdot K}$ and $R_p = R_u/MW_p = 293.6\,\mathrm{J/kg \cdot K}$, where $R_u = 8.31441\,\mathrm{J/mol \cdot K}$ is the universal gas constant (see Reference [27, in back]). The gas constant of a reactants-products mixture in the reaction chamber will lie somewhere in between these two values. It is approximately equal to the gas constant of the ambient environment. Thus, the chosen value for R is rather convenient: a different choice would yield a scaling density ρ_0 different from that of the ambient environment.

Specifying the specific heat and ratio of specific heats

Choosing proper values for the specific heat (c_p) and the associated ratio of specific heats ($\gamma = \frac{c_p}{c_p - R}$) is more complicated, since they depend on the temperature as well as on the composition of the mixture in the combustion chamber. The variation with the temperature of the specific heats of the products and reactants mixtures can be obtained from literature. Table 3s, p.346, from Reference [27] shows the temperature dependency of the molal specific heats at constant pressure, $\bar{c}_p$, for various gases. From this table, the molal specific heat

$$\bar{c}_p = a + bT + cT^2 + dT^3, \quad [T \text{ in K}, \bar{c}_p \text{ in J/mol} \cdot \text{K}]$$

Mixture	a	b	c	d
Reactants	26.88	1.416×10^{-2}	-0.1655×10^{-5}	-0.6336×10^{-9}
Products	28.65	0.6108×10^{-2}	0.3453×10^{-5}	-1.782×10^{-9}

Table 5.4: Temperature dependency of molal specific heats at constant pressure for the reactants and products. Range of validity: 273–1500 K. The values are compiled from Table 3s, p.346, in Reference [27].

of a mixture of compounds, $\bar{c}_{p,\text{mix}}$ can be obtained by using the relation (see Reference [27] for instance):

$$\bar{c}_{p,\text{mix}} = \sum_i \chi_i \bar{c}_{p,i}. \tag{5.93}$$

Here the sum is taken over all compounds of the mixture and χ_i and $\bar{c}_{p,i}$ are the corresponding mass fractions and molal specific heats, respectively. The resulting (polynomial) expressions in temperature for the molal specific heats of the reactants and products are given in Table 5.4. The specific heat at constant pressure of a mixture ($c_{p,\text{mix}}$) can be computed from the molal specific heat ($\bar{c}_{p,\text{mix}}$) by using the relation

$$c_{p,\text{mix}} = \frac{\bar{c}_{p,\text{mix}}}{\text{MW}_{\text{mix}}}, \tag{5.94}$$

where MW_{mix} is the mixture's molecular weight.

Figure 5.2 shows plots of the specific heats at constant pressure for the reactants and products over the temperature range 273–1500 K, the range of validity of the values from the consulted reference. The plots show that the specific heats vary significantly with the temperature. In the specified temperature range, the specific heat rises roughly by $30\,\text{J/kg} \cdot \text{K}$ for every $100\,\text{K}$ the temperature rises.

The mean temperature in the combustion chamber is not known beforehand. It will lie somewhere in between $300\,\text{K}$, the temperature of the reactants upon entrance, and $2267\,\text{K}$, the adiabatic flame temperature of a stoichiometric propane-air mixture (see Table B.1, p.543, in Reference [32]). Without additional information on the combustion process and associated temperatures it is difficult to make a sensible choice for the model parameter c_p.

Choosing parameters based on an average temperature from the numerical results of Richards et al. did not yield the same numerical results. Also, the numerical solution of the model equations is rather sensitive to the choice of the model parameters. Since several model parameters need to be 'guessed' in order to reproduce the numerical results of Richards et al., this means that a process of trial and error is laborious. In the end, the model parameters used for the numerical evaluation of the model equations were obtained from articles [8] (co-authored by Richards) and [12], in which the model of Richards et al. is used.

Both the articles use $c_p = 1200\,\text{J/kg} \cdot \text{K}$ and $\gamma = 1.27$. Using the relation $R = c_p \frac{\gamma - 1}{\gamma}$ gives $R = 255.1\,\text{J/kg} \cdot \text{K}$ for the gas constant, nowhere near the value for the mixture in the combustion chamber computed above. Besides, the numerical results when evaluating the model equations with these parameters
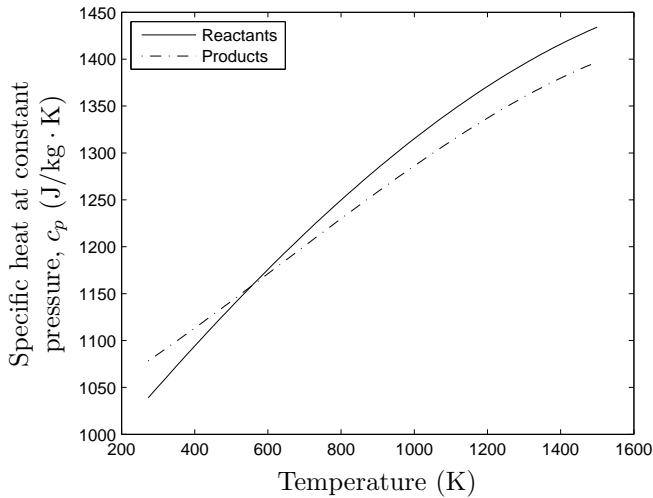
Figure 5.2: Temperature dependency of specific heats at constant pressure of the reactants and products.

are different from those of Richards et al. The specific heat associated with $\gamma = 1.27$ and $R = 287\,\mathrm{J/kg \cdot K}$ is given by $c_p = \frac{R\gamma}{\gamma-1} = 1350.0\,\mathrm{J/kg \cdot K}$. Using these values for the numerical evaluation of the model equations yields results very similar to those of Richards et al., if $\Delta H_f = 5 \times 10^7\,\mathrm{J/kg}$ is used for the heat of combustion. Table B.1, p.543, in Reference [32] gives $\Delta H_f = 4.6357 \times 10^7\,\mathrm{J/kg}$ for the heat of combustion (lower heating value) of propane, so the value used for obtaining the numerical results could be a rough approximation. It should be noted that the numerical solution of the model equations showed a very different behaviour for values of ΔH_f less than $4.88 \times 10^7\,\mathrm{J/kg}$, showing the sensitivity to the model parameters. The article [19] (also co-authored by Richards), found after the numerical results presented in this section were already obtained, also uses these model parameter values (for γ, c_p, R and ΔH_f). This makes it more likely that the values mentioned above were indeed used by Richards et al. in their original article.

A remark on the parameter choices is in order. In none of the articles is the choice for the model parameters c_p and γ motivated. In fact, the choices do not seem to correspond to the mean temperature in the combustion chamber that the numerical evaluation of the model equations yields. Also, the numerical solution of the model equations is sensitive to these parameters. This raises the question whether the solution to the model equations would not show a very different behaviour if the temperature dependency of c_p and γ were accounted for.

5.4 Numerical results and discussion

The model equations were solved with the MATLAB-codes presented in Appendix C. This appendix also contains all the codes that were used to produce the plots

Figure 5.3: Computed dimensionless pressure for the first 300 ms for three different values of the wall temperature. (Cf. Figure 3 in [25].)

in this section. Unless indicated otherwise, the default values presented in Tables 5.1–5.3 were used for the model parameters. To ease the comparison with the numerical results presented by Richards et al., the numerical results are presented in similar graphs. This also facilitates the discussion of the interpretation of the results by Richards et al. All graphs presented below very closely resemble those of Richards et al., but there are slight differences, most notable in the amplitude of the pressure oscillations and in the range of the parameter values over which an oscillatory solution exists (cf. Figures 5.6 and 5.9). The differences may come from a different implementation of the two factors about which the article of Richards et al. is unclear: the choice for certain model parameters and the isentropic acceleration/deceleration of the fluid into/from the tailpipe.

5.4.1 Steady combustion, oscillatory combustion, and flame extinction

Figure 5.3 shows three plots of the computed dimensionless pressure ($\widetilde{P}$) for the first 300 ms for three different values of the combustion chamber wall temperature (T_w). In all cases there are oscillations directly after the starting time, which are caused by the initial conditions. For wall temperatures of 1200 K and 750 K the oscillations quickly die away, while for a wall temperature of 1000 K the initial oscillations are amplified, until damping processes and nonlinearity
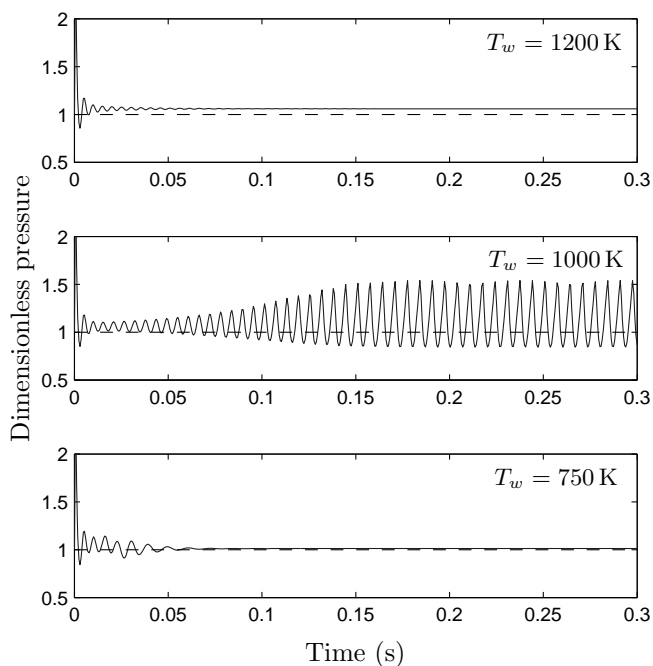
Figure 5.4: Computed dimensionless temperature for the first $50\,\mathrm{ms}$ for three different values of the wall temperature. (Cf. Figure 4 in [25].)

in the model equations limit further amplification.

Figure 5.4 shows graphs of the computed dimensionless temperature $(\widetilde{T})$ for the three wall temperatures for the first 50 ms. Figure 5.5 shows corresponding graphs of the computed fuel mass fraction (Y_f). These graphs indicate that for a wall temperature of 750 K the combustion ceases: the fuel mass fraction approaches the value at inflow and the temperature drops to about the ambient value. For a wall temperature of 1200 K the combustion becomes steady: the fuel mass fraction approaches a constant value below that of the inflow and the temperature approaches a constant value far above the ambient.

Richards et al. note that the three graphs for the temperature (cf. Figure 5.4) are very similar for the first 10 ms and that from this the influence of the wall temperature can be seen. A higher wall temperature slightly increases the temperature in the combustion chamber and "alters the relative phase during the initial oscillations."

Richards et al. attribute the extinguishing of the flame in case of a wall temperature of 750 K to heat loss. Why the case of a wall temperature of 1000 K shows an oscillating behaviour while the case of a wall temperature of 1200 K does not, is explained by Richards et al. as follows. If the reaction rate is lower than the supply rate, a surplus of fuel is built up in the combustion chamber. Reduction in the gas outflow causes the temperature to rise because more hot combustion products remain in the combustion chamber and because of adiabatic compression. This temperature rise increases the reaction rate, such that the fuel surplus is consumed by combustion. Richards et al. state that the two causes of temperature rise (the remaining of more hot products and the adiabatic compression) "[...] are associated with increasing pressure in the combustion chamber," and that "the result is an increasing reaction rate at the time of increasing pressure which is in accordance with the classic Rayleigh
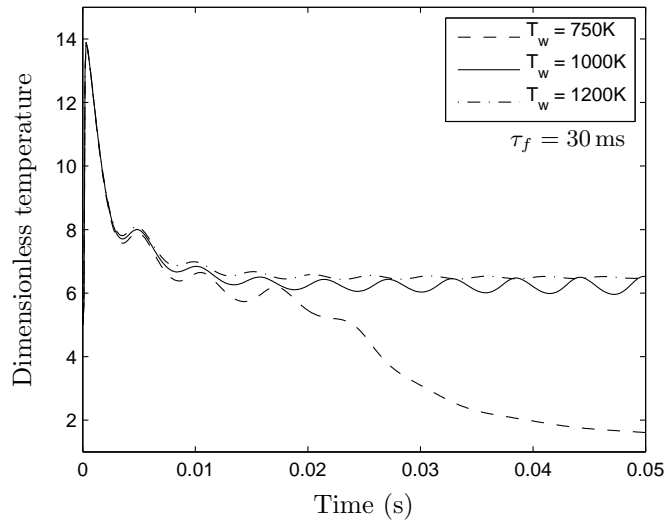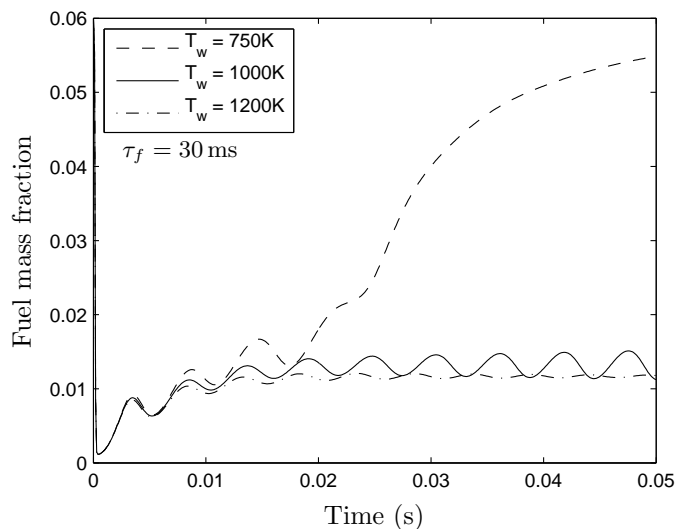
Figure 5.5: Computed fuel mass fraction for the first 50 ms for three different values of the wall temperature. (Cf. Figure 5 in [25].)

criterion for sustained combustion oscillations [...]." Richards et al. then suggest that with the lower wall temperature (1000 K), a fuel surplus needed to drive the oscillations can be build up, but that in case of the higher wall temperature (1200 K) "the faster reactions which result from higher gas temperatures do not allow a surplus of fuel, so that a limited variation in reaction rate occurs, and the oscillation eventually dies out." To illustrate these processes, they refer to graphs of the fuel mass fraction (cf. Figure 5.5), which show that "the peak fuel mass fraction is higher in the 1000 K case than the 1200 K case, providing the surplus fuel transients needed to drive the oscillations."

Two remarks on this explanation are given below. First, while the Rayleigh criterion is, of course, satisfied for the heat release caused by adiabatic compression, this may not be so for the heat release caused by the remaining of more hot products. That mechanism for temperature rise is coupled to the gas velocity in the tailpipe and therefore there is an associated phase difference with the pressure oscillations, which obscures its effect on these oscillations.

Second, the explanation is unsatisfactory in that it does not address how the faster reactions in case of higher wall temperatures prevent a build up of fuel surplus. In fact, it seems to confuse cause and effect. If heat release is in phase with the pressure oscillations (satisfying Rayleigh's criterion), the pressure oscillations are amplified. If the amplification is enough to overcome the damping processes, every cycle energy will be added to the oscillations. Thus, even the slightest of oscillations may grow to finite amplitude oscillations; no fuel surplus is needed for this. So, the question remains why the amplification of the oscillations (by heat release at moments of increased pressure) is enough to overcome the damping effects in case of a 1000 K wall temperature, while it is not enough in case of a 1200 K wall temperature.

The answer probably lies in the phasing of the heat release relative to the

pressure oscillations. The higher reaction rates associated with higher wall temperatures cause the reactants to be burnt *earlier* in the cycle. The more favorable the phasing of the heat release and the pressure oscillations is (i.e. peaking at the same moments), the more energy is added to the oscillations. It would seem that the phasing in case of the 1000 K wall temperature is favorable enough to overcome the damping effects, while it is not favorable enough (i.e. the reactants are burnt too early in the cycle) in case of the 1200 K wall temperature. Note that it remains to be seen whether the altering of "the relative phase during the initial oscillations" with increasing wall temperature (cf. Figure 5.4) that was mentioned by Richards et al., is caused by the phase difference of heat release and pressure oscillations, or that it is caused by other (or, additional) processes, for example by an increase in frequency due to increased temperature.

An indication, from preliminary results, that the phase difference between heat release and pressure oscillations changes with change in wall temperature as described above, is that the reaction rate for the 1200 K wall temperature peaks slightly before the moment of highest pressure, while the reaction rate for the 750 K wall temperature peaks slightly after the moment of highest pressure. The fact that with a wall temperature of 1200 K oscillations occur if the friction coefficient is chosen to be $f = 0.02$, shows that damping effects might be important in preventing oscillations (the default value is $f = 0.03$, resulting in steady combustion). An indication of the influence of the change in this phase difference, also from preliminary results, is the following. The reaction rate for the 1000 K wall temperature slightly leads the pressure oscillations in the beginning (the first 50 ms), where the amplitude of the oscillations is small. Thereafter, when the amplitude of the pressure oscillations increases, the reaction rate and pressure oscillations coincide more and more. At 200 ms, when the oscillations are stable, the graph of the reaction rate has changed from a sinusoidal shape to a shape much more peaked at moments of high pressure with broad troughs in between. The change in the shape of the graph of the reaction rate can be attributed to nonlinear effects, among which the build up of a fuel surplus. Eventually, the oscillations are stabilized by these nonlinear effects.

Comment on the characteristic times

To gain further insight into the processes that stimulate or dampen the oscillations, the different terms in the right-hand side of the differential equation for the pressure (5.73) contributing to the pressure change should be examined in more detail. This equation comes from an energy balance over the combustion chamber. The terms in the right-hand side are associated with heat release: addition of heat due to in- and outflow ($A - G\widetilde{Z}_e\widetilde{T}$, in minus out), heat release due to combustion ($B \cdot RR$), and heat addition due to heat transfer from the combustion chamber wall ($C(D - \widetilde{T})$). Note that Richards et al. associated with these terms three 'characteristic times' (a flow time $\tau_f = 1/A$, a combustion time $\tau_c = 1/(B \cdot RR)$, and a heat transfer time $\tau_{HT} = 1/CD$), but that they neglected to incorporate the heat addition/heat loss effects of the outflow from the combustion chamber ($-G\widetilde{Z}_e\widetilde{T}$) and the influence of the temperature on the heat loss to the combustion chamber wall ($-C\widetilde{T}$). A possible influence of the outflow term on the oscillations will be mentioned in Subsection 5.4.4, where the influence of the tailpipe length is discussed. An effect of the temperature in the combustion chamber on the heat loss to the combustion chamber wall

will be mentioned in Subsection 5.4.2, where the influence of the heat transfer coefficient is discussed. More appropriate characteristic times might be given by $1/\tau_f^* = A - G\widetilde{Z}_e^*\widetilde{T}^*$ for the flow time, $1/\tau_c^* = B \cdot RR^*$ for the combustion time and $1/\tau_{HT}^* = C(D - \widetilde{T}^*)$ for the heat transfer time. Here, the starred variables refer to values at some averaged state (i.e., at a mean pressure, temperature, fuel mass fraction and outflow velocity). Note that these characteristic times are only of use close to such an averaged state, since away from this state, nonlinear effects influence the other terms in the energy equation. Some insight into the behaviour of the combustion system can be obtained by exploring the steady states of the system. This is the subject of Section 5.5 entitled "Steady-state solutions and their stability."

5.4.2   Influence of the heat transfer coefficient

Richards et al. mention that the influence of the wall temperature is dependent upon the efficiency of heat transfer to the combustion chamber wall, which is influenced by the heat transfer coefficient. If the heat transfer time defined by Richards et al. ($\tau_{HT} = 1/CD$) were to be characteristic for the combustion process, one might expect a similar change in the behaviour of the system for an increase of either $C = \widehat{h}/L_1 c_p \rho_0$ or $D = T_w/T_0$ by a certain factor. But accounting for the fact that heat loss to the combustion chamber wall is dependent on the temperature in the combustion chamber ($1/\tau_{HT}^* = C(D - \widetilde{T}^*)$), shows that the effect of an increase of C is dependent on whether $D - \widetilde{T}^*$ is positive or negative. Since the combustion chamber wall temperature is usually less than the mean temperature in the combustion chamber, increasing C and increasing D have opposite effects. In case of the results presented in this report, the wall temperature is even below the minimum temperature if no flame extinction occurs, so heat is always lost from the combustion chamber.

Figure 5.6 shows the effect of the heat transfer coefficient on the amplitude of the pressure oscillations. The values of the heat transfer coefficient were varied from $\widehat{h} = 100\,\mathrm{W/m^2 \cdot K}$ to $\widehat{h} = 165\,\mathrm{W/m^2 \cdot K}$ with steps of $5\,\mathrm{W/m^2 \cdot K}$. The peak-to-peak amplitudes of the pressure oscillations were determined from a numerical solution of the pressure on the time interval 1–1.3 s by taking the difference between the maximum and minimum values of the pressure on this interval. For all values of the heat transfer coefficient, the oscillations were stable or had practically vanished on this time interval. When the amplitudes were practically zero, the fuel mass fraction on the time interval was used to determine whether steady combustion had occurred (if the fuel mass fraction was less than the value at inflow) or the combustion had ceased (if the fuel mass fraction was close to the value at inflow).

The graph shows that below $\widehat{h} = 110\,\mathrm{W/m^2 \cdot K}$ steady combustion occurs. This can be attributed to insufficient cooling down after combustion has occurred, due to a lower heat transfer rate: the temperature in the combustion chamber rises, causing the reactants to be burnt too early in the cycle. Somewhere between $\widehat{h} = 110\,\mathrm{W/m^2 \cdot K}$ and $\widehat{h} = 115\,\mathrm{W/m^2 \cdot K}$ the behaviour of the combustion system suddenly changes from steady combustion to an oscillating process. This can be explained by the amplification of pressure oscillations by combustion overcoming the damping terms, due to a more favorable phasing associated with a lower temperature in the combustion chamber. The first second
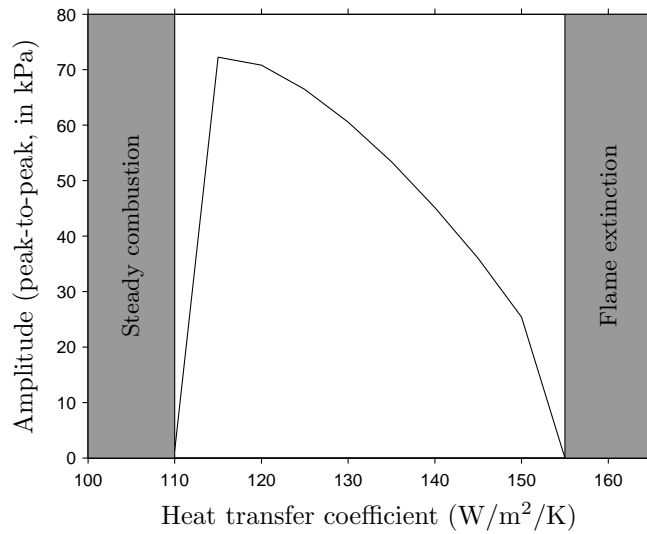
Figure 5.6: Effect of the heat transfer coefficient on the amplitude of the pressure oscillations. (Cf. Figure 6 in [25].)

was enough for the oscillations to be amplified until further increase was limited by nonlinear effects. For larger heat transfer coefficients, the graph shows a decrease in the amplitude. Exactly what processes are responsible for this decrease remains to be determined. One such process is the increased damping due to higher heat losses to the combustion chamber wall. Note that the heat transfer rates are greatest at moments of high temperature and smallest at moments of low temperature. By Rayleigh's criterion this means that the process of heat loss to the combustion chamber wall actually counteracts the oscillatory process. For values of the heat transfer coefficient past a critical value somewhere between $\widehat{h} = 150\,\mathrm{W/m^2 \cdot K}$ and $\widehat{h} = 155\,\mathrm{W/m^2 \cdot K}$, no oscillatory combustion process can be maintained.

5.4.3 Influence of the friction coefficient

Richards et al. noted that the effect of friction in the tailpipe is significant. The effect of decreasing the friction coefficient is to increase the pressure amplitude. This may be expected, since the friction is a damping factor. Figure 5.7 shows graphs of the pressure and velocity, normalized with respect to their maxima, for three values of the friction coefficient. The time interval used for the graphs is from $t = 0.9\,\mathrm{s}$ (when oscillations have become stable) to $t = 0.92\,\mathrm{s}$. The pressure amplitudes were determined from the maximum and minimum pressures on this time interval. Note that the pressure amplitude for the frictionless case (the bottom graph) is much larger than in the cases with friction.

For lower friction coefficients, the graphs show a flow returning to the combustion chamber: the velocity becomes negative. Apparently associated with the negative velocities, are the sudden pressure increases just after the velocity changes from negative to positive. Figure 5.8 shows graphs of the normalized
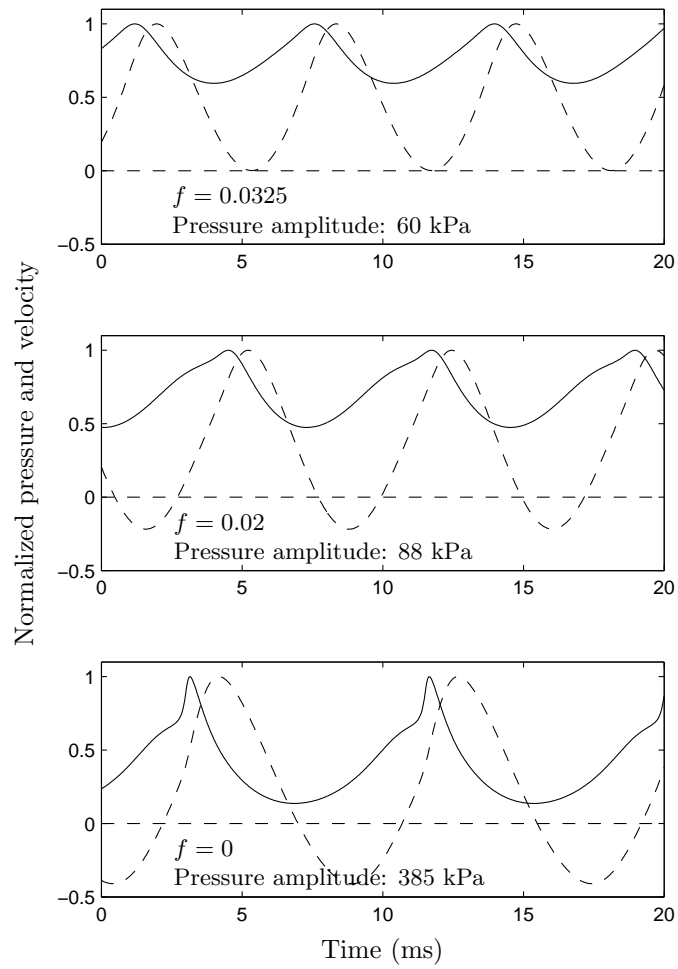
Figure 5.7: Effect of the friction coefficient on the pressure oscillations and the tailpipe gas velocity. (——— Normalized pressure, – – – Normalized velocity) (Cf. Figure 7 in [25].)
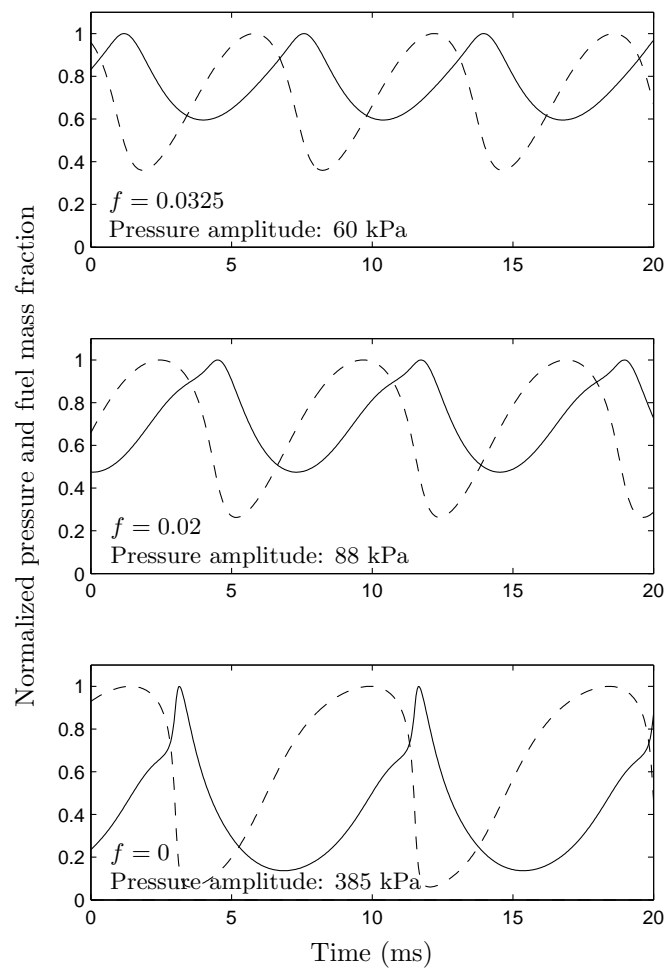
Figure 5.8: Effect of the friction coefficient on the pressure oscillations and the fuel mass fraction at the conditions of Figure 5.7. (—— Normalized pressure, − − − Normalized mass fraction) (Cf. Figure 8 in [25].)

pressure and fuel mass fractions on the same time interval. The drops in fuel mass fraction suggest that the (sudden) pressure rises are caused by increased combustion.

The exact effect of the friction on the combustion process is not clear from these figures. It should be mentioned that for friction coefficients between $f = 0.006$ and $f = 0.016$ the flame is extinguished, while for values below $f = 0.005$ or above $f = 0.017$ oscillations occur, although they are irregular. Closer to the boundary of values for which the flame is extinguished, the oscillation grows more irregular, and flame extinction may occur after longer periods of oscillation. Finally, it should be stressed that the model equations may introduce unrealistic effects if the fluid velocity in the tailpipe becomes negative, as a result of incorrect modelling of the flow into the combustion chamber. (See the remarks in the first new paragraphs after equations (5.10) and (5.40) in Section 5.2 on the derivation of the model equations.) Therefore it is not clear whether the peaks in pressure, occurring after the velocity changes from negative to positive, are 'real' effects, or an artificial result from incorrect modelling.

5.4.4   Influence of the tailpipe length

Following the presentation of Richards et al., the influence of the tailpipe length on the amplitude and frequency of the pressure oscillations is examined next.

The frequencies of the pressure oscillations for different values of the tailpipe length were determined from a discrete Fourier transformation (DFT) of the numerical solution on the time interval from $t = 0.3\,\mathrm{s}$ to $t = 1.3\,\mathrm{s}$. On this interval, the oscillations were either stable or had practically vanished for most values of the tailpipe length. The DFT was computed using the standard MATLAB-function fft, which is an implementation of the fast Fourier transform (FFT). Data used for the FFT were sampled from the numerical solution of the pressure on the time interval from $t = 0.3\,\mathrm{s}$ to $t = 1.3\,\mathrm{s}$ with a sample interval of $\Delta = 1/4096\,\mathrm{s}$. Since the data point $t = 1.3\,\mathrm{s}$ was not included, this gave $N = 4096$ sample values. The frequency resolution was, thus, $f_{\mathrm{res}} = 1/(N\Delta) = 1\,\mathrm{Hz}$ and the Nyquist frequency was $f_{\mathrm{Nyq}} = 2048\,\mathrm{Hz}$. The frequency of the oscillations for each tailpipe length was recognized as a distinct peak in the periodogram. The frequencies were automatically determined by searching for the frequency at which the periodogram was maximum. The peak-to-peak pressure amplitudes were determined by taking the difference of the maximum and minimum of the sampled values of the computed pressure on the time interval from $t = 1\,\mathrm{s}$ to $t = 1.3\,\mathrm{s}$.

The tailpipe values for which the frequencies and amplitudes were determined, range from 0.45 m to 0.85 m with steps of 0.025 m. As before, when the pressure amplitude was practically zero, the fuel mass fraction was used to determine whether there was steady combustion or flame extinction had occurred. The numerical results are shown in Figure 5.9.

Figure 5.9 shows that steady combustion occurs for tailpipe lengths less than some value between $L_{tp} = 0.525\,\mathrm{m}$ and $L_{tp} = 0.55\,\mathrm{m}$. (The computed value for the pressure amplitude at $L_{tp} = 0.525\,\mathrm{m}$ is not zero, but extending the time interval for the numerical solution reveals that the combustion becomes steady for the tailpipe length $L_{tp} = 0.525\,\mathrm{m}$.) The flame is extinguished for tailpipe lengths above a value somewhere between $L_{tp} = 0.75\,\mathrm{m}$ and $L_{tp} = 0.775\,\mathrm{m}$.
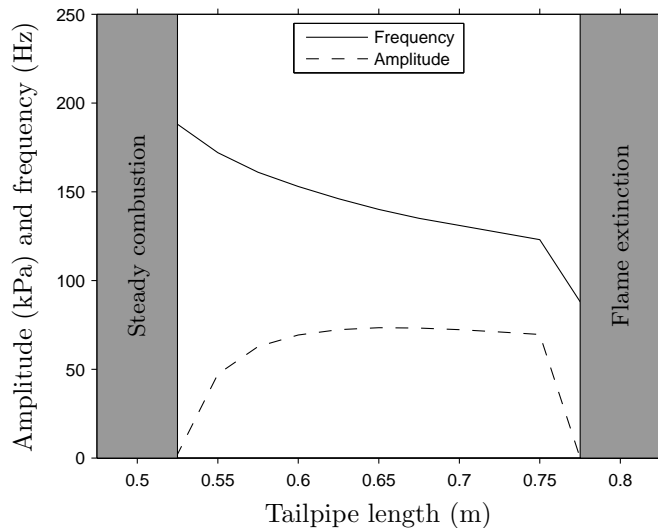
Figure 5.9: Effect of the tailpipe length on amplitude (peak-to-peak) and frequency of pressure oscillations. (Cf. Figure 9 in [25].)

The different behaviour of the modelled combustion system for different values of the tailpipe length can be explained by the phase difference between the heat release and pressure oscillations. For shorter tailpipes, the frequency of the Helmholtz oscillator is greater. Thus, the pressure waves return sooner after the combustion has accelerated. There is less time for the inflow of cold reactants (and the outflow of hot products) to reduce the temperature in the combustion chamber. The reaction rate is higher when the pressure wave returns and combustion occurs earlier in the cycle. If the amplification of the pressure oscillations is not enough to overcome the damping terms (i.e., combustion acceleration occurs too early), steady combustion will occur.

For longer tailpipes, the frequency of the Helmholtz oscillator is less. Thus, pressure waves caused by accelerated combustion take longer to return. In the meantime, the inflow of cold reactants (and the outflow of hot products) reduce the temperature in the combustion chamber. The reaction rate is lower when the pressure wave returns and combustion occurs later in the cycle. If the amplification of the pressure oscillations is not enough to overcome the damping terms (i.e., combustion acceleration occurs too late), the flame will be extinguished.

The outflow term $(-G\widetilde{Z}_e\widetilde{T})$ that was neglected by Richards et al. in defining the characteristic times, has an effect on the temperature of the combustion chamber. Therefore it has an influence on phase difference between heat release and pressure oscillations, and thus on the operation of the thermal pulse combustor.

It is interesting to note that the pressure oscillations at the transition from oscillatory combustion to flame extinction are very irregular, while those at the transition from steady combustion to oscillatory combustion grow from small amplitude oscillations to regular finite amplitude oscillations. The exact cause

of the irregular oscillations at the transition between oscillatory combustion and flame extinction should be examined more closely.

5.4.5   Influence of the flow time

To determine regions of stability for the flow time and the wall temperature, Richards et al. computed the pressure amplitudes and frequencies over a range of those parameters, and presented the numerical data in three-dimensional plots. Similar results are presented in Figure 5.10: the three-dimensional plots are replaced by contour plots, which makes the data somewhat easier to read.

The pressure amplitudes and frequencies were computed in the same way as before. That is, on the time-interval 0.3–1.3 s values from the numerical solution of the pressure were sampled with a sample interval of 1/4096 s. From these sampled values, the peak-to-peak pressure amplitude was determined by taking the difference between the maximum and minimum values on the time-interval 1–1.3 s. The frequency was determined from the maximum value in the periodogram of the sampled data. The wall temperature (T_w) was varied from 700 K to 1400 K, with steps of 25 K. The flow time (τ_f) was varied from 10 ms to 90 ms, with steps of 2.5 ms. This gave the pressure amplitudes and frequencies on a coarse 29×33 grid. The standard MATLAB-function `contour` was used to plot the contour lines. The levels for the contour plots were chosen to vary from 0 kPa to 100 kPa with steps of 10 kPa for the pressure amplitudes, and for the frequencies the levels were varied from 70 Hz to 200 Hz with steps of 10 Hz.

Thick solid lines were added to the plots to mark the regions of oscillation. In both plots the line was produced by plotting the contour line of the computed pressure amplitudes at a level of 1% of the ambient pressure, i.e. at the $0.01 \times 101.325 = 1.01325$ kPa level. Thick dashed lines were added to the plots to indicate the boundary between flame extinction and steady or oscillatory combustion. In both plots the line was produced by plotting the contour line for the computed mean fuel mass fractions, averaged over the time-interval 1–1.3 s, at the level of 99% of the fuel mass fraction at the inlet, i.e. at the $0.99 \times 0.06 = 0.0594$ level. It should be noted that the high density of contour lines close to the boundary between flame extinction and steady or oscillatory combustion is an artificial effect resulting from interpolation on the coarse 29×33 grid. It should be viewed at as a sudden drop in pressure amplitude or frequency when going from the region of steady or oscillatory combustion to the region of flame extinction. Note that Figure 5.10b shows the contour lines for the frequencies in the regions of steady combustion and flame extinction, even though there should not be any oscillations. These frequencies correspond to the small oscillations remaining from the initial oscillations (after 0.3–1.3 s). They were included in the plots, because they might provide additional insight.

Richards et al. noted that the lower frequencies occur at smaller flow times and added that one might have expected higher frequencies, because of a faster replenishment of the combustion zone. They explained the lower frequencies by a delay in the returning flow caused by "the higher (mean) exit flow associated with smaller flow times [...]." It is not clear that the flow time has such an effect on the frequency of the oscillations. Another, perhaps more satisfactory explanation is found in the temperature dependency of the frequency. An increase in wall temperature has the effect of increasing the temperature, so higher frequencies are expected to result. Smaller flow times are associated with a greater inflow
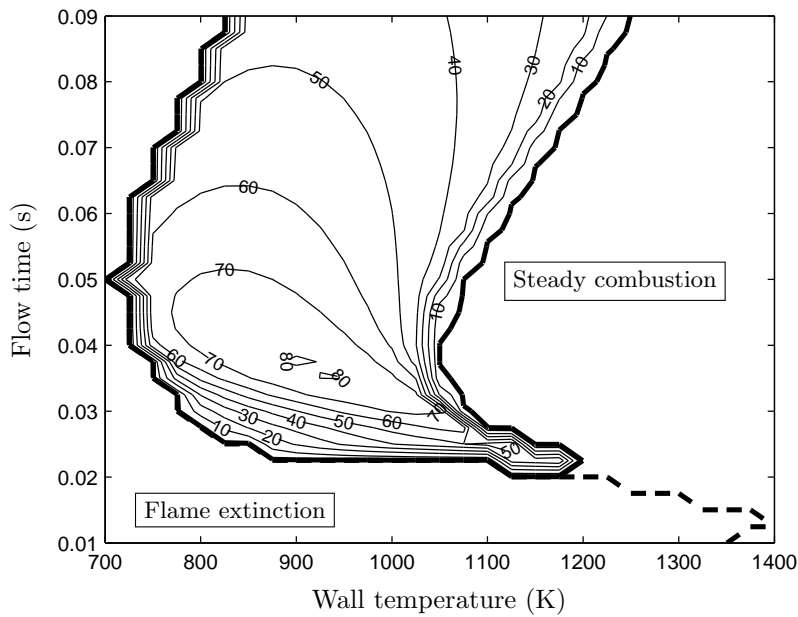
(a) Pressure amplitude (peak-to-peak, in kPa); maximum: 81 kPa
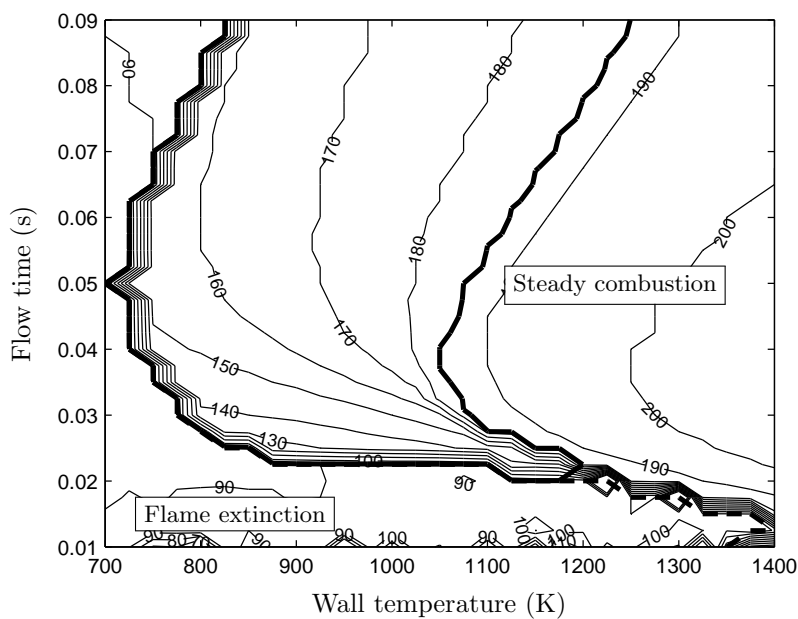
(b) Frequency (Hz); maximum: 188 Hz

Figure 5.10: Contour plots of (a) the pressure amplitude and (b) the frequency of the oscillations over a range of wall temperatures and flow times. The thick solid line encircles the region where oscillations occur; the thick dashed line is the boundary between flame extinction and steady or oscillatory combustion. (Cf. Figure 10 in [25].)

of cool reactants, resulting in lower temperatures and, thus, lower frequencies are to be expected. These two effects, the cooling by reactants inflow and the heat transfer to the combustion chamber wall, both contribute to the change in temperature, and the frequency is affected likewise. For smaller flow times, the temperature is influenced mainly by the inflow of the cool reactants, while for larger flow times the wall temperature is the more dominant factor. These effects can be observed in the contour plot of the frequencies (Figure 5.10b). The figure also shows that the flame is extinguished for flow times that are too low, and that steady combustion occurs for wall temperatures that are too high. Note that the frequency of the oscillations lies somewhere around 90–100 Hz when there is no combustion.

Richards et al. also noted that the pressure amplitudes were higher for smaller flow times and explained this by the presence of more reactants at the moment of combustion acceleration. It is interesting to note that the pressure amplitudes seem to be the greatest when the frequency is around 150–160 Hz. If the frequency can be used as a measure for the (mean) temperature, the pressure amplitudes can be explained for a large part by the phase difference between the heat release and pressure oscillations, determined predominantly by the temperature. Then, apparently, the phase difference is optimal for conditions that cause the frequency to be around 150–160 Hz. The difference in pressure amplitude along lines of constant frequency could be explained by the presence of more reactants for smaller flow times, as remarked by Richards et al. The factors that determine the frequency and the amplitudes of the pressure oscillations should be studied more closely by quantifying the energy put into the oscillations and determining the timing of this.

As a final remark on the contour plots, it should be noted that the inflow of reactants is proportional to the inverse of the flow time ($\frac{1}{\tau_f} = \frac{\dot{m}_i}{\rho_0 V_{cc}}$, see definitions (5.13) and (5.23)). Thus, for a certain change in flow time, the inflow of reactants changes more for smaller flow times than for larger flow times. It may be better to represent the data for the inverse of the flow time instead of the flow time, so that changes along the vertical axis correspond to proportional changes in the reactants inflow.

5.4.6   Influence of microscale mixing

As final part of the numerical evaluation of their model equations, Richards et al. discussed the influence of imperfect mixing in the combustion chamber. They distinguished imperfect mixing between microscale and macroscale inhomogeneities. They remarked that, while macroscale mixing imperfections depend on the internal flow field and are therefore difficult to incorporate in the present model, the microscale mixing imperfections can be incorporated by adjusting the combustion time. Richards et al. did this by adding a mixing time τ_m to the combustion time (τ_c), and replacing the combustion time in the original model equations by this combined combustion and mixing time:

$$\tau_{cm} = \tau_c + \tau_m. \tag{5.95}$$

Then they produced the three-dimensional plots as before, incorporating the microscale mixing effects in the manner just described.

In order to incorporate the microscale mixing in a similar manner in the model equations (5.73)–(5.89) that are implemented in this report, the reaction

rate RR, related to the inverse of the combustion time by the relation $1/\tau_c = B \cdot RR$, needs to be adjusted as follows. A new reaction rate $\widehat{RR}$, that is to correspond to the combined combustion and mixing time, is defined by

$$\widehat{RR} = \frac{1}{B\tau_{cm}}. \tag{5.96}$$

It can be expressed in terms of the old reaction rate RR:

$$\widehat{RR} = \frac{1}{B(\tau_c + \tau_m)} = \frac{RR}{1 + B \cdot RR\,\tau_m}. \tag{5.97}$$

The numerical implementation of this new reaction rate is straightforward: only a line of code computing the new reaction rate from the old one needs to be added. Note that with $\tau_m = 0$ the old reaction rate is recovered. Following the presentation of Richards et al., Figure 5.11 shows the numerical results similar to those presented in Figure 5.10 for a mixing time of $\tau_m = 1$ ms.

The regions of oscillatory and steady combustion are quite different from the ones for perfect mixing ($\tau_m = 0$ ms). Where in case of perfect mixing the boundary between oscillatory and steady combustion seems to follow the curves of constant frequency, it cuts these curves in case of the mixing time $\tau_m = 1$ ms. The transition of the stability regions when going from $\tau_m = 0$ ms to $\tau_m = 1$ ms can be better understood by making plots for a mixing time in between the two. Figure 5.12 shows the contour plots for the amplitudes and frequencies of the pressure oscillations for the mixing time $\tau_m = 0.5$ ms.

The contour plots for non-zero mixing times, with the corresponding stability regions, can be explained as follows. For low enough flow times or wall temperatures, the temperature in the combustion chamber is insufficient to maintain combustion, hence flame extinction occurs. For high enough wall temperatures, the temperature in the combustion chamber is always high enough to maintain steady combustion. In case of steady combustion, conditions (temperature, pressure, fuel mass fraction and products mass outflow) are such that the reaction rate is balanced with the reactants mass inflow. At the boundary between flame extinction and steady combustion, a small pressure disturbance takes just too long to return to the combustion chamber so that, due to cooling, the reaction rate will be too low to maintain combustion. Now, if the frequency can be seen as a measure for the (mean) temperature in the combustion chamber, the temperature is about constant along a line of constant frequency. The temperature is determined by three factors: cooling by reactants inflow, cooling by heat transfer to the combustion chamber wall and heating by combustion. Following a curve of constant frequency (read: temperature) toward a higher flow time, the cooling effect of the reactants inflow is shifted toward the wall temperature. Since the cooling by the wall temperature is least at moments of low temperature and greatest at moments of high temperature, the temperature in the combustion chamber will be somewhat higher when a pressure wave from a disturbance arrives. Thus, following a curve of constant frequency from a low flow time to a higher flow time, the phase difference will grow more favorable to maintain oscillations. At some point, the phase difference is favorable enough to overcome the damping terms, and pressure oscillations become possible.

The influence of the mixing time is to reduce the reaction rate (see equation (5.97)). This effect is more pronounced for higher reaction rates. Thus, in
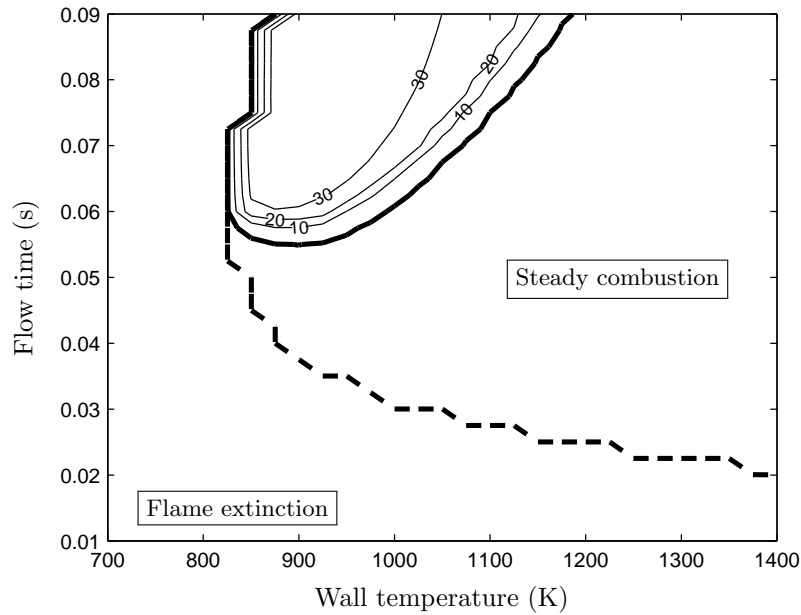
(a) Pressure amplitude (peak-to-peak, in kPa); maximum: 36 kPa
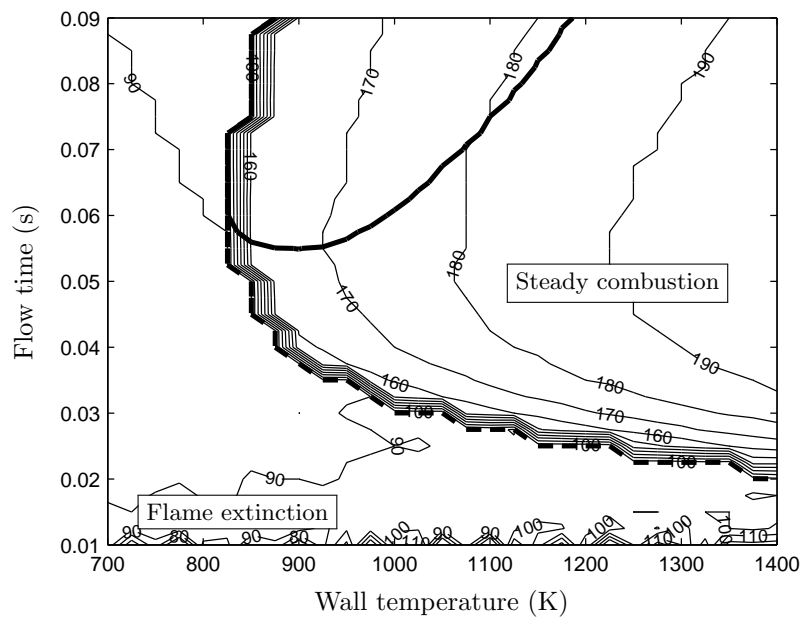
(b) Frequency (Hz); maximum: 182 Hz

Figure 5.11: Contour plots of (a) the pressure amplitude and (b) the frequency of the oscillations over a range of wall temperatures and flow times for the *mixing time* $\tau_m = 1\,\mathrm{ms}$. The thick solid line encircles the region where oscillations occur; the thick dashed line is the boundary between flame extinction and steady combustion. (Cf. Figure 11 in [25].)
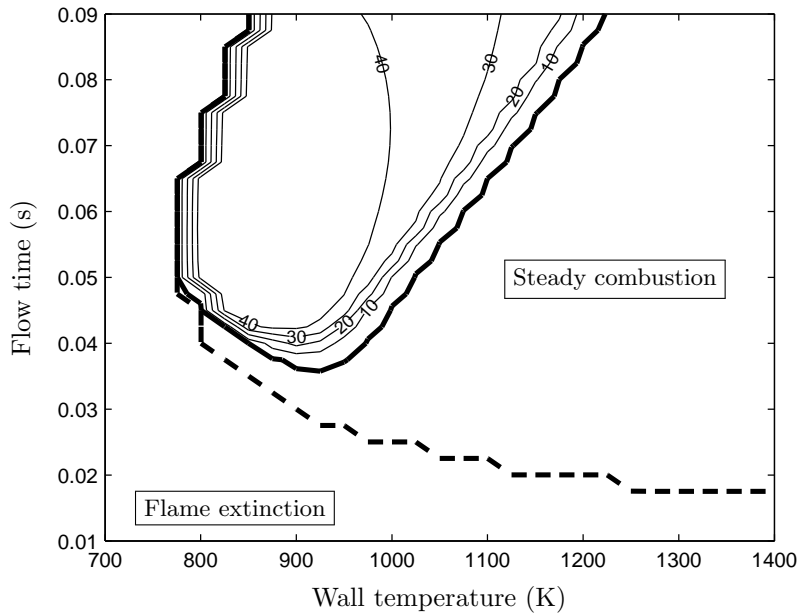
(a) Pressure amplitude (peak-to-peak, in kPa); maximum: 50 kPa
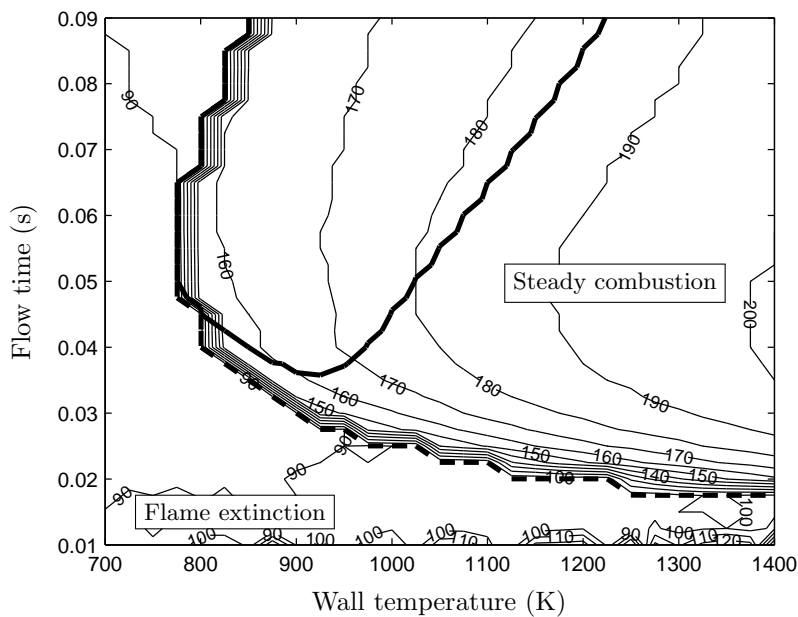
(b) Frequency (Hz); maximum: 188 Hz

Figure 5.12: Contour plots of (a) the pressure amplitude and (b) the frequency of the oscillations over a range of wall temperatures and flow times for the *mixing time* $\tau_m = 0.5$ ms. The thick solid line encircles the region where oscillations occur; the thick dashed line is the boundary between flame extinction and steady combustion.

order to obtain a situation of steady combustion, i.e. to reach a certain reaction rate, the temperature needs to be higher in case of longer mixing times. This explains the higher frequency close to the boundary between flame extinction and steady combustion for longer mixing times. Also, for longer mixing times, the influence of combustion is less, so that a more favorable phasing is needed to obtain oscillations. For high enough flow time the reaction rate will be less, because there is less reactants to burn. Thus, the effect of the mixing time will diminish with the increase of the flow time above a certain level. This can be seen by comparing the Figures 5.9–5.12.

Of course, the qualitative arguments that are given above are highly speculative. They should be quantified to confirm whether the proposed effects are occurring.

5.5   Steady-state solutions and their stability

The parameter study through numerical integration of the model equations, such as performed in the previous section, proves to be very time consuming. For example, producing Figure 5.10a (which shows for which values of wall temperature and flow time, steady combustion, flame extinction, or pulsating combustion occurs) takes about 20 minutes on the computer system that is used for the numerical integration. Doing the Fourier analysis to determine the associated frequencies (see Figure 5.10b) adds about 10 minutes of computing time. Thus, a similar analysis for a slightly different tailpipe length – to study the effect on the frequency, for example – will take another 30 minutes. Any substantial exploration of the model parameter space will take many hours. Furthermore, the insight gained in this way may be useless for any modifications of the model equations (e.g., modelling the reaction rate in a different way).

To gain insight into the influence of the parameters on the system's behaviour without a huge computational effort, the steady-state solutions are determined and their stability is investigated. At the least, this will provide information on regions in the model parameter space for which steady combustion or flame extinction can occur: such behaviour corresponds to a stable steady-state solution of the model equations. Besides, the numerical results of the previous section show, in case of pulsating combustion, a tendency to first approach a steady state, but then, close to a steady-state solution, to diverge by amplification of the oscillations until nonlinear effects limit further growth (see Figure 5.3, for example). Thus, an investigation of the steady-state solutions and their stability may also provide information regarding pulsating combustion.

5.5.1   Stability theory; application to model equations

When investigating the behaviour of an autonomous system of ordinary differential equations,

$$\frac{d\mathbf{y}}{dt} = \mathbf{f}(\mathbf{y}), \tag{5.98}$$

a first step is to determine the steady states (or, *critical points*), which are solutions of $\mathbf{f}(\mathbf{y}) = \mathbf{0}$, and to examine their stability. Under certain conditions on the smoothness of $\mathbf{f}$, the stability of a steady-state solution can be obtained

from the study of system (5.98) linearized in the neighbourhood of the steady state.

In particular, the following holds for the autonomous system

$$\frac{d\mathbf{x}}{dt} = A\mathbf{x} + \mathbf{g}(\mathbf{x}), \qquad (5.99)$$

with A a non-singular $n \times n$-matrix and $\mathbf{g}$ satisfying

$$\lim_{||\mathbf{x}|| \to 0} \frac{||\mathbf{g}(\mathbf{x})||}{||\mathbf{x}||} = 0. \qquad (5.100)$$

If the eigenvalues of matrix A all have negative real part, the trivial solution $\mathbf{x} = \mathbf{0}$ of (5.99) is asymptotically stable. If there is at least one eigenvalue of the matrix A with positive real part, the trivial solution $\mathbf{x} = \mathbf{0}$ of (5.99) is unstable. (See Chapters 3 and 7 in [34].)

Suppose the vector function $\mathbf{f}$ of system (5.98) is continuously differentiable in a critical point $\mathbf{y}^*$ (thus $\mathbf{f}(\mathbf{y}^*) = \mathbf{0}$). Then, in a neighbourhood of the critical point, the perturbation $\mathbf{y}(t) = \mathbf{y}^* + \mathbf{x}(t)$ of the steady-state solution $\mathbf{y}^*$ satisfies

$$\frac{d\mathbf{x}}{dt} = \frac{d\mathbf{y}}{dt} = \mathbf{f}(\mathbf{y}^* + \mathbf{x}) = A\mathbf{x} + \mathbf{g}(\mathbf{x}), \qquad (5.101)$$

where the matrix $A = \mathbf{f}'(\mathbf{y}^*)$ is the derivative of the vector function $\mathbf{f}$ in $\mathbf{y}^*$, and $\mathbf{g}$ satisfies condition (5.100). Conclusions about the stability of the trivial solution of (5.101) carry over to the stability of the steady-state solution $\mathbf{y}^*$. Thus, the stability of the steady-state solutions of system (5.98) can be determined from the eigenvalues of the Jacobian matrices $\mathbf{f}'$ evaluated in the critical points, provided that their real parts are all non-zero.

Application of stability theory to the model equations

The system of model equations (5.73)–(5.76) can be written in the general vector form of (5.98) by defining $\mathbf{y} = (y_i)$ and $\mathbf{f} = (f_i)$ $(i = 1, \ldots, 4)$ in the following way:

$$\mathbf{y} = \begin{pmatrix} \widetilde{P} \\ \widetilde{T} \\ \widetilde{u} \\ Y_f \end{pmatrix} \qquad (5.102)$$

and, writing $\widetilde{P}$, $\widetilde{T}$, $\widetilde{u}$, Y_f instead of y_1, y_2, y_3, y_4 (for easier reference to the model equations)

$$\mathbf{f}(\mathbf{y}) = \begin{pmatrix} \gamma \left(A - G\widetilde{Z}_e(\mathbf{y})\widetilde{T} + B \cdot RR(\mathbf{y}) + C(D - \widetilde{T}) \right) \\ \frac{1}{\widetilde{\rho}(\mathbf{y})} \left(f_1(\mathbf{y}) - (A - G\widetilde{Z}_e(\mathbf{y}))\widetilde{T} \right) \\ \frac{E}{\widetilde{\rho}_e(\mathbf{y})} \left(\widetilde{P}_e(\mathbf{y}) - 1 \right) - F\widetilde{u}\,|\widetilde{u}| \\ \frac{1}{\widetilde{\rho}(\mathbf{y})} \left(A\left(Y_{f,i} - Y_f\right) - RR(\mathbf{y}) \right) \end{pmatrix}. \qquad (5.103)$$

Note that $f_1(\mathbf{y})$ is used in defining $f_2(\mathbf{y})$, cf. (5.73) and (5.74). The factors in the right-hand side of (5.103) that are dependent on $\mathbf{y}$ are given by (see also

(5.77)–(5.80))

$$\widetilde{\rho}(\mathbf{y}) = \frac{\widetilde{P}}{\widetilde{T}}, \tag{5.104}$$

$$RR(\mathbf{y}) = A'\sqrt{\widetilde{T}}\,\widetilde{\rho}(\mathbf{y})^2 Y_f^2 \exp(-\widetilde{T}_{\mathrm{act}}/\widetilde{T}), \tag{5.105}$$

$$\widetilde{P}_e(\mathbf{y}) = \widetilde{P}\left(1 - \frac{\gamma-1}{2}\frac{u_0^2}{\gamma R T_0}\frac{\widetilde{u}^2}{\widetilde{T}}\right)^{\frac{\gamma}{\gamma-1}}, \tag{5.106}$$

$$\widetilde{T}_e(\mathbf{y}) = \widetilde{T}\left(1 - \frac{\gamma-1}{2}\frac{u_0^2}{\gamma R T_0}\frac{\widetilde{u}^2}{\widetilde{T}}\right), \tag{5.107}$$

$$\widetilde{\rho}_e(\mathbf{y}) = \frac{\widetilde{P}_e(\mathbf{y})}{\widetilde{T}_e(\mathbf{y})}, \tag{5.108}$$

$$\widetilde{Z}_e(\mathbf{y}) = \widetilde{\rho}_e(\mathbf{y})\,\widetilde{u}. \tag{5.109}$$

To incorporate the mixing time τ_m in the model equations, the function $RR(\mathbf{y})$ in (5.103), which is defined by (5.105), should be replaced by $\widehat{RR}(\mathbf{y})$ defined by

$$\widehat{RR}(\mathbf{y}) = \frac{RR(\mathbf{y})}{1 + B \cdot RR(\mathbf{y})\tau_m} \tag{5.110}$$

(see (5.97)).

  The physics of the problem that is modelled, requires that $\mathbf{y}$ lies in a domain with $\widetilde{P} > 0$, $\widetilde{T} > \frac{\gamma-1}{2}\frac{u_0^2}{\gamma R T_0}\widetilde{u}^2$, and $0 \leq Y_f \leq 1$. It is easy to see that $\mathbf{f}$ is a continuously differentiable function on such a domain. Thus, the theory that is presented above, can be applied to investigate the stability of the steady-state solutions of the model equations.

5.5.2   Computation of the critical points

The critical points of the system of model equations are found by solving the nonlinear equations $\mathbf{f}(\mathbf{y}) = \mathbf{0}$. For a critical point $\mathbf{y}^* = (\widetilde{P}^*, \widetilde{T}^*, \widetilde{u}^*, Y_f^*)^\top$, it follows from $f_1(\mathbf{y}^*) = 0$, and the requirements that $\widetilde{\rho}(\mathbf{y}^*) > 0$, $\widetilde{\rho}_e(\mathbf{y}^*) > 0$ and $\widetilde{T}^* > 0$, that

$$\left(A - G\widetilde{Z}_e(\mathbf{y}^*)\widetilde{T}^*\right) + B \cdot RR(\mathbf{y}^*) + C\left(D - \widetilde{T}^*\right) = 0, \tag{5.111}$$

$$A - G\widetilde{Z}_e(\mathbf{y}^*) = 0, \tag{5.112}$$

$$E\left(\widetilde{P}_e(\mathbf{y}^*) - 1\right) - F\,\widetilde{Z}_e(\mathbf{y}^*)|\widetilde{u}^*| = 0, \tag{5.113}$$

$$A\left(Y_{f,i} - Y_f^*\right) - RR(\mathbf{y}^*) = 0. \tag{5.114}$$

  The nonlinear equations (5.111)–(5.114) are valid for a steady-state solution $\mathbf{y}^*$ of the model equations, and they have clear physical interpretations. Equation (5.111) expresses the balance that must exist between the net heat flux out of the combustion chamber (minus the first term), the heat released by combustion (the second term), and the heat transfer to the combustion chamber wall (minus the third term). Equation (5.112) expresses the balance in mass inflow and outflow rates. Note that the mass conservation equation was used earlier to derive the differential equation for the temperature from the energy equation

(see page 50). The equilibrium required by mass conservation is recovered from the equilibrium condition for the temperature ($f_2(\mathbf{y}^*) = 0$) by combining it with the equilibrium condition for the energy ($f_1(\mathbf{y}^*) = 0$). Equation (5.113) expresses the balance between the force that drives the tailpipe fluid flow (due to a pressure difference), and the friction force. Equation (5.114) relates the difference between the fuel mass fraction at inflow and that in the combustion chamber to the fuel mass consumption rate (i.e. the reaction rate RR).

Next, it will be shown that this system of nonlinear equations can be reduced to a single nonlinear equation for the (dimensionless) steady-state temperature $\widetilde{T}^*$ between certain bounds: $\widetilde{T}_{\min} \leq \widetilde{T}^* \leq \widetilde{T}_{\max}$. For that purpose, the (dimensionless) steady-state pressure $\widetilde{P}^*$, tailpipe fluid velocity $\widetilde{u}^*$, and fuel mass fraction Y_f^* are expressed in terms of the steady-state temperature $\widetilde{T}^*$. It is helpful to keep the physical interpretation of equations (5.111)–(5.114) in mind.

Heat release rate; bounds for steady-state temperature

In this part, the steady-state heat release rate will be linked to the steady-state temperature $\widetilde{T}^*$, and minimum and maximum values for $\widetilde{T}^*$ will be determined. Also, the steady-state fuel mass fraction Y_f^* will be expressed in terms of $\widetilde{T}^*$.

With equation (5.112) (requiring a balance between the mass inflow and outflow rates), the (dimensionless) mass outflow rate immediately follows from the given mass inflow rate:

$$\widetilde{Z}_e(\mathbf{y}^*) = \widetilde{\rho}_e(\mathbf{y}^*)\widetilde{u}^* = \frac{A}{G}. \tag{5.115}$$

With the (dimensionless) mass outflow rate given by (5.115), equation (5.111) (requiring a balance between the heat terms of the energy equation) relates the heat losses from the combustion chamber to the heat release term:

$$B \cdot RR(\mathbf{y}^*) = A\left(\widetilde{T}^* - 1\right) + C\left(\widetilde{T}^* - D\right). \tag{5.116}$$

Since $RR(\mathbf{y}^*)$ must be positive, this relation gives a minimum $\widetilde{T}_{\min}$ for the steady-state temperature $\widetilde{T}^*$, associated with $RR = 0$ (i.e. zero heat release rate):

$$\widetilde{T}^* \geq \widetilde{T}_{\min} = \frac{A + CD}{A + C}. \tag{5.117}$$

Combining equation (5.114) (requiring a balance between the fuel mass fraction that is converted and the fuel mass consumption rate) with expression (5.116) for the reaction rate, gives

$$Y_f^* = Y_{f,i} - \frac{1}{AB}\left(A\left(\widetilde{T}^* - 1\right) + C\left(\widetilde{T}^* - D\right)\right). \tag{5.118}$$

Since Y_f^* must be positive, this relation gives a maximum $\widetilde{T}_{\max}$ for the steady-state temperature $\widetilde{T}^*$, associated with $Y_f^* = 0$ (i.e. maximum fuel consumption):

$$\widetilde{T}^* \leq \widetilde{T}_{\max} = \frac{AB}{A + C}Y_{f,i} + \frac{A + CD}{A + C}. \tag{5.119}$$

Using $\widetilde{T}_{\max} - \widetilde{T}_{\min} = \frac{AB}{A+C} Y_{f,i}$, the steady-state fuel mass fraction can be written as

$$Y_f^* = Y_{f,i} \left(1 - \frac{\widetilde{T}^* - \widetilde{T}_{\min}}{\widetilde{T}_{\max} - \widetilde{T}_{\min}} \right) = Y_{f,i} \left(\frac{\widetilde{T}_{\max} - \widetilde{T}^*}{\widetilde{T}_{\max} - \widetilde{T}_{\min}} \right). \tag{5.120}$$

Expressing a critical point in the steady-state temperature

In this part, the critical point $\mathbf{y}^* = (\widetilde{P}^*, \widetilde{T}^*, \widetilde{u}^*, Y_f^*)^\top$ will be expressed in terms of the steady-state temperature $\widetilde{T}^*$ alone. The steady-state fuel mass fraction is already expressed in terms of the steady-state temperature by (5.120).

Using the expression (5.115) for the mass outflow rate $\widetilde{Z}_e(\mathbf{y}^*)$ in equation (5.113) (which gives the balance between the force driving the tailpipe fluid flow and the friction force) gives for the pressure $\widetilde{P}_e(\mathbf{y}^*)$ at the tailpipe entrance

$$\widetilde{P}_e(\mathbf{y}^*) = 1 + \frac{AF}{GE} |\widetilde{u}^*|. \tag{5.121}$$

With the requirement that $\widetilde{\rho}_e(\mathbf{y}^*) > 0$, it follows from expression (5.115) for the mass outflow rate that $\widetilde{u}^* > 0$, so that the absolute value bars in (5.121) may be omitted. With both $\widetilde{P}_e(\mathbf{y}^*)$ and $\widetilde{\rho}_e(\mathbf{y}^*)$ expressed in the steady-state tailpipe fluid velocity $\widetilde{u}^*$ (see (5.121) and (5.115)), the temperature $\widetilde{T}_e(\mathbf{y}^*)$ can also be expressed in $\widetilde{u}^*$ by using relation (5.108):

$$\widetilde{T}_e(\mathbf{y}^*) = \frac{\widetilde{P}_e(\mathbf{y}^*)}{\widetilde{\rho}_e(\mathbf{y}^*)} = \widetilde{u}^* \left(\frac{G}{A} + \frac{F}{E} \widetilde{u}^* \right). \tag{5.122}$$

From (5.107), which gives the isentropic relation between $\widetilde{T}_e(\mathbf{y}^*)$ and $\widetilde{T}^*$, it follows that

$$\widetilde{T}^* = \widetilde{T}_e(\mathbf{y}^*) + \alpha \widetilde{u}^{*2} = \widetilde{u}^* \left(\frac{G}{A} + \left(\alpha + \frac{F}{E} \right) \widetilde{u}^* \right), \tag{5.123}$$

where $\alpha = \frac{\gamma - 1}{2} \frac{u_0^2}{\gamma R T_0}$ is introduced to ease the notation. Since $\widetilde{u}^* > 0$, (5.123) is a one-to-one relationship between $\widetilde{T}^*$ and $\widetilde{u}^*$, which is given by

$$\widetilde{u}^* = \frac{-\frac{G}{A} + \sqrt{\left(\frac{G}{A} \right)^2 + 4 \left(\alpha + \frac{F}{E} \right) \widetilde{T}^*}}{2 \left(\alpha + \frac{F}{E} \right)}. \tag{5.124}$$

By multiplying numerator and denominator with $\frac{G}{A} + \sqrt{\left(\frac{G}{A} \right)^2 + 4 \left(\alpha + \frac{F}{E} \right) \widetilde{T}^*}$, relation (5.124) can equivalently be written as

$$\widetilde{u}^* = \frac{2 \widetilde{T}^*}{\frac{G}{A} + \sqrt{\left(\frac{G}{A} \right)^2 + 4 \left(\alpha + \frac{F}{E} \right) \widetilde{T}^*}}. \tag{5.125}$$

This latter expression for $\widetilde{u}^*$ is better to use in a numerical implementation than the former, because it prevents cancellation errors.

The steady-state pressure $\widetilde{P}^*$ is related to the pressure $\widetilde{P}_e(\mathbf{y}^*)$ at the tailpipe entrance by the isentropic relation

$$\widetilde{P}^* = \widetilde{P}_e(\mathbf{y}^*) \left(\frac{\widetilde{T}^*}{\widetilde{T}_e(\mathbf{y}^*)} \right)^{\frac{\gamma}{\gamma - 1}}, \tag{5.126}$$

see (5.106) and (5.107). With (5.122) and (5.123) it follows that

$$\widetilde{P}^* = \widetilde{P}_e(\mathbf{y}^*) \left(\frac{\frac{G}{A} + \left(\alpha + \frac{F}{E}\right)\widetilde{u}^*}{\frac{G}{A} + \frac{F}{E}\widetilde{u}^*} \right)^{\frac{\gamma}{\gamma-1}}. \tag{5.127}$$

Now the steady-state pressure $\widetilde{P}^*$, tailpipe fluid velocity $\widetilde{u}^*$, and fuel mass fraction Y_f^* can all be expressed in terms of the steady-state temperature $\widetilde{T}^*$: $Y_f^*(\widetilde{T}^*)$ is given by (5.120), $\widetilde{u}^*(\widetilde{T}^*)$ is given by (5.125), and $\widetilde{P}^*(\widetilde{T}^*)$ follows from combining (5.127) with (5.121) and (5.125).

Finding the critical points

Let $\widetilde{T}$ be a candidate steady-state temperature. From the foregoing analysis, it follows that there is exactly one candidate critical point $\mathbf{y}(\widetilde{T}) = (\widetilde{P}, \widetilde{T}, \widetilde{u}, Y_f)^\top$ associated with it. The elements $\widetilde{P}$, $\widetilde{u}$, and Y_f of the vector $\mathbf{y}$ are given by

$$\widetilde{u}(\widetilde{T}) \ = \ \frac{2\widetilde{T}}{\frac{G}{A} + \sqrt{\left(\frac{G}{A}\right)^2 + 4\left(\alpha + \frac{F}{E}\right)\widetilde{T}}}, \tag{5.128}$$

$$\widetilde{P}(\widetilde{T}) \ = \ \widetilde{P}_e(\widetilde{u}(\widetilde{T}))\left(\frac{\frac{G}{A} + \left(\alpha + \frac{F}{E}\right)\widetilde{u}(\widetilde{T})}{\frac{G}{A} + \frac{F}{E}\widetilde{u}(\widetilde{T})} \right)^{\frac{\gamma}{\gamma-1}}, \tag{5.129}$$

$$Y_f(\widetilde{T}) \ = \ Y_{f,i}\left(\frac{\widetilde{T}_{\max} - \widetilde{T}}{\widetilde{T}_{\max} - \widetilde{T}_{\min}} \right), \tag{5.130}$$

where

$$\widetilde{P}_e(\widetilde{u}(\widetilde{T})) = \left(1 + \frac{AF}{GE}\widetilde{u}(\widetilde{T}) \right), \tag{5.131}$$

and

$$\widetilde{T}_{\min} = \frac{A + CD}{A + C}, \quad \widetilde{T}_{\max} = \widetilde{T}_{\min} + \frac{AB}{A + C}Y_{f,i}. \tag{5.132}$$

Associated with this candidate critical point $\mathbf{y}(\widetilde{T})$ is the reaction rate $RR_1(\widetilde{T}) = RR(\mathbf{y}(\widetilde{T}))$ given by (5.105):

$$RR_1(\widetilde{T}) = RR(\mathbf{y}(\widetilde{T})) = A'\sqrt{\widetilde{T}}\ \widetilde{\rho}(\mathbf{y}(\widetilde{T}))^2 Y_f(\widetilde{T})^2 \exp(-\widetilde{T}_{\mathrm{act}}/\widetilde{T}), \tag{5.133}$$

where $\widetilde{\rho}(\mathbf{y}(\widetilde{T})) = \widetilde{P}(\widetilde{T})/\widetilde{T}$. Let $RR_2(\widetilde{T})$ be the reaction rate that is required for a balance between heat release and heat losses (see (5.116)), i.e.

$$RR_2(\widetilde{T}) = \frac{A + C}{B}\left(\widetilde{T} - \frac{A + CD}{A + C} \right) = AY_{f,i}\left(\frac{\widetilde{T} - \widetilde{T}_{\min}}{\widetilde{T}_{\max} - \widetilde{T}_{\min}} \right). \tag{5.134}$$

If the reaction rate that is associated with the candidate critical point $\mathbf{y}(\widetilde{T})$ equals the reaction rate that is needed for a balance in heat release and heat losses, i.e. if $RR_1(\widetilde{T}) = RR_2(\widetilde{T})$, all the equations $\mathbf{f}(\mathbf{y}(\widetilde{T})) = \mathbf{0}$ are satisfied, and we have found a critical point of the model equations. Since all steady-state temperatures lie between $\widetilde{T}_{\min}$ and $\widetilde{T}_{\max}$, the critical points of the model equations can be found by solving the nonlinear equation

$$RR_1(\widetilde{T}) = RR_2(\widetilde{T}) \tag{5.135}$$

for $\widetilde{T}_{\min} \leq \widetilde{T} \leq \widetilde{T}_{\max}$.

Note that the reaction rate that is needed for a balance between the heat release and the heat losses, i.e. RR_2 given by (5.134), is independent of the actual heat release rate in the model, i.e. RR_1 given by (5.133). This means that for a different heat release model, the steady states can be found by solving equation (5.135), with the reaction rate RR_1 replaced by the new reaction rate. In particular, if the mixing time τ_m is incorporated in the reaction rate (see (5.110)), the critical points can be found by solving the nonlinear equation

$$\widehat{RR_1}(\widetilde{T}) = RR_2(\widetilde{T}), \tag{5.136}$$

for $\widetilde{T}_{\min} \leq \widetilde{T} \leq \widetilde{T}_{\max}$, where $\widehat{RR_1}(\widetilde{T})$ is defined by

$$\widehat{RR_1}(\widetilde{T}) = \frac{RR_1(\widetilde{T})}{1 + B \cdot RR_1(\widetilde{T})\tau_m}. \tag{5.137}$$

The nonlinear equation (5.135) for the steady-state temperature can be solved numerically. This is done for varying model parameter values in Subsection 5.5.4, under the heading "Investigation of the critical points."

5.5.3   Computation of the Jacobian matrices

It was noted before, that Richards et al. used the mass conservation equation

$$\frac{d\widetilde{\rho}}{dt} = A - G\widetilde{Z}_e \tag{5.138}$$

(cf. (5.27)) to derive a differential equation for the temperature from the energy conservation equation (cf. (5.21)). The equation for the temperature is in fact a second energy conservation equation, which is related to the first and to the mass conservation equation by the perfect gas law:

$$\frac{d\widetilde{\rho}}{dt} = \frac{1}{\widetilde{T}}\frac{d\widetilde{P}}{dt} - \frac{\widetilde{P}}{\widetilde{T}^2}\frac{d\widetilde{T}}{dt}. \tag{5.139}$$

It may be preferred to use the mass conservation equation directly, instead of 'hiding the information' in two energy conservation equations. But using the mass conservation equation instead of the differential equation for the temperature will give a different right-hand side function, and there is a different Jacobian matrix associated with it. In this section, the elements of Jacobian matrices are determined for three choices of variables in which to express the model equations: $\widetilde{P}, \widetilde{T}, \widetilde{u}, Y_f$ of the original system, or using $\widetilde{\rho}$ instead of $\widetilde{T}$, or using $\widetilde{\rho}$ instead of $\widetilde{P}$.

The three different systems of equations, resulting from each of the choices of (independent) variables, can be related to each other by variable transformations. For example, expressing the equations in $\mathbf{z} = (\widetilde{P}, \widetilde{u}, Y_f, \widetilde{\rho})^{\top}$ is equivalent to applying the variable transformation $\boldsymbol{\zeta} : \mathbf{y} \to (y_1, y_3, y_4, \frac{y_1}{y_2})^{\top}$ to the original system of equations, which is expressed in $\mathbf{y} = (\widetilde{P}, \widetilde{T}, \widetilde{u}, Y_f)^{\top}$. It is shown below, that *in a critical point* the Jacobian matrix for a transformed system of differential equations is similar to the Jacobian matrix of the original system *in the corresponding critical point*. Similar matrices share the same Jordan form, which means that they have the same eigenvalues, and each eigenvalue has the same number of eigenvectors associated with it. Thus, the results from stability analysis will be independent from the choice of variables.

Jacobian matrices for three choices of independent variables

The three choices of independent variables that are considered, are the sets formed by $\widetilde{P}$, $\widetilde{T}$, $\widetilde{u}$, Y_f, $\widetilde{\rho}$, and then leaving out $\widetilde{P}$, $\widetilde{T}$ or $\widetilde{\rho}$. In order to compute the Jacobian matrices for these three choices all at once, the original system of model equations (5.103) is extended with the mass conservation equation (5.138). The extended system of equations can be written as

$$\frac{d\widehat{\mathbf{y}}}{dt} = \widehat{\mathbf{f}}(\widehat{\mathbf{y}}), \tag{5.140}$$

where $\widehat{\mathbf{y}} = (\widehat{y}_i)$ and $\widehat{\mathbf{f}} = (\widehat{f}_i)$ $(i = 1, \ldots, 5)$ are given by $\widehat{\mathbf{y}} = (\widetilde{P}, \widetilde{T}, \widetilde{u}, Y_f, \widetilde{\rho})^\top$ and

$$\widehat{f}_1(\widehat{\mathbf{y}}) = \gamma \left(A + B \cdot RR(\widehat{\mathbf{y}}) + CD \right) - \gamma \left(C + G\widetilde{Z}_e(\widehat{\mathbf{y}}) \right) \widetilde{T}, \tag{5.141}$$

$$\widehat{f}_2(\widehat{\mathbf{y}}) = \frac{1}{\widetilde{\rho}} \left(\widehat{f}_1(\widehat{\mathbf{y}}) - \widehat{f}_5(\widehat{\mathbf{y}})\widetilde{T} \right), \tag{5.142}$$

$$\widehat{f}_3(\widehat{\mathbf{y}}) = \frac{E}{\widetilde{\rho}_e(\widehat{\mathbf{y}})} \left(\widetilde{P}_e(\widehat{\mathbf{y}}) - 1 \right) - F\,\widetilde{u}\,|\widetilde{u}|, \tag{5.143}$$

$$\widehat{f}_4(\widehat{\mathbf{y}}) = \frac{1}{\widetilde{\rho}} \left(A \left(Y_{f,i} - Y_f \right) - RR(\widehat{\mathbf{y}}) \right), \tag{5.144}$$

$$\widehat{f}_5(\widehat{\mathbf{y}}) = A - G\widetilde{Z}_e(\widehat{\mathbf{y}}), \tag{5.145}$$

cf. equations (5.73)–(5.76) and (5.138). The terms RR, $\widetilde{Z}_e$, $\widetilde{\rho}_e$, and $\widetilde{P}_e$ are functions of $\widehat{\mathbf{y}}$. With the constant $\alpha = \frac{\gamma-1}{2} \frac{u_0^2}{\gamma R T_0}$ and a newly introduced variable $\mu = \frac{\widetilde{u}^2}{\widetilde{T}}$ (to ease the notation), these terms are given by

$$RR(\widehat{\mathbf{y}}) = A' \sqrt{\widetilde{T}} \, \widetilde{\rho}^2 \, Y_f^2 \, \exp\left(-\frac{\widetilde{T}_{\mathrm{act}}}{\widetilde{T}} \right), \tag{5.146}$$

$$\widetilde{Z}_e(\widehat{\mathbf{y}}) = \widetilde{\rho}_e \widetilde{u}, \tag{5.147}$$

$$\mu(\widehat{\mathbf{y}}) = \frac{\widetilde{u}^2}{\widetilde{T}}, \tag{5.148}$$

$$\widetilde{\rho}_e(\widehat{\mathbf{y}}) = \widetilde{\rho} \left(1 - \alpha\mu(\widehat{\mathbf{y}}) \right)^{\frac{1}{\gamma-1}}, \tag{5.149}$$

$$\widetilde{P}_e(\widehat{\mathbf{y}}) = \widetilde{P} \left(1 - \alpha\mu(\widehat{\mathbf{y}}) \right)^{\frac{\gamma}{\gamma-1}}. \tag{5.150}$$

Now, if $\widetilde{\rho}$ is eliminated from these equations using the perfect gas law, the original system of model equations results. Eliminating $\widetilde{P}$ or $\widetilde{T}$ from the extended system of equations (using the perfect gas law) is equivalent to applying a variable transformation of the original system.

We can consider $\widehat{\mathbf{y}}$ to be a function of $\mathbf{z} = (z_1, \ldots, z_4)^\top$, which is formed from $\widehat{\mathbf{y}}$ by removing $\widehat{y}_1 = \widetilde{P}$, $\widehat{y}_2 = \widetilde{T}$, or $\widehat{y}_5 = \widetilde{\rho}$. Let $\widehat{y}_k$ be the variable that is removed (i.e., it is eliminated from the extended system of equations). Using the chain rule for differentiation, the derivatives $\frac{\partial \widehat{f}_i}{\partial z_j}$, $i = 1, \ldots, 5$, $j = 1, \ldots, 4$, can be expressed in the derivatives $\frac{\partial \widehat{y}_i}{\partial z_j}$. With the perfect gas law, $\widehat{y}_k$ can be expressed in $\mathbf{z}$, so all the derivatives $\frac{\partial \widehat{y}_i}{\partial z_j}$ can be determined. The Jacobian matrix associated with the system of equations (which is expressed in $\mathbf{z}$) can then be formed from $\frac{\partial \widehat{f}_i}{\partial z_j}$ for $i \neq k$.

In deriving the elements of the Jacobian matrices, the following differential relationship is used repeatedly: the derivative of $\Phi(\xi) = \prod_{i=1}^{n} \phi_i(\xi)^{\nu_i}$ is given by $\frac{d\Phi}{d\xi} = \sum_{i=1}^{n} \nu_i \frac{\Phi}{\phi_i} \frac{d\phi_i}{d\xi}$. (Of course, certain smoothness conditions need to be satisfied. For $\phi_i(\xi) = 0$, we can take the limit of $\xi \to 0$ in the right-hand side.)

The elements $\frac{\partial \widehat{f}_i}{\partial z_j}$ ($i = 1, \ldots, 5$, $j = 1, \ldots, 4$) are given by

$$\frac{\partial \widehat{f}_1}{\partial z_j} = \gamma B \frac{\partial RR}{\partial z_j} - \gamma \left(C + G\widetilde{Z}_e \right) \frac{\partial \widetilde{T}}{\partial z_j} - \gamma G\widetilde{T} \frac{\partial \widetilde{Z}_e}{\partial z_j}, \qquad (5.151)$$

$$\frac{\partial \widehat{f}_2}{\partial z_j} = -\frac{\widehat{f}_2}{\widetilde{\rho}} \frac{\partial \widetilde{\rho}}{\partial z_j} + \frac{1}{\widetilde{\rho}} \left(\frac{\partial \widehat{f}_1}{\partial z_j} - \frac{\partial \widehat{f}_5}{\partial z_j} \widetilde{T} - \widehat{f}_5 \frac{\partial \widetilde{T}}{\partial z_j} \right), \qquad (5.152)$$

$$\frac{\partial \widehat{f}_3}{\partial z_j} = -\frac{1}{\widetilde{\rho}_e^2} \frac{\partial \widetilde{\rho}_e}{\partial z_j} E \left(\widetilde{P}_e - 1 \right) + \frac{E}{\widetilde{\rho}_e} \frac{\partial \widetilde{P}_e}{\partial z_j} - 2F|\widetilde{u}| \frac{\partial \widetilde{u}}{\partial z_j}, \qquad (5.153)$$

$$\frac{\partial \widehat{f}_4}{\partial z_j} = -\frac{\widehat{f}_4}{\widetilde{\rho}} \frac{\partial \widetilde{\rho}}{\partial z_j} - \frac{1}{\widetilde{\rho}} \left(A \frac{\partial Y_f}{\partial z_j} + \frac{\partial RR}{\partial z_j} \right), \qquad (5.154)$$

$$\frac{\partial \widehat{f}_5}{\partial z_j} = -G \frac{\partial \widetilde{Z}_e}{\partial z_j}, \qquad (5.155)$$

where

$$\frac{\partial RR}{\partial z_j} = 2 \frac{RR}{\widetilde{\rho}} \frac{\partial \widetilde{\rho}}{\partial z_j} + 2 \frac{RR}{Y_f} \frac{\partial Y_f}{\partial z_j} + \left(\frac{1}{2} + \frac{\widetilde{T}_{\text{act}}}{\widetilde{T}} \right) \frac{RR}{\widetilde{T}} \frac{\partial \widetilde{T}}{\partial z_j}, \quad (5.156)$$

$$\frac{\partial \widetilde{Z}_e}{\partial z_j} = \widetilde{u} \frac{\partial \widetilde{\rho}_e}{\partial z_j} + \widetilde{\rho}_e \frac{\partial \widetilde{u}}{\partial z_j}, \qquad (5.157)$$

$$\frac{\partial \widetilde{\rho}_e}{\partial z_j} = \frac{\widetilde{\rho}_e}{\widetilde{\rho}} \frac{\partial \widetilde{\rho}}{\partial z_j} + \frac{1}{\gamma - 1} \frac{\widetilde{\rho}_e}{(1 - \alpha\mu)} \left(-\alpha \frac{\partial \mu}{\partial z_j} \right), \qquad (5.158)$$

$$\frac{\partial \widetilde{P}_e}{\partial z_j} = \frac{\widetilde{P}_e}{\widetilde{P}} \frac{\partial \widetilde{P}}{\partial z_j} + \frac{\gamma}{\gamma - 1} \frac{\widetilde{P}_e}{(1 - \alpha\mu)} \left(-\alpha \frac{\partial \mu}{\partial z_j} \right), \qquad (5.159)$$

$$\frac{\partial \mu}{\partial z_j} = \frac{\widetilde{u}}{\widetilde{T}} \left(2 \frac{\partial \widetilde{u}}{\partial z_j} - \frac{\widetilde{u}}{\widetilde{T}} \frac{\partial \widetilde{T}}{\partial z_j} \right). \qquad (5.160)$$

If the mixing time τ_m is incorporated in the reaction rate (see (5.110)), the derivatives $\frac{\partial \widehat{f}_i}{\partial z_j}$ are adjusted in the following way. By using the chain rule for differentiation, it is easy to show that

$$\frac{\partial \widehat{RR}}{\partial z_j} = \left(1 - B \cdot \tau_m \widehat{RR} \right) \frac{\widehat{RR}}{RR} \frac{\partial RR}{\partial z_j}. \qquad (5.161)$$

The derivatives $\frac{\partial \widehat{f}_i}{\partial z_j}$ are found by replacing the term $\frac{\partial RR}{\partial z_j}$ in (5.151) and (5.154) by $\frac{\partial \widehat{RR}}{\partial z_j}$, which is given by (5.161).

Let us make the derivatives explicit. If $k = 1$ (thus, $\widehat{y}_1 = \widetilde{P}$ is expressed in $\widehat{y}_2 = \widetilde{T}$ and $\widehat{y}_5 = \widetilde{\rho}$), we have $\widehat{\mathbf{y}} = (\widetilde{T}\widetilde{\rho}, \widetilde{T}, \widetilde{u}, Y_f, \widetilde{\rho})^\top$ and $\mathbf{z} = (\widetilde{T}, \widetilde{u}, Y_f, \widetilde{\rho})^\top$. The

derivatives $\frac{\partial \widehat{y}_i}{\partial z_j}$ ($i = 1, \ldots, 5$ and $j = 1, \ldots, 4$) are given by

$$\frac{\partial \widehat{y}_i}{\partial z_j} = \frac{\partial}{\partial z_j} \begin{pmatrix} \widetilde{T}\widetilde{\rho} \\ \widetilde{T} \\ \widetilde{u} \\ Y_f \\ \widetilde{\rho} \end{pmatrix}_{(i)} = \begin{pmatrix} \widetilde{\rho} & 0 & 0 & \widetilde{T} \\ 1 & 0 & 0 & 0 \\ 0 & 1 & 0 & 0 \\ 0 & 0 & 1 & 0 \\ 0 & 0 & 0 & 1 \end{pmatrix}_{(i,j)} , \qquad (5.162)$$

where the subscript (i) denotes the element in the ith row of the vector, and (i, j) denotes the element in the ith row and jth column of the matrix. Now, the Jacobian matrix is formed from the matrix with the (i, j)-element equal to $\frac{\partial \widehat{f}_i}{\partial z_j}$ ($i = 1, \ldots, 5$, $j = 1, \ldots, 4$) by throwing away the first row ($k = 1$).

Similarly, if $k = 2$ ($\widetilde{T}$ is eliminated) we have $\widehat{\mathbf{y}} = (\widetilde{P}, \widetilde{P}/\widetilde{\rho}, \widetilde{u}, Y_f, \widetilde{\rho})^\top$ and $\mathbf{z} = (\widetilde{P}, \widetilde{u}, Y_f, \widetilde{\rho})^\top$, and the derivatives $\frac{\partial \widehat{y}_i}{\partial z_j}$ are given by

$$\frac{\partial \widehat{y}_i}{\partial z_j} = \frac{\partial}{\partial z_j} \begin{pmatrix} \widetilde{P} \\ \widetilde{P}/\widetilde{\rho} \\ \widetilde{u} \\ Y_f \\ \widetilde{\rho} \end{pmatrix}_{(i)} = \begin{pmatrix} 1 & 0 & 0 & 0 \\ 1/\widetilde{\rho} & 0 & 0 & -\widetilde{P}/\widetilde{\rho}^2 \\ 0 & 1 & 0 & 0 \\ 0 & 0 & 1 & 0 \\ 0 & 0 & 0 & 1 \end{pmatrix}_{(i,j)} . \qquad (5.163)$$

Now, the Jacobian matrix is formed from the matrix with the (i, j)-element equal to $\frac{\partial \widehat{f}_i}{\partial z_j}$ ($i = 1, \ldots, 5$, $j = 1, \ldots, 4$) by throwing away the second row ($k = 2$).

Finally, if $k = 5$ ($\widetilde{\rho}$ is eliminated) we have $\widehat{\mathbf{y}} = (\widetilde{P}, \widetilde{T}, \widetilde{u}, Y_f, \widetilde{P}/\widetilde{T})^\top$ and $\mathbf{z} = (\widetilde{P}, \widetilde{T}, \widetilde{u}, Y_f)^\top$, and the derivatives $\frac{\partial \widehat{y}_i}{\partial z_j}$ are given by

$$\frac{\partial \widehat{y}_i}{\partial z_j} = \frac{\partial}{\partial z_j} \begin{pmatrix} \widetilde{P} \\ \widetilde{T} \\ \widetilde{u} \\ Y_f \\ \widetilde{P}/\widetilde{T} \end{pmatrix}_{(i)} = \begin{pmatrix} 1 & 0 & 0 & 0 \\ 0 & 1 & 0 & 0 \\ 0 & 0 & 1 & 0 \\ 0 & 0 & 0 & 1 \\ 1/\widetilde{T} & 0 & 0 & -\widetilde{P}/\widetilde{T}^2 \end{pmatrix}_{(i,j)} . \qquad (5.164)$$

Now, the Jacobian matrix is formed from the matrix with the (i, j)-element equal to $\frac{\partial \widehat{f}_i}{\partial z_j}$ ($i = 1, \ldots, 5$, $j = 1, \ldots, 4$) by throwing away the last row ($k = 5$).

Stability analysis is independent of the choice of variables

The solution of the system of model equations is, of course, independent of the choice of variables in which they are expressed (e.g. using $\widetilde{\rho}$ instead of $\widetilde{T}$). That the stability analysis will give results that are independent of the choice of variables, will be shown next. But first we introduce some notation.

In this subsection, vectors are printed in bold, and their elements are displayed in normal font with an index. The notation $\mathbf{y} = (y_i)$ means that $\mathbf{y}$ is a vector with elements y_i, with $i = 1, 2, \ldots, d$, where d is the dimension of the vector $\mathbf{y}$. Matrices are printed in capitals, and their elements are displayed in normal font with two indices. The notation $A = (a_{ij})$ means that A is a matrix with elements a_{ij}, with $i = 1, 2, \ldots, m$, and $j = 1, 2, \ldots, n$, where $m \times n$ gives the

dimensions of the matrix A. The derivative of a vector function $\mathbf{f}(\mathbf{x}) = (f_i(\mathbf{x}))$ is denoted by $\mathbf{f}' = (f'_{ij})$. The elements of the functional matrix $\mathbf{f}'$ are given by $f'_{ij} = \frac{\partial f_i}{\partial x_j}$, with $i = 1, \ldots, m$ and $j = 1, \ldots, n$, where m is the dimension of $\mathbf{f}(\mathbf{x})$ and n is the dimension of $\mathbf{x}$, the argument of $\mathbf{f}$.

Consider a (sufficiently smooth) invertible function $\boldsymbol{\eta} : D \to E$, which maps $\mathbf{z} \in D \subset \mathbb{R}^n$ to $\mathbf{y} = \boldsymbol{\eta}(\mathbf{z}) \in E \subset \mathbb{R}^n$. Applying the chain rule of differentiation gives

$$\frac{dy_i}{dt} = \sum_{k=1}^{n} \frac{\partial \eta_i}{\partial z_k} \frac{dz_k}{dt}, \tag{5.165}$$

or, using vector notation,

$$\frac{d\mathbf{y}}{dt} = \boldsymbol{\eta}'(\mathbf{z}) \frac{d\mathbf{z}}{dt}, \tag{5.166}$$

where $\mathbf{y} = (y_i)$, $\mathbf{z} = (z_i)$, and $\boldsymbol{\eta}' = (\eta'_{ij})$, with $\eta'_{ij} = \frac{\partial \eta_i}{\partial z_j}$. With the derivative $\boldsymbol{\eta}'$ being invertible (under sufficient conditions on the smoothness of $\boldsymbol{\eta}$), the system of equations

$$\frac{d\mathbf{y}}{dt} = \mathbf{f}(\mathbf{y}) \tag{5.167}$$

is transformed to

$$\frac{d\mathbf{z}}{dt} = \boldsymbol{\eta}'(\mathbf{z})^{-1} \mathbf{f}(\boldsymbol{\eta}(\mathbf{z})) = B(\mathbf{z}) \mathbf{f}(\boldsymbol{\eta}(\mathbf{z})) = \mathbf{g}(\mathbf{z}), \tag{5.168}$$

where the matrix $B(\mathbf{z}) = (b_{ij}) = \boldsymbol{\eta}'(\mathbf{z})^{-1}$ is introduced to ease subsequent notation, and the function $\mathbf{g} = (g_i)$ is defined by the last equality relation. The elements $g'_{ij} = \frac{\partial g_i}{\partial z_j}$ of the Jacobian matrix $\mathbf{g}' = (g'_{ij})$ are given by

$$g'_{ij} = \frac{\partial g_i}{\partial z_j} = \frac{\partial}{\partial z_j} \sum_{k=1}^{n} b_{ik} (f \circ \eta)_k = \sum_{k=1}^{n} \left(\frac{\partial b_{ik}}{\partial z_j} (f \circ \eta)_k + b_{ik} \frac{\partial (f \circ \eta)_k}{\partial z_j} \right), \tag{5.169}$$

where $(f \circ \eta)_k$ denotes the kth element of the vector function $\mathbf{f}(\boldsymbol{\eta}(\mathbf{z}))$. The stability analysis is based on the properties of the Jacobian matrix associated with the system, evaluated in a critical point. For a critical point $\mathbf{y}^*$ of the original system (5.167) we have $\mathbf{f}(\mathbf{y}^*) = \mathbf{0}$. The associated critical point $\mathbf{z}^*$ for the transformed system (5.168) is given by $\mathbf{y}^* = \boldsymbol{\eta}(\mathbf{z}^*)$ (i.e. $\mathbf{z}^* = \boldsymbol{\eta}^{-1}(\mathbf{y}^*)$, where $\boldsymbol{\eta}^{-1}$ is the inverse of the function $\boldsymbol{\eta}$). It follows that $\mathbf{f}(\boldsymbol{\eta}(\mathbf{z}^*)) = \mathbf{0}$, so the first term of the sum in the right-hand side of (5.169) vanishes in a critical point. With

$$\frac{\partial (f \circ \eta)_k}{\partial z_j} = \sum_{m=1}^{n} \frac{\partial f_k}{\partial \eta_m} \frac{\partial \eta_m}{\partial z_j} = \sum_{m=1}^{n} a_{km} c_{mj}, \tag{5.170}$$

where $a_{km} = \frac{\partial f_k}{\partial \eta_m}$ and $c_{mj} = \frac{\partial \eta_m}{\partial z_j}$, the relation (5.169) can be written as

$$g'_{ij} = \sum_{k=1}^{n} \sum_{m=1}^{n} b_{ik} a_{km} c_{mj}. \tag{5.171}$$

This can be written in the matrix form $\mathbf{g}' = BAC$, where $A = (a_{ij})$ and $C = (c_{ij})$. Since $a_{ij} = \frac{\partial f_i}{\partial \eta_j} = f'_{ij}$ and $c_{ij} = \frac{\partial \eta_i}{\partial z_j} = \eta'_{ij}$, we have $A = \mathbf{f}'$ and $C = B^{-1}$. It follows that in a critical point $\mathbf{z}^*$ of the transformed system (5.168),

the Jacobian matrix $\mathbf{g}'$ is similar to the Jacobian matrix $\mathbf{f}'$ of the original system (5.167) in the corresponding critical point $\mathbf{y}^* = \boldsymbol{\eta}(\mathbf{z}^*)$:

$$\mathbf{g}'(\mathbf{z}^*) = \boldsymbol{\eta}'(\mathbf{z}^*)^{-1}\mathbf{f}'(\mathbf{y}^*)\boldsymbol{\eta}'(\mathbf{z}^*). \tag{5.172}$$

Since similar matrices share the same Jordan form, the stability analysis will give the same results for the original system (5.167) as for the transformed system (5.168).

5.5.4 Results from stability analysis

In this subsection the steady states of the system of model equations are determined for various model parameter sets. The influence of parameter variation on the steady states is investigated. Then, the stability of the steady states is investigated by examining the eigenvalues of the corresponding Jacobian matrices. Finally, results from the stability analysis are compared to numerical results that were obtained from numerical integration.

Investigation of the critical points

It was shown earlier that the critical points of the system of model equations (5.73)–(5.76) can be determined from the steady-state temperatures: with $\widetilde{T}^*$ a steady-state temperature of the system of model equations, the corresponding critical point $\mathbf{y}^*(\widetilde{T}^*) = (\widetilde{P}^*, \widetilde{T}^*, \widetilde{u}^*, Y_f^*)^\top$ is given by the expressions (5.128)–(5.132). The steady-state temperatures are found by solving the nonlinear equation $RR_1(\widetilde{T}) = RR_2(\widetilde{T})$ for $\widetilde{T}_{\min} \leq \widetilde{T} \leq \widetilde{T}_{\max}$, where RR_1 is the reaction rate associated with the critical point:

$$RR_1(\widetilde{T}) = RR(\mathbf{y}(\widetilde{T})) = A'\sqrt{\widetilde{T}}\,\widetilde{\rho}(\mathbf{y}(\widetilde{T}))^2 Y_f(\widetilde{T})^2 \exp(-\widetilde{T}_{\mathrm{act}}/\widetilde{T}), \tag{5.173}$$

and RR_2 is the reaction rate that is needed for $\widetilde{T}$ to be a steady-state temperature (i.e. to obtain a balance in the heat release terms):

$$RR_2(\widetilde{T}) = \frac{A+C}{B}\left(\widetilde{T} - \frac{A+CD}{A+C}\right) = AY_{f,i}\left(\frac{\widetilde{T} - \widetilde{T}_{\min}}{\widetilde{T}_{\max} - \widetilde{T}_{\min}}\right). \tag{5.174}$$

The boundaries for the temperature are given by

$$\widetilde{T}_{\min} = \frac{A+CD}{A+C}, \quad \widetilde{T}_{\max} = \widetilde{T}_{\min} + \frac{AB}{A+C}Y_{f,i}, \tag{5.175}$$

which resulted from the minimum steady-state reaction rate ($RR^* = 0$) and the maximum steady-state fuel conversion ($Y_f^* = 0$), see expressions (5.132)–(5.134).

In Figure 5.13, graphs for RR_1 and RR_2 are plotted as functions of the temperature $\widetilde{T}$, using default parameter values. The steady-state temperatures are found from the intersections of the graphs on the temperature interval $[\widetilde{T}_{\min}, \widetilde{T}_{\max}]$. These are indicated with bullets just below the horizontal axis.

Arrows show how the graphs respond to an increase of the wall temperature T_w. The response of the reaction rate RR_2 to an increase of the wall temperature is particularly simple: T_w is only present in the definition of the constant D
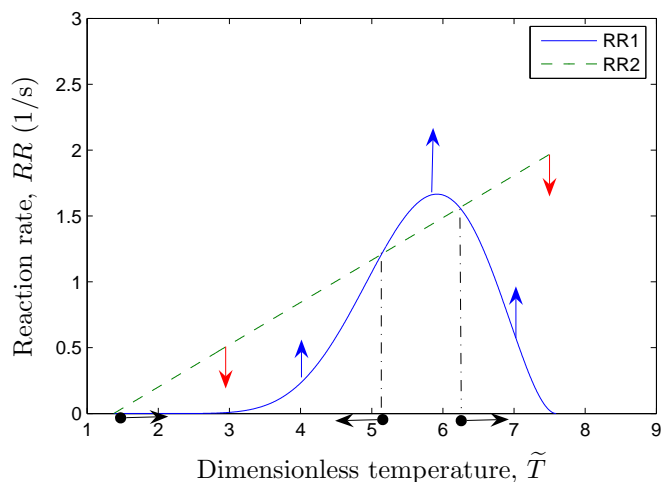
Figure 5.13: Graphs of the reaction rates $RR_1(\widetilde{T})$ and $RR_2(\widetilde{T})$. The steady-state temperatures are indicated by the bullets just below the axis. Arrows indicate the responses to an increase of the wall temperature T_w.

(see (5.84)). It follows directly from (5.174) that the graph of RR_2 is just shifted downward if T_w is increased. With RR_1 increasing for increasing wall temperatures, the responses of the steady-state temperatures to an increase of T_w are as indicated in Figure 5.13 by the arrows attached to the bullets. The responses to a decrease of the wall temperature are of course just in the opposite directions.

Note that $RR_2(\widetilde{T}_{\min}) = 0$, while $RR_1(\widetilde{T}_{\min}) > 0$, and that $RR_1(\widetilde{T}_{\max}) = 0$, while $RR_2(\widetilde{T}_{\max}) > 0$. Thus, there is always at least one steady-state temperature in the interval $[\widetilde{T}_{\min}, \widetilde{T}_{\max}]$. The graph of RR_2 is a straight line (with a zero at $\widetilde{T} = \widetilde{T}_{\min}$) for all model parameter values. For different model parameter values, we may expect similar shapes of the graph of RR_1 as the one shown in Figure 5.13. From this, we may expect for any set of model parameter values, one, two, or three critical points. (Two is only possible if the straight line of RR_2 is tangent to the curve of RR_1.) In particular, we may expect one critical point for very low values of the wall temperature T_w, while by increasing T_w we get (first two and immediately thereafter) three critical points. Increasing T_w even further, if necessary beyond any value of practical relevance, we may again expect only one critical point (with at the exact moment of transition two critical points). Thus, with varying values of the wall temperature, the system may show bifurcation of the critical points.

The bifurcation of the critical points is illustrated in Figure 5.14, which shows the steady-state temperatures for varying wall temperature, while all other model parameter values are held constant at their default values. It shows that for wall temperatures below 778 K, there is only one steady-state temperature. It is very low: this steady-state temperature is the result of flame extinction. If the wall temperature is higher than 778 K, there are three critical points. This may alter the behaviour of the system significantly. For example, if the critical point with the highest steady-state temperature is stable, the sys-
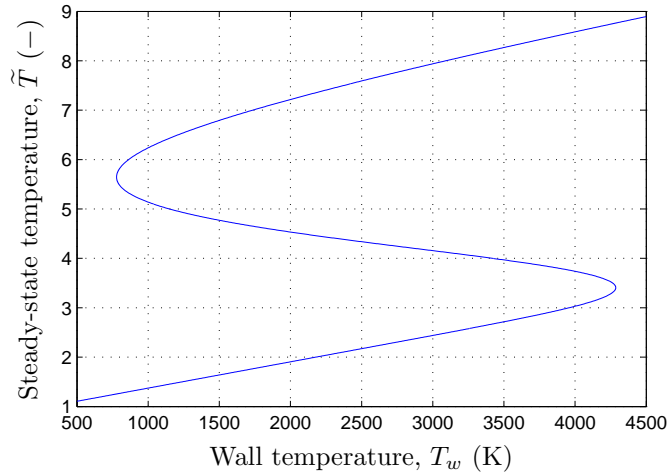
Figure 5.14: Bifurcation of steady-state temperatures takes place for wall temperatures around $T_w \approx 778\,\mathrm{K}$ and around $T_w \approx 4286\,\mathrm{K}$

tem may be in a state of steady combustion. This would not be possible for wall temperatures below 778 K. The stability of the steady states can be established from examining the eigenvalues of the Jacobian matrices of the system of model equations, evaluated in the critical points. Such an investigation for varying wall temperature can be found below under the heading "Inspection of the eigenvalues."

We may expect similar results from varying other parameter values. Figure 5.15 shows how the steady-state temperatures change if the model parameters are varied over a range of 50%–150% of their default values, while keeping the other model parameters constant at their default values. The vertical lines in these plots indicate the default values of the model parameters. (Since the default value of the mixing time τ_m is 0 ms, it was changed temporarily to 0.7 ms to obtain a plot over a range of values.)

From these plots, we get an impression of the sensitivity of the system to changes in the model parameters. For example, it can be seen that for values of ΔH_f below $4.8 \times 10^7\,\mathrm{J/kg}$, and all other parameters at their default values, there is only one steady state, which is associated with flame extinction. This is in agreement with the earlier observation that pulse combustion does not occur for values of ΔH_f below $4.88 \times 10^7\,\mathrm{J/kg}$ (see p. 63). The plot for the heat transfer coefficient $\widehat{h}$ shows that flame extinction for values of $\widehat{h}$ above $159\,\mathrm{W/m^2/K}$ is due to bifurcation of the critical points. Through numerical integration of the model equations, it was found earlier that flame extinction occurs for $\widehat{h}$ between 150 and $155\,\mathrm{W/m^2/K}$ (see Subsection 5.4.2, p. 68). The seeming discrepancy results from the choice of initial conditions. If the initial conditions are chosen close to the critical point with the highest steady-state temperature, the numerical integration suggests there is a stable limit cycle for $\widehat{h} = 155\,\mathrm{W/m^2/K}$. Flame extinction is not always associated with steady-state bifurcation, as can be seen by comparing the numerical results for varying tailpipe lengths (see Subsection 5.4.4, p. 72) with the plot for L_{tp} in Figure
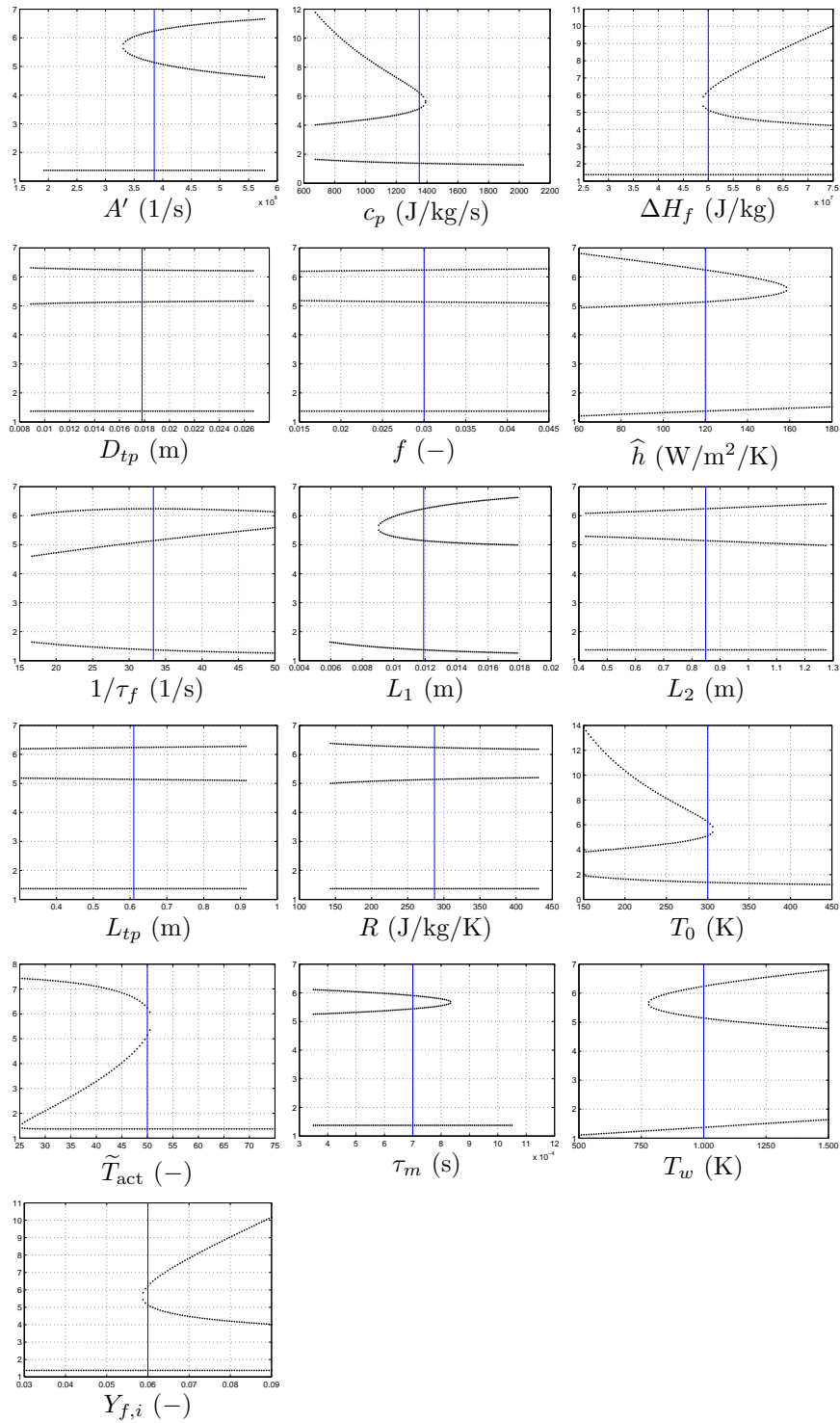
Figure 5.15: Bifurcation of critical points. Default parameter values are indicated with a vertical line. (To get a plot for τ_m, its default value has been changed temporarily from 0 ms to 0.7 ms.)

Figure 5.16: Bifurcation of critical points. T_w is set to 778.5 K, close to its bifurcation value if the other parameters have their default values. Default parameter values are indicated with a vertical line.

5.15. Results from numerical integration show that flame extinction occurs for tailpipe lengths above $0.775\,\mathrm{m}$ and that there is steady combustion for values below $0.525\,\mathrm{m}$, while the steady-state temperatures hardly change in that range of values.

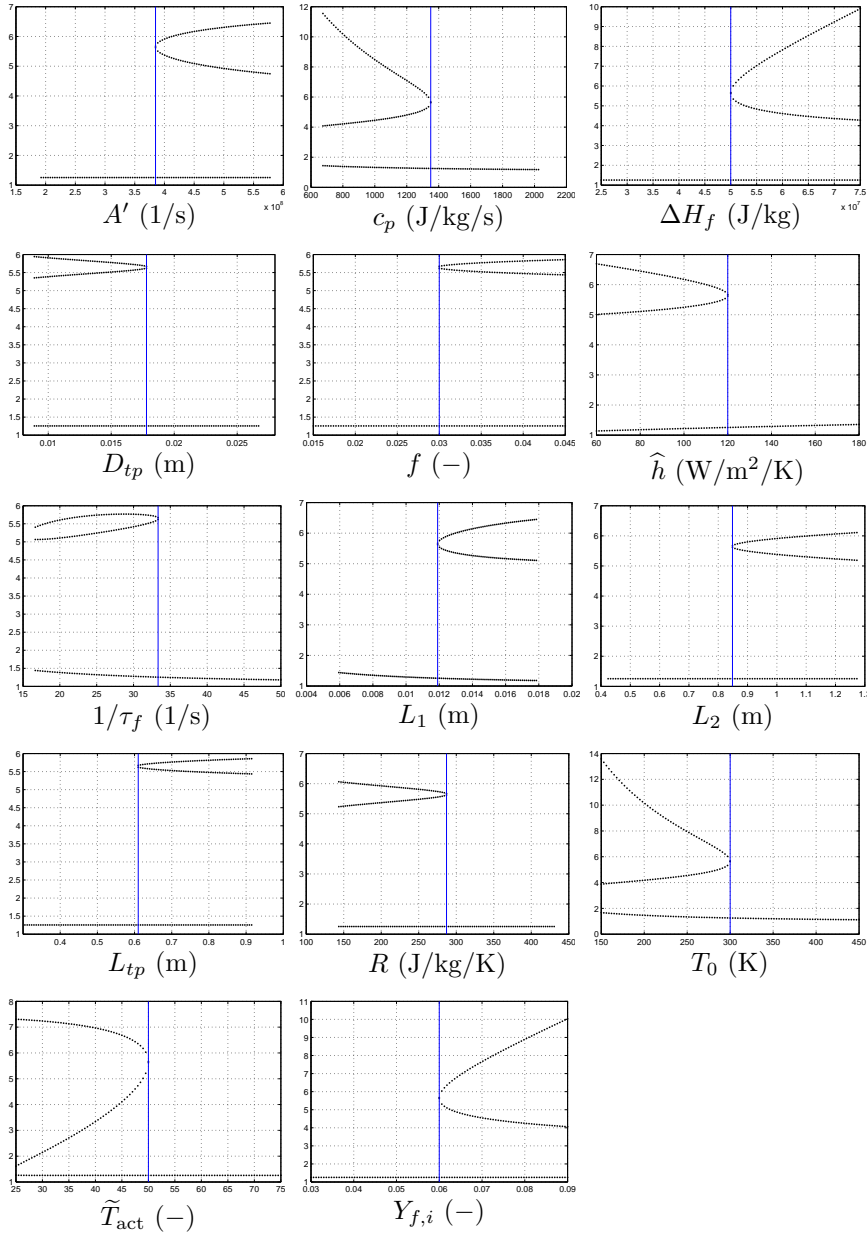As was mentioned before, the vertical lines in Figure 5.15 indicate the defaults values of the model parameters. Since in the plots only one parameter is changed from its default value, the steady-state temperature on the vertical line must be the same in all the plots. Thus, if we change the default value of one model parameter to a value for which steady-state bifurcation occurs, the vertical line will have two steady-state temperatures for all the plots. So, the system will show steady-state bifurcation for all the default parameter values. This is shown in Figure 5.16, which was obtained by changing the default value for the wall temperature T_w to $778.5\,\mathrm{K}$. Comparing the plots to those of Figure 5.15 gives an impression of how the steady-state temperatures change if two parameters are modified (the parameter of the plot and T_w). It is not difficult to see that plotting the steady-state temperatures for pairs of model parameters, would give a surface in 3-dimensional space with folds at the values for which bifurcation occurs.

Inspection of the eigenvalues

The eigenvalues of the Jacobian matrix of the system, evaluated in a critical point, give an indication for the stability of the critical point (or, steady-state solution): a steady-state solution is stable if all the eigenvalues have negative real part; it is unstable if at least one eigenvalue has a positive real part. In the phase plane, stable critical points attract phase paths, and if the solution of the system of model equations evolves along such a path, it will end up in a stable state: either flame extinction or steady combustion will occur. For pulsating combustion, starting close to a steady state, the oscillations must be amplified, until nonlinear effects limit further growth, and a limit cycle is attained. Thus, we are interested in the parts of the model parameter space that allow for unstable critical points. (In case that combustion oscillations may be harmful, or otherwise undesirable, one of course tries to keep the system away from unstable critical points.) We will investigate the eigenvalues associated with the steady-state temperatures over a range of wall temperatures. Refer to Figure 5.14 to see how the steady-state temperatures depend on the wall temperature.

As can be seen in Figure 5.14, there are ranges of wall temperatures for which there is only one critical point, and there are ranges for which there are three. On grounds of continuity, it may be expected that small changes in the steady-state temperature lead to small changes in the associated eigenvalues. Following the curve of Figure 5.14 from the low steady-state temperatures to the high temperatures, the associated eigenvalues were computed and plotted. In Figure 5.17 the results are shown per branch of the graph in Figure 5.14: (a) shows the eigenvalues for the lower branch, (b) shows the eigenvalues for the middle branch, and (c) shows the eigenvalues for the upper branch. Note that the scales of the plots are different. Also note that for most wall temperatures there are less than four values plotted for the real parts of the eigenvalues. This indicates that there are pairs of complex conjugate eigenvalues, which of course have equal real parts. In Figure (d) the eigenvalues are plotted for all three branches.

(a) For lower branch of Fig. 5.14

(b) For middle branch of Fig. 5.14

(c) For upper branch of Fig. 5.14

(d) For all branches of Fig. 5.14

(e) Zoom in of Subfig. (d)

(f) Further zoom in of Subfig. (d)

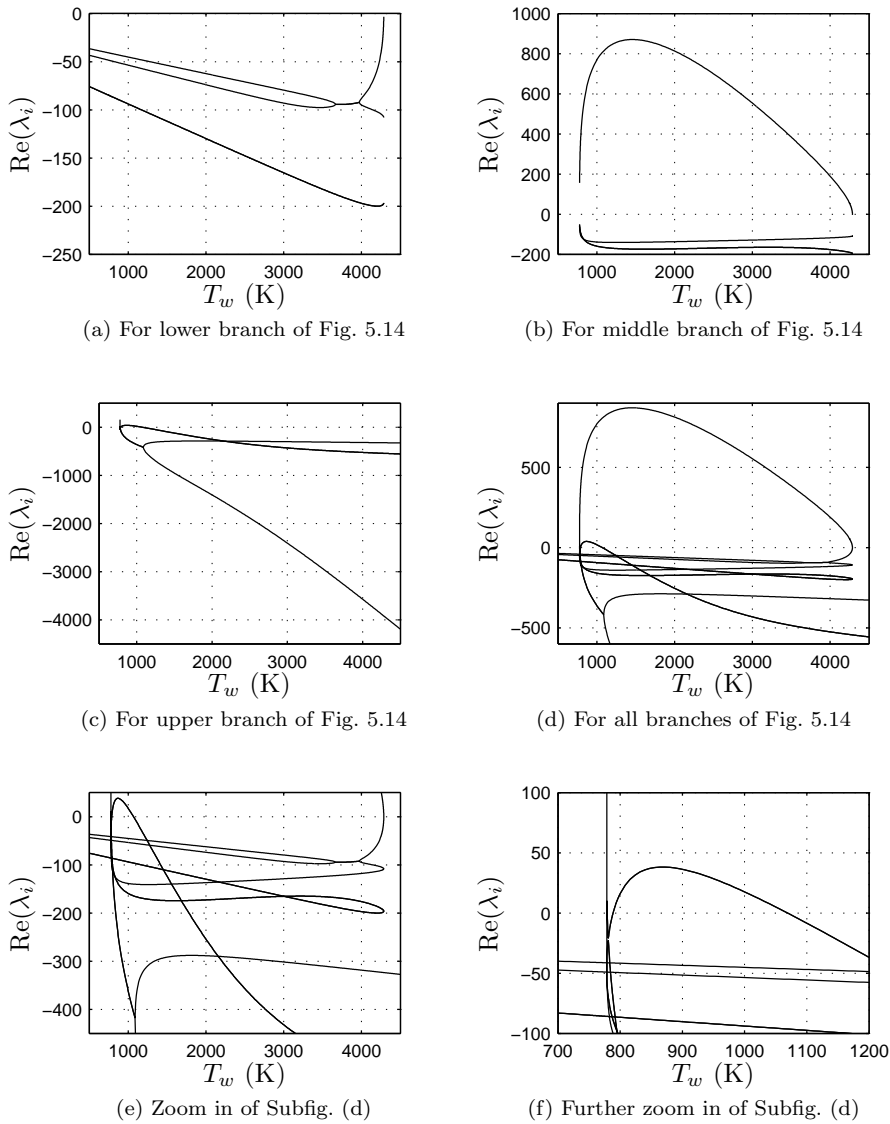Figure 5.17: The real parts of the eigenvalues λ_i, $i = 1, \ldots, 4$, of the Jacobian matrices associated with the steady-state temperatures of the graph in Figure 5.14: (a) for the lower branch of the graph, (b) for the middle branch, and (c) for the upper branch. In (d) the eigenvalues for the three branches are shown in one plot. An enlarged portion of (d) is shown in (e), and (f) is zoomed in even further.

The plots show that the steady states associated with the lower branch of the graph in Figure 5.14, are all stable; the steady states associated with the middle branch are all unstable, while those associated with the upper branch may be stable or unstable. These results are not surprising: for low temperatures, the reaction rate is too low to maintain combustion, and flame extinction occurs. For high temperatures, the reaction rate may increase until the limited fuel supply prevents further increase. For intermediate temperatures, there are no mechanisms that limit the self-excited decrease or increase of the temperature: a steady state can only result from a delicate balance. If the system starts close to a steady state with an intermediate temperature, we may expect it to evolve toward a critical point with a higher temperature, or to a critical point with a lower temperature. Therefore, to study conditions for which pulse combustion may be possible, we are the most interested in the stability of the critical points with the highest temperatures.

The eigenvalues associated with the upper branch of Figure 5.14 (i.e., the highest steady-state temperatures) are shown in Figure 5.17c, and they can also be found in Figure 5.17d. The interesting parts of these curves are where one of the eigenvalues for the upper branch has positive real part. This can be better viewed in Figure 5.17e, which is an enlargement of Figure 5.17d. Figure 5.17f is zoomed in even further, and a range of wall temperatures for which the upper branch has an unstable critical point, can be read from the axis. The stability changes from unstable to stable if the wall temperature is increased beyond 1069 K. This coincides with the boundary between pulsating and steady combustion, which can be established by numerically integrating the model equations for varying wall temperatures.

Comparing results from stability analysis and numerical integration

In Section 5.4.5, the model equations were numerically integrated for three different mixing times (τ_m), and varying flow times and wall temperatures. In that way, regions in the model parameter space were established for which the model predicts pulsating combustion, steady combustion, or flame extinction. We will apply the stability analysis to the model equations and compare the results with those from numerical integration.

Figure 5.18a (at the end of this section) shows the results that were obtained previously from numerical integration for $\tau_m = 0$ ms (see also Figure 5.10a), and Figure 5.18b shows the results from stability analysis. We are interested in the eigenvalues that are associated with the highest steady-state temperature, and of these, those with the largest real parts. (If the largest real part is negative, all four critical points are stable.) The contour plot of Figure 5.18b shows these largest real parts.

The stability boundaries between regions with stable and unstable critical points are indicated with thick solid lines. They were obtained by plotting the contour lines for which the largest real part of the eigenvalues is equal to zero. For values below zero, all four critical points are stable, and the system may be expected to evolve toward a steady state: either flame extinction (for low temperatures), or steady combustion (for high temperatures). The boundary between regions for which there is only one critical point and regions for which there are three, is indicated with a dashed line. It was obtained by determining the number of critical points for combinations of flow time and wall temperature,

and then plotting the contour line for the value 2. It is not clearly visible in the contour plot, because it almost completely coincides with the left stability boundary. This shows that the transition from pulsating combustion to flame extinction is due to bifurcation of the steady states. On the other hand, the transition from steady combustion to pulsating combustion is due to the real parts of the eigenvalues passing through zero (with nonzero imaginary part). This is typically associated with a Hopf-bifurcation. The emergence of limit cycles may be related to this.

The contour plots for the results from numerical integration and from stability analysis are very similar, except for the lower flow times. By comparing the two contour plots, we see that flame extinction may occur, while the critical point with the highest steady-state temperature is unstable. In part, the discrepancy is due to the initial conditions: starting close enough to the critical point, the numerical integration may show pulsating behaviour. But there are also combinations of flow times and wall temperatures, for which the solution will not stay close to the critical point, resulting eventually in flame extinction. Thus, we may not conclude that pulse combustion will result if the steady-state is unstable. For that, we also need nonlinear effects that prevent the solution from wandering off in the phase plane.

With Figures 5.19 and 5.20, the results from numerical integration and from stability analysis can be compared for *mixing times* $\tau_m = 1\,\mathrm{ms}$ and $\tau_m = 0.5\,\mathrm{ms}$, respectively. The contour plots are very similar. From the contour plots of Figures 5.19b and 5.20b, it can be seen that the transition from steady combustion to flame extinction is associated with bifurcation of the critical points. The transition from steady combustion to pulsating combustion is due to the real parts of the eigenvalues passing through zero, while the imaginary parts are nonzero.

Close inspection of the boundaries indicated in each of the Figures 5.19 and 5.20, shows that they do not agree exactly. The boundaries obtained from stability analysis are more accurate than those obtained from numerical integration. Extending the time span of the numerical integration shows that the inconsistencies are caused by residual pressure oscillations, which eventually would fade away.

We see that the stability analysis provides results very similar to those from numerical integration. The biggest advantage of stability analysis over numerical integration is the reduced CPU-time that is needed to compute the results. For example, the data for the contour plot of Figure 5.18a took about 30 minutes to compute, while computing the data for contour plot of Figure 5.18b took only about 15 seconds. From this, we see that stability analysis is a valuable tool for exploring the model parameter space.
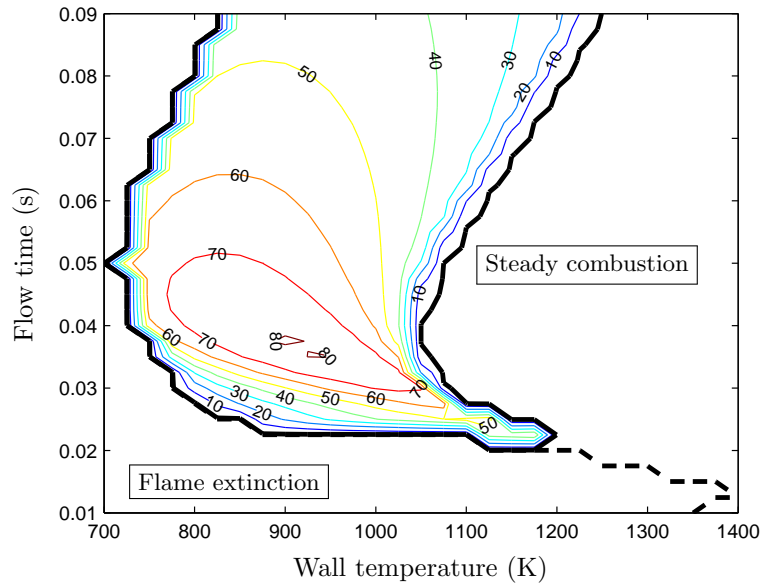
(a) Pressure amplitude (peak-to-peak, in kPa); maximum: 81 kPa
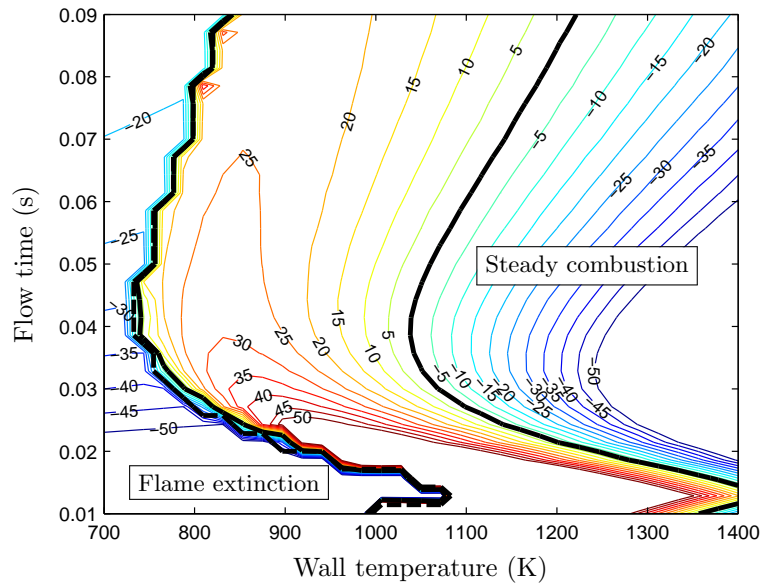
(b) Largest of real parts of eigenvalues for highest steady-state temperature

Figure 5.18: Comparison of the results obtained from (a) numerical integration (cf. Figure 5.10a) and (b) stability analysis; the *mixing time* is $\tau_m = 0$ ms. The lower contour plot shows the largest of the real parts of the eigenvalues associated with the critical point with the highest steady-state temperature. Thick solid line indicates the boundary between stable and unstable critical points. The boundary for bifurcation of the critical points is indicated with a thick dashed line; it coincides with the left stability boundary.
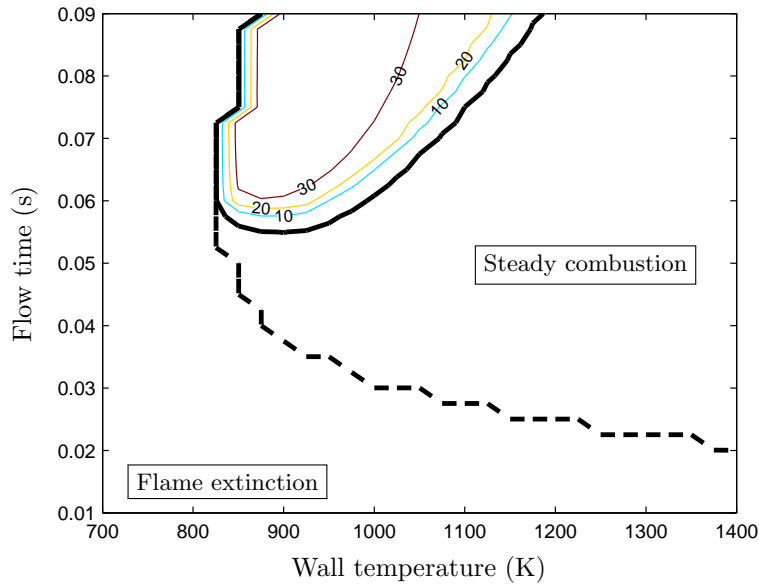
(a) Pressure amplitude (peak-to-peak, in kPa); maximum: 81 kPa
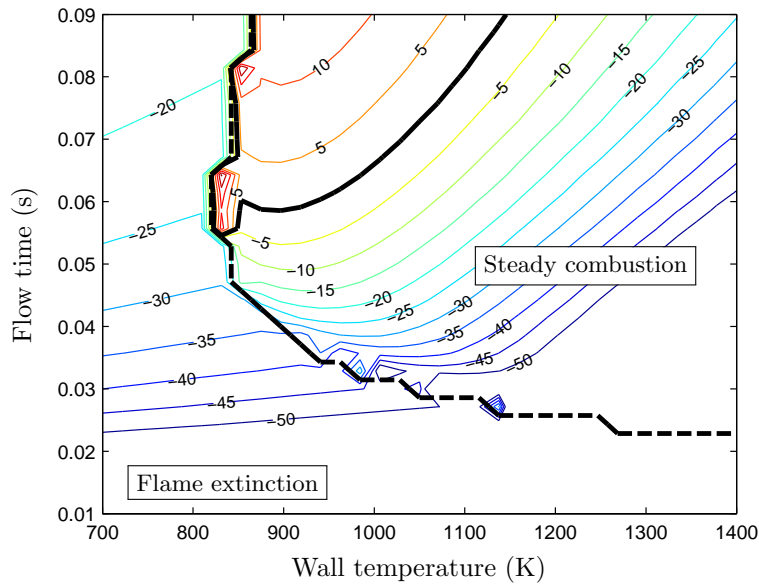
(b) Largest of real parts of eigenvalues for highest steady-state temperature

Figure 5.19: Comparison of the results obtained from (a) numerical integration (cf. Figure 5.11a) and (b) stability analysis; the *mixing time* is $\tau_m = 1\,\text{ms}$. The lower contour plot shows the largest of the real parts of the eigenvalues associated with the critical point with the highest steady-state temperature. Thick solid line indicates the boundary between stable and unstable critical points. The boundary for bifurcation of the critical points is indicated with a thick dashed line; it coincides in part with the stability boundary.

(a) Pressure amplitude (peak-to-peak, in kPa); maximum: 81 kPa
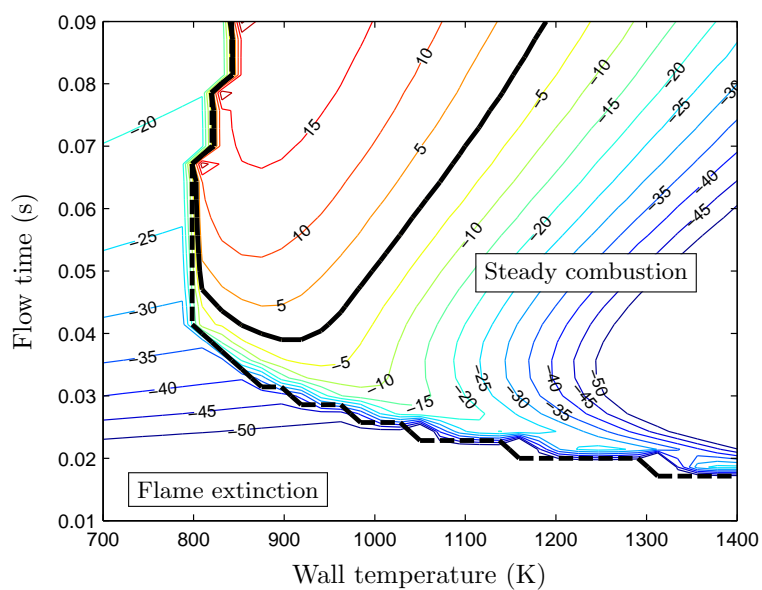
(b) Largest of real parts of eigenvalues for highest steady-state temperature

Figure 5.20: Comparison of the results obtained from (a) numerical integration (cf. Figure 5.12a) and (b) stability analysis; the *mixing time* is $\tau_m = 0.5$ ms. The lower contour plot shows the largest of the real parts of the eigenvalues associated with the critical point with the highest steady-state temperature. Thick solid line indicates the boundary between stable and unstable critical points. The boundary for bifurcation of the critical points is indicated with a thick dashed line; it coincides in part with the stability boundary.

5.6   Comment on related literature

The model of Richards et al. has been employed in a number of further studies. Two papers, one by Daw et al. [8] and one by In et al. [12], were already mentioned as sources for establishing certain model parameters that Richards et al. did not prescribe in their article. In these papers, chaotic behaviour of a thermal pulse combustor that is observed when the flow rate is increased toward the flameout limit, is investigated both experimentally and theoretically. The goal of these studies is to control operating parameters in such a way that chaos can be maintained, thereby extending the limits of operation. This can be useful for running combustors on lean fuel-air ratios, which show a chaotic behaviour near the flameout limit. The advantage of lean combustion is that it may increase fuel efficiency and lower emissions. These papers use the model of Richards et al. in an unaltered form, i.e. the same modelling assumptions and errors are applied.

There are studies that extend and/or modify the model of Richards et al. For example, Heravi [11] coupled the model equations to a chemical kinetic scheme, and implemented an adjustment to better account for an oscillatory heat transfer process. The purpose of this study was to predict NO_x and CO emissions. Another example is the paper of Datta et al. [7], in which they extend the model equations of Richards et al. to incorporate radiation from the combustor gases, and investigate perturbations of the mass inflow rate. They also observe signs of chaos in the numerical solutions of the model equations near the flameout limit. Again, the same modelling assumptions and errors are applied.

The articles of Narayanaswami and Richards [19] and of Richards and Gemmen [24] are of interest, because in these articles aerovalved combustion (thus, a variable mass inflow instead of a constant one) and mixing of cold and hot gases is incorporated into the model. It may be expected that the behaviour of a combustion system with an aerovalve differs from that with a steady mass inflow. In case of an aerovalve, the inflow of reactants (and with it, the mass fuel fraction, temperature, etc.) is dependent on the pressure amplitude of the combustion osc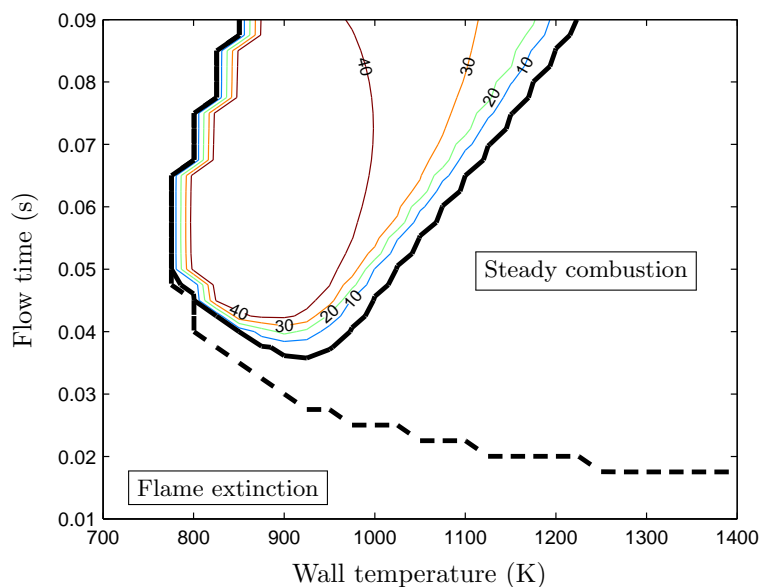illations, while in case of steady reactants inflow, it is independent of the pressure amplitude. With keeping track of the fluid properties of hot and cold gases separately, the error in the modelling of flow back into the combustion chamber that was introduced in the original model of Richards et al. is avoided. The purpose of these studies is to predict under what conditions pressure gain can be achieved. It could then be applied in a gas turbine instead of steady combustion to get an improved overall cycle efficiency.

Of particular interest are the articles of Keller et al. [14,15] and Barr et al. [3], to which Richards et al. referred in their article. In these articles, the importance of characteristic times to the operation of pulse combustors is demonstrated. The characteristic times they mention, consist of a species mixing time (to mix oxidizer and fuel, in case of non-premixed combustion), a mixing time for the reactants and hot products, a chemical reaction time and a resonance time. The first three characteristic times contribute to a total ignition delay time. These characteristic times are not the same as those mentioned by Richards et al. in their article. In the articles, Rayleigh's criterion is referred to, and a phase difference between heat release and pressure oscillations is expected to affect the operation of the pulse combustor, both in frequency and amplitude of the

oscillations.

5.7　Conclusions

In their article, Richards et al. [25] presented modelling results and experimental data for a so-called thermal pulse combustor. Contrary to a conventional pulse combustor, a thermal pulse combustor has a constant fuel and air supply. They have shown that an oscillatory combustion process is possible without using valves.

The model they presented, is a lumped parameter model with the combustion chamber as control volume. The combustion process is modelled by a one-step Ahrrenius law, depending on fuel and oxygen concentrations. Assuming that material properties are constant, that the perfect gas law holds, that the mixing in the combustion chamber is perfect and that combustion takes place at stoichiometric conditions, they derived a system of four ordinary differential equations. These come from applying conservation of energy, mass and species to the combustion chamber and conservation of momentum to the tailpipe flow, which is coupled to the combustion chamber conditions by isentropic acceleration of the combustion products. The tailpipe flow is treated as a slug flow, driven by the pressure difference over the tailpipe. Richards et al. incorporated friction in the tailpipe and heat transfer to the combustion chamber wall in their model.

In this chapter, the mathematical model presented by Richards et al. has been examined and implemented numerically. The derivation of the model equations has been given, largely following the presentation of Richards et al. In the course of deriving the model equations, the following comments on the mathematical model were given.

- The model equations do not correctly represent flow from the tailpipe back into the combustion chamber. To correct this, some kind of average values for the temperature, density and fuel mass fraction of the tailpipe gases need to be determined.

- The reaction rate in the model does not explicitly depend on the equivalence ratio, and is only valid for stoichiometric conditions. Although Richards et al. suggest that it may be used for simulation of lean combustion, the reaction rate given by Kretschmer and Odgers [18], on which Richards et al. based their reaction rate, is dependent on the equivalence ratio. It needs to be considered whether the reaction rate model needs to be adjusted in case of lean combustion.

- The density of the gases in the tailpipe is given by its value at the entrance. This means that slight modifications in the density at the entrance of the tailpipe, lead to a disproportional change of the mass of the tailpipe gases. This will have an effect on the velocity of the tailpipe gases. This can be corrected by introducing an extra ordinary differential equation, which continuously updates the average density of the tailpipe gases. Preliminary numerical results, incorporating such a correction, indicate that the effect may be significant.

- In order to obtain consistent results when varying the model parameters during numerical simulation, it was found necessary to rewrite the model equations. In particular, the inflow of reactants needed to be decoupled from the tailpipe fluid velocity by introducing a different parameter to non-dimensionalize the tailpipe fluid velocity.

- The characteristic time for the heat transfer (τ_{HT}) that was introduced by Richards et al. is not a characteristic parameter for the thermal pulse combustion process. The characteristic time for combustion (τ_c) is not a constant, but rather an expression for the reaction rate. Thus, it is not a characteristic parameter.

- The specific heats may vary significantly over the wide temperature range associated with pulse combustion. Since the solution of the model equations is strongly dependent on these parameters, the effect of the specific heats varying with the temperature needs to be examined more closely.

Difficulties arose when trying to reproduce the numerical results of Richards et al. These difficulties were due to uncertainty of the model parameters used by Richards et al. (in particular the specific heat for constant pressure) and by uncertainty of how Richards et al. have implemented the isentropic coupling of the tailpipe flow and the combustion chamber conditions. In the end, parameters were chosen based on values used in related articles. With the chosen parameters, the numerical results presented in this report closely resemble those of Richards et al. Differences are most notable in the pressure amplitudes and the ranges of parameters over which oscillatory solutions exist.

All the numerical results can be explained heuristically by referring to the phase difference between heat release and the acoustic oscillations. Although this may be expected because of Rayleigh's criterion, the discussion of the numerical results by Richards et al. did not focus on this issue. More insight in thermal pulse combustion may be gained by quantifying the contributions of the various physical processes to the energy of the oscillations.

To establish regions in the model parameter space for which stable pulse combustion may occur, the model equations can be integrated numerically. However, such an approach proves to be very time consuming. A study of the steady states of the model equations and their stability has been performed. The stability analysis proved to be a very useful tool for exploring the model parameter space. Regions in the model parameter space for which pulse combustion may occur, can be established in a fraction of the time that would be needed by numerical integration.

Finally, some literature related to the model of Richards et al. was presented. The model of Richards et al. was used, and extended, in a number of studies. The comments on the mathematical model given above, are particularly relevant for these studies. It was noted that aerovalved pulse combustion may be different from thermal pulse combustion. References to literature extending the mathematical model of Richards et al. to include the case of aerovalved pulse combustion have been given. Also, references were given to papers that characterize pulse combustion by a total ignition delay time and a resonance time. These papers, and related studies, appear to be very valuable for understanding the pulse combustion process.

Chapter 6

Conclusions and suggestions for future research

In this work we have analyzed three simple models to determine conditions under which they can describe stable operation of a pulse combustor. Each model is described and analyzed its own chapter. We refer to the end of those chapters for conclusions on the models.

According to our analysis, the models of Kilicarslan and of Ahrens et al. seem to be too simplified to describe a stably pulsating combustion process. In contrast to these two, the model of Richards et al. accounts for heat transfer to the combustion chamber wall and friction of the tailpipe flow and uses a more detailed description of the burning rate. Numerical experiments show that by incorporating these physical processes, stable pulsations can be achieved. Stability analysis of the steady states has been shown to be very useful for establishing conditions under which stable pulse combustor operation may be possible, in a fraction of the time that would be needed for numerical integration of the model equations.

In our opinion, for a sufficiently realistic description of an (aerovalved) pulse combustor, the three models lack two important features. Firstly, a more detailed description of the wave dynamics is needed. Secondly, they do not model the effect of an *aerovalve* on the operation of a pulse combustor. While aerovalved pulse combustion has been modelled in the work of Narayanaswami and Richards [19] and of Richards and Gemmen [24] by extending the model of Richards et al. (which was discussed in Chapter 5), it still results in a lumped parameter model, that provides little insight into the wave dynamics. Therefore, the development of a one-dimensional model, capable of providing an approximation to the wave dynamics inside an aerovalved pulse combustor, should be the first step in the follow-up research.

The one-dimensional modelling of aerovalved pulse combustion can be divided into a number of submodelling problems.

- The one-dimensional equations of gas dynamics need to be formulated, including energy sources (from combustion) and energy sinks and dissipative processes (such as heat transfer, wall friction). These describe the wave dynamics in the system, driven by combustion and damped by dissipative processes.

- The heat released by combustion needs to be quantified. Factors of influence on this are the mixing processes of fuel and oxidizer, the mixing of reactants and hot products, and a chemical reaction rate. In turn, the mixing processes depend on the flow field and injection characteristics.

- The geometry of the pulse combustor needs to be specified. It could be considered as a continuous volume, including aerovalve, combustion chamber and tailpipe, in which the wave dynamics are described.

- Finally, boundary conditions, describing the effects of the aerovalve inlet and the tailpipe exit, need to be specified.

These submodels can be taken from literature, with the model presented by Barr and Dwyer [4] as an interesting starting point. In the modelling process, the temperature dependency of the specific heat needs to be considered. To gain insight into the pulse combustion process, the contributions of the various physical terms to the energy of the oscillations need to be quantified.

The main focus of a follow-up research project should be on developing a numerical scheme, that is capable of approximating the solution of the model equations for given geometry and boundary conditions with sufficient accuracy. Of course, a simple mathematical model will not be able to predict the exact behaviour of a real pulse combustor, so it may be questioned how accurate the numerical method needs to be. It is desirable that the calculated contributions of the various physical processes to the operation characteristics are not affected by artificial effects introduced by the numerical model. Specifically:

- **Numerical dispersion.** Phase differences between heat release by combustion and the acoustic waves drive the pulse combustion process, and it is very sensitive to these differences. Therefore, the numerical method needs to limit the numerical dispersion.

- **Numerical dissipation.** Damping processes affect the amplification of the system's acoustics, which may significantly affect the amplitude of the oscillations in the system. Also, damping processes may affect the system's frequency, which in turn affects the phase difference between heat release and the acoustic waves. Therefore, the numerical method also needs to limit the numerical dissipation.

- **Numerical accuracy.** Finally, the nature of pulse combustion operation is in the amplification and maintenance of disturbances, by favorably linking heat release to resonant acoustics. Thus, a numerical method for solving model equations that capture this nature, will be susceptible to (numerical) disturbances. Therefore, the numerical method needs to be sufficiently accurate.

Of course, the important question is: How accurate is 'sufficiently accurate,' and how much numerical dispersion and dissipation may be allowed? Also, are these properties of a numerical scheme indeed as important as suggested above? These questions are important elements in the verification of the numerical model (i.e., the process of establishing whether the numerical model accurately represents the model equations). For verification purposes, benchmark problems and/or problems with an analytical solution need to be selected.

The final question is: Is the model capable of capturing the behaviour of a pulse combustor, at least in a qualitative sense? Of course, a one-dimensional model cannot describe the pulse combustion process accurately. Conditions for which the one-dimensional approximation may be acceptable for describing (the characteristics of) the pulse combustion process, need to be established. The geometry of the modelled pulse combustor can be expected to be a major factor in this respect. To address the final question, the model should be validated against experimental results (of course under the conditions for which the model is intended).

Bibliography

[1] Milton Abramowitz and Irene A. Stegun. *Handbook of Mathematical Functions: with formulas, graphs and mathematical tables.* Dover Publications, Inc., New York, 1965. For an online copy of the tenth printing (1972) of this work, see web-site `http://www.math.sfu.ca/~cbm/aands/`.

[2] Frederick W. Ahrens, Choong Kim, and Shiu-Wing Tam. An analysis of the pulse combustion burner. *ASHRAE Transactions*, 84, Part 1:488–507, 1978.

[3] P. K. Barr, J. O. Keller, T. T. Bramlette, C. K. Westbrook, and J. E. Dec. Pulse combustor modeling demonstration of the importance of characteristic times. *Combustion and Flame*, 82:252–269, 1990.

[4] Pamela K. Barr and Harry A. Dwyer. *Pulse Combustor Dynamics: A Numerical Study*, chapter 22, pages 673–710. Volume 135 of Oran and Boris [21], 1991.

[5] Paul F. Byrd and Morris D. Friedman. *Handbook of Elliptic Integrals for Engineers and Physicists.* Die Grundlehren der Mathematischen Wissenschaften, Band LXVII. Springer-Verlag, Berlin, 1954.

[6] Boa-Teh Chu. On the energy transfer to small disturbances in fluid flow (Part I). *Acta Mechanica*, 1(3):215–234, September 1965. (Printed.).

[7] Subhashis Datta, Achintya Mukhopadhyay, and Dipankar Sanyal. Modeling and analysis of the nonlinear dynamics of a thermal pulse combustor. *42nd AIAA/ASME/SAE/ASEE Joint Propulsion Conference & Exhibit*, 2006. 9–12 July 2006, Sacramento, California. American Institute of Aeronautics and Astronautics, Paper AIAA 2006-4396.

[8] C. Stuart Daw, John F. Thomas, George A. Richards, and Lakshmanan L. Narayanaswami. Chaos in thermal pulse combustion. *Chaos*, 5(4):662–670, 1995.

[9] John E. Dec and Jay O. Keller. Pulse combustor tail-pipe heat-transfer dependence on frequency, amplitude, and mean flow rate. *Combustion and Flame*, 77:359–374, 1989.

[10] John E. Dec, Jay O. Keller, and Vedat S. Arpaci. Heat transfer enhancement in the oscillating turbulent flow of a pulse combustor tail pipe. *International Journal of Heat and Mass Transfer*, 35(9):2311–2325, 1992.

[11] H. M. Heravi, J. R. Dawson, P. J. Bowen, and N. Syred. Primary pollutant prediction from integrated thermofluid-kinetic pulse combustor models. *Journal of Propulsion and Power*, 21(6):1092–1097, November-December 2005.

[12] Visarath In, Mark L. Spano, Joseph D. Neff, William L. Ditto, C. Stuart Daw, K. Dean Edwards, and Ke Nguyen. Maintenance of chaos in a computational model of a thermal pulse combustor. *Chaos*, 7(4):605–613, 1997.

[13] Dominic William Jordan and Peter Smith. *Nonlinear ordinary differential equations*. Oxford applied mathematics and computing series. Oxford University Press Inc., New York, 1994.

[14] J. O. Keller, T. T. Bramlette, J. E. Dec, and C. K. Westbrook. Pulse combustion: The importance of characteristic times. *Combustion and Flame*, 75:33–44, 1989.

[15] J. O. Keller, T. T. Bramlette, C. K. Westbrook, and J. E. Dec. Pulse combustion: The quantification of characteristic times. *Combustion and Flame*, 79:151–161, 1990.

[16] J. O. Keller and I. Hongo. Pulse combustion: The mechanisms of NO_x production. *Combustion and Flame*, 80:219–237, 1990.

[17] Ali Kilicarslan. Frequency evaluation of a gas-fired pulse combustor. *International Journal of Energy Research*, 29:439–454, 2005.

[18] D. Kretschmer and J. Odgers. Modeling of gas turbine combustors—a convenient reaction rate equation. *Journal of Engineering for Power (Transactions of the ASME)*, pages 173–180, July 1972.

[19] L. Narayanaswami and G. A. Richards. Pressure-gain combustion: Part I—Model development. *Journal of Engineering for Gas Turbines and Power*, 118(3):461–468, July 1996.

[20] F. Nicoud and T. Poinsot. Thermoacoustic instabilities: Should the Rayleigh criterion be extended to include entropy changes? *Combustion and Flame*, 142:153–159, 2005.

[21] Elaine S. Oran and Jay P. Boris, editors. *Numerical Approaches to Combustion Modeling*, volume 135 of *Progress in Astronautics and Aeronautics*. The American Institute of Aeronautics and Astronautics, Inc., Washington, DC, 1991.

[22] A. A. Putnam, F. E. Belles, and J. A. C. Kentfield. Pulse combustion. *Progress in Energy and Combustion Science*, 12:43–79, 1986.

[23] Rayleigh. The explanation of certain acoustical phenomena. *Nature*, 18(455):319–321, July 1878.

[24] G. A. Richards and R. S. Gemmen. Pressure-gain combustion: Part II—Experimental and model results. *Journal of Engineering for Gas Turbines and Power*, 118(3):469–473, July 1996.

[25] G. A. Richards, G. J. Morris, D. W. Shaw, S. A. Keeley, and M. J. Welter. Thermal pulse combustion. *Combustion Science and Technology*, 94:57–85, 1993.

[26] H. Schlichting. *Boundary Layer Theory*. McGraw-Hill, New York, 1979.

[27] Philip S. Schmidt, Ofodike A. Ezekoye, John R. Howell, and Derek K. Baker. *Thermodynamics: An integrated learning system*. John Wiley & Sons, Inc., New York, 2006.

[28] Lawrence F. Shampine and Mark W. Reichelt. The MATLAB ODE Suite. *SIAM Journal of Scientific Computing*, 18(1):1–22, January 1997.

[29] The MathWorks, Inc. MATLAB, version 7.3.0.298 (R2006b), 2006. Web-site: http://www.mathworks.com.

[30] Philip A. Thompson. *Compressible-Fluid Dynamics*. Advanced Engineering Series. McGraw-Hill, Inc., New York, 1972.

[31] N. A. W. Tiemessen and R. J. M. Bastiaans. Aerovalved pulse combustion. Bachelor's Thesis Project, Eindhoven University of Technology, Eindhoven, October 2006. (In Dutch.).

[32] Stephen R. Turns. *An Introduction to Combustion: Concepts and applications*. McGraw-Hill Series in Mechanical Engineering. McGraw-Hill, Inc., New York, 1996.

[33] D. J. van Mullem and R. J. M. Bastiaans. Modelleren van een pulse combustor. Bachelor's Thesis Project, Eindhoven University of Technology, Eindhoven, January 2007. (In Dutch.).

[34] Ferdinand Verhulst. *Nonlinear Differential Equations and Dynamical Systems*. Universitext. Springer-Verlag, Berlin, 2nd rev. and enlarged edition, 2000.

Appendix A

MATLAB codes for model of Kilicarslan

In this chapter, the system of ordinary differential equations (ODEs) of Kilicarslan's model (see (3.16)–(3.22)) is numerically implemented using MATLAB [29] software. The standard MATLAB ODE solver `ode45` is used to solve the equations. It is assumed that the user is familiar with MATLAB, and the ODE solver.

The MATLAB ODE solvers for initial value problems (e.g. the solver `ode45`) can be used to solve systems of ODEs written in the general form

$$\frac{d\mathbf{y}}{dt} = \mathbf{f}(t, \mathbf{y}), \tag{A.1}$$

$$\mathbf{y}(0) = \mathbf{y}_0, \tag{A.2}$$

where $\mathbf{y}$ is a vector, $\mathbf{f}$ is a vector function, t is time, and $\mathbf{y}_0$ is a vector of initial values. To obtain a numerical solution, a function implementing the right-hand side of (A.1) must be passed to the solver, together with the initial values vector $\mathbf{y}_0$. The function that is passed to the solver, should return a column vector.

In Section A.1 the model equations of Kilicarslan are written in the general form of (A.1) and (A.2), and the function that can be passed to the solver is given. In Section A.2 the code is given that was used to generate the data for the figures of Section 3.5. Finally, Section A.3 presents the code that was used to plot the figures of Section 3.5, using the generated data.

It should be mentioned that the code was written rather quickly, and no attempt has been made to optimize it. In the implementation of the functions, no attention is paid to checking whether the input arguments are of the correct form. Thus, the user should take care when prescribing the input arguments, although eventually an error will be produced if the input is of an unexpected form. Also, plots produced by the code of Section A.3 may differ somewhat from the figures in Section 3.5. This is because they were manipulated manually (e.g. by resizing them, replacing labels) before including them in the report.

A.1   Numerical implementation

The model equations of Kilicarslan (see (3.16)–(3.22)) can be written in the general form of (A.1) and (A.2) by defining $\mathbf{y}$ and $\mathbf{f}$ in the following way:

$$\mathbf{y} = \left(\begin{array}{c} p \\ \dot{m}_e \end{array} \right), \tag{A.3}$$

$$\mathbf{f}(t, \mathbf{y}) = \left(\begin{array}{c} AF(y_1) - B\,y_2 \\ C\,y_1 \end{array} \right), \tag{A.4}$$

where A, B and C, expressed in the model parameters, are:

$$A \;=\; k_g(1+r)\frac{(\gamma-1)h_e}{V_{cc}}, \tag{A.5}$$

$$B \;=\; \frac{(\gamma-1)h_e}{V_{cc}}, \tag{A.6}$$

$$C \;=\; \frac{A_{tp}}{L_{tp}}, \tag{A.7}$$

$$F(p) \;=\; \sqrt{|p|}\,\mathbf{1}_{(-\infty,0)}(p). \tag{A.8}$$

The function that must be passed to the solver (implementing $\mathbf{f}(t, \mathbf{y})$), depends on the model parameters. To be able to vary all of the model parameters, it was chosen to pass a structure of model parameters to that function. The structure has fields in which the model parameter values are stored; the fieldnames correspond to the model parameters. Such a structure can be generated with help of the function `setKilicarslan` (see Listing A.1.1 at the end of this section). Calling the function without any input arguments returns a structure with the model parameters set to their default values. Calling the function with input of the form `'par1',val1,...` (i.e. in pairs of fieldnames and values), sets the model parameters specified by the fieldnames `par`n to the corresponding values `val`n, while the other parameters are set to their default values. Together, Tables A.1 and A.2 list the model parameters that are stored in a parameter structure, their fieldnames, and the default values.

Not all model parameters can be specified independently: those that can, are listed in Table A.1, while those that depend on others are listed in Table A.2. While no error is produced if the input of the function `setKilicarslan` contains one of the dependent model parameters, it will have no effect on the output. Its value in the resulting structure will just be the value specified by the definition given in Table A.2, which can be rewritten using solely independent parameters. Of course, it is possible to generate, or manipulate, a model parameter structure directly, but in doing so, one risks that the dependent model parameter values are inconsistent with the independent parameter values. Thus, it is advised to set the model parameters using the function `setKilicarslan`.

The function `setKilicarslan` uses the auxiliary function `setparam`, which sets specified fields of a given structure to specified values. In the process, it checks whether the specified fields exist in the structure, and it gives an error if that is not the case. Since the function `setparam` is also used to set parameters in the numerical implementation of the models of Ahrens et al. (see Appendix B) and Richards et al. (see Appendix C), its implementation and usage is discussed in Appendix D.

Parameter	Fieldname	Default value	Unit
$A_{v,g}$	Avg	6.26×10^{-5}	m^2
$C_{D,g}$	CDg	0.6	−
c_p	cp	1009.7	J/kg/K
ΔH_f	DHf	50.016×10^6	J/kg
D_{tp}	Dtp	0.042	m
L_{tp}	Ltp	2	m
MW_g	MWg	16.043	kg/kmol
P_0	P0	1.01325×10^5	Pa
r	r	17.12	−
R_a	Ra	287	J/kg/K
R_u	Ru	8.31441×10^3	J/kmol/K
T_0	T0	300	K
V_{cc}	Vcc	2.609705×10^{-3}	m^3

Table A.1: Independent model parameters of Kilicarslan's model, the fieldnames under which they are stored in the parameter structure, their default values, and the units in which they are expressed.

Parameter	Fieldname	Defined by	Unit
A_{tp}	Atp	$= \pi D_{tp}^2/4$	m^2
γ	gam	$= \frac{c_p}{c_p - R_a}$	−
h_e	he	$= h_r + \frac{\Delta H_f}{1+r}$	J/kg
h_r	hr	$= c_p T_0$	J/kg
k_g	kg	$= \sqrt{2\rho_g C_{D,g} A_{v,g}}$	$\text{kg}^{1/2}\,\text{m}^{1/2}$
R_g	Rg	$= R_u/\text{MW}_g$	J/kg/K
ρ_g	rhog	$= \frac{P_0}{R_g T_0}$	kg/m^3

Table A.2: Dependent model parameters of Kilicarslan's model, the fieldnames under which they are stored in the parameter structure, expressions defining their values, and the units in which they are expressed.

Function	Input	Description
`odeKilicarslan`	`t,y,s`	Returns the value of the function $\mathbf{f}(t,\mathbf{y})$ of (A.4), for specified time `t`, vector `y`, and the model parameters stored in structure **s**.
`setKilicarslan`	none	Returns a parameter structure with *default* values, that can be passed to the function `odeKilicarslan`.
	`'par1',val1,...`	Returns a parameter structure with the *independent* parameters `par`n set to the specified values `val`n; the other parameters have default values. The structure can be passed to the function `odeKilicarslan`.
`setparam`	`s,'fld1',val1,...`	See Appendix D.

Table A.3: Overview of the functions that are defined in Section A.1.

The function `odeKilicarslan` is an implementation of the function $\mathbf{f}(t,\mathbf{y})$ of (A.4). Besides the time t and the vector $\mathbf{y}$, the implemented function also needs a parameter structure specifying the model parameters as input. The code of the function `odeKilicarslan` is given in Listing A.1.2 at the end of this section.

An overview of the MATLAB functions defined in this section, is presented in Table A.3.

Listing A.1.1: Function setKilicarslan. Given a paired list of fieldnames and values, it returns a structure of model parameters, which can be passed to the function `odeKilicarslan`. Model parameter values that are not specified, are set to their default values.

```matlab
                      _____ setKilicarslan.m _____
 1    function sOut = setKilicarslan(varargin);
 2
 3    % Set default values
 4
 5    s = struct(...
 6        'Atp' , []              ,... % (calculated, see below)
 7        'Avg' , 6.26e-5         ,... % [ m^2 ]
 8        'CDg' , 0.6             ,... % [ - ]
 9        'cp'  , 1009.7          ,... % [ J/kg/K ]
10        'DHf' , 50.016e+6       ,... % [ J/kg ]
11        'Dtp' , 0.042           ,... % [ m ]
12        'gam' , []              ,... % (calculated, see below)
13        'he'  , []              ,... % (calculated, see below)
14        'hr'  , []              ,... % (calculated, see below)
15        'kg'  , []              ,... % (calculated, see below)
```

```
16        'Ltp' , 2            ,... % [ m ]
17        'MWg' , 16.043       ,... % [ kg/kmol ]
18        'P0'  , 1.01325e+5   ,... % [ Pa ]
19        'r'   , 17.12        ,... % [ - ]
20        'Ra'  , 287          ,... % [ J/kg/K ]
21        'Rg'  , []           ,... % (calculated, see below)
22        'rhog', []           ,... % (calculated, see below)
23        'Ru'  , 8.31441e+3   ,... % [ J/kmol/K ]
24        'T0'  , 300          ,... % [ K ]
25        'Vcc' , 2.609705e-3 );   % [ m^3 ]
26
27   % Set user specified model parameters
28
29   if nargin > 0
30       s = setparam(s,varargin{:});
31   end
32
33   % Calculate dependent model parameters
34
35   s.Atp = 0.25*pi*s.Dtp^2;          % [ m^2 ]
36   s.gam = s.cp/(s.cp - s.Ra);       % [ - ]
37   s.hr  = s.cp*s.T0;                % [ J/kg ]
38   s.he  = s.hr + s.DHf/(1 + s.r);   % [ J/kg ]
39   s.Rg  = s.Ru/s.MWg;               % [ J/kg/K ]
40
41   s.rhog = s.P0/(s.Rg*s.T0);         % [ kg/m^3 ]
42   s.kg   = sqrt(2*s.rhog)*s.CDg*s.Avg;  % [ kg^0.5 m^0.5 ]
43
44   % Assign output structure
45
46   sOut = s;
```
───── setKilicarslan.m ─────

Listing A.1.2: Function odeKilicarslan. Given the following input arguments: time t, the vector $\mathbf{y}$ (see (A.3)), and a model parameter structure, it returns the vector $\mathbf{f}(t,\mathbf{y})$ defined by (A.4).

───── odeKilicarslan.m ─────
```
1    function dydt = odeKilicarslan(t,y,s);
2
3    % Compute auxiliary constants
4
5    B = (s.gam - 1)/s.Vcc*s.he;
6    A = s.kg*(1 + s.r)*B;
7    C = s.Atp/s.Ltp;
8
9    F = @(p) sqrt(abs(min(p,0)));  % function of gauge pressure, p
10
11   % Compute dydt
12   %    y(1) == gauge pressure, [ Pa ]
13   %    y(2) == mass flux at chamber exit, [ kg/s ]
14
```

```
15    dy1dt = A*F(y(1)) - B*y(2);
16    dy2dt = C*y(1);
17
18    dydt  = [dy1dt; dy2dt];
```
─────────── odeKilicarslan.m ───────────

A.2   Generating data for graphs

The script file `dataKilicarslan.m` (see Listing A.2.1) contains the code that
was used to generate the data for the figures of Section 3.5. By setting the
Matlab variable `identifier` in Line 16 to a certain string and running the
script, data for the figure associated with the identifier are generated, and stored
under an appropriate name. The available choices for the identifier are listed in
Table A.4, together with descriptions of the data that are generated for those
choices and the filenames under which the data are stored. The data that are
stored in the `.mat` files are: the model parameter structure and the initial values
vector that were passed to the ODE solver `ode45`, and the solution structure
that was returned by the solver. The initial conditions that were used, are given
in Table A.5.

Listing A.2.1: Script file dataKilicarslan.m. Generates data for the figures of
Section 3.5. The choice of the identifier set in Line 16 determines the data that
are generated.
─────────── dataKilicarslan.m ───────────

```
1     % dataKilicarslan.m
2
3     % Clear workspace, close figure windows, and clear command window
4
5     clear all
6     close all
7     clc
8
9     % Set identifier for generation of data for a certain figure from
10    % the Interim Report, Chapter 3. Choose from:
11    %
12    %   'Figure3_3'  = default parameter values; no oscillations
13    %   'Figure3_4'  = parameter values adjusted to show some
14    %                    oscillations
15
16    identifier = 'Figure3_3';
17
18    % Set initial values for ODE-solver
19    %    y(1) == gauge pressure, [ Pa ]
20    %    y(2) == mass flux at chamber exit, [ kg/s ]
21
22    y1ini = 1.01325e+5;  % [ Pa ]
23    y2ini = 0;           % [ kg/s ]
24
25    y0 = [y1ini; y2ini];
26
```

Identifier	Filename	Description
'Figure3_3'	dataFigure3_3.mat	Generates data for Figure 3.3. Default parameter values are used.
'Figure3_4'	dataFigure3_4.mat	Generates data for Figure 3.4. Three parameter values are changed from their defaults to get an oscillatory solution.

Table A.4: Identifier choices for the script file `dataKilicarslan.m` (see Line 16 of Listing A.2.1), and the filenames under which the generated data are stored. The following data are stored in the `.mat` files: the parameter structure (`s`), the initial values vector (`y0`), and the solution structure (`sol`) that is returned by the ODE solver.

Initial condition		Value used	Unit
`y0(1)`	$= p(0)$	1.01325×10^5	Pa
`y0(2)`	$= \dot{m}_e(0)$	0	kg/s

Table A.5: Initial values, stored in the vector `y0` that was passed to the ODE solver to generate the data for the figures of Section 3.5.

```matlab
27   % Set options for ODE-solver
28
29   options = odeset('AbsTol',1e-8,'RelTol',1e-6);
30
31   % Set time-span for ODE-solver
32
33   tmin  = 0;      % [ s ]
34   tmax  = 0.15;   % [ s ]
35   tspan = [tmin tmax];
36
37   % Initialize structure of model parameters (default values)
38
39   s = setKilicarslan;
40
41   % Select data to generate for plotting the figure, and save it
42
43   switch identifier
44
45       case 'Figure3_3'
46
47           % Run ODE-solver with default parameter values, and save
48
49           sol = ode45(@odeKilicarslan,tspan,y0,options,s);
50           save(['data',identifier],'s','y0','sol')
51
52       case 'Figure3_4'
53
54           % Run ODE-solver with parameter values adjusted to show
55           % some oscillations, and save
56
57           s = setKilicarslan(...
58               'Avg', 0.5  * s.Avg ,...
59               'Ltp', 0.25 * s.Ltp ,...
60               'Vcc', 10   * s.Vcc );
61           sol = ode45(@odeKilicarslan,tspan,y0,options,s);
62           save(['data',identifier],'s','y0','sol')
63
64       otherwise
65
66           error('Unknown identifier choice.');
67
68   end  % switch
```
───────────── dataKilicarslan.m ─────────────

A.3   Plotting graphs

The script file `plotKilicarslan.m` (see Listing A.3.1) contains the code that was used to plot the figures of Section 3.5, using the data generated with the script `dataKilicarslan` (see Section A.2). By setting the MATLAB variable `identifier` in Line 15 to a certain string and running the script, data for the figure associated with that identifier is loaded, and a graph is plotted and saved under an appropriate name. The available choices for the identifier are listed

Identifier	Filename ⟨needed⟩	Description
'Figure3_3'	Figure3_3.fig ⟨dataFigure3_3.mat⟩	Plots Figure 3.3.
'Figure3_4'	Figure3_4.fig ⟨dataFigure3_4.mat⟩	Plots Figure 3.4.

Table A.6: Identifier choices for the script file `plotKilicarslan.m` (see Line 15 of Listing A.3.1). The figures are saved as `.fig` files. Data that is needed to plot the figures, is loaded from the `.mat` files; they are indicated by angular brackets.

in Table A.6. It mentions which figures are produced for those choices, and the filenames under which the figures are saved (i.e. the `.fig` files). The data files (extension: `.mat`) that are needed to plot the figures, are shown between angular brackets.

Listing A.3.1: Script file plotKilicarslan.m. Plots the figures from Section 3.5, using data generated with `dataKilicarslan.m` (see Section A.2). The choice of the identifier set in Line 15 determines the graph that is plotted.

```
                        ─── plotKilicarslan.m ───
1    % plotKilicarslan.m
2
3    % Clear workspace, close figure windows, and clear command window
4
5    clear all
6    close all
7    clc
8
9    % Set identifier to plot a certain graph from the Interim Report,
10   % Chapter 3. Choose from:
11   %
12   %    'Figure3_3'  = plot Figure 3.3 from Interim Report
13   %    'Figure3_4'  = plot Figure 3.4 from Interim Report
14
15   identifier = 'Figure3_3';
16
17   % Select data to load, plot requested figure, and save it
18
19   switch identifier
20
21       case 'Figure3_3'
22
23           % Load data
24
25           load 'dataFigure3_3';
26
27           % Extract data for time and gauge pressure from solution
28           % structure
29
30           t = sol.x.';
```

```matlab
31          y = sol.y.';
32          p = y(:,1);       % gauge pressure, [ Pa ]

34          % Plot graph, annotate, and save

36          h = figure('Name','Figure 3.3 of Interim Report');
37          plot(t,p*1e-3)  % time in [ s ], gauge pressure in [ kPa ]

39          title('Figure 3.3')
40          xlabel('Time (s)')
41          ylabel('Gauge pressure (kPa)')
42          xlim([0 max(t)])
43          grid on

45          saveas(h,'Figure3_3','fig')

47      case 'Figure3_4'

49          % Load data

51          load 'dataFigure3_4';

53          % Extract data for time and gauge pressure from solution
54          % structure

56          t = sol.x.';
57          y = sol.y.';
58          p = y(:,1);       % gauge pressure, [ Pa ]

60          % Plot graph, annotate, and save

62          h = figure('Name','Figure 3.4 of Interim Report');
63          plot(t,p*1e-3)  % time in [ s ], gauge pressure in [ kPa ]

65          title('Figure 3.4')
66          xlabel('Time (s)')
67          ylabel('Gauge pressure (kPa)')
68          xlim([0 max(t)])
69          grid on

71          saveas(h,'Figure3_4','fig')

73      otherwise

75          error('Unknown identifier choice.');

77  end  % switch
```

plotKilicarslan.m

Appendix B

MATLAB codes for model of Ahrens et al.

In this chapter, the system of ordinary differential equations (ODEs) of the model of Ahrens et al. (see (4.12)–(4.19)) is numerically implemented using MATLAB [29] software. The standard MATLAB ODE solver `ode45` is used to solve the equations. It is assumed that the user is familiar with MATLAB, and the ODE solver.

The MATLAB ODE solvers for initial value problems (e.g. the solver `ode45`) can be used to solve systems of ODEs written in the general form

$$\frac{d\mathbf{y}}{dt} = \mathbf{f}(t, \mathbf{y}), \tag{B.1}$$

$$\mathbf{y}(0) = \mathbf{y}_0, \tag{B.2}$$

where $\mathbf{y}$ is a vector, $\mathbf{f}$ is a vector function, t is time, and $\mathbf{y}_0$ is a vector of initial values. To obtain a numerical solution, a function implementing the right-hand side of (A.1) must be passed to the solver, together with the initial values vector $\mathbf{y}_0$. The function that is passed to the solver, should return a column vector.

In Section B.1 the model equations of Ahrens et al. are written in the general form of (B.1) and (B.2), and the function that can be passed to the solver is given. In Section B.2 the code is given that was used to generate the data for the figures of Section 4.6. Finally, Section B.3 presents the code that was used to plot the figures of Section 4.6, using the generated data.

It should be mentioned that the code was written rather quickly, and no attempt has been made to optimize it. In the implementation of the functions, no attention is paid to checking whether the input arguments are of the correct form. Thus, the user should take care when prescribing the input arguments, although eventually an error will be produced if the input is of an unexpected form. Also, plots produced by the code of Section B.3 may differ somewhat from the figures in Section 4.6. This is because they were manipulated manually (e.g. by resizing them, replacing labels) before including them in the report.

B.1   Numerical implementation

The model equations of Ahrens et al. (see (4.12)–(4.19)) can be written in the general form of (B.1) and (B.2) by defining $\mathbf{y}$ and $\mathbf{f}$ in the following way:

$$\mathbf{y} = \begin{pmatrix} p \\ \dot{m}_e \end{pmatrix}, \tag{B.3}$$

$$\mathbf{f}(t, \mathbf{y}) = \begin{pmatrix} AF(y_1) + B(y_1 + P_0) - C\,y_2 \\ D\,y_1 \end{pmatrix}, \tag{B.4}$$

where A, B, C and D, expressed in the model parameters, are:

$$A = k_g(1+r)\frac{\gamma - 1}{V_{cc}}h_r \tag{B.5}$$

$$B = \frac{A_b U_f}{RT_0}\frac{\gamma - 1}{V_{cc}}\frac{\Delta H_f}{1+r}, \tag{B.6}$$

$$C = \frac{(\gamma - 1)h_e}{V_{cc}}, \tag{B.7}$$

$$D = \frac{A_{tp}}{L_{tp}}, \tag{B.8}$$

$$F(p) = \sqrt{|p|}\,\mathbf{1}_{(-\infty, 0)}(p). \tag{B.9}$$

The function that must be passed to the solver (implementing $\mathbf{f}(t, \mathbf{y})$), depends on the model parameters. To be able to vary all of the model parameters, it was chosen to pass a structure of model parameters to that function. The structure has fields in which the model parameter values are stored; the fieldnames correspond to the model parameters. Such a structure can be generated with help of the function `setAhrensEa` (see Listing B.1.1 at the end of this section). Calling the function without any input arguments returns a structure with the model parameters set to their default values. Calling the function with input of the form `'par1','val1',...` (i.e. in pairs of fieldnames and values), sets the model parameters specified by the fieldnames `par`n to the corresponding values `val`n, while the other parameters are set to their default values. Together, Tables B.1 and B.2 list the model parameters that are stored in a parameter structure, their fieldnames, and the default values.

Not all model parameters can be specified independently: those that can, are listed in Table B.1, while those that depend on others are listed in Table B.2. While no error is produced if the input of the function `setAhrensEa` contains one of the dependent model parameters, it will have no effect on the output. Its value in the resulting structure will just be the value specified by the definition given in Table B.2, which can be rewritten using solely independent parameters. Of course, it is possible to generate, or manipulate, a model parameter structure directly, but in doing so, one risks that the dependent model parameter values are inconsistent with the independent parameter values. Thus, it is advised to set the model parameters using the function `setAhrensEa`.

The function `setAhrensEa` uses the auxiliary function `setparam`, which sets specified fields of a given structure to specified values. In the process, it checks whether the specified fields exist in the structure, and it gives an error if that is not the case. Since the function `setparam` is also used to set parameters in the numerical implementation of the models of Kilicarslan (see Appendix A) and

Parameter	Fieldname	Default value	Unit
A_b	Ab	8.11×10^{-3}	m^2
A_{tp}	Atp	7.92×10^{-4}	m^2
$A_{v,g}$	Avg	6.26×10^{-5}	m^2
$C_{D,g}$	CDg	0.6	−
c_p	cp	1009.7	J/kg/K
ΔH_f	DHf	50.016×10^6	J/kg
L_{tp}	Ltp	1.52	m
MW_g	MWg	16.043	kg/kmol
P_0	P0	1.01325×10^5	Pa
r	r	19.8	−
R_a	Ra	287	J/kg/K
R_u	Ru	8.31441×10^3	J/kmol/K
T_0	T0	300	K
V_{cc}	Vcc	1.97×10^{-3}	m^3

Table B.1: Independent model parameters of the model of Ahrens et al., the fieldnames under which they are stored in the parameter structure, their default values, and the units in which they are expressed.

Parameter	Fieldname	Defined by	Unit
γ	gam	$= \frac{c_p}{c_p - R_a}$	−
h_e	he	$= h_r + \frac{\Delta H_f}{1+r}$	J/kg
h_r	hr	$= c_p T_0$	J/kg
k_g	kg	$= \sqrt{2\rho_g} C_{D,g} A_{v,g}$	$\text{kg}^{1/2}\,\text{m}^{1/2}$
$p_{\max}$	pmax	$= \frac{1}{0.75} \frac{P_0(1+r)h_r}{\Delta H_f}$	Pa
R_g	Rg	$= R_u / \text{MW}_g$	J/kg/K
ρ_g	rhog	$= \frac{P_0}{R_g T_0}$	kg/m^3
U_f	Uf	$= \sqrt{0.1875 \frac{RT_0(1+r)^{3/2}}{A_b\sqrt{P_0}}} \sqrt{\frac{h_r}{\Delta H_f}}$	m/s

Table B.2: Dependent model parameters of the model of Ahrens et al., the fieldnames under which they are stored in the parameter structure, expressions defining their values, and the units in which they are expressed.

Function	Input	Description
odeAhrensEa	t,y,s	Returns the value of the function $\mathbf{f}(t, \mathbf{y})$ of (B.4), for specified time t, vector y, and the model parameters stored in structure s.
setAhrensEa	none	Returns a parameter structure with *default* values, that can be passed to the function odeAhrensEa.
	'par1',val1,...	Returns a parameter structure with the *independent* parameters par$n$ set to the specified values val$n$; the other parameters have default values. The structure can be passed to the function odeAhrensEa.
setparam	s,'fld1',val1,...	See Appendix D.

Table B.3: Overview of the functions that are defined in Section B.1.

Richards et al. (see Appendix C), its implementation and usage is discussed in Appendix D.

The function odeAhrensEa is an implementation of the function $\mathbf{f}(t, \mathbf{y})$ of (B.4). Besides the time t and the vector $\mathbf{y}$, the implemented function also needs a parameter structure specifying the model parameters as input. The code of the function odeAhrensEa is given in Listing B.1.2 at the end of this section.

An overview of the MATLAB functions defined in this section, is presented in Table B.3.

Listing B.1.1: Function setAhrensEa. Given a paired list of fieldnames and values, it returns a structure of model parameters, which can be passed to the function odeAhrensEa. Model parameter values that are not specified, are set to their default values.

```
                          ─── setAhrensEa.m ───
1   function sOut = setAhrensEa(varargin);
2
3   % Set default values
4
5   s = struct(...
6       'Ab'  , 8.11e-3    ,... % [ m^2 ]
7       'Atp' , 7.92e-4    ,... % [ m^2 ]
8       'Avg' , 6.26e-5    ,... % [ m^2 ]
9       'CDg' , 0.6        ,... % [ - ]
10      'cp'  , 1009.7     ,... % [ J/kg/K ]
11      'DHf' , 50.016e+6  ,... % [ J/kg ]
12      'gam' , []         ,... % (calculated, see below)
13      'he'  , []         ,... % (calculated, see below)
14      'hr'  , []         ,... % (calculated, see below)
15      'kg'  , []         ,... % (calculated, see below)
16      'Ltp' , 1.52       ,... % [ m ]
```

```
17        'MWg' , 16.043     ,... % [ kg/kmol ]
18        'P0'  , 1.01325e+5 ,... % [ Pa ]
19        'pmax', []         ,... % (calculated, see below)
20        'r'   , 19.8       ,... % [ - ]
21        'Ra'  , 287        ,... % [ J/kg/K ]
22        'Rg'  , []         ,... % (calculated, see below)
23        'rhog', []         ,... % (calculated, see below)
24        'Ru'  , 8.31441e+3 ,... % [ J/kmol/K ]
25        'T0'  , 300        ,... % [ K ]
26        'Uf'  , []         ,... % (calculated, see below)
27        'Vcc' , 1.97e-3    );   % [ m^3 ]
28
29    % Set user specified model parameters
30
31    if nargin > 0
32        s = setparam(s,varargin{:});
33    end
34
35    % Calculate dependent model parameters
36
37    s.gam = s.cp/(s.cp - s.Ra);      % [ - ]
38    s.hr  = s.cp*s.T0;               % [ J/kg ]
39    s.he  = s.hr + s.DHf/(1 + s.r);  % [ J/kg ]
40    s.Rg  = s.Ru/s.MWg;              % [ J/kg/K ]
41
42    s.rhog = s.P0/(s.Rg*s.T0);           % [ kg/m^3 ]
43    s.kg   = sqrt(2*s.rhog)*s.CDg*s.Avg; % [ kg^0.5 m^0.5 ]
44
45    s.pmax = s.hr*(1 + s.r)*s.P0/s.DHf/0.75;  % [ Pa ]
46    s.Uf   = sqrt(0.1875*s.hr/s.DHf/s.P0)*s.kg*(1 + s.r)^1.5*s.Ra* ...
47        s.T0/s.Ab;  % [ m/s ]
48
49    % Assign output structure
50
51    sOut = s;
```
setAhrensEa.m

Listing B.1.2: Function odeAhrensEa. Given the following input arguments: time t, the vector $\mathbf{y}$ (see (B.3)), and a model parameter structure, it returns the vector $\mathbf{f}(t, \mathbf{y})$ defined by (B.4).

odeAhrensEa.m
```
1    function dydt = odeAhrensEa(t,y,s);
2
3    % Compute auxiliary constants
4
5    tmp = (s.gam - 1)/s.Vcc;
6
7    A = s.kg*(1 + s.r)*tmp*s.hr;
8    B = s.Ab*s.Uf/s.Ra/s.T0*tmp*s.DHf/(1 + s.r);
9    C = tmp*s.he;
10   D = s.Atp/s.Ltp;
```

```
11
12    F = @(p) sqrt(abs(min(p,0)));   % function of gauge pressure, p
13
14    % Compute dydt
15    %    y(1) == gauge pressure, [ Pa ]
16    %    y(2) == mass flux at chamber exit, [ kg/s ]
17
18    dy1dt = A*F(y(1)) + B*(y(1) + s.P0)- C*y(2);
19    dy2dt = D*y(1);
20
21    dydt  = [dy1dt; dy2dt];
```
──────────── odeAhrensEa.m ────────────

B.2   Generating data for graphs

The script file `dataAhrensEa.m` (see Listing B.2.1) contains the code that was used to generate the data for the figures of Section 4.6. By setting the MATLAB variable `identifier` in Line 17 to a certain string and running the script, data for the figure associated with the identifier are generated, and stored under an appropriate name. The available choices for the identifier are listed in Table B.4, together with descriptions of the data that are generated for those choices and the filenames under which the data are stored. The data that are stored in the `.mat` files are: the model parameter structure, the parameter δ (needed to specify the initial conditions, see below), the initial values vector, and the solution structure that was returned by the ODE solver.

   The initial conditions that were used, are given in Table B.5. The constants B and C (see (B.6) and (B.7)) in specifying the initial conditions conceal the dependency on the model parameters somewhat. To keep the code in the script file `dataAhrensEa.m` clear, the function `iniOdeAhrensEa` was written to produce the initial conditions. It needs the model parameter structure and the 'fine tuning' parameter δ as input arguments. The code of the function `iniOdeAhrensEa` is given in Listing B.2.2.

   For completeness, an overview of the MATLAB functions defined in this section, is presented in Table B.6.

Listing B.2.1: Script file `dataAhrensEa.m`. Generates data for the figures of Section 4.6. The choice of the identifier set in Line 17 determines the data that are generated.

──────────── dataAhrensEa.m ────────────
```
1     % dataAhrensEa.m
2
3     % Clear workspace, close figure windows, and clear command window
4
5     clear all
6     close all
7     clc
8
9     % Set identifier for generation of data for a certain figure from
10    % the Interim Report, Chapter 4. Choose from:
```

Identifier	Filename	Description
'Figure4_3a'	dataFigure4_3a.mat	Generates data for Figure 4.3a. Default parameter values are used, $\delta = 0.242$.
'Figure4_3b'	dataFigure4_3b.mat	Generates data for Figure 4.3b. Default parameter values are used, $\delta = 0.243$.
'Figure4_4'	dataFigure4_3a.mat dataFigure4_3b.mat	Generates data for Figure 4.4. Same as running the script with the identifier choices 'Figure4_3a' and 'Figure4_3b' consecutively.

Table B.4: Identifier choices for the script file `dataAhrensEa.m` (see Line 17 of Listing B.2.1), and the filenames under which the generated data are stored. The following data are stored in the `.mat` files: the parameter structure (`s`), the parameter δ (`delta`), the initial values vector (`y0`), and the solution structure (`sol`) that is returned by the ODE solver.

Initial condition		Value used	Unit
y0(1)	$= p(0) = p_0$	$(1 + \delta)p_{\max}$	Pa
y0(2)	$= \dot{m}_e(0) = \dot{m}_{e,0}$	$\frac{B}{C}(p_0 + P_0)$	kg/s

Table B.5: Initial values, stored in the vector `y0` that was passed to the ODE solver to generate the data for the figures of Section 4.6, expressed in model parameters. In the code, they can be obtained with the function `iniOdeAhrensEa` (see Listing B.2.2), which needs the parameter structure and the parameter δ as input arguments.

Function	Input	Description
iniOdeAhrensEa	s,delta	Returns the vector of initial values y0 as specified in Table B.5, which depend on the model parameters (stored in structure `s`) and the parameter δ (`delta`).

Table B.6: Overview of the functions that are defined in Section B.2.

```matlab
11   %
12   %    'Figure4_3a'  = default parameter values, delta = 0.242
13   %    'Figure4_3b'  = default parameter values, delta = 0.243
14   %    'Figure4_4'   -> produces same data as 'Figure4_3a' and
15   %                     'Figure4_3b' separately
16
17   identifier = 'Figure4_3a';
18
19   % Set options for ODE-solver
20
21   options = odeset('AbsTol',1e-8,'RelTol',1e-6);
22
23   % Set time-span for ODE-solver
24
25   tmin  = 0;      % [ s ]
26   tmax  = 0.18;  % [ s ]
27   tspan = [tmin tmax];
28
29   % Initialize structure of model parameters (default values)
30
31   s = setAhrensEa;
32
33   if ~strcmp(identifier,'Figure4_3a') && ...
34           ~strcmp(identifier,'Figure4_3b') && ...
35           ~strcmp(identifier,'Figure4_4')
36       error('Unknown identifier choice.');
37   end
38
39   % Select data to generate for plotting the figure, and save it
40
41   if strcmp(identifier,'Figure4_3a') || strcmp(identifier,'Figure4_4')
42
43       % Set initial values for ODE-solver for default values with
44       % delta = 0.242
45       %    y0(1) == initial gauge pressure, [ Pa ]
46       %    y0(2) == initial mass flux at chamber exit, [ kg/s ]
47
48       delta = 0.242;
49       y0 = iniOdeAhrensEa(s,delta);
50
51       % Run ODE-solver, and save
52
53       sol = ode45(@odeAhrensEa,tspan,y0,options,s);
54       save('dataFigure4_3a','s','delta','y0','sol')
55
56   end
57
58   if strcmp(identifier,'Figure4_3b') || strcmp(identifier,'Figure4_4')
59
60       % Set initial values for ODE-solver for default values with
61       % delta = 0.243
62       %    y0(1) == initial gauge pressure, [ Pa ]
63       %    y0(2) == initial mass flux at chamber exit, [ kg/s ]
64
```

```
65      delta = 0.243;
66      y0 = iniOdeAhrensEa(s,delta);
67
68      % Run ODE-solver, and save
69
70      sol = ode45(@odeAhrensEa,tspan,y0,options,s);
71      save('dataFigure4_3b','s','delta','y0','sol')
72
73  end
```

dataAhrensEa.m

Listing B.2.2: Function iniOdeAhrensEa. Given a model parameter structure (`s`) and the parameter δ (`delta`), the function returns the vector of initial values $(p_0, \dot{m}_{e,0})^T$ specified in Table B.5.

iniOdeAhrensEa.m

```
1   function y0 = iniOdeAhrensEa(s,delta);
2
3   % Compute auxiliary constants B and C (needed for specifying initial
4   % mass flux)
5
6   tmp = (s.gam - 1)/s.Vcc;
7
8   B = s.Ab*s.Uf/s.Ra/s.T0*tmp*s.DHf/(1 + s.r);
9   C = tmp*s.he;
10
11  % Set initial values for ODE-solver
12  %    y0(1) == initial gauge pressure, [ Pa ]
13  %    y0(2) == initial mass flux at chamber exit, [ kg/s ]
14
15  y01 = (1 + delta)*s.pmax;
16  y02 = B*(y01 + s.P0)/C;
17
18  y0 = [y01; y02];
```

iniOdeAhrensEa.m

B.3 Plotting graphs

The script file `plotAhrensEa.m` (see Listing B.3.1) contains the code that was used to plot the figures of Section 4.6, using the data generated with the script `dataAhrensEa` (see Section B.2). By setting the MATLAB variable `identifier` in Line 16 to a certain string and running the script, data for the figure associated with that identifier is loaded, and a graph is plotted and saved under an appropriate name. The available choices for the identifier are listed in Table B.7. It mentions which figures are produced for those choices, and the filenames under which the figures are saved (i.e. the `.fig` files). The data files (extension: `.mat`) that are needed to plot the figures, are shown between angular brackets.

In Figure 4.4, the graph of the time-derivative of the gauge pressure ($\frac{dp}{dt}$) is plotted versus the gauge pressure (p). The time-derivative was not computed within the script `dataAhrensEa`, so it must be computed within the script

Identifier	Filename ⟨ needed ⟩	Description
'Figure4_3a'	Figure4_3a.fig ⟨ dataFigure4_3a.mat ⟩	Plots Figure 4.3a.
'Figure4_3b'	Figure4_3b.fig ⟨ dataFigure4_3b.mat ⟩	Plots Figure 4.3b.
'Figure4_4'	Figure4_4.fig ⟨ dataFigure4_3a.mat ⟩ ⟨ dataFigure4_3b.mat ⟩	Plots Figure 4.4.

Table B.7: Identifier choices for the script file `plotAhrensEa.m` (see Line 16 of Listing B.3.1). The figures are saved as `.fig` files. Data that is needed to plot the figures, is loaded from the `.mat` files; they are indicated by angular brackets.

Function	Input	Description
derivative	p,medot,s	Given a vector `p` of gauge pressures, a vector `medot` of fuel mass fluxes at the combustion chamber exit, and a model parameter structure `s`, it returns the time-derivative of the vector of gauge pressures. The time-derivative is determined element-wise by the function $f_1(t, \mathbf{y})$, see (B.4), p.104.

Table B.8: Overview of the functions that are used in Section B.3.

`plotAhrensEa`. To keep the code of the script clear, the function `derivative` was written, and included as a subfunction in the script file `plotAhrensEa.m` (see Listing B.3.1, Lines 138ff.). Given the following input arguments: gauge pressure p (`p`), fuel mass flux at the combustion chamber exit $\dot{m}_e$ (`medot`), and a model parameter structure (`s`), it returns the time-derivative of the gauge pressure $\frac{dp}{dt}$ as given by $f_1(t, \mathbf{y})$ in equation (B.4).

For completeness, an overview of the MATLAB functions defined in this section, is presented in Table B.8.

Listing B.3.1: Script file plotAhrensEa.m. Plots the figures from Section 4.6, using data generated with `dataAhrensEa.m` (see Section B.2). The choice of the identifier set in Line 16 determines the graph that is plotted.

```
                          plotAhrensEa.m
1   % plotAhrensEa.m
2
3   % Clear workspace, close figure windows, and clear command window
4
5   clear all
6   close all
7   clc
8
9   % Set identifier to plot a certain graph from the Interim Report,
10  % Chapter 4. Choose from:
11  %
```

```matlab
12   %    'Figure4_3a'   = plot Figure 4.3a from Interim Report
13   %    'Figure4_3b'   = plot Figure 4.3b from Interim Report
14   %    'Figure4_4'    = plot Figure 4.4  from Interim Report
15
16   identifier = 'Figure4_3a';
17
18   % Select data to load, plot requested figure, and save it
19
20   switch identifier
21
22       case 'Figure4_3a'
23
24           % Load data
25
26           load dataFigure4_3a
27
28           % Extract data for time and gauge pressure from solution
29           % structure
30
31           t = sol.x.';
32           y = sol.y.';
33           p = y(:,1);        % gauge pressure, [ Pa ]
34
35           % Plot graph, annotate, and save
36
37           h = figure('Name','Figure 4.3(a) of Interim Report');
38           plot(t,p*1e-3)  % time in [ s ], gauge pressure in [ kPa ]
39
40           title('Figure 4.3(a), delta = 0.242')
41           xlabel('Time (s)')
42           ylabel('Gauge pressure (kPa)')
43           xlim([0 max(t)])
44           ylim([-s.P0 s.P0]/500)
45           grid on
46
47           saveas(h,'Figure4_3a','fig')
48
49       case 'Figure4_3b'
50
51           % Load data
52
53           load dataFigure4_3b
54
55           % Extract data for time and gauge pressure from solution
56           % structure
57
58           t = sol.x.';
59           y = sol.y.';
60           p = y(:,1);        % gauge pressure, [ Pa ]
61
62           % Plot graph, annotate, and save
63
64           h = figure('Name','Figure 4.3(b) of Interim Report');
65           plot(t,p*1e-3)  % time in [ s ], gauge pressure in [ kPa ]
```

```
66
67              title('Figure 4.3(b), delta = 0.243')
68              xlabel('Time (s)')
69              ylabel('Gauge pressure (kPa)')
70              xlim([0 max(t)])
71              ylim([-s.P0 s.P0]/500)
72              grid on
73
74              saveas(h,'Figure4_3b','fig')
75
76          case 'Figure4_4'
77
78              % Load data for delta = 0.242
79
80              load dataFigure4_3a
81
82              % Extract data for time, gauge pressure, and mass flux at
83              % combustion chamber exit
84
85              t = sol.x.';
86              y = sol.y.';
87              p = y(:,1);      % gauge pressure, [ Pa ]
88              medot = y(:,2);  % mass flux at chamber exit, [ kg/s ]
89
90              % Compute time-derivative of gauge pressure from ODEs
91
92              dpdt = derivative(p,medot,s);
93
94              % Plot graph
95
96              h = figure('Name','Figure 4.4 of Interim Report');
97              plot(p*1e-3,dpdt*1e-3)  % gauge pressure in [ kPa ],
98                                      % time in [ s ]
99
100             % Load data for delta = 0.243
101
102             load dataFigure4_3b
103
104             % Extract data for time, gauge pressure, and mass flux at
105             % combustion chamber exit
106
107             t = sol.x.';
108             y = sol.y.';
109             p = y(:,1);      % gauge pressure, [ Pa ]
110             medot = y(:,2);  % mass flux at chamber exit, [ kg/s ]
111
112             % Compute time-derivative of gauge pressure from ODEs
113
114             dpdt = derivative(p,medot,s);
115
116             % Add to previous graph, annotate, and save
117
118             hold on
119             plot(p*1e-3,dpdt*1e-3)  % gauge pressure in [ kPa ], its
```

```
120                                  % time-derivative in [ kPa/s ]
121
122          title('Figure 4.4')
123          xlabel('Gauge pressure p (kPa)')
124          ylabel('dp/dt (kPa/s)')
125          axis([-100 100 -5e4 5e4])
126          grid on
127
128          saveas(h,'Figure4_4','fig')
129
130      otherwise
131
132          error('Unknown identifier choice.');
133
134   end  % switch
```
─────────── plotAhrensEa.m ───────────

Listing B.3.2: Function derivative. Given the following input arguments: a vector of gauge pressures p (p), a vector of fuel mass fractions at the combustion chamber exit $\dot{m}_e$ (medot), and a model parameter structure (s), it returns a vector of time-derivatives of the gauge pressures, $\frac{dp}{dt}$ (given by the function $f_1(t, \mathbf{y})$, see (B.4)), p.104 of the report.

─────────── derivative.m ───────────
```
1   function dpdt = derivative(p,medot,s);
2
3   % Compute auxiliary constants
4
5   tmp = (s.gam - 1)/s.Vcc;
6
7   A = s.kg*(1 + s.r)*tmp*s.hr;
8   B = s.Ab*s.Uf/s.Ra/s.T0*tmp*s.DHf/(1 + s.r);
9   C = tmp*s.he;
10
11  F = @(p) sqrt(abs(min(p,0)));  % function of gauge pressure, p
12
13  % Compute dpdt, [ Pa/s ]
14
15  dpdt = A*F(p) + B*(p + s.P0)- C*medot;
```
─────────── derivative.m ───────────

Appendix C

MATLAB codes for model of Richards et al.

In this chapter, the system of ordinary differential equations (ODEs) of the model of Richards et al. (see (5.73)–(5.89)) is numerically implemented using MATLAB [29] software. The standard MATLAB ODE solver `ode45` is used to solve the equations. It is assumed that the user is familiar with MATLAB, and the ODE solver.

The MATLAB ODE solvers for initial value problems (e.g. the solver `ode45`) can be used to solve systems of ODEs written in the general form

$$
\begin{aligned}
\frac{d\mathbf{y}}{dt} &= \mathbf{f}(t, \mathbf{y}), & \text{(C.1)} \\
\mathbf{y}(0) &= \mathbf{y}_0, & \text{(C.2)}
\end{aligned}
$$

where $\mathbf{y}$ is a vector, $\mathbf{f}$ is a vector function, t is time, and $\mathbf{y}_0$ is a vector of initial values. To obtain a numerical solution, a function implementing the right-hand side of (C.1) must be passed to the solver, together with the initial values vector $\mathbf{y}_0$. The function that is passed to the solver, should return a column vector.

In Section C.1 the model equations of Richards et al. are written in the general form of (C.1) and (C.2), and the function that can be passed to the solver is given. In Section C.2 the code is given that was used to generate the data for the figures of Section 5.4. Finally, Section C.4 presents the code that was used to plot the figures of Section 5.4, using the generated data.

It should be mentioned that the code was written rather quickly, and no attempt has been made to optimize it. In the implementation of the functions, no attention is paid to checking whether the input arguments are of the correct form. Thus, the user should take care when prescribing the input arguments, although eventually an error will be produced if the input is of an unexpected form. Also, plots produced by the code of Section C.4 may differ somewhat from the figures in Section 5.4. This is because they were manipulated manually (e.g. by resizing them, replacing labels) before including them in the report.

C.1   Numerical implementation

The model equations of Richards et al. (see (5.73)–(5.89), (5.97)), can be written
in the general form of (C.1) and (C.2) by defining $\mathbf{y}$ and $\mathbf{f}$ in the following way:

$$
\mathbf{y} = \begin{pmatrix} \widetilde{P} \\ \widetilde{T} \\ \widetilde{u} \\ Y_f \end{pmatrix},
\tag{C.3}
$$

and, writing $\widetilde{P}$, $\widetilde{T}$, $\widetilde{u}$, Y_f instead of y_1, y_2, y_3, y_4, respectively, (for easier reference to the model equations)

$$
\mathbf{f}(t,\mathbf{y}) = \begin{pmatrix}
\gamma \left(A + B \cdot RR + CD - (C + G\widetilde{Z}_e)\widetilde{T} \right) \\
\left(f_1(t,\mathbf{y}) - (A - G\widetilde{Z}_e)\widetilde{T} \right) \dfrac{\widetilde{T}}{\widetilde{P}} \\
E(\widetilde{P}_e - 1)\dfrac{\widetilde{T}_e}{\widetilde{P}_e} - F\,\widetilde{u}\,|\widetilde{u}| \\
\left(A(Y_{f,i} - Y_f) - RR \right)\dfrac{\widetilde{T}}{\widetilde{P}}
\end{pmatrix},
\tag{C.4}
$$

where RR, $\widetilde{P}_e$, $\widetilde{T}_e$ and $\widetilde{Z}_e$ are functions of $\widetilde{P}$, $\widetilde{T}$, $\widetilde{u}$ and Y_f given by

$$
RR = A' \frac{\widetilde{P}^2}{\widetilde{T}^{3/2}} Y_f^2 \exp(-\widetilde{T}_{\mathrm{act}}/\widetilde{T}),
\tag{C.5}
$$

$$
\widetilde{T}_e = \widetilde{T}\left(1 - \frac{\gamma-1}{2}\frac{u_0^2}{\gamma R T_0}\frac{\widetilde{u}^2}{\widetilde{T}} \right),
\tag{C.6}
$$

$$
\widetilde{P}_e = \widetilde{P}\left(\frac{\widetilde{T}_e}{\widetilde{T}} \right)^{\frac{\gamma}{\gamma-1}},
\tag{C.7}
$$

$$
\widetilde{Z}_e = \frac{\widetilde{P}_e}{\widetilde{T}_e}\widetilde{u}
\tag{C.8}
$$

and A, B, C, D, E, F and G are expressed in the model parameters by:

$$
A = \frac{1}{\tau_f} = \frac{\dot{m}_i}{\rho_0 V_{cc}},
\tag{C.9}
$$

$$
B = \frac{\Delta H_f}{c_p T_0},
\tag{C.10}
$$

$$
C = \frac{\widehat{h}}{L_1 c_p \rho_0},
\tag{C.11}
$$

$$
D = \frac{T_w}{T_0},
\tag{C.12}
$$

$$
E = \frac{R T_0}{L_{tp} u_0},
\tag{C.13}
$$

$$
F = \frac{u_0 f}{2 D_{tp}},
\tag{C.14}
$$

$$
G = \frac{u_0}{L_2}.
\tag{C.15}
$$

Parameter	Fieldname	Default value	Unit
A'	`Aprime`	3.85×10^8	1/s
c_p	`cp`	1350	J/kg/K
ΔH_f	`DHf`	5×10^7	J/kg
D_{tp}	`Dtp`	0.0178	m
f	`f`	0.03	–
$\widehat{h}$	`h`	120	W/m^2/K
$1/\tau_f$	`itauf`	1/0.030	1/s
L_1	`L1`	0.0119	m
L_2	`L2`	0.8486	m
L_{tp}	`Ltp`	0.6100	m
P_0	`P0`	1.01325×10^5	Pa
R	`R`	287	J/kg/K
T_0	`T0`	300	K
$\widetilde{T}_{\mathrm{act}}$	`Tact`	50	–
τ_m	`taum`	0	s
T_w	`Tw`	1000	K
$Y_{f,i}$	`Yfi`	0.06	–

Table C.1: Independent model parameters of the model of Richards et al., the fieldnames under which they are stored in the parameter structure, their default values, and the units in which they are expressed.

Note that $f_2(t, \mathbf{y})$ is defined using $f_1(t, \mathbf{y})$; it makes the notation more compact. In fact, the numerical implementation of the vector function $\mathbf{f}$ of (C.4) is done in an analogous way. To incorporate the mixing time τ_m in the model equations, the term RR in the expression for f_1 should be replace by $\widehat{RR}$ defined by $\widehat{RR} = \frac{RR}{1+B \cdot RR \tau_m}$ (see (5.97)).

The function that must be passed to the solver (implementing $\mathbf{f}(t, \mathbf{y})$), depends on the model parameters. To be able to vary all of the model parameters, it was chosen to pass a structure of model parameters to that function. The structure has fields in which the model parameter values are stored; the fieldnames correspond to the model parameters. Such a structure can be generated with help of the function `setRichardsEa` (see Listing C.1.1 at the end of this section). Calling the function without any input arguments returns a structure with the model parameters set to their default values. Calling the function with input of the form `'par1',val1,...` (i.e. in pairs of fieldnames and values), sets the model parameters specified by the fieldnames `par`n to the corresponding values `val`n, while the other parameters are set to their default values. Together, Tables C.1 and C.2 list the model parameters that are stored in a parameter structure, their fieldnames, and the default values.

Not all model parameters can be specified independently: those that can, are listed in Table C.1, while those that depend on others are listed in Table C.2. While no error is produced if the input of the function `setRichardsEa` contains one of the dependent model parameters, it will have no effect on the output. Its value in the resulting structure will just be the value specified by the definition given in Table C.2, which can be rewritten using solely independent parameters. Of course, it is possible to generate, or manipulate, a model parameter structure

Parameter	Fieldname	Defined by	Unit
γ	`gam`	$= \frac{c_p}{c_p - R}$	$-$
ρ_0	`rho0`	$= \frac{P_0}{RT_0}$	kg/m^3
u_0	`u0`	$= \sqrt{\gamma R T_0}$	m/s

Table C.2: Dependent model parameters of the model of Richards et al., the fieldnames under which they are stored in the parameter structure, expressions defining their values, and the units in which they are expressed.

Function	Input	Description
`odeRichardsEa`	`t,y,s`	Returns the value of the function $\mathbf{f}(t,\mathbf{y})$ of (C.4), for specified time `t`, vector `y`, and the model parameters stored in structure `s`.
`setparam`	`s,'fld1',val1,...`	See Appendix D.
`setRichardsEa`	none	Returns a parameter structure with *default* values, that can be passed to the function `odeRichardsEa`.
	`'par1',val1,...`	Returns a parameter structure with the *independent* parameters `par`n set to the specified values `val`n; the other parameters have default values. The structure can be passed to the function `odeRichardsEa`.

Table C.3: Overview of the functions that are defined in Section C.1.

directly. As long as none of the model parameters γ, ρ_0, or u_0 are changed, there is no objection against manipulating the structure of model parameters without using the function setRichardsEa. However, care should be taken to spell the fieldnames of the structure correctly, because if an incorrect name is used, a field will be added to the structure (instead of changing the contents of the intended field). No warning will be given in such a case, while if a similar mistake is made using the function setRichardsEa, an error will be given.

The function setRichardsEa uses the auxiliary function setparam, which sets specified fields of a given structure to specified values. In the process, it checks whether the specified fields exist in the structure, and it gives an error if that is not the case. Since the function setparam is also used to set parameters in the numerical implementation of the models of Kilicarslan (see Appendix A) and Ahrens et al. (see Appendix B), its implementation and usage is discussed in Appendix D.

The function odeRichardsEa is an implementation of the function $\mathbf{f}(t, \mathbf{y})$ in (C.4). Besides the time t and the vector $\mathbf{y}$, the implemented function also needs a parameter structure specifying the model parameters as input. The code of the function odeRichardsEa is given in Listing C.1.2 at the end of this section.

An overview of the MATLAB functions defined in this section, is presented in Table C.3.

Listing C.1.1: Function setRichardsEa. Given a paired list of fieldnames and values, it returns a structure of model parameters, which can be passed to the function odeRichardsEa. Model parameter values that are not specified, are set to their default values.

```
                              ─── setRichardsEa.m ───
1    function sOut = setRichardsEa(varargin);
2
3    % Set default values
4
5    s = struct(...
6        'Aprime', 3.85e+8    ,... % [ 1/s ]
7        'cp'    , 1350        ,... % [ J/kg/K ]
8        'DHf'   , 5e+7        ,... % [ J/kg ]
9        'Dtp'   , 0.0178      ,... % [ m ]
10       'f'     , 0.03        ,... % [ - ]
11       'gam'   , []          ,... % (calculated, see below)
12       'h'     , 120         ,... % [ W/m^2/K ]
13       'itauf' , 1/0.030     ,... % [ 1/s ] (inverse of tauf)
14       'L1'    , 0.0119      ,... % [ m ]
15       'L2'    , 0.8486      ,... % [ m ]
16       'Ltp'   , 0.6100      ,... % [ m ]
17       'P0'    , 1.01325e+5  ,... % [ Pa ]
18       'R'     , 287         ,... % [ J/kg/K ]
19       'rho0'  , []          ,... % (calculated, see below)
20       'T0'    , 300         ,... % [ K ]
21       'Tact'  , 50          ,... % [ - ]
22       'taum'  , 0           ,... % [ s ]
23       'Tw'    , 1000        ,... % [ K ]
24       'u0'    , []          ,... % (calculated, see below)
```

```
25        'Yfi'    , 0.06        );   % [ - ]
26
27   % Set user specified model parameters
28
29   if nargin > 0
30       s = setparam(s,varargin{:});
31   end
32
33   % Calculate dependent model parameters
34
35   s.gam  = s.cp/(s.cp - s.R);     % [ - ]
36   s.rho0 = s.P0/(s.R*s.T0);       % [ kg/m^3 ]
37   s.u0   = sqrt(s.gam*s.R*s.T0);  % [ m/s ]
38
39   % Assign output structure
40
41   sOut = s;
```
———————— setRichardsEa.m ————————

Listing C.1.2: Function odeRichardsEa. Given the following input arguments:
time t, the vector $\mathbf{y}$ (see (C.3)), and a model parameter structure, it returns the
vector $\mathbf{f}(t, \mathbf{y})$ defined by (C.4).

———————— odeRichardsEa.m ————————
```
1    function dydt = odeRichardsEa(t,y,s);
2
3    % Compute auxiliary constants
4
5    A = s.itauf;
6    B = s.DHf/(s.cp*s.T0);
7    C = s.h/(s.L1*s.cp*s.rho0);
8    D = s.Tw/s.T0;
9    E = s.R*s.T0/(s.Ltp*s.u0);
10   F = 0.5*s.u0*s.f/s.Dtp;
11   G = s.u0/s.L2;
12
13   % Compute time dependent variables
14
15   P  = y(1);
16   T  = y(2);
17   u  = y(3);
18   Yf = y(4);
19
20   Te = T*(1 - 0.5*(s.gam - 1)*s.u0^2*u^2/(s.gam*s.R*s.T0*T));
21   Pe = P*(Te/T)^(s.gam/(s.gam - 1));
22   Ze = u*Pe/Te;
23   RR = s.Aprime*(P^2/T^1.5)*Yf^2*exp(-s.Tact/T);
24   RR = RR/(1 + B*RR*s.taum);  % Reaction rate with mixing incorporated
25
26   % Compute dydt
27
28   dPdt  = s.gam*(A + B*RR + C*D) - s.gam*(G*Ze + C)*T;
```

```
29   dTdt  = (dPdt - (A - G*Ze)*T)*T/P;
30   dudt  = E*(Pe - 1)*Te/Pe - F*u*abs(u);
31   dYfdt = (A*(s.Yfi - Yf) - RR)*T/P;
32
33   dydt  = [dPdt; dTdt; dudt; dYfdt];
```
────────────────── odeRichardsEa.m ──────────────────

C.2 Generating data for graphs

The script file `dataRichardsEa.m` (see Listing C.2.1) contains the code that was
used to generate the data for the figures of Section 5.4. By setting the MATLAB
variable `identifier` in Line 28 to a certain string and running the script, data
for the figure associated with the identifier are generated, and stored under an
appropriate name. The available choices for the identifier are listed in Table
C.4, together with descriptions of the data that are generated for those choices
and the filenames under which the data are stored. The initial conditions that
were used, are given in Table C.5. They are the same for all choices of the
identifier. For uniformity in the generated data, the time span that was passed
to the ODE solver was also the same for all identifier choices, namely 0–1.3 s.
Although this is somewhat larger than is necessary to plot some of the figures,
it is the interval that is needed for generating nearly all of the data used for
plotting the figures of Section 5.4.

For each of the identifier choices, one or two parameter values are varied
over a certain range, using a fixed step size. The parameter values are stored
in an array named $\langle par\rangle$`Data`, where $\langle par\rangle$ is the name of the parameter that is
varied. For each of the parameter values in the array, a corresponding solution
structure can be obtained from the ODE solver. These solution structures are
stored in a cell array with the name `sol`$\langle par\rangle$, where $\langle par\rangle$ is the name of the
parameter that is varied. The parameters that are varied, the names of the
arrays in which the various values are stored, and the names of the cell arrays
with the corresponding solution structures are given in Table C.6 for each of the
identifier choices.

Before running the script, a word of caution is in order:

> **Warning:** Running the script `dataRichardsEa` with one of the
> choices ’`Figure5_10`’, ’`Figure5_11`’, or ’`Figure5_12`’ for the vari-
> able `identifier` (see Line 28 of Listing C.2.1) may take a consider-
> able time to finish! Also, very large data structures are generated,
> so one should have a large amount of memory and storage space
> available! See Table C.7 for an indication of how much time and
> memory/storage space is needed.

As can be seen from Table C.7, the amount of data generated is larger for smaller
values of the mixing time τ_m. The reason for this is, that for smaller mixing
times the model equations have oscillatory solutions for a wider range of the
model parameters τ_f and T_w, as can be seen from Figures 5.10–5.12. Since the
ODE solver can use a larger step size if the solution does not change very rapidly,
the solution structures that are returned by the ODE solver, are much smaller if
flame extinction or steady combustion occurs than for an oscillatory combustion
process. The amounts of data that are generated for the three choices of the

Identifier	Filename	Description
'Figure5_3' 'Figure5_4' 'Figure5_5'	dataFigures5_3-4-5.mat	Generates data for Figures 5.3–5.5.
'Figure5_6'	dataFigure5_6.mat	Generates data for Figure 5.6.
'Figure5_7' 'Figure5_8'	dataFigures5_7-8.mat	Generates data for Figures 5.7–5.8.
'Figure5_9'	dataFigure5_9.mat	Generates data for Figure 5.9.
'Figure5_10'	dataFigure5_10.mat	Generates data for Figure 5.10.
'Figure5_11'	dataFigure5_11.mat	Generates data for Figure 5.11.
'Figure5_12'	dataFigure5_12.mat	Generates data for Figure 5.12.

Table C.4: Identifier choices for the script file `dataRichardsEa.m` (see Line 28 of Listing C.2.1), and the filenames under which the generated data are stored. The data that are saved in the `.mat` files, are: the parameter structure (`s`), the initial values vector (`y0`), the array of values of the parameter that was varied (see Table C.6) and the corresponding cell array containing the solution structures (see Table C.6).

Initial condition		Value used	Unit
`y0(1)`	$= \widetilde{P}(0)$	1	–
`y0(2)`	$= \widetilde{T}(0)$	5	–
`y0(3)`	$= \widetilde{u}(0)$	0	–
`y0(4)`	$= Y_f(0) = Y_{f,i}$	0.06	–

Table C.5: Initial values, stored in the vector `y0` that was passed to the ODE solver to generate the data for the figures of Section 5.4.

Identifier	Par	Range	Unit	Array	Structure
'Figure5_3' 'Figure5_4' 'Figure5_5'	T_w	$750, 1000, 1200$	K	TwData	solTw
'Figure5_6'	$\widehat{h}$	$100 : 5 : 165$	W/m^2/K	hData	solh
'Figure5_7' 'Figure5_8'	f	$0, 0.02, 0.0325$	$-$	fData	solf
'Figure5_9'	L_{tp}	$0.4 : 0.025 : 0.8$	m	LtpData	solLtp
'Figure5_10'	τ_f	$0.01 : 0.0025 : 0.09$	s	taufData	soltaufTw
	T_w	$700 : 25 : 1400$	K	TwData	
	τ_m	$= 0$	s		
'Figure5_11'	τ_f	$0.01 : 0.0025 : 0.09$	s	taufData	soltaufTw
	T_w	$700 : 25 : 1400$	K	TwData	
	τ_m	$= 1.0 \times 10^{-3}$	s		
'Figure5_12'	τ_f	$0.01 : 0.0025 : 0.09$	s	taufData	soltaufTw
	T_w	$700 : 25 : 1400$	K	TwData	
	τ_m	$= 0.5 \times 10^{-3}$	s		

Table C.6: The model parameters that are varied to obtain data for the figures of Section 5.4, associated with the identifier choices. The ranges over which the parameters are varied (expressed in the listed units), are given in the format start:step:end, or as a list of values. The parameter values are stored in arrays and the corresponding solution structures in cell arrays; their names are listed in the last two columns.

Identifier	τ_m (ms)	CPU time (min.)	Data (MB)
'Figure5_10'	0	21.0	889
'Figure5_11'	1.5	10.7	453
'Figure5_12'	0.5	15.1	638

Table C.7: CPU time taken and size of data generated by running the script `dataRichardsEa` for the three listed identifier choices (see Line 28 of Listing C.2.1). Each identifier choice is associated with a mixing time τ_m. The CPU times were measured with the MATLAB command `cputime`. The size of the data is the storage space occupied in the workspace after the script has finished. (In storage on hard disk less space is occupied, because MATLAB compresses it by default.) Used computer configuration: desktop with Intel Core 2 Duo-processor E6300 and 1024MB DDR2 SDRAM memory (533MHz, 64-bits), and Windows XP as operating system.

identifier are very large, because the model parameters τ_f and T_w are varied over 33 and 29 values, respectively, resulting in cell arrays that store $33 \times 29 = 957$ solution structures.

Of course, one way of limiting the demand on time and storage space is by varying these parameters over less values. This can be done without any problems by modifying the script file `dataRichardsEa.m` in Lines 127 and 128, where `taufData` and `TwData` are specified. (In fact, all model parameter ranges can be adjusted in an analogous manner, without a need to rewrite other code.) Then, when plotting the figures using the modified data, a graph of lower resolution will result.

The data that were generated with the script `dataRichardsEa` was used to examine the time history of the solutions for many different parameter values. But if the data is only needed to plot the Figures 5.10–5.12 of Section 5.4, it would be better to combine the code of the script file `dataRichardsEa.m` with the code of the script file `freqDataRichardsEa.m`, which is given in the next section. It was written to determine the amplitudes and frequencies of the oscillatory solutions. By determining and storing the amplitude and frequency information directly after a solution structure has been obtained, there is no need to store the solution structures for later use. Then, the demands on memory or storage capacity are minimal. It will probably not make much difference on the needed CPU time.

Listing C.2.1: Script file `dataRichardsEa.m`. Generates data for the figures of Section 5.4. The choice of the identifier set in Line 28 determines the data that are generated.

```
                          ──────── dataRichardsEa.m ────────
1   % dataRichardsEa.m
2
3   % Clear workspace, close figure windows, and clear command window
4
5   clear all
6   close all
7   clc
8
9   % Set identifier for generation of data for a certain figure from
10  % the Interim Report, Chapter 5. Choose from:
11  %
12  %   'Figure5_3'  = Three wall temperature values
13  %   'Figure5_4'  = -> produces same data as 'figure5_3'
14  %   'Figure5_5'  = -> produces same data as 'figure5_3'
15  %   'Figure5_6'  = Range of heat transfer coefficients
16  %   'Figure5_7'  = Three friction coefficient values
17  %   'Figure5_8'  = -> produces same data as 'figure5_7'
18  %   'Figure5_9'  = Range of tailpipe lengths
19  %   'Figure5_10' = Range of flow times and wall temperatures, ...
20  %                     taum = 0 s
21  %   'Figure5_11' = (idem), taum = 1.0e-3 s
22  %   'Figure5_12' = (idem), taum = 0.5e-3 s
23  %
24  % WARNING! Choices 'Figure5_10', 'Figure5_11', 'Figure5_12' may take
```

```
25   % a considerable time to process and they produce very large data
26   % structures!
27
28   identifier = 'Figure5_3';
29
30   % Set initial values for ODE-solver
31
32   Pini  = 1;     % [ - ]
33   Tini  = 5;     % [ - ]
34   uini  = 0;     % [ - ]
35   Yfini = 0.06;  % [ - ]
36
37   y0 = [Pini; Tini; uini; Yfini];
38
39   % Set options for ODE-solver
40
41   options = odeset('AbsTol',1e-8,'RelTol',1e-6);
42
43   % Set time-span for ODE-solver
44
45   tmin  = 0;     % [ s ]
46   tmax  = 1.3;   % [ s ]
47   tspan = [tmin tmax];
48
49   % Initialize structure of model parameters
50
51   s = setRichardsEa;
52
53   % Select data to generate for plotting the figure, and save it
54
55   switch identifier
56
57       case {'Figure5_3','Figure5_4','Figure5_5'}
58
59           % Run ODE-solver with default values for three wall
60           % temperature values
61
62           TwData = [750, 1000, 1200];  % [ K ]
63           for n = 1:length(TwData)
64               s.Tw = TwData(n);
65               sol = ode45(@odeRichardsEa,tspan,y0,options,s);
66               solTw(n) = {sol};
67           end
68           filename = 'dataFigures5_3-4-5';
69           save(filename,'s','y0','TwData','solTw')
70
71       case 'Figure5_6'
72
73           % Run ODE-solver with default values for a range of heat
74           % transfer coefficients
75
76           hData = linspace(100,165,14); % [ W/m^2/K ], step = 5
77           for n = 1:length(hData)
78               s.h = hData(n);
```

```
79              sol = ode45(@odeRichardsEa,tspan,y0,options,s);
80              solh(n) = {sol};
81          end
82          filename = ['data',identifier];
83          save(filename,'s','y0','hData','solh')

85      case {'Figure5_7','Figure5_8'}

87          % Run ODE-solver with default values for three friction
88          % coefficient values

90          fData = [0, 0.02, 0.0325];  % [ - ]
91          for n = 1:length(fData)
92              s.f = fData(n);
93              sol = ode45(@odeRichardsEa,tspan,y0,options,s);
94              solf(n) = {sol};
95          end
96          filename = 'dataFigures5_7-8';
97          save(filename,'s','y0','fData','solf')

99      case 'Figure5_9'

101         % Run ODE-solver with default values for a range of tailpipe
102         % lengths

104         LtpData = linspace(0.4,0.8,17);  % [ m ], step = 0.025
105         for n = 1:length(LtpData)
106             s.Ltp = LtpData(n);
107             sol = ode45(@odeRichardsEa,tspan,y0,options,s);
108             solLtp(n) = {sol};
109         end
110         filename = ['data',identifier];
111         save(filename,'s','y0','LtpData','solLtp')

113     case {'Figure5_10','Figure5_11','Figure5_12'}

115         switch identifier
116             case 'Figure5_10'
117                 s.taum = 0;       % [ s ]
118             case 'Figure5_11'
119                 s.taum = 1.0e-3;  % [ s ]
120             case 'Figure5_12'
121                 s.taum = 0.5e-3;  % [ s ]
122         end

124         % Run ODE-solver with default values for a range of flow
125         % times and wall temperatures

127         taufData = linspace(0.01,0.09,33);  % [ 1/s ], step = 0.0025
128         TwData   = linspace(700,1400,29);   % [ K ],   step = 25
129         for n = 1:length(taufData)
130             s.itauf = 1/taufData(n);
131             for m = 1:length(TwData)
132                 s.Tw = TwData(m);
```

```
133              sol = ode45(@odeRichardsEa,tspan,y0,options,s);
134              soltaufTw(n,m) = {sol};
135           end
136        end
137        filename = ['data',identifier];
138        save(filename,'s','y0','taufData','TwData','soltaufTw')
139
140     otherwise
141
142        error('Unknown identifier choice.');
143
144  end  % switch
```

dataRichardsEa.m

C.3   Calculating amplitudes and frequencies

The script file `freqDataRichardsEa.m` (see Listing C.3.1) contains the code that was used to extract the amplitude and frequency information for the Figures 5.9–5.12 of Section 5.4 from the data generated with `dataRichardsEa.m` (see Section C.2). By setting the MATLAB variable `identifier` in Line 21 to a certain string and running the script, data for the figure associated with the identifier are generated, and stored under an appropriate name. The available choices for the identifier are listed in Table C.8, together with descriptions of the data that are generated for those choices, the filenames under which the data are stored, and the data files that are needed for execution of the script with the given identifier. The data files that are needed for execution of the script are generated with the script `dataRichardsEa` (see Section C.2).

The frequencies of the numerical solutions that were obtained with the script `dataRichardsEa`, are determined from a Discrete Fourier Transformation, using MATLAB's Fast Fourier Transform algorithm `fft`. They are the frequencies that maximize the approximated periodogram. To obtain the frequency information for the periodogram, the time interval $[0.3, 1.3]$ (in s) is divided into 4096 equally spaced intervals, giving 4096 samples points (the point $t = 1.3\,$s is not included). The time interval and the number of sample points were chosen after testing on given combinations of sine functions, and on some of the numerical solutions of the model equations. Although the testing was not done rigorously, it was found that a (much) shorter time interval would be unsuitable, because the time domain truncation disturbs the frequency information of the signal. The number of sample points that was chosen (4096), was found to be sufficient to prevent serious aliasing of the frequencies. Note that it is a power of 2; the `fft` is the most efficient for vector lengths that are powers of 2.

The testing that was done to determine the interval length and the number of sample points, suggested that the (discrete) Fourier analysis would not give the amplitudes of the time signal with satisfactory accuracy. The main cause for lack of accuracy of the amplitudes is the time domain truncation. It was found that increasing the time interval gave better results, but that would mean very long computing times. Therefore, the (peak-to-peak) amplitudes were estimated from the sampled data by taking the difference of the maximum and the minimum of the pressure on the time interval 1–1.3 s.

The amplitude information can be used to distinguish between steady com-

bustion or flame extinction (amplitude nearly zero) and oscillatory combustion. To distinguish between flame extinction and combustion (steady, or oscillatory), the (mean) fuel mass fraction can be used. Therefore, for Figures 5.10–5.12, the mean fuel mass fraction is determined over the same time interval as the pressure amplitudes, i.e. 1–1.3 s.

Before running the script, a word of caution is in order:

> **Warning:** Running the script `freqDataRichardsEa` with one of the choices `'Figure5_10'`, `'Figure5_11'`, or `'Figure5_12'` for the variable `identifier` (see Line 21 of Listing C.3.1) may take a considerable time to finish! See Table C.9 for an indication of how much time is needed.

The differences in the CPU times that the script needs to finish, come from the different amounts of data that needs to be analyzed for the frequency content. The smaller the mixing time τ_m, the larger the amount of data, as was explained in Section C.2.

Listing C.3.1: Script freqDataRichardsEa.m

```
                       ──── freqDataRichardsEa.m ────

1    % freqDataRichardsEa.m
2
3    % Clear workspace, close figure windows, and clear command window
4
5    clear all
6    close all
7    clc
8
9    % Set identifier to generate frequency data (and amplitude data) for
10   % one of the Figures 5.9-5.12 from the Interim Report, Chapter 5.
11   % Choose from:
12   %
13   %    'Figure5_9'  = generate frequency data for Figure 5.9
14   %    'Figure5_10' = generate frequency data for Figure 5.10
15   %    'Figure5_11' = generate frequency data for Figure 5.11
16   %    'Figure5_12' = generate frequency data for Figure 5.12
17   %
18   % WARNING! Choices 'Figure5_10', 'Figure5_11', 'Figure5_12' may take
19   % a considerable time to process!
20
21   identifier = 'Figure5_9';
22
23   % Select data to load, plot requested figure, and save it
24
25   switch identifier
26
27       case 'Figure5_9'
28
29           % Load data
30
31           load dataFigure5_9
32
```

Identifier	Filename ⟨needed⟩	Description
'Figure5_9'	`freqDataFigure5_9.mat` ⟨`dataFigure5_9.mat`⟩	Extracts amplitude and frequency information for Figure 5.9.
'Figure5_10'	`freqDataFigure5_10.mat` ⟨`dataFigure5_10.mat`⟩	Extracts amplitude and frequency information for Figure 5.10.
'Figure5_11'	`freqDataFigure5_11.mat` ⟨`dataFigure5_11.mat`⟩	Extracts amplitude and frequency information for Figure 5.11.
'Figure5_12'	`freqDataFigure5_12.mat` ⟨`dataFigure5_12.mat`⟩	Extracts amplitude and frequency information for Figure 5.12.

Table C.8: Identifier choices for the script file `freqDataRichardsEa.m` (see Line 21 of Listing C.3.1), the filenames under which the generated data are stored, and the files that are needed for execution of the script (in angular brackets). The data that are saved in the `.mat` files, are: the arrays with the computed the amplitudes (`Amp`) and frequencies (`Freq`), in addition to the parameter structure (`s`), the initial values vector (`y0`), and the arrays of values of the parameters that were varied (cf. Table C.6 in Section C.2). For the contour plots of Figures 5.10–5.12, the computed mean fuel mass fraction (`YfMean`) is also added to the data files.

Identifier	τ_m (ms)	CPU time (min.)
'Figure5_10'	0	9.5
'Figure5_11'	1.5	4.7
'Figure5_12'	0.5	6.5

Table C.9: CPU time taken by running the script `freqDataRichardsEa` for the three listed identifier choices (see Line 21 of Listing C.3.1). Each identifier choice is associated with a mixing time τ_m. The CPU times were measured with the MATLAB command `cputime`. Used computer configuration: desktop with Intel Core 2 Duo-processor E6300 and 1024MB DDR2 SDRAM memory (533MHz, 64-bits), and Windows XP as operating system.

```matlab
33              % Select points in time, in [ s ], which are used for the
34              % frequency analysis of the pressure oscillations
35
36              tstart = 0.3;
37              tend   = 1.3;
38              N = 4096;
39              t = linspace(tstart,tend,N+1);   % sample times, N intervals
40              t(end) = [];                % do not include t = 1.3 -> N points
41
42              freqRes = 1/(tend - tstart);  % frequency resolution
43              freqFFT = (0:N-1)*freqRes;    % frequencies [ Hz ] from fft
44
45              % Pre-allocate space
46
47              nLtp = length(LtpData);
48              nt   = length(t);
49
50              Amp   = zeros(nLtp,1);
51              Freq  = zeros(nLtp,1);
52
53              FFT_P = zeros(nt,1);
54              y     = zeros(nt,4);
55              P     = zeros(nt,1);
56
57              % The frequency information of the pressure oscillations
58              % is contained in the entries 2:N/2 of the FFT.
59              % To determine the pressure amplitudes, only the points in
60              % time > 1 sec. are used.
61
62              Ifreq = 2:N/2;
63              freqFFT = freqFFT(Ifreq);
64              I = find((t > 1),1);  % index of first t > 1
65
66              % Extract data for pressure from solution structure, and
67              % determine peak-to-peak amplitudes [ kPa ] and frequencies
68              % [ Hz ]
69
70              for i = 1:nLtp
71                  y(:,:) = deval(t,solLtp{i}).';
72                  P(:,1) = y(:,1);
73                  Amp(i) = max(P(I:end)) - min(P(I:end));
74                  FFT_P(:,1) = fft(P);
75                  [val,ind]  = max(abs(FFT_P(Ifreq)));  % determine max.
76                                                        % in periodogram
77                  Freq(i) = freqFFT(ind);
78              end
79              Amp = Amp*s.P0*1e-3;  % pressure amplitude [ kPa ]
80
81              % Save frequency and amplitude data
82
83              filename = ['freqData',identifier];
84              save(filename,'s','y0','LtpData','Amp','Freq')
85
86          case {'Figure5_10','Figure5_11','Figure5_12'}
```

```
87
88          % Load data
89
90          filename = ['data',identifier];
91          load(filename)
92
93          % Select points in time, in [ s ], which are used for the
94          % frequency analysis of the pressure oscillations
95
96          tstart = 0.3;
97          tend   = 1.3;
98          N = 4096;
99          t = linspace(tstart,tend,N+1);   % sample times, N intervals
100         t(end) = [];              % do not include t = 1.3 -> N points
101
102         freqRes = 1/(tend - tstart);  % frequency resolution
103         freqFFT = (0:N-1)*freqRes;    % frequencies [ Hz ] from fft
104
105         % Pre-allocate space
106
107         ntauf = length(taufData);
108         nTw   = length(TwData);
109         nt    = length(t);
110
111         Amp    = zeros(ntauf,nTw);
112         Freq   = zeros(ntauf,nTw);
113         YfMean = zeros(ntauf,nTw);
114
115         FFT_P = zeros(nt,1);
116         y     = zeros(nt,4);
117         P     = zeros(nt,1);
118         Yf    = zeros(nt,1);
119
120         % The frequency information of the pressure oscillations
121         % is contained in the entries 2:N/2 of the FFT.
122         % To determine the pressure amplitudes and mean fuel mass
123         % fraction, only the points in time > 1 sec. are used.
124
125         Ifreq = 2:N/2;
126         freqFFT = freqFFT(Ifreq);
127         I = find((t > 1),1);  % index of first t > 1
128
129         % Extract data for pressure from solution structure and
130         % determine peak-to-peak amplitudes [ kPa ], mean fuel mass
131         % fractions [ - ], and frequencies [ Hz ]
132
133         for i = 1:ntauf
134             for j = 1:nTw
135                 y(:,:)  = deval(t,soltaufTw{i,j}).';
136                 P(:,1)  = y(:,1);
137                 Yf(:,1) = y(:,4);
138                 Amp(i,j)   = max(P(I:end)) - min(P(I:end));
139                 FFT_P(:,1) = fft(P);
140                 [val,ind]  = max(abs(FFT_P(Ifreq)));
```

```
141                                        % determine max. in periodogram
142               Freq(i,j)   = freqFFT(ind);
143               YfMean(i,j) = mean(Yf(I:end));
144            end
145         end
146         Amp = Amp*s.P0*1e-3;  % pressure amplitude [ kPa ]
147
148         % Save frequency and amplitude data
149
150         filename = ['freqData',identifier];
151         save(filename,'s','y0','taufData','TwData','Amp','Freq',...
152            'YfMean')
153
154      otherwise
155
156         error('Unknown identifier choice.');
157
158   end  % switch
```
———————————— freqDataRichardsEa.m ————————————

C.4   Plotting graphs

The script file `plotRichardsEa.m` (see Listing C.4.1) contains the code that was used to plot the figures of Section 5.4, using the data generated with the scripts `dataRichardsEa` (see Section C.2) and `freqDataRichardsEa` (see Section C.3). By setting the MATLAB variable `identifier` in Line 23 to a certain string and running the script, data for the figure associated with that identifier is loaded, and a graph is plotted and saved under an appropriate name. The available choices for the identifier are listed in Table C.10. It mentions which figures are produced for those choices, and the filenames under which the figures are saved (i.e. the .fig files). The data files (extension: .mat) that are needed to plot the figures, are shown between angular brackets.

For Figures 5.6–5.8 amplitude information is needed, which was not generated with the scripts `dataRichardsEa` or `freqDataRichardsEa`. It is therefore computed in the script `plotRichardsEa` in this section. To be able to compare the amplitude information of Figure 5.6 directly with those of Figures 5.9–5.12, the amplitudes are determined in the exact same way, using the same sample times.

A last remark on the code of `plotRichardsEa.m`: labels for the contour plots of Figures 5.10–5.12 must be placed manually in the plots by pointing and clicking the mouse on contour lines. You continue by pressing the 'Return' key. The contour plots are always produced in pairs: part (a) of the figure (the amplitude information), and part (b) of the figure (the frequency information). It may happen that the second contour plot is hidden behind the first, when you are asked to place the labels manually. Just select the second figure window to put it in the foreground, and continue with placing labels.

Identifier	Filename ⟨ needed ⟩	Description
'Figure5_3'	`Figure5_3.fig` ⟨ `dataFigures5_3-4-5.mat` ⟩	Plots Figure 5.3.
'Figure5_4'	`Figure5_4.fig` ⟨ `dataFigures5_3-4-5.mat` ⟩	Plots Figure 5.4.
'Figure5_5'	`Figure5_5.fig` ⟨ `dataFigures5_3-4-5.mat` ⟩	Plots Figure 5.5.
'Figure5_6'	`Figure5_6.fig` ⟨ `dataFigure5_6.mat` ⟩	Plots Figure 5.6.
'Figure5_7'	`Figure5_7.fig` ⟨ `dataFigures5_7-8.mat` ⟩	Plots Figure 5.7.
'Figure5_8'	`Figure5_8.fig` ⟨ `dataFigures5_7-8.mat` ⟩	Plots Figure 5.8.
'Figure5_9'	`Figure5_9.fig` ⟨ `freqDataFigure5_9.mat` ⟩	Plots Figure 5.9.

'Figure5_10'	`Figure5_10a.fig`
	`Figure5_10b.fig`
	⟨ `freqDataFigure5_10.mat` ⟩
		Plots Figures 5.10a
		and 5.10b.

'Figure5_11'	`Figure5_11a.fig`
	`Figure5_11b.fig`
	⟨ `freqDataFigure5_11.mat` ⟩
		Plots Figures 5.11a
		and 5.11b.

'Figure5_12'	`Figure5_12a.fig`
	`Figure5_12b.fig`
	⟨ `freqDataFigure5_12.mat` ⟩
		Plots Figures 5.12a
		and 5.12b.

Table C.10: Identifier choices for the script file `plotRichardsEa.m` (see Line 23 of Listing C.4.1). The figures are saved as `.fig` files. Data that is needed to plot the figures, is loaded from the `.mat` files; they are indicated by angular brackets.

Listing C.4.1: Script file plotRichardsEa.m. Plots the figures from Section 5.4, using data generated with `dataRichardsEa.m` (see Section C.2) and `freq-DataRichardsEa.m` (see Section C.3). The choice of the identifier set in Line 23 determines the graph that is plotted.

```
                     ──────── plotRichardsEa.m ────────
1    % plotRichardsEa.m
2
3    % Clear workspace, close figure windows, and clear command window
4
5    clear all
6    close all
7    clc
8
9    % Set identifier to plot a certain graph from the Interim Report,
10   % Chapter 5. Choose from:
11   %
12   %    'Figure5_3'  = plot Figure 5.3 from Interim Report
13   %    'Figure5_4'  = plot Figure 5.4 from Interim Report
14   %    'Figure5_5'  = plot Figure 5.5 from Interim Report
15   %    'Figure5_6'  = plot Figure 5.6 from Interim Report
16   %    'Figure5_7'  = plot Figure 5.7 from Interim Report
17   %    'Figure5_8'  = plot Figure 5.8 from Interim Report
18   %    'Figure5_9'  = plot Figure 5.9 from Interim Report
19   %    'Figure5_10' = plot Figure 5.10 from Interim Report
20   %    'Figure5_11' = plot Figure 5.11 from Interim Report
21   %    'Figure5_12' = plot Figure 5.12 from Interim Report
22
23   identifier = 'Figure5_3';
24
25   % Select data to load, plot requested figure, and save it
26
27   switch identifier
28
29       case 'Figure5_3'
30
31           % Load data
32
33           load dataFigures5_3-4-5
34
35           % Select time-span, time in [ s ]
36
37           tstart = 0;
38           tend   = 0.3;
39           t = linspace(tstart,tend,501);
40
41           % Plot graph
42
43           h = figure('Name','Figure 5.3 of Interim Report');
44           nTwData = length(TwData);
45
46           for i = 1:nTwData
47
48               % Extract data for pressure at specified points in time
```

```
49              % from solution structure
50
51              y = deval(t,solTw{i}).';
52              P = y(:,1);    % pressure, [ - ]
53
54              % Plot pressure versus time in subplot, and annotate
55
56              subplot(nTwData,1,nTwData - i + 1)
57              plot(t,P)       % time in [ s ], pressure in [ - ]
58              axis([tstart tend 0.5 2])
59
60              xlabel('Time (s)')
61              ylabel({'Dimensionless','pressure'})
62              text(0.25,1.75,0,...
63                  ['T_w = ',num2str(TwData(i))],'FontSize',9)
64
65              % Plot horizontal, dashed line at P = 1 (for reference)
66
67              hold on
68              plot([tstart tend],[1 1],'k--')
69
70          end
71
72          % Save graph
73
74          saveas(h,'Figure5_3','fig')
75
76      case 'Figure5_4'
77
78          % Load data
79
80          load dataFigures5_3-4-5
81
82          % Select time-span, time in [ s ]
83
84          tstart = 0;
85          tend   = 0.05;
86          nt = 501;
87          t  = linspace(tstart,tend,nt);
88
89          % Extract data for temperature from solution structure;
90          % collect data in array, with Tw varying over the columns
91
92          TArray = zeros(nt,length(TwData));
93          for i = 1:length(TwData)
94              y = deval(t,solTw{i}).';
95              TArray(:,i) = y(:,2);    % temperature, [ - ]
96          end
97
98          % Plot graph
99
100         h = figure('Name','Figure 5.4 of Interim Report');
101         plot(t,TArray)
102         axis([tstart tend 1 15]);
```

```
103
104              % Annotate graph
105
106              for i = 1:length(TwData)
107                  strLegend{i} = ['T_w = ', num2str(TwData(i)), ' K'];
108              end
109
110              hleg = legend(strLegend{:});
111              set(hleg,'FontSize',9)
112              text(0.041,10.75,0,...
113                  ['\tau_f = ',num2str(round(1/s.itauf*1e3)),' ms'],...
114                  'FontSize',9)
115              title('Figure 5.4')
116              xlabel('Time (s)')
117              ylabel('Dimensionless temperature')
118
119              % Save graph
120
121              saveas(h,'Figure5_4','fig')
122
123          case 'Figure5_5'
124
125              % Load data
126
127              load dataFigures5_3-4-5
128
129              % Select time-span, time in [ s ]
130
131              tstart = 0;
132              tend   = 0.05;
133              nt = 501;
134              t  = linspace(tstart,tend,nt);
135
136              % Extract data for fuel mass fraction from solution
137              % structure; collect data in array, with Tw varying over the
138              % columns
139
140              YfArray = zeros(nt,length(TwData));
141              for i = 1:length(TwData)
142                  y = deval(t,solTw{i}).';
143                  YfArray(:,i) = y(:,4);    % fuel mass fraction, [ - ]
144              end
145
146              % Plot graph
147
148              h = figure('Name','Figure 5.5 of Interim Report');
149              plot(t,YfArray)
150              axis([tstart tend 0 s.Yfi]);
151
152              % Annotate graph
153
154              for i = 1:length(TwData)
155                  strLegend{i} = ['T_w = ', num2str(TwData(i)), ' K'];
156              end
```

```
157            hleg = legend(strLegend{:},...
158                'Location','NorthWest');
159            set(hleg,'FontSize',9)
160            text(0.007,0.042,0,...
161                ['\tau_f = ',num2str(round(1/s.itauf*1e3)),' ms'],...
162                'FontSize',9)
163            title('Figure 5.5')
164            xlabel('Time (s)')
165            ylabel('Fuel mass fraction')
166
167            % Save graph
168
169            saveas(h,'Figure5_5','fig')
170
171        case 'Figure5_6'
172
173            % Load data
174
175            load dataFigure5_6
176
177            % Select points in time, in [ s ], which are used to
178            % determine the peak-to-peak pressure amplitude (i.e, use
179            % the points in time consistent with those used for Figures
180            % 5.9-5.12 of the Interim Report)
181
182            tstart = 0.3;
183            tend   = 1.3;
184            N = 4096;
185            t = linspace(tstart,tend,N + 1);  % N intervals
186            I = find((t > 1),1);              % index first t > 1
187            t = t(I:(end - 1));               % time span from 1 to 1.3,
188                                              % not including t = 1.3
189
190            % Extract data for pressure from solution structure,
191            % and determine peak-to-peak amplitude, in [ kPa ]
192
193            nh  = length(hData);
194            Amp = zeros(nh,1);
195
196            for i = 1:nh
197                y = deval(t,solh{i}).';
198                Amp(i) = max(y(:,1)) - min(y(:,1));  % amplitude, [ - ]
199            end
200            Amp = s.P0*Amp*1e-3;  % peak-to-peak amplitude [ kPa ]
201
202            % Plot graph
203
204            h = figure('Name','Figure 5.6 of Interim Report');
205            plot(hData,Amp)
206
207            axis([100 165 0 80]);
208            set(gca,'Box','on','TickDir','out')
209
210            % Annoatate, indicate areas of steady combustion and flame
```

```matlab
211            % extinction
212
213            hold on
214            fill([100 110 110 100],[0 0 80 80],[.6 .6 .6])
215            text(105,40,'Steady combustion',...
216                'Rotation',90,...
217                'HorizontalAlignment','center')
218            fill([155 165 165 155],[0 0 80 80],[.6 .6 .6])
219            text(160,40,'Flame extinction',...
220                'Rotation',90,...
221                'HorizontalAlignment','center')
222
223            title('Figure 5.6')
224            xlabel('Heat transfer coefficient (W/m^2/K))')
225            ylabel('Amplitude (peak-to-peak, in kPa)')
226
227            % Save graph
228
229            saveas(h,'Figure5_6','fig')
230
231        case 'Figure5_7'
232
233            % Load data
234
235            load dataFigures5_7-8
236
237            % Select time-span, time in [ s ]
238
239            tstart = 0.9;
240            tend   = 0.92;
241            t = linspace(tstart,tend,501);
242            tplot  = (t - tstart)*1e3;    % time in [ ms ]
243
244            % Plot graph
245
246            h = figure('Name','Figure 5.7 of Interim Report');
247            nfData = length(fData);
248
249            for i = 1:nfData
250
251                % Extract data for pressure and velocity at specified
252                % points in time from solution structure
253
254                y = deval(t,solf{i}).';
255                P = y(:,1);   % pressure, [ - ]
256                u = y(:,3);   % velocity, [ - ]
257
258                % Compute pressure amplitude, normalized pressure,
259                % and normalized velocity
260
261                Amp = s.P0*(max(P) - min(P))*1e-3; % pressure amplitude
262                                                   % in [ kPa ]
263                P = P/max(P);  % pressure normalized to its maximum
264                u = u/max(u);  % velocity normalized to its maximum
```

```
265
266              % Plot pressure and velocity versus time in subplot,
267              % and annotate
268
269              subplot(length(fData),1,nfData - i + 1)
270              plot(tplot,[P u])   % pressure and velocity,
271                                  % time in [ ms ]
272
273              axis([tplot(1) tplot(end) -0.5 1.1])
274              hleg = legend('Normalized pressure',...
275                  'Normalized velocity','Location','NorthOutside');
276              set(hleg,'FontSize',9)
277              xlabel('Time (ms)')
278              ylabel({'Normalized pressure','and velocity'})
279              text(0.5,-0.3,0,...
280                  {['f = ',num2str(fData(i))],...
281                  ['Pressure amplitude = ',num2str(round(Amp)),...
282                  ' kPa']},...
283                  'FontSize',9)
284
285              % Plot horizontal, dashed line at y = 0 (for reference)
286
287              hold on
288              plot([tplot(1) tplot(end)],[0 0],'k--')
289
290          end % for
291
292          % Save graph
293
294          saveas(h,'Figure5_7','fig')
295
296      case 'Figure5_8'
297
298          % Load data
299
300          load dataFigures5_7-8
301
302          % Select time-span, time in [ s ]
303
304          tstart = 0.9;
305          tend   = 0.92;
306          t = linspace(tstart,tend,501);
307          tplot  = (t - tstart)*1e3;    % time in [ ms ]
308
309          % Plot graph
310
311          h = figure('Name','Figure 5.8 of Interim Report');
312          nfData = length(fData);
313
314          for i = 1:nfData
315
316              % Extract data for pressure and fuel mass fraction at
317              % specified points in time from solution structure
318
```

```
319                    y  = deval(t,solf{i}).';
320                    P  = y(:,1);    % pressure, [ - ]
321                    Yf = y(:,4);    % fuel mass fraction, [ - ]
322
323                    % Compute pressure amplitude, normalized pressure,
324                    % and normalized fuel mass fraction
325
326                    Amp = s.P0*(max(P) - min(P))*1e-3;  % pressure amplitude
327                                                        % in [ kPa ]
328                    P  = P/max(P);   % pressure normalized to its maximum
329                    Yf = Yf/max(Yf); % fuel mass fraction normalized to its
330                                     % maximum
331
332                    % Plot pressure and fuel mass fraction versus time in
333                    % subplot, and annotate
334
335                    subplot(length(fData),1,nfData - i + 1)
336                    plot(tplot,[P Yf]) % pressure and fuel mass fraction,
337                                       % time in [ ms ]
338
339                    axis([tplot(1) tplot(end) 0 1.1])
340                    hleg = legend('Normalized pressure',...
341                        'Normalized fuel mass fraction',...
342                        'Location','NorthOutside');
343                    set(hleg,'FontSize',9)
344                    xlabel('Time (ms)')
345                    ylabel({'Normalized pressure','and fuel mass fraction'})
346                    text(0.5,0.2,0,...
347                        {['f = ',num2str(fData(i))],...
348                        ['Pressure amplitude = ',num2str(round(Amp)),...
349                        ' kPa']},...
350                        'FontSize',9)
351
352                end % for
353
354            % Save graph
355
356            saveas(h,'Figure5_8','fig')
357
358        case 'Figure5_9'
359
360            % Load data
361
362            load freqDataFigure5_9
363
364            % Plot graph
365
366            h = figure('Name','Figure 5.9 of Interim Report');
367            plot(LtpData,[Freq,Amp])
368            legend('Frequency','Amplitude','Location','North')
369            axis([0.475 0.825 0 250]);
370            set(gca,'Box','on','TickDir','out')
371
372            % Annoatate, indicate areas of steady combustion and flame
```

```
373        % extinction
374
375        hold on
376        fill([0.475 0.525 0.525 0.475],[0 0 250 250],[.6 .6 .6])
377        text(0.5,125,'Steady combustion',...
378            'Rotation',90,...
379            'HorizontalAlignment','center')
380        fill([0.775 0.825 0.825 0.775],[0 0 250 250],[.6 .6 .6])
381        text(0.8,125,'Flame extinction',...
382            'Rotation',90,...
383            'HorizontalAlignment','center')
384
385        title('Figure 5.9')
386        xlabel('Tailpipe length (m)')
387        ylabel('Amplitude (kPa) and frequency (Hz)')
388
389        % Save graph
390
391        saveas(h,'Figure5_9','fig')
392
393    case {'Figure5_10','Figure5_11','Figure5_12'}
394
395        % Load data
396
397        filename = ['freqData',identifier];
398        load(filename)
399
400        % Plot graph, part (a) contour plot of amplitudes
401
402        strFigure = ['Figure 5.',identifier(end-1:end),'(a)'];
403        h = figure('Name',[strFigure,'a of Interim Report']);
404
405        % Plot pressure amplitude contour lines
406
407        [XTw,Ytauf] = meshgrid(TwData,taufData);
408        [C,hC] = contour(XTw,Ytauf,Amp,[0:10:100],'k');
409        axis([700 1400 0.01 0.09])
410
411        % Add lines indicating boundary between steady and
412        % oscillatory combustion
413
414        hold on
415        contour(XTw,Ytauf,Amp,0.01*s.P0*1e-3*[1 1],'k',...
416            'LineWidth',2)
417
418        % Add lines indicating boundary between combustion and
419        % flame extinction
420
421        contour(XTw,Ytauf,YfMean,0.99*s.Yfi*[1 1],'k--',...
422            'LineWidth',2)
423
424        % Annotate graph
425
426        title(strFigure)
```

```
427            xlabel('Wall temperature (K)')
428            ylabel('Flow time (s)')
429            text(1200,0.05,'Steady combustion')
430            text(750,0.015,'Flame extinction')
431
432            % Label contour lines manually by pointing and clicking with
433            % the mouse (press <Return> to continue)
434
435            clabel(C,hC,'manual','FontSize',7)
436
437            % Save graph, part (a) contour plot of amplitudes
438
439            saveas(h,[identifier,'a'],'fig')
440            %close(h)
441
442            % Plot graph, part (b) contour plot of frequencies
443
444            strFigure = ['Figure 5.',identifier(end-1:end),'(b)'];
445            h = figure('Name',[strFigure,'b of Interim Report']);
446
447            % Plot pressure frequency contour lines
448
449            [XTw,Ytauf] = meshgrid(TwData,taufData);
450            [C,hC] = contour(XTw,Ytauf,Freq,[70:10:200],'k');
451            axis([700 1400 0.01 0.09])
452
453            % Add lines indicating boundary between steady and
454            % oscillatory combustion
455
456            hold on
457            contour(XTw,Ytauf,Amp,0.01*s.P0*1e-3*[1 1],'k',...
458                'LineWidth',2)
459
460            % Add lines indicating boundary between combustion and
461            % flame extinction
462
463            contour(XTw,Ytauf,YfMean,0.99*s.Yfi*[1 1],'k--',...
464                'LineWidth',2)
465
466            % Annotate graph
467
468            title(strFigure)
469            xlabel('Wall temperature (K)')
470            ylabel('Flow time (s)')
471            text(1200,0.05,'Steady combustion')
472            text(750,0.015,'Flame extinction')
473
474            % Label contour lines manually by pointing and clicking with
475            % the mouse (press <Return> to continue)
476
477            clabel(C,hC,'manual','FontSize',7)
478
479            % Save graph
480
```

```
481          saveas(h,[identifier,'b'],'fig')
482
483      otherwise
484
485          error('Unknown identifier choice.');
486
487  end  % switch
```
──────────────── plotRichardsEa.m ────────────────

Appendix D

MATLAB codes of auxiliary functions

D.1   Adjusting model parameter structure

The function `setparam` (see Listing D.1.1) was written to specify the contents of multiple fields of a structure in an easy way. It also checks if the fieldnames exist for which the contents is to be set, and it returns an error message if that is not the case. So, by using the function `setparam`, the contents of multiple fields of a structure can be set in one go, and the user is sure that the correct fields are modified. However, since the input arguments of the function are not checked for correctness, the user should take care that the input is specified in the intended way. Otherwise, an unexpected error message may appear.

The input of the function `setparam` should be of the following form: a structure (say, **s**), followed by a paired list of strings of fieldnames and values (say, `...,'fld`n`',val`n`,...`). Thus, the input is: `s,'fld1',val1,...`. The function then returns an identical structure, except that the fields with the names `fld`n are given the values `val`n.

The function `setparam` is used by the functions `setKilicarslan` (see Section A.1), `setAhrensEa` (see Section B.1), and `setRichardsEa` (see Section C.1).

For completeness, an overview of the MATLAB functions defined in this section, is presented in Table D.1.

Function	Input	Description
`setparam`	`s,'fld1',val1,...`	Returns a structure equal to **s**, except that the fields `fld`n are given the specified values `val`n.

Table D.1: Overview of the functions that are defined in Section D.1.

Listing D.1.1: Function setparam. Given a structure and a paired list of field-names and values, it returns an identical structure, except that the specified fields are set to the corresponding values.

```
                              setparam.m
1   function sOut = setparam(sIn,varargin);

2

3   % Copy input structure

4

5   sOut = sIn;

6

7   % Adjust user specified fields to user specified values

8

9   for i = 1:2:length(varargin)
10      if ~isfield(sOut,varargin{i})
11          error('Unknown parameter.');
12      end
13      sOut = setfield(sOut,varargin{i},varargin{i+1});
14  end
                              setparam.m
```

This report was provided with a CD-ROM in the back, on which all the MATLAB codes can be found that were presented in the appendices.